Peptide-Based Biocompatible Hydrogels for Biomedical Applications

A thesis submitted in partial fulfilment of the requirements

for the award of the degree of

DOCTOR of PHILOSOPHY

By

SHUBHANGINI SINGH VERMA

DEPARTMENT OF BIOSCIENCES AND BIOENGINEERING

INDIAN INSTITUTE OF TECHNOLOGY GUWAHATI

GUWAHATI, ASSAM - 781 039, India

March, 2026

Dedicated to my family

Source and pillars of my motivation and strength…

INDIAN INSTITUTE OF TECHNOLOGY GUWAHATI

DEPARTMENT OF BIOSCIENCES AND BIOENGINEERING

DECLARATION

The research work presented in this thesis is an original work carried out by me in the Department of Biosciences and Bioengineering, Indian Institute of Technology Guwahati, India, for the degree of the Doctor of Philosophy. The research work was carried out under the guidance of my supervisor, Prof. Nitin Chaudhary. The work reported herein has not been submitted to any other Institute/University for any degree or diploma. Consistent with the standard practice of scientific reporting, appropriate acknowledgments have been made, and references to the original sources have been cited whenever the work is based on findings of other researchers.

Date: March 02, 2026
Place: Guwahati

Shubhangini Singh

Shubhangini Singh Verma

INDIAN INSTITUTE OF TECHNOLOGY GUWAHATI

DEPARTMENT OF BIOSCIENCES AND BIOENGINEERING

CERTIFICATE

This is to certify that the thesis entitled "Peptide-Based Biocompatible Hydrogels for Biomedical Applications" submitted by Ms. Shubhangini Singh Verma, for the award of the degree of Doctor of Philosophy is a record of an original research work carried out by her under my supervision and guidance at the Department of Biosciences and Bioengineering, Indian Institute of Technology Guwahati, India. The thesis has fulfilled all requirements as per the regulations of the institute and, in my opinion, has reached the standard needed for submission. The results embodied in this thesis have not been submitted to any other University or Institute for the award of any degree or diploma.

Date: March 02, 2026
Place: Guwahati

Prof. Nitin Chaudhary
(Thesis supervisor)
Department of Biosciences and Bioengineering
Indian Institute of Technology Guwahati

ACKNOWLEDGEMENTS

Words alone cannot adequately express the profound gratitude I feel for this transformative journey that has broadened my perspective and deepened my appreciation for life itself.

I extend my most sincere and heartfelt thanks to my supervisor, Prof. Nitin Chaudhary, for his invaluable guidance, unwavering support, and constant encouragement. His emphasis on critical thinking, fundamental understanding, and exposure to real-world problems has shaped me as a researcher and individual. I am forever grateful for his mentorship and the opportunities he provided.

I am deeply thankful to my doctoral committee members: Prof. Sachin Kumar (Chairman), Prof. Vibin Ramakrishnan, and Dr. Shirisha Nagotu from the Department of Biosciences and Bioengineering. Their insightful critiques, valuable advice, and constructive suggestions during my progress seminars significantly enhanced the quality of this research.

I would also like to express my heartfelt gratitude to my B.Sc. supervisor, Prof. Chandra Sekhar Gahan, for his constant encouragement and unwavering support throughout my journey in both life and research.

I acknowledge the facilities and support provided by Department of Biosciences and Bioengineering, Departmental Central Instrument Facility (DCIF), Param-Ishan Supercomputing Facility and Central Instrument Facility (CIF), IIT Guwahati. Special thanks to Dr. Arun Sathyan and Dr. Debolina Ghosh from the Centre for Environment, IIT Guwahati, for their assistance with FTIR analysis. I also thank Shinjini Bhattacharya for her valuable assistance in cell-culture experiments.

I gratefully acknowledge the Ministry of Human Resource Development, India, for providing the fellowship that enabled me to pursue this PhD.

I am particularly indebted to Mr. Vishnu G from the Department of Civil Engineering, IITG for his unconditional support and invaluable assistance with experiments and analyses beyond my expertise.

My heartfelt gratitude to present and former lab members Dr. Anshuman Mohapatra, Dr. Vinay Kumar Belwal, Dr. Vivek Prakash, Dr. Yvonne Christian, Dr. Feba Francis, Dr. Kalpana, Aishwarya, Amrita, Kamini, Sakshi, Kunal, Naveen, Dikshita, Mouli, Amay, Sushmita,

Debarshee, Aishee, and Saraswati from NC, and VR lab for their support, motivation and meaningful discussions, throughout this journey. I am immensely grateful to my senior and mentor, Dr. Shubham Srivastava from Central University of Rajasthan for his constant guidance, encouragement, and invaluable support.

Special mention goes to the Volleyball Club, IIT Guwahati, which played a pivotal role in maintaining my mental well-being throughout this PhD journey. I would like to extend my heartfelt gratitude to my wonderful friends I made through the game: Vijay, Shreya, Ichchha, Ritika, Meghna, Chongpi, Sarjeeta, Sonal, Nandini, Kalyani, Shivighn, Rohit, Gowtham, Shreyansh, and Amey for bringing balance, energy, and joy to my life outside of research.

I cherish the friendship and camaraderie of my colleagues and friends Dr. Sumona, Dr. Debolina, Sreekanth, Anil, Dr. Abhay Pratap Singh, Akash, Jaideep, and Dr. Ashish. The memories we created together through community gatherings, events, and sports activities will always hold a special place in my heart. I extend heartfelt appreciation to my best friends Anuradha dixit and Dr. Lavi Chouhan who have stood by me through all my ups and downs.

From the depths of my heart, I express my profound gratitude to my beloved parents, Mr. Shelender Singh Verma and Mrs. Asha Verma, whose sacrifices, love, and unwavering faith enabled me to pursue my ambitions. I am equally thankful to my sister Ms. Nandini Singh and my brother Mr. Tanmay Singh for their constant love and support.

Above all, I bow with reverence to Lord Shiva, whose divine blessings, strength, and guidance have been my constant source of perseverance, clarity, and inspiration throughout this journey.

Finally, I express my gratitude to everyone who contributed directly or indirectly to the completion of this thesis. It is through their collective efforts and support that this journey became possible.

Shubhangini Singh Verma

Table of Contents

List of abbreviations

Aβ	β-amyloid
ATR	Attenuated total reflectance
Boc	tert-Butoxycarbonyl
Calcein AM	Calcein acetoxymethyl ester
CD	Circular dichroism
DIPEA	*N,N*-diisopropylethylamine
DMEM	Dulbecco's Modified Eagle's Medium
DMF	*N,N*-dimethylformamide
FBS	Fetal bovine serum
Fmoc	Fluorenylmethyloxycarbonyl
GAPDH	Glyceraldehyde 3-phosphate dehydrogenase
FRET	Förster resonance energy transfer
FTIR	Fourier-transform infrared spectroscopy
HBTU	*N,N,N′,N′*-tetramethyl-*O*-(1*H*-benzotriazol-1-yl)uronium hexafluorophosphate
HCCA	α-Cyano-4-hydroxycinnamic acid
HEK-293	Human embryonic kidney cells
HOBt	1-Hydroxybenzotriazole hydrate
HPLC	High performance liquid chromatography
IAPP	Human islet amyloid polypeptide
MALDI-TOF	Matrix-assisted laser desorption ionization-time of flight
MD	Molecular dynamics
MTT	3-(4,5-Dimethylthiazol-2-yl)-2,5-diphenyltetrazolium bromide
PA	Peptide amphiphile
PBS	Phosphate-buffered saline
RPMI 1640	Roswell Park Memorial Institute 1640 Medium
TEM	Transmission electron microscopy
TFA	Trifluoroacetic acid
ThT	Thioflavin T
TIPS	Triisopropylsilane

Synopsis

Hydrogels are soft materials known for their exceptionally high-water content. Hydrogelators, the compounds that bring about gelation, have extensive chemical and structural diversity. Given the wide range of biomedical applications of hydrogels, there is growing interest in developing biocompatible hydrogelators. Peptides have emerged as promising candidates for this purpose due to their inherent structural versatility, well-established synthetic protocols, and well-understood folding and self-assembly mechanisms. Numerous peptides are reported in the literature that can spontaneously organize into β-sheet-rich fibrillar networks, leading to hydrogel formation. However, most peptide-based hydrogelators incorporate bulky, non-natural aromatic groups, such as naphthalene or Fmoc, which promote self-assembly through π–π stacking interactions. While effective in facilitating hydrogelation, the presence of such foreign moieties raises safety concerns for biomedical use. As a result, there is an increasing focus on developing hydrogelators composed exclusively of natural amino acids. Native peptide sequences are further advantageous for therapeutic applications as they are non-immunogenic. Amyloid-forming peptides are particularly notable for their ability to self-assemble into fibrillar structures and have been widely studied for their hydrogel-forming capabilities.

In my doctoral research, I investigated the hydrogel-forming ability of Ac-PHF6 and its including aromatic and aliphatic analogs. PHF6 is a peptide fragment derived from the human tau protein ($tau^{306-311}$), which is known to play a key role in Alzheimer's disease through the formation of paired helical filaments (PHFs). The effects of salt and the aromatic tyrosine residue were systematically examined by designing and synthesizing analogs with either aromatic or aliphatic substitutions to understand the influence of specific structural features on gelation. Additionally, I investigated the gelation of Ac-PHF6*, a native peptide similar to Ac-PHF6 lacking aromatic residues.

The content of this thesis is arranged in six chapters.

Chapter 1: Introduction

This chapter overviews peptide-based hydrogels, including their classification and diverse biomedical applications. It discusses various classes such as Fmoc-protected peptides, peptide amphiphiles, amphiphilic peptides, and amyloid-derived peptides, with emphasis on their self-assembly and hydrogelation. Special focus is on amyloidogenic peptides, known to form β-

sheet-rich fibrils. The chapter also introduces the rationale behind selecting native short peptide stretches for hydrogelation without foreign aromatic moieties, enhancing biocompatibility.

Chapter 2: Ac-PHF6 as a promising injectable hydrogelator

Native short peptide sequences with self-assembling potential were screened for salt-induced gelation. Peptides were shortlisted based on three key criteria: (i) the presence of one or more charged residues, (ii) at least one aromatic residue, and (iii) the ability to self-assemble via parallel β-sheet structures, preferably with in-register arrangement. These criteria led to the identification of the tau-derived hexapeptide VQIVYK ($tau^{306-311}$). I evaluated the hydrogelation propensity of the uncapped (VQIVYK) and capped (CH_3CO-VQIVYK-NH_2, also called Ac-PHF6) peptides. Both peptides readily dissolved in water. However, upon dilution in PBS, the uncapped peptide failed to induce gelation at concentrations up to 20 mM. In contrast, Ac-PHF6 formed soft hydrogels at 10 and 15 mM, and a much stronger gel at 20 mM concentration. Ac-PHF6 caused gelation of cell culture media as well. The hydrogel was characterized using rheology, and the underlying superstructures were characterized using CD and FTIR spectroscopy, fluorescence spectroscopy, and TEM. The structures underlying hydrogels were found to be β-sheet-rich amyloid-like fibrils. The hydrogel was found to be biocompatible, which allowed cell culture, as demonstrated using HEK-293 cells. Besides, the drug entrapment followed by sustained release was also investigated. Ac-PHF6 was turned out to be a potent injectable hydrogelator.

Chapter 3: Investigations into the self-assembly and hydrogelation of Ac-PHF6 analogs with electron-deficient aromatic rings

The findings from Chapter 2 inspired a follow-up investigation focused on the role of the Tyr residue in Ac-PHF6, specifically by exploring the impact of aromatic substitutions. In this study, Tyr was replaced with Phe, and the phenyl ring was further modified with various para-substituted electron-withdrawing groups (H, F, CN, NO_2, CF_3). While most analogs formed viscous solutions in water, only Ac-VQIVF(CF_3)K-am induced hydrogelation upon heating to 70 °C, followed by cooling to room temperature. Notably, all analogs formed stable, self-supporting hydrogels in PBS at 20 mM concentration with comparable mechanical strength. Among the analogs, Ac-VQIVF(CF_3)K-am showed the highest mechanical strength, likely due to its increased hydrophobicity. These hydrogels were comprehensively characterized using rheology, CD, fluorescence spectroscopy, FTIR, and TEM imaging. MD simulations of the steric zipper assemblies for Ac-PHF6 and its analogs revealed comparable stability across all

systems. The results suggest that hydrophobicity, rather than electronic effects of the aromatic substituents, plays a dominant role in promoting hydrogelation. Thus, the function of the Tyr residue in Ac-PHF6 appears to be more related to its bulky hydrophobic nature than its aromaticity.

Chapter 4: Investigating the hydrogelation of Ac-PHF6 aliphatic analogs

The results in chapter 3 show that Ac-PHF6 analogs, wherein tyrosine's phenolic group is substituted with phenyl or electron-deficient phenyl groups, also form hydrogels. The formation of hydrogels with comparable rheological properties, irrespective of the aromatic moiety, led me to speculate that the Tyr310 residue contributes to Ac-PHF6 hydrogelation through its hydrophobicity, rather than its aromaticity. This hypothesis was tested in chapter 4. Ac-PHF6 analogs wherein Tyr was replaced with aliphatic amino acids with different side-chain hydrophobicities, *viz.* Lys, Ala, Met, Val, and Ile, were investigated, along with Ac-PHF6* (tau$^{275\text{-}280}$). Ac-PHF6* (CH_3CO-VQIINK-NH_2) is another peptide motif similar to Ac-PHF6, but without an aromatic residue. All the peptides caused instant gelation of PBS, except Ac-VQIVKK-am, which formed a soft gel after about 2 h. Peptides containing Val and Ile formed stiffer hydrogels than Ac-PHF6. Met and Ala have lower hydrophobicities relative to Val and Ile, and form hydrogels with lower stiffness. Ac-VQIVKK-am formed softer gel with a storage modulus of about 1 kPa. Ac-PHF6* had lower solubility compared to that of Ac-PHF6, but formed hydrogel at 10 mM concentration. These data establish that tyrosine's role in Ac-PHF6 self-assembly is primarily due to its hydrophobicity rather than its aromaticity. Additionally, Ac-PHF6* shows cytocompatibility and cell-viability against HEK-293 cells.

Chapter 5: Hydrogelation by Ac-PHF6 and Ac-PHF6* analogs with cationic N-terminus

Tuttle and coworkers suggested that the terminal charge coupling in tripeptides, such as a cationic N-terminus and/or an anionic C-terminus, contributes to hydrogelation propensity. Guided by these insights, this chapter examined Ac-PHF6 and Ac-PHF6* analogs harboring an N-terminal Lys residue. The peptides were systematically designed and synthesized to assess the influence of terminal charge coupling on self-assembly and gelation. The study included a retropeptide (KYVIQV), bola-amphiphilic variants (Ac-KVQIVYK-am, and Ac-KVQIINK-am), and charged-flipped analogs (KVQIVY-am, Ac-KVQIVY-am, and Ac-KVQIIN-am). Among these, KYVIQV-am and Ac-KVQIVYK-am formed clear, viscous solutions in water and successfully formed transparent hydrogels in PBS at 20 mM concentration. Analogs of Ac-PHF6* form rigid hydrogels at 15 mM concentration with

rheological properties comparable to 20 mM Ac-PHF6 hydrogel. Ac-KVQIVY-am also formed PBS hydrogel at 15 mM concentration. The gel, however, was turbid, and the storage modulus was ~8 kPa. Rheological analysis showed that the retropeptide formed a softer gel than Ac-PHF6, whereas the bola-amphiphilic analog demonstrated greater mechanical strength than Ac-PHF6 at 20 mM. Cytocompatibility assays conducted with the retropeptide and bola-amphiphilic gels using HEK 293 cells demonstrated their ability to support cell growth, highlighting their potential for biomedical applications.

Chapter 6: Conclusions and future directions

This chapter concludes the thesis by summarizing its major outcomes, discussing the unexplored possibilities of Ac-PHF6 and its analogs, and provides future directions with relevant examples.

List of publications

(1.) **Verma SS**, Bhattacharya S, Kumar S, Chaudhary N*. The amyloidogenic peptide stretch in human tau, tau306–311 is a promising injectable hydrogelator. *Biophysical Chemistry*, 2025, 322: 107438.

(2.) **Verma SS**, Chaudhary N*. Substitution of tyrosine with electron-deficient aromatic amino acids improves Ac-PHF6 self-assembly and hydrogelation. *RSC Advances*, 2025, 15(28): 22216–27.

(3.) **S. S. Verma**, S. Bhattacharya, S. Kumar, and N. Chaudhary, "Tyr310 is Superfluous for Ac-PHF6 Hydrogelation: Ac-PHF6* is also a Hydrogelator," *Int. J. Pept. Res. Ther.*, vol. 32, no. 1, p. 21, 2026, doi: 10.1007/s10989-026-10803-9.

CHAPTER 1

Introduction

1. Peptide self-assembly and hydrogelation

The spontaneous formation of ordered structures from discrete molecular building blocks has garnered significant attention due to its relevance in chemistry, materials science, and biology. Molecular self-assembly is a reversible and spontaneous process whereby molecules organize into well-defined architectures without external direction [1]. This process is driven primarily by non-covalent interactions, including hydrogen bonding, hydrophobic interactions, electrostatic forces, π-π stacking, and van der Waals interactions that may occur intra- and/or intermolecularly. Two key prerequisites for efficient self-assembly are chemical complementarity and structural compatibility of the constituent molecules [2]. Another factor is the balance between attractive and repulsive forces: sufficient attraction (hydrophobic, hydrogen bonding, aromatic stacking) must overcome repulsion (electrostatics, solvation effects, conformational entropy) to nucleate assembly. Among the various classes of self-assembling molecules, proteins and peptides are particularly attractive when it comes to biocompatible materials [3], [4], [13]–[20], [5]–[12]. They are native to biological systems and are made up of diverse functional groups that bring chemical diversity. Chemical moieties such as hydrophobic groups, aromatic rings, charged groups, and hydrogen-bond donors and acceptors collectively drive assembly into higher-order structures. This chemical versatility not only underlies natural processes such as protein folding but also enables the design of minimal peptide motifs capable of forming fibers, sheets, or other nanostructures in vitro [21]. In materials science, peptides can be rationally designed to assemble into nanostructures with tunable physicochemical properties, offering a biomimetic route to functional materials. Aromatic residues, for instance, promote stacking interactions, while charged residues impart solubility or responsiveness to ionic conditions. The modular nature of peptides allows for systematic variation to elucidate sequence–structure relationships, making them ideal model systems for studying self-assembly principles at the molecular level.

Notably, such processes reinforce the formation of many functional soft materials. A prominent example is the peptide-based hydrogels, where nanofibrous peptide network immobilizes water to yield three-dimensional, hydrated matrices [22], [23]. In these systems, self-assembly dictates the formation, stability, and responsiveness of the gel, illustrating how fundamental supramolecular principles can be translated into practical biomaterials [24]. Conventional hydrogels are often derived from natural or synthetic high-molecular-weight polymers [9]. Peptide-based hydrogels and their different classes have been discussed in the following section.

1.1. Peptide-based hydrogels

Natural or synthetic polymers, including proteins and carbohydrates, make up the vast bulk of hydrogels. In the last two decades, a distinct class of hydrogels has emerged: peptide-based hydrogels, built from amino acids or their derivatives [25]. Owing to their modularity, these systems offer an attractive alternative to conventional polymeric matrices. Unlike large biomacromolecules, short peptides are easier and less expensive to synthesize yet retain the essential motifs required for supramolecular self-assembly [26]–[28]. In the standard approach to fabricating peptide-based hydrogels, individual peptide units adopt specific secondary structures and self-assemble into nanoscale assemblies, most frequently fibrillar architectures. As these fibrils elongate and assemble, they form larger supramolecular aggregates that, through non-covalent cross-linking and physical entanglement, generate a continuous, self-supporting network. The resulting mechanical properties of such hydrogels are influenced by multiple parameters, including the peptide's primary sequence, concentration, and the balance between hydrophobic and hydrophilic residues. Furthermore, the incorporation of non-natural amino acids or chemical modifications at termini allows fine control over properties such as hydrophobicity, charge, pKa, and isoelectric point, dramatically expanding the structural and functional diversity accessible to these materials [29].

Peptide-based hydrogels are typically classified as low-molecular-weight gelators whose assembly is driven by non-covalent interactions such as hydrogen bonding, hydrophobic effects, electrostatic attractions, van der Waals forces, and π-π stacking [30]. These interactions direct the peptides to adopt secondary structures such as β-sheets, α-helices, or turns. The resulting ordered motifs then aggregate hierarchically into nanostructures (fibrils, ribbons, or tapes) that entangle or cross-link to form a percolating network capable of trapping large volumes of water [31]. This hierarchical organization mirrors natural protein folding and offers tunable viscoelasticity and mechanical strength suitable for biomedical use [32]. Because peptides are inherently biocompatible and biodegradable, their hydrogels can be engineered to provide defined microenvironments for cells, encapsulate and release bioactive molecules, or respond to environmental cues such as pH, temperature, and light. Stimuli-responsive hydrogels adapt their structure to environmental changes, making them valuable for biomedical uses [33]–[38]. The pH-responsive hydrogels contain ionizable groups whose protonation shifts with pH, altering electrostatic and hydrogen-bonding interactions to drive swelling, collapse, or re-gelation [39]–[41]. Temperature-sensitive hydrogels exploit the thermal dependence of non-covalent forces; many peptide systems show sol-gel transitions near body

temperature, enabling injectable delivery and in situ solidification [42]–[45]. Light-responsive hydrogels incorporate photoactive moieties (e.g., azobenzene, photolabile linkers) that change conformation or break cross-links upon irradiation, enabling reversible sol-gel transitions or spatial control over mechanical properties [46][47][48]. These attributes make them highly attractive for applications ranging from three-dimensional cell culture, tissue engineering, and wound healing to drug delivery, microfluidic systems, and self-healing biomaterials [49]–[52]. Notably, the modular chemistry of amino acids allows precise tailoring of gelation kinetics, mesh size, and degradation profiles, enabling customization for specific therapeutic or industrial needs.

Most peptide-based hydrogels rely on β-sheet-rich assemblies in which individual gelators form fibrils that bundle into larger fibers through supramolecular forces [53]. These extended aggregates establish a self-supporting, water-laden network without requiring covalent crosslinkers. Such supramolecular gels not only mimic aspects of the extracellular matrix (ECM) but also offer controllable nanostructure and mechanical properties, positioning them as promising next-generation biomaterials. The major types of β-sheet peptide hydrogelators are discussed in the following subsections.

1.1.1. Fmoc-protected amino acids and peptides

Short peptides containing an aromatic group at their N-termini have a strong tendency to self-assemble in aqueous environments, often causing hydrogelation [54]. The self-assembly of very short gelators strongly depends on aromatic stacking interactions and hydrogen bonding. The modification at the N-terminus with aromatic moieties such as Fmoc [N-(fluorenyl-9-methoxycarbonyl)] makes up a considerable portion of peptide-based gelators reported in the literature (Fig. 1.1) [25], [55]–[58].

One of the simplest scaffolds used to manufacture a variety of hydrogels is an aromatic Phe-Phe dipeptide (FF) [59]. Fmoc-Phe-Phe self-assembled through aromatic stacking interactions, forming transparent hydrogel [55]. Substitution of C_α hydrogen atom with methyl group in one or both Phe groups in Fmoc-FF significantly impacts the self-assembly and hydrogelation [54]. Selected examples of the Fmoc-protected peptide-based hydrogels are listed in Table 1.1.

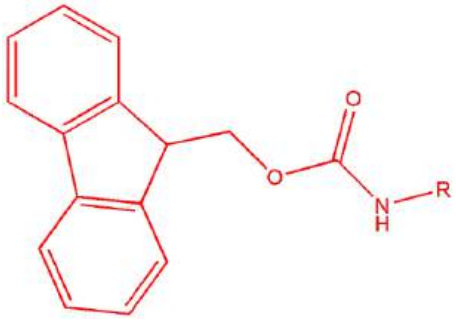

Figure 1.1. Structure of the Fmoc moiety coupled to primary amine *via* the urethane linkage.

Table 1.1 Selected examples of Fmoc-protected amino acid and peptide hydrogelators.

Peptides	**Finding**	**Reference**
Fmoc-Leu-Asp Fmoc-Ala-Asp Fmoc-Ile-Asp	Role of aromatic stacking in hydrogelation.	[60]
Fmoc-^{D}Ala-^{D}Ala	Ligand-receptor interaction of Vancomycin with Fmoc-^{D}Ala-^{D}Ala.	[61]
Fmoc-Tyr	Gelation study by dephosphorylation of Fmoc-Tyr phosphate in the presence of alkaline phosphatase enzyme.	[62]
Fmoc-Phe	Entrapment of model dyes (Direct Red and Naphthol Yellow) and their release from hydrogel.	[63]
Fmoc-F_2 and Fmoc-F2-X (X = Lys, Ser, Asp)	Chemical functionalization of the peptide scaffolds improves cell compatibility and enables tunable chemical and mechanical properties for in vitro cell culture.	[64]
Fmoc-FRGD/RGDF/2-Nal/FG/FF (2-Nal = 2-naphthyl-L-alanine)	A new library of aromatic Fmoc-dipeptides was developed, and a biophysical study of Fmoc-peptide hydrogels reveals how aromatic interactions govern their structure, thermal stability, and self-assembly for medical applications.	[65]
Fmoc-FF/RGD	Biomimetic peptide-derived nanofibrous hydrogel self-assembles into 3D scaffolds that support anchorage-	[66]

	dependent cell adhesion, proliferation, and in vitro tissue regeneration.	
Fmoc-F5-Phe	Enhancement in gelation due to fluorous effect and hydrophobicity.	[67]
Fmoc-VLK(Boc) Fmoc-K(Boc)LV	Self-assembly of peptides shows sequence inversion markedly alters fibril morphology and hydrogel properties, enabling tunable material design.	[68]
Fmoc-FF/KGM	The hybrid hydrogel shows enhanced stability and mechanical strength with tunable sustained release of hydrophobic drugs, making it a promising drug delivery carrier.	[69]
Fmoc-βAla-Val Fmoc-βAla-Phe	Incorporation of β-amino acid to prepare proteolytically resistant and mechanically strong hydrogel.	[70]
Fmoc-FFF or Fmoc-F*F*F* (F* = ^{D}Phe)	The obtained hydrogels of varying chirality were evaluated as tissue-engineering and controlled drug-delivery scaffolds.	[71]
Fmoc-X-Car (X = Ala, Val, Leu, Ile, Met, Phe, Tyr; and Car = L-carnosine)	Fmoc-protected tripeptides form pH-sensitive and proteolytically stable supramolecular hydrogels.	[72]
Fmoc-FF	Preparation of self-supporting hydrogels at physiological pH with tunable properties and morphology for tissue engineering and drug delivery.	[31] [73]
Fmoc-XX (X= F/mF/^{D}F)	Introduction of the methyl group at the α-carbon of Phe (mF) to observe its influence on self-assembly and gelation.	[54]
Fmoc-FF/Cationic peptide	Multicomponent peptide blends yield seven self-sorted hydrogels with tunable rigidity, high biocompatibility, and enhanced cell adhesion.	[74]
Fmoc-FFpY	Formation of NaCl-induced supramolecular hydrogels with self-healing, thermo-responsive behavior, and mixed β-sheet/α-helical structures.	[75]

1.1.2. Peptide amphiphiles

Peptide amphiphiles (PAs) are hybrid molecules combining a hydrophobic component, often an alkyl lipid tail, with a peptide segment that can include charged or bioactive residues (Fig. 1.2) [15]. This design allows PAs to self-assemble into well-ordered supramolecular nanostructures under aqueous conditions, such as nanofibers, micelles, or vesicles [15], [76]–[78]. Their amphiphilic nature yields a strong driving force for hierarchical assembly, mediated by hydrophobic collapse, hydrogen bonding, and often π-π interactions when aromatic residues are present [79].

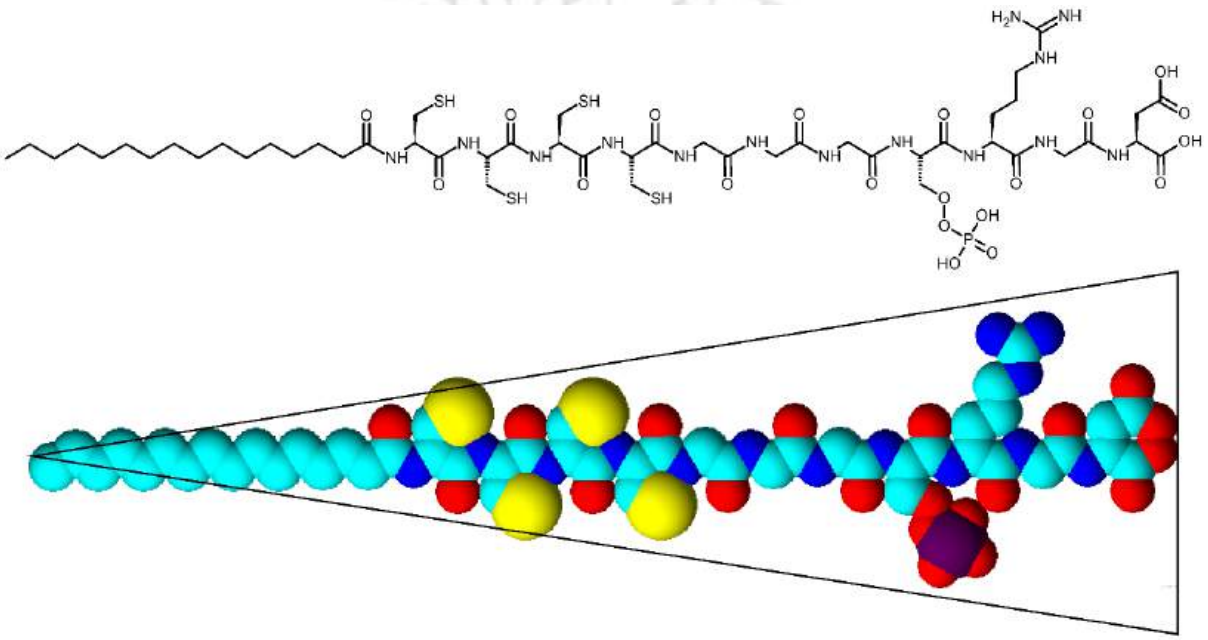

Figure 1.2. Peptide amphiphile designed by Stupp and coworkers. (A) Chemical structure, and (B) molecular structure of peptide amphiphile depicting conical shape of the molecule [15], [17].

PAs are particularly promising for biomedical applications because they mimic native ECM features while being biodegradable and biocompatible. The peptide region can be engineered to present cell-adhesion motifs, enzymatic cleavage sites, or responsive elements that react to environmental stimuli like pH, ions, or temperature [80]–[82]. Moreover, their nanoscale morphology and gelation behavior can be tuned by modifying tail length, sequence composition, or ionic headgroups, enabling control over mechanical stiffness, porosity, and degradation rate. Such tunable peptide amphiphile hydrogels have been successfully used as scaffolds for tissue engineering, platforms for controlled drug delivery, wound healing matrices, and in 3D cell culture systems [82]–[84]. Studies revealed that peptide amphiphiles self-assemble into nanofibers directing hydroxyapatite mineralization, while double-chain

alkyl amphiphiles with oligo-L-glutamic acid head groups enhanced aggregation control, mimicking bone-like structural and functional properties [85], [86]. Due to their overall conical geometry, ionic peptides bearing long alkyl chains tend to self-assemble in water into supramolecular nanostructures, such as cylindrical micelles, which can further organize into fibrous assemblies [86]. Rational design of the peptide segment allows the formation of β-sheet domains near the alkyl tail, while distal charged or bioactive residues enhance solubility and functional activity. The resulting nanofibers may be reversibly cross-linked, providing tunable internal architectures that modulate hydrogel formation [78].

The first systematic demonstration of PAs was reported by Stupp and coworkers in 2001, who synthesized a peptide amphiphile bearing a C16 alkyl chain conjugated to a peptide segment containing tetra-cysteine, glycine spacers, a phosphoserine residue, and a C-terminal RGD motif. This PA self-assembled into nanofibrous scaffolds mimicking extracellular matrix (ECM) features and promoted hydroxyapatite mineralization upon treatment with $CaCl_2$ and Na_2HPO_4 solutions [15]. Subsequently, the same group investigated a series of analogs by varying the alkyl tail length (from none to C22), substituting the tetra-cysteine domain (e.g., Cys → Ala), modifying ionic head groups, and incorporating cell adhesion motifs. These derivatives displayed pH-responsive gelation and could also be triggered to self-assemble by surface drying or treatment with divalent cations (Ca^{2+}) [76].

They further advanced the field by introducing branching architectures via orthogonal protecting-group strategies at lysine residues to incorporate multiple bioactive epitopes. For instance, RGDS motif was introduced into the branched PAs to produce nanofibrous 3D matrices suitable for regenerative medicine applications and in situ cell encapsulation [87]. In a related study, histidine-functionalized branched PAs exhibited esterase-like activity, catalyzing the hydrolysis of 2,4-dinitrophenyl acetate at their fiber surfaces [88]. In another study, they showed that the mechanical properties of self-assembled peptide-amphiphile nanofiber gels could be tuned by altering intermolecular interactions; for example, gels formed with $CaCl_2$ exhibited stronger cross-linking and higher strain tolerance. In contrast, those prepared with HCl displayed superior recovery after deformation, enabling the design of materials with tailored mechanics for specific biological responses [89]. Since these seminal reports, numerous peptide amphiphile-based hydrogelators with diverse architectures and bioactivities have been developed, establishing PAs as versatile scaffolds for biomedical applications [5]. Kokkoli and colleagues reported the development of peptide-amphiphile nanofibers, particularly PR_g (fibronectin-mimetic peptide-amphiphile) hydrogels, which

served as effective scaffolds for tissue engineering. These materials outperformed conventional gels in supporting cell adhesion and ECM deposition, demonstrating strong potential as ECM-mimetic scaffolds [90]. Das and coworkers examined the influence of counterion variation on the antimicrobial activity and biocompatibility of amino-acid-based hydrogelating amphiphiles, demonstrating enhanced efficacy against Gram-positive bacteria and fungi and improved cytocompatibility, with further broad-spectrum antimicrobial action achieved through the incorporation of silver nanoparticles [91]. Banerjee and coworkers explored a series of peptide amphiphiles capable of forming thermoresponsive hydrogels with nanofibrillar network architectures, which exhibited antimicrobial activity against both Gram-positive and Gram-negative bacteria, low cytotoxicity, and proteolytic stability, thereby highlighting their promise as next-generation antimicrobial materials [81]. Sleep and coworkers developed an injectable PA scaffold ($C_{16}V_nA_nE_n$) with liquid-crystalline order that closely resembled the ECM, which improved the survival, alignment, and differentiation of transplanted muscle stem cells and enhanced tissue regeneration [92].

1.1.3. Amphiphilic peptides

Amphiphilic peptides, *i.e.* the composed of alternating hydrophobic and hydrophilic amino acid residues, have emerged as a powerful class of biomaterials owing to their predictable self-assembly, tunable properties, and high compatibility with biological systems. Such peptides derive amphiphilicity from arranging residues like Leu, Val, and Phe (hydrophobic) alternately with Lys, Arg, Glu, or Asp (hydrophilic). This periodic polarity leads to a well-defined interface that drives self-assembly, aggregating into fibers, tapes, or sheet-like networks [93]. These principles, like alternate polar/non-polar residues, charge balance, and hydrophobic face exposure, allow amphiphilic peptides to offer precise control over assembly morphology, mechanics, biodegradability, and responsiveness. Such peptides were designed by emulating the native protein patterns that comprise regular repetitions of oppositely charged residues separated by 1 or 2 hydrophobic residues [2].

Peptides designed with alternating polar and nonpolar amino acid residues, such as CH_3CO-$(AEAEAKAK)_2$-NH_2 (EAK16), have been shown to readily adopt β-sheet conformations [94]. In these assemblies, nonpolar residues are typically oriented toward the interior of the β-sheet, while polar residues are exposed on the exterior surface, conferring both structural stability and aqueous compatibility [95]. The first of such sequences was identified as part of the yeast protein zuotin, a factor initially characterized by its binding affinity to left-handed Z-DNA [96]. Self-assembling scaffolds based on analogous sequences, such as CH_3CO-

RADARADARADARADA-NH_2 (RADA16-I) and CH_3CO-RARADADARARADADA-NH_2 (RADA16-II), have been investigated for their ability to support cell adhesion and differentiation, promote neurite extension, and facilitate the formation of functional synapses in primary and cultured neuronal cells [97].

Building on these findings, Ruan and coworkers reported a nine-residue peptide (PSFCFKFEP) that organizes into a robust, fishnet-like nanostructure whose morphology depends on peptide concentration and mechanical perturbation. Remarkably, this peptide demonstrated self-healing characteristics and could encapsulate hydrophobic model drugs such as pyrene, enabling their gradual release from coated microcrystals or liposomal carriers [2]. Similarly, alternating co-polypeptides such as poly(Glu-Val-Lys-Val) and others demonstrated highly stable β-sheet structures over wide ranges of pH and ionic strength, underscoring the robustness of sequences with hydrophobic-hydrophilic alternation [98]. Recent studies have shown that amphiphilic peptides can be engineered into highly functional biomaterials with remarkable biomedical potential. An investigation by Seow and coworkers described an ultrashort amphiphilic peptide hydrogel that formed transparent hydrogel with high shape fidelity, creating a moist and biocompatible matrix that significantly accelerated the healing of full-thickness skin wounds in mice [99]. A separate study used enzymatic triggers to guide the self-assembly of the amphiphilic peptide A_9K_2, demonstrating that its morphology could be switched between micelles, fibers, and gels under physiological conditions, which allowed fine control over the rate of gel formation and its mechanical strength [100]. Collectively, these findings illustrate how rationally designed amphiphilic peptides can generate a wide variety of nanostructured hydrogels and scaffolds, whose properties can be tuned by cross-linking, enzymatic cues, or molecular ordering to meet the demands of applications ranging from wound dressings to cell-delivery systems.

Another notable study varied the balance between hydrophobic and hydrophilic residues in designer α-helical peptides, systematically altering Leu/Lys ratios to study how relative hydrophobic area influences self-association, membrane interaction, and assembly [101].

1.1.4. Amyloidogenic peptides

One class of peptides extensively studied for self-assembly and hydrogelation is amyloids [102], [103]. Amyloid fibrils are insoluble protein/peptide assemblies that are associated with many diseases [104], [105]. Their accumulation in tissues is widely implicated in pathological processes, with Alzheimer's disease being one of the most well-known examples [106]. During

fibrillization, the peptide molecules self-assemble to adopt a cross-β-sheet architecture, in which β-strands run perpendicular to the fibril axis, a structural hallmark historically linked to disease [107], [108]. The cytotoxicity of amyloids is largely caused by the prefibrillar amyloid oligomers [109]–[111]. Even though amyloid fibrils were first discovered as disease associated pathogenic structures, research over the past two decades has identified amyloid-like architectures in native proteins, establishing cross-β sheet as a legitimate and functional protein fold [112]–[117]. The discovery of amyloid as a functional fold led to the proposition that amyloidogenic peptides could turn out to be interesting biomaterials [118], [119]. Their nativeness opens up new opportunities for their use as functional biomaterials [103], [120]–[123].

Short amyloidogenic peptides have been widely explored for hydrogel formation. Short peptides offer several advantages. They are easy to synthesize, and therefore cost-effective. Besides, the self-assembly is dictated by a smaller number of interactions, enabling better control over self-assembly and hydrogelation. Hydrogels comprising amyloid nanofibrils derived from Fmoc-protected di- and tri-peptides have since been developed to support cell culture and stem-cell differentiation [124]. Jean and coworkers investigated islet amyloid polypeptide associated with type II diabetes, which was shown to form gels in bulk solution and at hydrophobic-hydrophilic interfaces, producing condensed fibril matrices stabilized by non-covalent β-sheet interactions [125]. Hen egg-white lysozyme (HEWL) was reported to form amyloid-like fibrillar hydrogels upon thermal cycling between 60 °C and 25 °C [126]. Ma and coworkers produced an injectable HEWL-derived hydrogel by pre-incubating peptides under acidic conditions with Mg^{2+} to accelerate fibrillation; the lyophilized powder formed a colloidal solution in phosphate buffer (pH 7.4) and rapidly gelled at 37 °C [123]. Juszczak and coworkers demonstrated that the N-terminal $tau_{2\text{-}19}$ peptide forms hydrogel with polyproline-II like fibrils resembling collagen I, stabilized by weak proline carbonyl hydrogen bonds. Studies suggest that the presence of water critically shaped gel architecture, and spectroscopic assays suggest a sequential gelation, syneresis, and aggregation process in Alzheimer's disease, with fibril formation driven by entropy from water release [127]. Krysmann and coworkers demonstrated the self-assembly of the $A\beta_{16\text{-}20}$ fragment (KLVFF) into a hydrogel at 3 wt% in phosphate-buffered saline (PBS) [128]. Paik ad coworkers examined hydrogel formation by α-synuclein, where horseradish peroxidase was successfully immobilized within the gel and catalyzed 3,3′,5,5′-tetramethylbenzidine oxidation [129]. Chaudhary and coworkers investigated the hydrogelation of $A\beta_{16\text{-}22}$ (CH_3CO-KLVFFAE-NH_2) and its analog $A\beta_{16\text{-}}$

$_{22}$(F20Y). The Aβ$_{16-22}$ was turned out to be a non-gelator up to 20 mM concentration while the analog Aβ$_{16-22}$(F20Y) formed hydrogel at 2 mM concentration [121]. Interestingly when two peptide units were connected via β-turn-supporting motifs, both the peptides caused hydrogelation [122].

Although self-assembly into β-sheets underlies the vast majority of peptide hydrogelators reported in the literature, assembly through α-helical coiled-coil motifs can also lead to hydrogelation. These peptides have repeating heptapeptide units such as (HPPHPPP), where H represents a hydrophobic residue and P a polar residue [130]. However, the relatively long sequences (20-40 residues) and high concentrations (1-12% w/v) required for gelation have limited their broader application. Nevertheless, peptide-based hydrogels are inherently biocompatible and proteolytically degradable, making them promising candidates for various biomedical and therapeutic uses [131].

1.2. Applications

Hydrogels, particularly those composed of peptides, look promising for many biomedical applications. They can be used for drug delivery, wound healing, gene therapy, cell and tissue culture, organoid formation, among other applications (Fig. 1.3). The unique structure of peptide hydrogels, characterized by their network of interconnected fibers, enables them to effectively encapsulate and release small molecules, making them highly suitable for drug delivery applications [121], [132], [133].

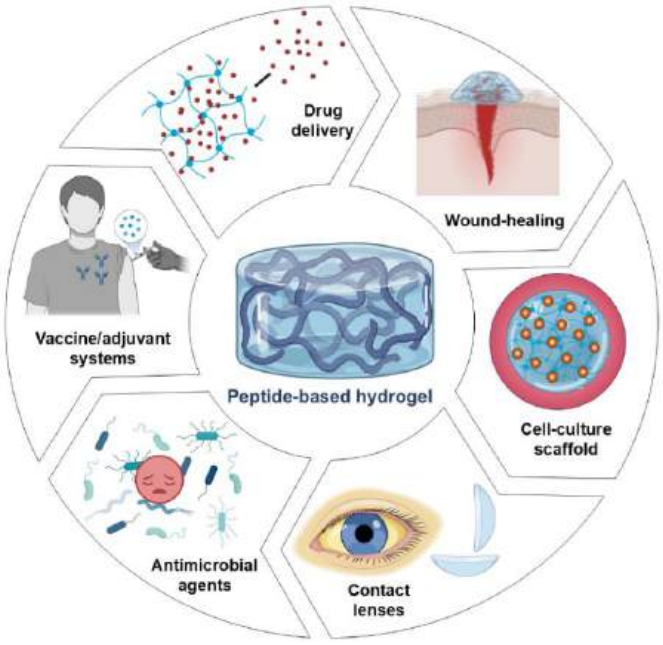

Figure 1.3. Applications of peptide-based hydrogels.

These hydrogels can offer controlled release profiles by responding to environmental stimuli such as pH or enzymes, which can trigger the release of drugs at targeted sites, enhancing therapeutic efficacy while minimizing side effects [52]. Peptide-based gels conjugated with antigenic peptides can serve as adjuvant systems capable of eliciting antibody responses [134]. Several amyloidogenic peptide hydrogels have been shown to effectively encapsulate and release the anticancer drug doxorubicin [44], [121], [123]. Besides controlled drug delivery, these hydrogels provide a protective milieu for cells, facilitating nutrient transport and creating a favorable environment for cell adhesion. [135]. These hydrogels mimic native extracellular matrices by forming stable, biocompatible networks with tunable mechanical properties and enhanced bioactivity through functional motifs [136], [137]. They support cell adhesion, proliferation, migration, and differentiation, while enabling controlled growth factor delivery, making them promising platforms for regenerative medicine and organotypic tissue models with superior structural and biological performance [138]–[141]. Due to their high-water content and close resemblance to the ECM, these have also been evaluated for wound-healing efficacy and infection control. Ultrashort peptides facilitated rapid autolytic debridement and re-epithelialization, whereas multidomain hydrogels promoted angiogenesis and neurogenesis [99], [142]–[144]. The resveratrol-loaded hydrogels were found to suppress inflammation and minimize scarring, enhancing tissue regeneration [145]. As far as antimicrobial activity of the hydrogels is concerned, they can be broadly classified into two categories: (i) hydrogels with intrinsic antibacterial activity, typically constructed from antimicrobial peptides (AMPs), and (ii) hydrogel platforms designed for the controlled delivery of conventional antibiotics [146], [147]. Peptide-based hydrogels display significant and selective antimicrobial activity, with several studies confirming their efficacy against both Gram-positive and Gram-negative bacteria, including drug-resistant strains like MRSA and *E. coli* [81], [100], [148]–[152]. These hydrogels kill bacteria chiefly by disrupting cell membranes, demonstrating low cytotoxicity and excellent biocompatibility with mammalian cells. Their promising versatility and safety pave the way for future breakthroughs in clinical therapies.

1.3. Rationale behind the thesis work

A large number of peptides have been reported in the literature that self-assemble to form β-sheet-rich fibrils, eventually causing hydrogelation. A vast majority of these peptides, however, employ bulky non-native aromatic moieties, such as fluorene and naphthalene. Hydrogelators with foreign aromatic moieties are usually very small in size. Incorporation of foreign aromatic moieties, however, raises safety concerns as far as biomedical applications are concerned. For

instance, the degradation of Fmoc-FF hydrogel causes cell death through necrosis [153]. Therefore, the peptides that lack foreign moieties have gained considerable attention as biocompatible hydrogelators. Unfortunately, peptide hydrogelators lacking foreign aromatic moieties are generally much larger [76], [154]. The large size of the designed peptides raises concerns about immune response when it comes to applications such as drug delivery or scaffolds in regenerative medicine. An interesting approach, therefore, could be identifying short native peptide stretches that can undergo hydrogelation under physiological conditions or be engineered into hydrogelators through minimal modifications. Tuttle and coworkers investigated the tripeptide sequence space with free termini and proposed certain guidelines that promote tripeptide gelation [155]. They proposed that a positively charged residue is preferred at the N-terminus, while aromatic residues are more favourable at positions 2 and 3 in the tripeptide. Position 3 of a tripeptide is the C-terminal residue. I surveyed short self-assembling native peptide sequences that could be salt-triggered to self-assemble. The following three criteria were applied to shortlist the peptides: (i) the peptide has one or more charged residues, (ii) there is at least one aromatic residue, and (iii) the peptide self-assembles through parallel β-sheet formation, preferably the in-register β-sheet. Parallel in-register β-sheet has been observed for many amyloidogenic proteins/peptides [156]. Such an arrangement places the identical residues juxtaposed in the strands of the β-sheet. These selection criteria led me to the peptide VQIVYK (tau$^{306\text{-}311}$). Mandelkow and coworkers first identified this peptide as the minimal interaction motif for tau self-assembly [157], [158]. The hexapeptide, termed PHF6, was shown to form fibrils in the presence of heparin. Kirschner and coworkers investigated the end-capped tau$^{306\text{-}311}$, where the N-terminus of the peptide was acetylated while the C-terminus was an amide (CH_3CO-VQIVYK-NH_2, also known in the literature as Ac-PHF6). The peptide rapidly forms amyloid fibrils in the presence of 150 mM salt [159]. Eisenberg and coworkers subsequently investigated the microcrystals formed by VQIVYK, the peptide with free termini. They find that the peptide self-assembles through parallel in-register β-sheets [160]. These two studies convinced me that VQIVYK could be a promising salt-triggered gelator. Tau$^{306\text{-}311}$ self-assembly has been extensively investigated using theoretical as well as various experimental methods [161]–[165]. Despite a large volume of literature on the tau$^{306\text{-}311}$ self-assembly, there is no report on its hydrogelation. In this thesis, I report that the peptide forms hydrogel as soon as it encounters the salt, an attribute that makes it a promising injectable hydrogelator.

1.4. Tau protein

Tau is a microtubule-associated protein predominantly found in neuronal cells, where it plays a key role in stabilizing microtubule structure [166]. Characterized as an intrinsically disordered protein, it contains an unusually high proportion of polar and charged amino acids, with Gly, Lys, Ser, Thr, and Pro making roughly half of its composition [167]. Under physiological conditions, tau is phosphorylated with approximately two to three phosphate groups per protein molecule [168]. In Alzheimer's disease and related tauopathies, tau protein undergoes hyperphosphorylation and accumulates within neurons as filamentous aggregates [169]. This leads to microtubule disassembly and promotes the aggregation of free tau molecules into paired helical filaments (PHFs). In the brains of individuals with Alzheimer's disease, tau aggregates are present as neurofibrillary tangles (NFTs), neuropil threads, and neuritic plaques, with the burden of NFTs being most strongly associated with neuronal degeneration [169]. These NFTs were thought to consist of PHFs, which predominantly adopt a β-sheet conformation [170]–[172]. Tau protein exists in six isoforms due to alternative RNA splicing. The primary structure organization of the longest isoform is shown in Fig. 1.3. The primary structure can be broadly divided into two regions: an N-terminal projection domain of approximately 120, predominantly acidic residues, and a complementary region that interfaces with the microtubule surface. The latter contains proline-rich segments along with 3-4 pseudo-repeats (R1-R4) and inter-repeat sequences, which together form the core microtubule-binding region (MTBR) (Fig. 1.4) [173]–[176]. The MTBR domain, other than microtubule binding, is recognized as a key region driving tau aggregation [177], [178].

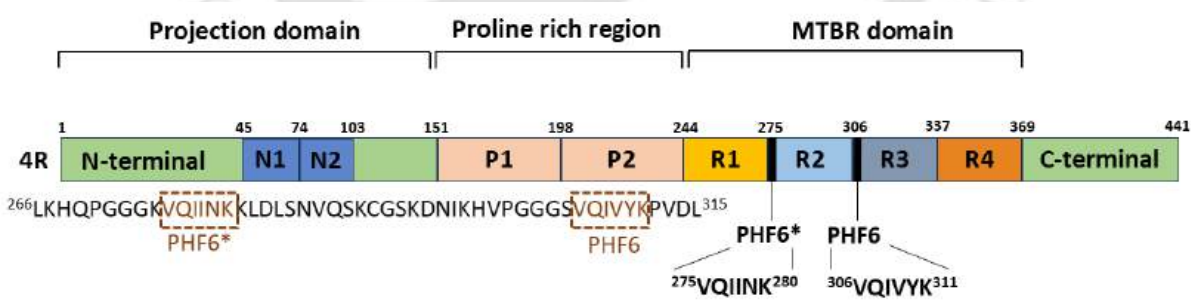

Figure 1.4. The 4R isoform of tau protein showing projection domain, protein rich region, and the MTBR domain. The positions of hexapeptide stretches PHF6, and another related hexapeptide stretch PHF6* are also indicated.

Two hexapeptide stretches, *viz.* ^{306}VQIVYK^{311} and ^{275}VQIINK^{280}, commonly referred to as PHF6 and PHF6*, respectively, are key stretches that drive tau aggregation in Alzheimer's disease. PHF6, located at the start of the R3 repeat, is conserved across all tau isoforms. PHF6*,

by contrast, is located at the start of the R2 repeat and is present exclusively in the 4R tau isoform. Owing to their strong aggregation tendencies and ability to form fibrils, both peptide segments were chosen for this study. Nevertheless, information on hydrogel formation by tau-derived peptides remains limited. Literature reports indicate that tau can undergo liquid-liquid phase separation (LLPS) within cells, producing dynamic droplets that gradually transition into gel-like states and ultimately promote the pathological aggregation of tau observed in Alzheimer's disease and related tauopathies. Ambadipudi and coworkers demonstrated that under physiological conditions, tau's lysine-rich microtubule-binding repeats undergo electrostatically driven liquid-liquid phase separation (LLPS). They showed that polyanions such as heparin or RNA accelerate amyloid formation. Their study revealed that alternative splicing and phosphorylation modulate Tau's LLPS propensity, suggesting a mechanistic link between splicing, phase separation, and neurotoxicity in tauopathies [179]. Wegmann et al. showed that soluble tau, including phosphorylated, mutant, and Alzheimer's-derived forms, undergoes LLPS in cells and model systems, forming droplets that mature into gel-like, amyloid-competent aggregates [180]. Their study showed that the phosphorylation and the aggregation-prone mutations caused enhanced droplet formation, that in turn promoted tau aggregation and seeding, implicating LLPS as a critical intermediate in tauopathies. Amyloid-based hydrogels remain relatively underexplored. Emerging research, however, is exploring them as promising materials for biomedical applications. While some initial investigations have demonstrated promising results, widespread practical applications of hydrogels in areas such as drug transport and cellular scaffolding are still developing.

CHAPTER 2

Ac-PHF6 as a promising injectable hydrogelator

2.1. Introduction

As discussed in Chapter 1, a vast majority of peptide hydrogelators harbor a bulky, non-native aromatic moiety. Such foreign moieties raise safety concerns as far as biomedical applications of hydrogels are concerned [153]. The hydrogel research, therefore, has branched to another dimension; to identify native or native-like short peptide stretches that could cause the gelation of biological fluids. Schneider and coworkers designed peptides with a β-turn-inducing motif that self-assembled under specific cues, causing hydrogelation [154], [181], [182]. Stupp and coworkers designed a peptide amphiphile wherein a palmitoyl chain was attached to the N-terminus of the peptidic moiety [86]. The peptide self-assembles at acidic pH, forming hydrogels that direct the hydroxyapatite mineralization when treated with calcium chloride and dibasic sodium phosphate. Peptide amphiphile is an interesting template for designing self-assembling peptides with different properties and applications [12], [76], [77], [149]. Native peptides are attractive gelators for biomedical applications as concerns about toxicity and immunogenicity are not there. Amyloid fibrils constitute an important class of self-assembling peptides [183]–[185]. Hauser and coworkers have reported hydrogelation by several short native N-acetylated amyloidogenic peptides [186]. Banerjee and coworkers reported hydrogel formed by a tetrapeptide from human amylin, $hIAPP_{24-27}$ [44]. Maji and coworkers have also reported several amyloid peptide hydrogelators [187], [188]. The potential of amyloid peptides as hydrogelators has been reviewed elsewhere [103].

My aim was to identify native peptide(s) that could be dissolved in water to a very high concentration without gelation and diluted in PBS to obtain the gel. I surveyed short amyloidogenic peptides and applied simple selection criteria *i.e.* presence of one or more charged residues with non-zero net charge, presence of one or more aromatic residues, and self-assembly through parallel β-sheets. These criteria led me to PHF6. The peptide harbors a lysine residue, a tyrosine residue, and self-assembled via parallel β-sheet formation [160]. In this chapter, the uncapped (VQIVYK) and the end-capped (CH_3CO-VQIVYK-NH_2) $tau^{306-311}$ were investigated. The uncapped peptide remained a clear solution in water as well as in PBS (137 mM NaCl, 2.7 mM KCl, 10 mM Na_2HPO_4, and 1.8 mM KH_2PO_4, pH 7.4). The end-capped peptide CH_3CO-VQIVYK-NH_2 (Ac-PHF6), on the other hand, formed a clear solution in water but caused instant gelation of PBS as well as the cell culture media DMEM and RPMI.

2.2. Materials and methods

2.2.1. Materials

Rink amide resin, Fmoc-protected amino acids, 1-Hydroxybenzotriazole hydrate (HOBt), and *N,N,N′,N′*-tetramethyl-*O*-(1*H*-benzotriazol-1-yl)uronium hexafluorophosphate (HBTU) were acquired from Novabiochem. Fmoc-Lys(Boc)-Wang resin was purchased from GL Biochem (Shanghai) Ltd., China. *N,N*-dimethylformamide, *N,N*-diisopropylethylamine (DIPEA), trifluoroacetic acid (TFA), acetic anhydride, thioflavin T (ThT), calcein, calcein-AM, diethyl ether, triisopropylsilane (TIPS), and rhodamine B were procured from Merck. Doxorubicin hydrochloride was purchased from Tokyo Chemical Industry (India) Pvt. Ltd. HEK cell line was obtained from the National Centre for Cell Science (NCCS), Pune, India. Dulbecco's Modified Eagle Medium (DMEM) and fetal bovine serum (FBS) for cell culture were procured from HiMedia, while RPMI 1640 medium and antibiotic-antimycotic cocktail were procured from Gibco. RNAiso Plus reagent was purchased from Takara Bio, Shiga, Japan, while MultiScribe^{TM} Reverse Transcriptase was purchased from Applied Biosystems, Waltham, Massachusetts, USA. 3-(4,5-Dimethylthiazol-2-yl)-2,5-diphenyltetrazolium bromide (MTT) was procured from Sisco Research Laboratories Pvt. Ltd. (India).

2.2.2. Peptides synthesis and characterization

The peptides were synthesized by employing Fmoc chemistry with HBTU/HOBt/DIPEA activation. The uncapped peptide (VQIVYK) was assembled on Fmoc-Lys(Boc)-Wang resin, while Ac-PHF6 was assembled on Rink amide resin. N-terminal acetylation for Ac-PHF6 was carried out on-resin using 10-equivalents each of acetic anhydride and DIPEA. The peptides were cleaved from the resins using a cleavage cocktail containing 95% TFA, 2.5% TIPS, and 2.5% water. The peptides were precipitated in ice-chilled diethyl ether, followed by multiple rounds of washing with diethyl ether. The peptides were air-dried and dissolved in water for analytical reversed-phase HPLC and purification. The identities of the peptides were ascertained using MALDI-TOF mass spectrometry on a Bruker Autoflex Speed MALDI-TOF mass spectrometer.

2.2.3. Peptide dissolution, hydrogelation, and rheology

Both peptides readily dissolved in water to very high concentrations (>20 mM). The peptide stock solutions were prepared in water, and their concentrations were estimated using the Tyr molar absorption coefficient of 1280 $M^{-1}cm^{-1}$ at 280 nm. Both peptides formed clear, viscous solutions up to about 25 mM concentration. The 10-fold concentrated PBS (10% of the final

gel volume) was taken in the clean vials. Peptide stock solution (1.11 times the desired concentration in the hydrogel) was added to obtain the hydrogel. The cases wherein the stock concentration was higher than 1.11X, required amount of deionized water was added to the 10X PBS, followed by addition of peptide. All gelation reactions were carried out at 27 °C and incubated undisturbed for 24 hours. The mixing order was same for all the subsequent studies carried out in this thesis. Gelation of PBS was attempted by diluting the peptide solutions to achieve 5, 10, 15, and 20 mM concentrations. Hydrogelation was established by gently inverting the 24-hour-old tubes. Rheology measurements of 20 mM PBS gel were carried on an Anton Paar Rheometer MCR 102 using 25 cm parallel plates at 0.5 mm gap. The amplitude sweep test was carried out at an angular frequency of 10 rad/s by varying shear strain from 0.01% to 10%. The gel showed a linear regime up to at least 0.2% strain. Frequency sweep data was recorded with 0.1% strain. Unless mentioned otherwise, all subsequent studies were carried out with 20 mM Ac-PHF6 samples prepared in water or PBS that were incubated at room temperature for 24 h.

2.2.4. Intrinsic tyrosine fluorescence spectroscopy

Intrinsic tyrosine fluorescence spectra were recorded for the 20 mM Ac-PHF6 samples prepared in water and PBS on a Jasco FP8500 spectrofluorometer. As 20 mM is a very high concentration, the spectra were recorded by diluting the samples in respective dispersants (water or PBS) to 100 µM concentration. Fluorescence emission spectra were recorded from 290-400 nm with 5 nm slit width by exciting the samples at 280 nm (2.5 nm slit width).

2.2.5. Tyrosine fluorescence quenching

Tyrosine fluorescence quenching assay was carried out for the water and PBS samples at 100 and 200 µM concentrations. As ionic strength plays a critical role in the self-assembly of Ac-PHF6, acrylamide was used as the collisional quencher. The samples were excited at 280 nm, and fluorescence emission spectra were recorded. An increasing amount of acrylamide was added, and fluorescence emission spectra were recorded. The fluorescence intensities were taken at the emission λ_{max} corresponding to the unquenched samples, and data are presented as Stern-Volmer plots.

2.2.6. Thioflavin T (ThT) fluorescence spectroscopy

The ThT fluorescence emission spectrum for the Ac-PHF6 gel sample was recorded in PBS. As ThT fluorescence quantum yield strongly depends on pH, the fluorescence emission spectrum for the water sample was not recorded in water but in 10 mM phosphate buffer, pH

7.4, to enable direct comparison with the gel sample. The assay was carried out at 100 µM peptide concentration and 10 µM ThT concentration. The samples were excited at 450 nm (slit width = 2.5 nm), and emission spectra were recorded from 465-555 nm with 5 nm slit width.

2.2.7. Circular dichroism (CD) spectroscopy

Far-UV electronic CD spectra were recorded on a Jasco J-1500 spectropolarimeter. The 24-hour-old 20 mM peptide samples were diluted to the desired concentrations in respective dispersants, and spectra were recorded in a 1 mm path-length quartz cell. The spectra were recorded from 250-195 nm at 1 nm bandwidth with a 100 nm/min scanning speed. Each spectrum is the average of 8 accumulations. The spectra were corrected by subtracting the respective dispersant's spectrum. The data was converted to mean residue ellipticity using the following formula (Equation 2.1):

$$\theta_{MRE}\ (deg.cm^2.dmol^{-1}) = \frac{\theta\ (mdeg) \times 10^6}{Pathlength\ (mm) \times Peptide\ (\mu M) \times (n-1)} \quad \text{(Equation 2.1)}$$

where n is the number of amino acids in the peptide.

2.2.8. Fourier transform infrared (FTIR) spectroscopy

FTIR spectra were recorded on a Shimadzu IRAffinity-1S Fourier transform infrared spectrometer equipped with a diamond ATR crystal. The samples were diluted 2-fold, and ~5 µl volume of the diluted sample was deposited on the diamond crystal and allowed to dry. Each spectrum is the average of 40 scans recorded at 4 cm^{-1} resolution.

2.2.9. Transmission electron microscopy

The samples were diluted 2-fold in water and deposited on the carbon-coated copper grids. After 10 minutes, the excess solvent was removed using lint-free tissue paper, and grids were stained with uranyl acetate for 10 minutes. The grids were air-dried, and the images were captured at 200 kV using a JEM-2100F transmission electron microscope (JEOL, Japan).

2.2.10. Hydrogel stability

The stability/degradation of Ac-PHF6 hydrogel was investigated by monitoring the release of peptide molecules from hydrogel to the bulk solution. The 20 mM Ac-PHF6 hydrogel (100 µl) was prepared in PBS. The gel was washed once with 100 µl PBS, and 1.4 ml PBS was carefully added on top of the hydrogel. The concentration of Ac-PHF6, released into PBS from the hydrogel, was estimated using Tyr molar absorption coefficient of 1280 $M^{-1}cm^{-1}$ at 280 nm. The hydrogel was subsequently sheared by vigorous vortexing and diluted 10-fold in PBS to

measure the absorbance. The concentration of the sheared hydrogel was considered to be 100% degradation.

2.2.11. Calcein release assay

Calcein at 500 µM concentration was trapped inside the gel. Briefly, 5 µl of 5 mM calcein stock solution prepared in 10X PBS was added to the cuvette. 45 µl of 22 mM peptide stock solution in water was subsequently added. The cuvette was left undisturbed for 24 hours, resulting in a colored gel. The release of calcein was studied by gently adding 700 µl of PBS on top of the dye-containing gel and monitoring fluorescence emission intensity at 520 nm after exciting at 490 nm. The excitation and emission slit widths were 2.5 and 5 nm, respectively.

2.2.12. Doxorubicin release assay

Doxorubicin (23 µM) was trapped inside the Ac-PHF6 gel. Briefly, 5 µl of 0.23 mM doxorubicin stock solution prepared in 10X PBS was added to a quartz fluorescence cuvette. Subsequently, 45 µl of 22 mM peptide stock solution in water was added, and the cuvette was left undisturbed for 24 h at room temperature. After 24 h, 700 µl of PBS was gently added on top of the doxorubicin-loaded gel. Doxorubicin release was monitored by recording fluorescence emission intensity at 560 nm over time by exciting at 490 nm. The excitation and emission slit widths were 2.5 and 5 nm, respectively.

2.2.13. Drug loading efficiency

The drug loading efficiency of Ac-PHF6 hydrogel was assessed using doxorubicin as the representative drug. A 20 mM Ac-PHF6 hydrogel was prepared (100 µl volume). A 10 mM doxorubicin stock solution was prepared in PBS, 100 µl volume was carefully added on top of the gel, and incubated for 18 hours. After 18 h incubation, the doxorubicin solution was removed, and the hydrogel was quickly washed once with 100 µl PBS. PBS (1.4 ml) was then added to the hydrogel, and the gel was sheared by vortexing. The sheared sample was 10-fold diluted, and absorbance was recorded at 495 nm. The concentration of doxorubicin was estimated using a molar absorption coefficient of 9250 M^{-1} cm^{-1} at 495 nm [189].

2.2.14. Injectability

The experiment was designed to qualitatively assess whether Ac-PHF6 instantaneously gels upon contact with PBS. A 20 mM Ac-PHF6 stock solution was prepared in water that contained 0.4 mM rhodamine B. The peptide was carefully injected into a glass cuvette containing 3 ml PBS. While injecting the peptide, the pipette tip was gently withdrawn from the cuvette**.** Instant

gelation resulted in a colored thread of peptide hydrogel dispersed in PBS. Immediate thread formation was visually monitored and images of the glass cuvette containing the hydrogel thread were captured at different times to see the rhodamine B release from the gel thread.

2.2.15. Cell culture assay

Human embryonic kidney (HEK-293) cells were cultured in a T25 flask using Dulbecco's Modified Eagle's Medium (DMEM) supplemented with 10% fetal bovine serum (FBS) and 1% antibiotic-antimycotic cocktail. The cells were incubated at 37 °C with 5% CO_2 for growth and maintenance. The cells were harvested using trypsin. The 10 or 15 mM PBS gels (70 µl volume) were set up in a 96-well plate. After 24 h, 200 µl complete DMEM was added to the wells having gels, and the gels were incubated at 37 °C with 5% CO_2 for 24 h. The medium was removed, and the gels were equilibrated with fresh complete medium for 10 minutes. Finally, the medium was removed, and the gels were seeded with HEK-293 cells (10^4 cells/well) and kept at 37 °C with 5% CO_2 for 48 h. The wells were subsequently washed with PBS. A 5 µM calcein-AM solution was prepared in incomplete DMEM, and 200 µl volume was added to the wells for staining the cells. After 30 minutes of incubation, the cells were washed with PBS thrice, and images were recorded using a Nikon Eclipse Ts2R fluorescence microscope.

2.2.16. RNA isolation and polymerase chain reaction

The total RNA was isolated from HEK-293 cells using RNAiso Plus reagent (Takara Bio, Shiga, Japan). The cDNA was synthesized using MultiScribe™ Reverse Transcriptase (Applied Biosystems, Waltham, Massachusetts, USA). PCR (40 cycles) was carried out using primers designed for GAPDH amplification as described elsewhere [121].

2.2.17. Cell viability assay

The biocompatibility of Ac-PHF6 was assessed through MTT assay [149]. Briefly, 10,000 HEK-293 cells in complete DMEM were seeded in a 96-well plate and incubated at 37 °C with 5% CO_2 for 24 h. The cells were then treated with Ac-PHF6 (50, 100, 150, 200 µM), and further incubated for 24 h. Subsequently, the growth medium was discarded, 100 µl of MTT (1 mg/ml in plain DMEM) was added to each well and incubated for 3 hours. The MTT solution was then removed, and 100 µl dimethylsulfoxide was added to each well. The absorbance was recorded at 570 nm in a multiwell plate reader (Multiskan GO, Thermo Scientific).

2.2.18. Molecular dynamics simulation

The extended conformation ($\phi = \psi = 180^o$) of VQIVYK was created using UCSF Chimera. N-terminal acetylation and C-terminal amidation were carried out using BIOVIA Discovery Studio. The self-assembly was investigated by including 216 randomly oriented peptide molecules in a cubic box having 8157.38 nm^3 volume. NaCl (150 mM) was subsequently added to the box. This setup corresponds to a peptide concentration of about 44 mM, a concentration much higher than the concentration at which gelation was experimentally observed. The C-terminal lysine residue contributes a positive charge to the peptide chain. Therefore, a chloride ion per peptide molecule was added to achieve an electrically-neutral system. Molecular dynamics simulation was performed with the GROMACS software package utilizing the CHARMM27 force field and a TIP3P water model [190], [191]. The modelled system was subjected to energy minimization using the steepest descent algorithm and was equilibrated through NVT and NPT ensembles (500 ns each) before a 200 ns production MD run. The simulation employed the leap-frog integration method along with the Verlet cutoff scheme. Long-range electrostatic interactions were handled using the Particle Mesh Ewald (PME) method, while bond lengths were constrained with the LINCS algorithm. Periodic boundary conditions were applied throughout the simulation. The results were analyzed using VMD, UCSF-Chimera, and Gromacs built-in tools.

Additionally, fully extended peptide molecules of Ac-PHF6 ($\phi = \psi = 180^o$) were further investigated for their capability to attain parallel β-sheet conformation by incorporating some turn inducing residues between the strands of peptide. Gly and Pro are known to induce turns in the protein chains. Both residues are associated with unusual conformational flexibility. To investigate the parallel β-sheet formation, 3 diglycine motifs ($\phi_{i+1} = 60$, $\psi_{i+1} = 30$, $\phi_{i+2} = 90$, and $\psi_{i+2} = 0$) were incorporated between four strands of Ac-PHF6 (named VGGK). The peptide was prepared in UCSF-Chimera and the N-terminal acetylation was done in BIOVIA Discovery Studio. CHARMM36 (all atom protein forcefield) forcefield was used for the simulation [192]. The forcefield has parameters for acetyl and amide groups. For C-terminal amidation, I need to choose CT2 option and no need to add amide group beforehand. The peptides were placed in the box with a 1 nm distance from the edges followed by solvation, ion addition (with 150 mM NaCl), energy minimization, and equilibration with NVT (100 ns) and NPT ensembles (200 ns). The system was then subjected to 200 ns production MD run, and results were analyzed.

2.2.19. Fluorescence resonance energy transfer

To further confirm whether Ac-PHF6 molecules assemble in parallel or antiparallel β-sheet arrangements, fluorescence resonance energy transfer was employed wherein efficiency of energy transfer was determined using time-correlated single photon counting (TCSPC). At pH >10, excitation of tyrosine residue gives appreciable fluorescence from the tyrosinate form. The tyrosinate emission is red-shifted, with an emission maximum around 350 nm, the wavelength at which the dansyl moiety absorbs. Ac-K(dan)VQIVYK-am was employed for the study. Stock solutions of Ac-PHF6 and Ac-K(dan)VQIVYK-am were prepared in water with concentrations of 22 mM and 18.72 mM, respectively. These stocks were diluted in PBS and NaOH (0.1 M) to achieve the final concentration of 100 μM. The samples were excited at 280 nm, and emission spectra were collected from 290-690 nm. Fluorescence intensities at 350 nm of Ac-PHF6 and Ac-K(dan)VQIVYK-am were analyzed to investigate energy transfer. No significant difference in the intensity could be observed. Therefore, I sought to compare the tyrosine fluorescence lifetime for Ac-PHF6 and Ac-K(dan)VQIVYK-am. The stock solutions of Ac-PHF6 and Ac-K(dan)VQIVYK-am were diluted in PBS to a final concentration of 20 μM. The samples were excited using a 290 nm LED light source, and the emission was recorded at 303 nm, with 1,000 photons in the highest intensity channel.

2.3. Results and discussion

The synthesized peptides were characterized using analytical HPLC and MALDI-TOF mass spectrometry. The peptides were found to be ≥ 95% pure, as ascertained by the areas under the peaks in the chromatograms. The MALDI-TOF mass spectra confirmed the identity of the peptides.

2.3.1. Hydrogelation and rheology

Both peptides (VQIVYK and CH_3CO-VQIVYK-NH_2) readily dissolved in deionized water to >20 mM concentration, giving clear, viscous solutions that could be easily pipetted out. The peptides were diluted to achieve 5, 10, 15, and 20 mM concentrations in PBS. Instant gelation was observed for Ac-PHF6 at 20 mM concentration. All the samples were kept undisturbed for 24 h and assessed visually for gelation by gently inverting the vials. Ac-PHF6 formed soft and fragile gels at 10 and 15 mM concentrations but a much stronger gel at 20 mM (~1.6 wt%) concentration. The 10 and 20 mM gels in inverted tubes are shown in Fig. 2.1. The peptide caused instant gelation of cell culture media DMEM and RPMI 1640 as well at 20 mM concentration. The inverted tube showing DMEM gel is shown in Fig. 2.1D. The stock solution

prepared in water remained viscous for at least a week and could also be stored at 4 °C without gelation. These attributes make Ac-PHF6 a promising injectable hydrogelator. The uncapped peptide VQIVYK, on the other hand, failed to cause gelation. Both water and PBS samples of VQIVYK remained as solutions up to at least 20 mM peptide concentration. VQIVYK, therefore, was not further investigated. Unless mentioned otherwise, all investigations were carried out for 20 mM Ac-PHF6 samples that were incubated for 24 h at room temperature. The 20 mM Ac-PHF6 hydrogel was subjected to rheological characterization. An oscillatory strain sweep was carried out to identify the linear viscoelastic region, *i.e.,* the oscillatory strain through which the complex stress varies linearly [193]. The gel displays a linear relationship for at least up to 0.2% strain. Frequency sweep, therefore, was carried out at a strain of 0.1% (Fig. 2.1E). The gel exhibits a storage modulus of around 20 kPa in the entire frequency range (624 - 0.01 rad/s).

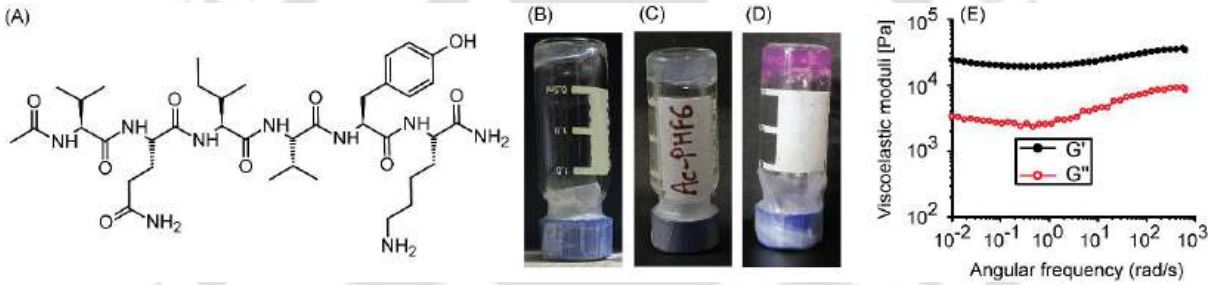

Figure 2.1. Hydrogelation caused by Ac-PHF6. (A) Chemical structure of Ac-PHF6, (B) PBS gel formed by 10 mM peptide, (C) PBS gel formed by 20 mM peptide, (D) DMEM gel formed by 20 mM peptide, and (E) frequency sweep rheological characterization of 20 mM PBS gel.

2.3.2. Secondary structure characterization

The CD spectra were recorded by diluting the 20 mM samples to 100 µM concentration (Fig. 2.2A). The CD spectrum of the water sample suggests a largely unstructured peptide. On the other hand, the PBS sample displays a negative band around 225 nm and a positive band around 200 nm, suggesting a distinct β-sheet conformation. Interestingly, however, attenuated total reflectance-Fourier transform infrared (ATR-FTIR) spectra of the dried peptide exhibit amide I band ~1626 cm^{-1} for both the samples, indicating β-sheet structure (Fig. 2.2B) [194]. At first, the infrared spectroscopy data may appear to contradict the CD data. However, it is important to note that ATR-FTIR spectra were recorded in the dried form, while CD spectra were recorded in solution. Drying is associated with a gradual increase in peptide concentration that can facilitate self-assembly in water as well, eventually showing the amide I band around 1626 cm^{-1}. To validate this interpretation, I recorded the CD spectra for 20 mM water sample by

diluting it to 400 and 200 µM concentrations (Fig. 2.2C). The spectrum recorded at 400 µM concentration shows distinct bands around 219 and 206 nm, suggesting a mixture of β-sheet and random coil conformations. At 200 µM concentration, these bands are blue-shifted. Besides, the intensity of the 214 nm band is much smaller than the 198 nm band, suggesting a larger contribution from random coil conformation. These data indicate that the peptide takes up a β-sheet conformation at high concentrations, and dilution shifts the equilibrium towards unordered conformation.

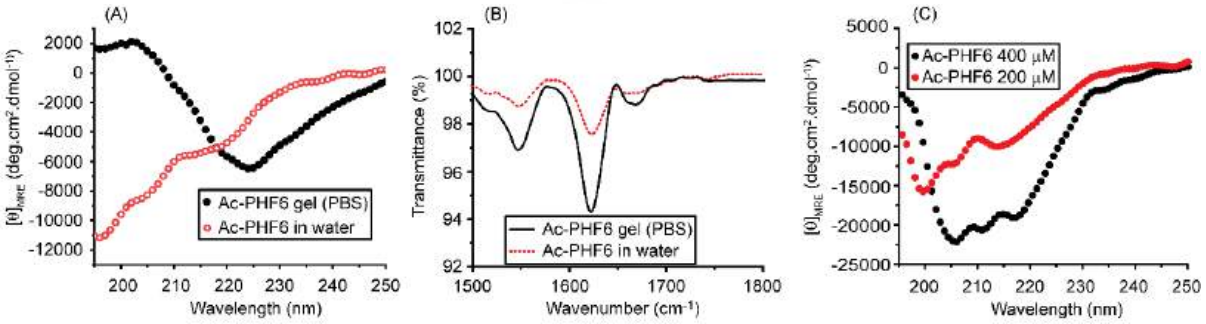

Figure 2.2. Characterization of self-assembled structures underlying the hydrogel. (A) CD spectra at 100 µM, (B) FTIR spectra, (C) CD spectra of water sample at 200 and 400 µM.

2.3.3. Molecular dynamics simulation

MD simulation of 216 Ac-PHF6 molecules in 150 mM NaCl was carried out for 200 ns. The peptide molecules in extended conformation were randomly oriented in the box. The 200 ns snapshot is shown in Fig. 2.3A, where peptide molecules can be seen forming clusters, some of them elongated. The simulation time (200 ns), however, was insufficient to attain the equilibrium, as suggested by the increasing root mean squared deviation throughout the 200 ns simulation (Fig. 2.3B).

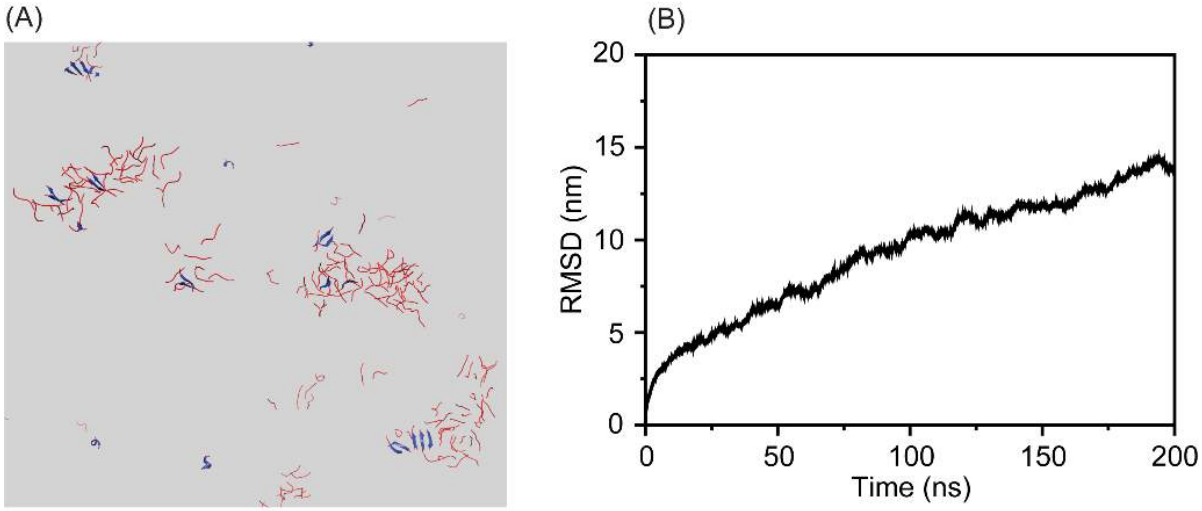

Figure 2.3. MD simulation of Ac-PHF6. Snapshots after 200 ns molecular dynamics simulation, showing clustering of peptide molecules in 150 mM NaCl (A). RMSD plotted against time, showing that the peptide assembly did not attain equilibrium (B).

The MD simulation of GG mediated peptide structure was carried out for 200 ns in 150 mM NaCl to gain insight about the conformation obtained by Ac-PHF6. The trajectory was analyzed for cluster analysis to obtain the predominant conformation of peptide, RMSD calculation, and to calculate distance between the α-carbons of terminal residues and residues present before and after the GG. The initial structure is shown in Fig. 2.4A. The middle structure of the largest cluster of simulated system was obtained at 61 ns (Fig. 2.4B). Strands 1 and 3 can be seen arranged somewhat parallel to each other. The second largest cluster shows stands 1 and 3 forming a 2-stranded parallel β-sheet (Fig. 2.4C). It was clearly evident that Ac-PHF6 stretches prefer to arrange in parallel orientation. The RMSD plot show that the system had large fluctuations at starting of simulation which got stable when it forms contacts in parallel assembly and RMSD value decreased to 0.6 nm (Fig. 2.4D). The distances were calculated between the α-carbons of Val1 and Val17 and between Tyr5 and Val20 (Fig. 2.4E). The distance between Val1 and Val17 was higher initially (~2 nm) which reduced to 0.6 nm when these two strands came in contact. The distance between Tyr5 and Lys22 was 1 nm initially and during the simulation it reduced to 0.4 nm. These simulation data indicate that Ac-PHF6 prefers to be in parallel β-sheet assembly.

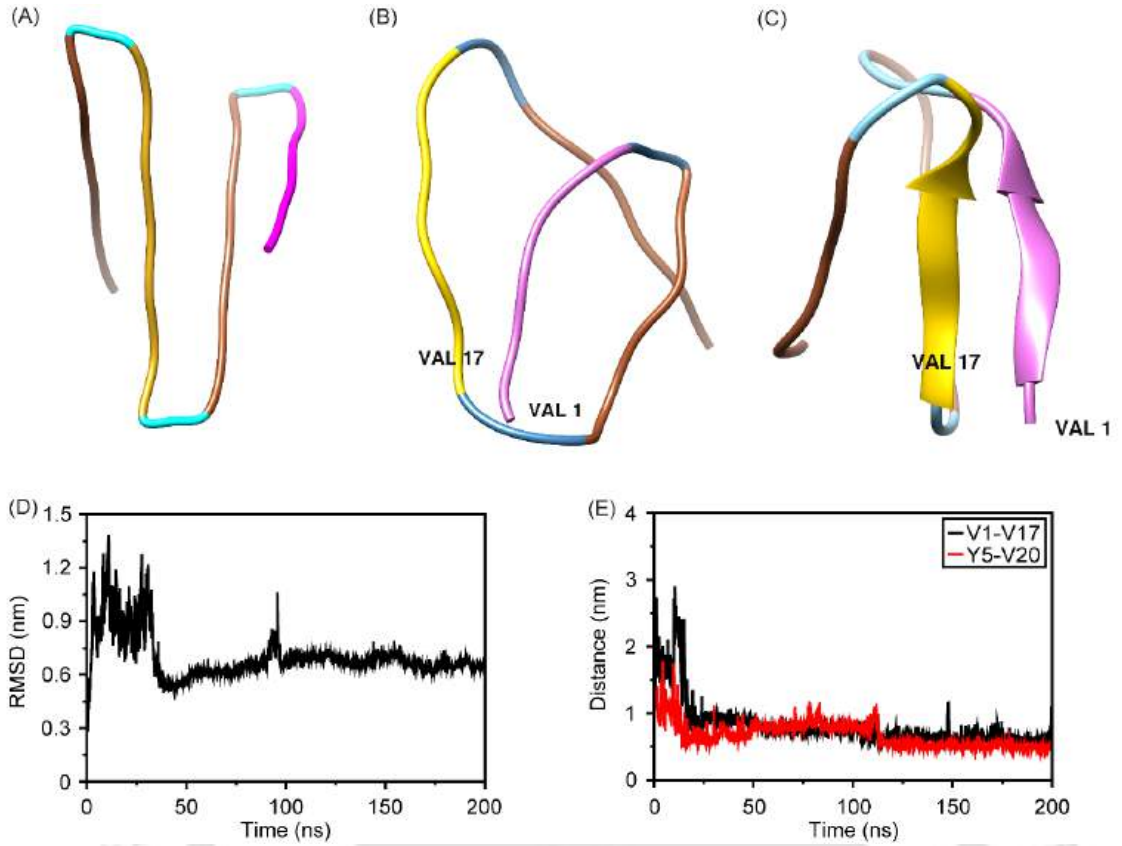

Figure 2.4. MD simulation of Ac-PHF6 with GG mediated turn. (A) Initial structure of peptide, (B) middle structure of the largest cluster, (C) middle structure of the second largest cluster, (D) RMSD plot, and (E) distance between V1Cα and V17Cα (black traces) and between Y5Cα and V20Cα (red traces).

2.3.4. Fluorescence resonance energy transfer

Computational data for parallel β-sheets assembly of Ac-PHF6 was reported by Eisenberg and coworkers and the simulations ran by me also indicate that it prefers parallel β-sheet formation [160]. To investigate it through experimental data, I carried out FRET and TCSPC. First approach was to convert Tyr into tyrosinate at pH > 10, which is a weakly fluorescent moiety with an emission maximum around 350 nm. This was carried out to make tyrosinate-dansyl pair for energy transfer. Unfortunately, in basic environment (0.1 M NaOH), the emission of tyrosinate at 350 nm was too weak to accurately determine the efficiency of energy transfer. No appreciable difference in fluorescence intensity was observed between Ac-PHF6 and Ac-K(dan)VQIVYK-am. Therefore, the energy transfer through TCSPC was carried out by investigating the lifetime decay of Ac-PHF6 and Ac-K(dan)VQIVYK-am (Fig. 2.5A). The decay observed for Ac-PHF6 was slower than the dansyl-labeled peptide, on the basis of which the distance between donor (Tyr) and acceptor (dansyl) was calculated. The lifetimes of donor

in the absence of acceptor (τ_0) and in the presence of acceptor (τ) were 2.116 and 0.945 ns, respectively. The relation between r (distance between donor and acceptor) and R_0 (Förster distance) is calculated as follows:

$$\text{The efficiency of energy transfer, } E = 1 - \frac{\tau}{\tau_0} = 1 - \frac{0.945}{2.116} = 0.553$$

$$E = \frac{R_0^6}{r^6 + R_0^6}$$

$$\left(\frac{r}{R_0}\right)^6 = \frac{1}{E} - 1 = \frac{1}{0.553} - 1 = 0.81$$

$$r = 0.96R_0$$

I could not find the R_0 for Tyr-dansyl pair in the literature. The R_0, however, is reported for the Trp-dansyl pair, which is 21 Å. Assuming that Tyr-dansyl pair also has the same Förster distance, the distance between Tyr and dansyl in the peptide would turn out to be around 20 Å. However, it is important to note that the Förster distance depends on the quantum yield of the donor and the spectral overlap between donor's emission and acceptors absorption maxima. In neutral aqueous solutions, there is not much difference in the quantum yields of Trp and Tyr. Therefore, the Förster distance is largely determined by the spectral overlap. The molar absorption coefficient of dansyl at 303 nm is about two-third of that at 350 nm, the wavelength at which Trp-dansyl Förster distance is reported in the literature. Therefore, it is safe to assume that the Trp-dansyl R_0 used for distance calculation can only be an overestimation. This implies that the distance between Tyr and dansyl in the self-assembled Ac-K(dan)VQIVYK-am is ≤ 20 Å. In proteins, the distance between the α-carbons of adjacent residues is ~3.5 Å. Considering a distance between two strands in amyloid-like structure to be ~4.7 Å, the theoretical distance between the Tyr residue and dansyl moiety in parallel in-register structure of Ac-K(dan)VQIVYK-am would be ~17-18 Å. This data, though not very conclusively, suggests that Ac-PHF6 self-assembles through parallel β-sheet formation.

2.3.5. ThT fluorescence

ThT fluorescence spectra were recorded to investigate the nature of self-assembled structures. ThT is a benzothiazole dye that displays enhanced fluorescence emission intensity when bound to cross-β sheet-rich fibrillar structures, the structure that forms the core of amyloid fibrils [195]. As ThT fluorescence emission quantum yield is sensitive to pH, the spectrum for the water sample was recorded in low ionic strength buffer (10 mM phosphate buffer, pH 7.4)

instead of water. The PBS sample causes a large enhancement in ThT fluorescence intensity, whereas no significant enhancement is observed for the water sample (Fig. 2.5B).

2.3.6. Intrinsic tyrosine fluorescence

As very high concentration brings in the inner-filter effect, intrinsic tyrosine fluorescence spectra for 20 mM samples were recorded by diluting them to 100 µM concentration in the respective dispersant. Excitation at 280 nm resulted in emission spectra with λ_{max} around 303 nm for both samples (Fig. 2.5C). The PBS sample, however, displays a much lower quantum yield than the water sample. The lower quantum yield could be multifactorial. These factors include absorption flattening due to self-assembly-induced local increase in chromophore (Tyr) concentration, the self-quenching of the stacked tyrosine side chains, and quenching by 150 mM chloride ions present in PBS.

Tyrosine fluorescence quenching data are presented as Stern-Volmer plots (Fig. 2.6A-D). The data for both water and PBS samples could be fit linearly. The Stern-Volmer constants (K_{SV}) observed for water samples at 100 and 200 µM peptide concentrations were 15.6 ± 3.1 M^{-1} (Fig. 6A) and 15.11 ± 2.77 M^{-1} (Fig. 2.6B), respectively. The K_{SV} values obtained for PBS samples, on the other hand, were lower. The 100 and 200 µM PBS samples displayed K_{SV} values of 11.4 ± 2.96 M^{-1} (Fig. 2.6C) and 10.6 ± 2.44 M^{-1} (Fig. 2.6D), respectively. The lower K_{SV} values observed for PBS samples suggest that the peptide self-assembly in PBS shields the tyrosine residues from the aqueous quencher.

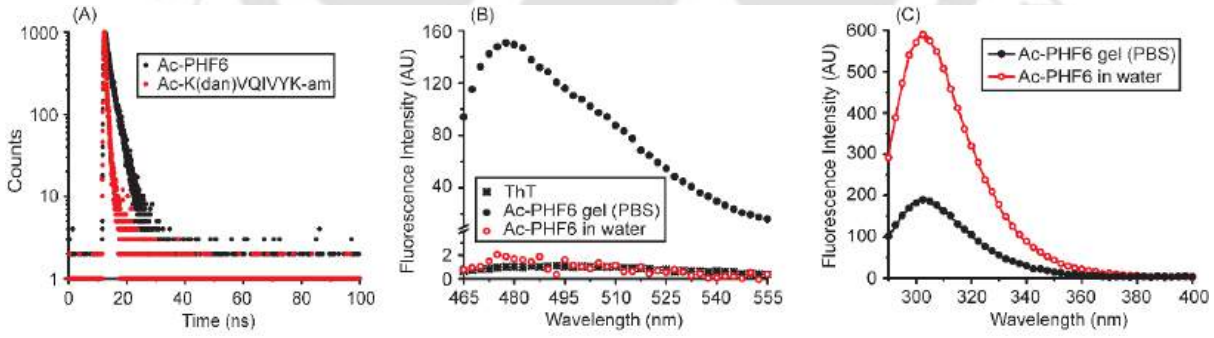

Figure 2.5. Fluorescence spectroscopy. TCSPC spectra of Ac-PHF6 and Ac-K(dan)VQIVYK-am (A). ThT fluorescence spectra of Ac-PHF6 samples in water and PBS (B). Intrinsic tyrosine fluorescence emission spectra (C).

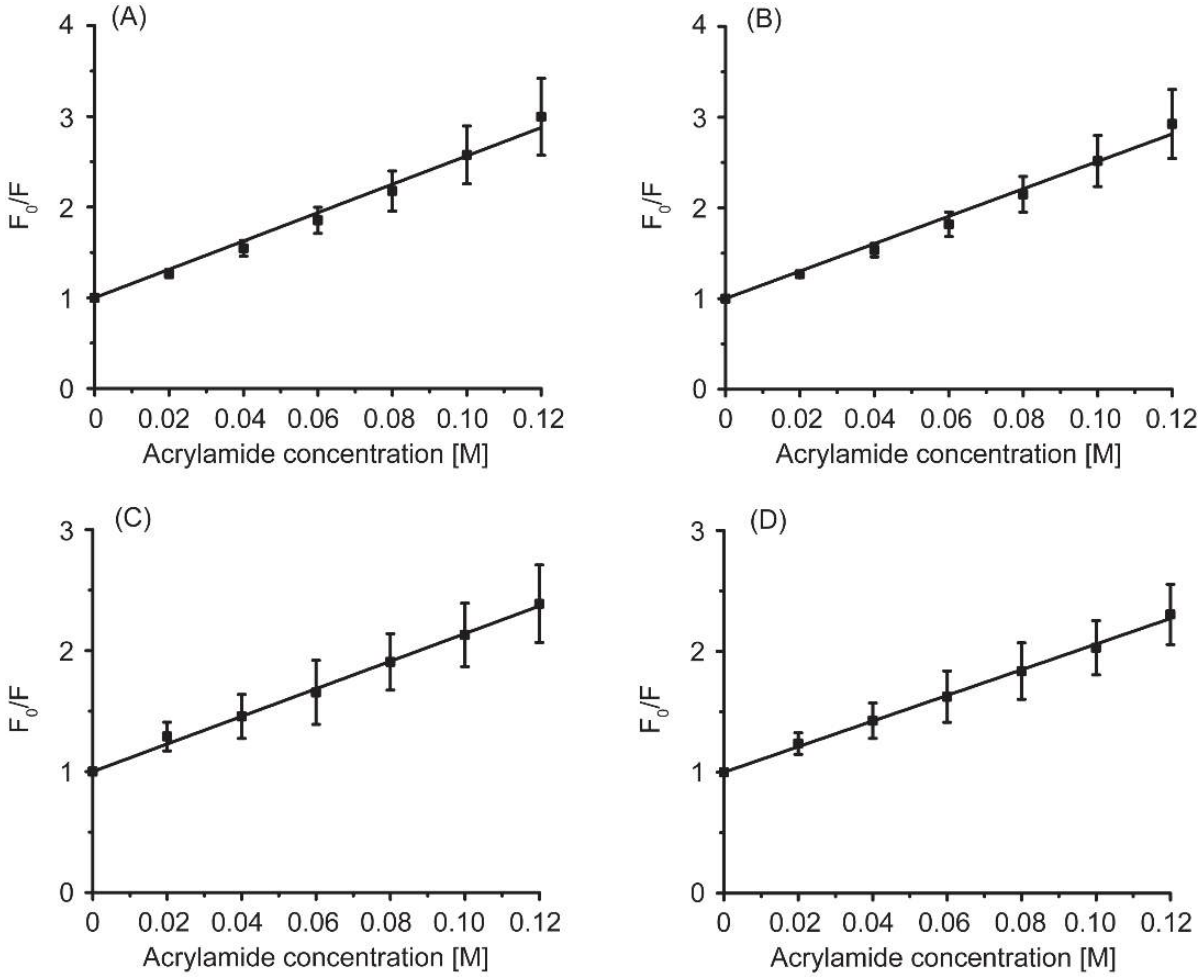

Figure 2.6. Stern-Volmer plots for Ac-PHF6 in water at 100 µM (A) and 200 µM (B) peptide concentrations, and Stern-Volmer plots for Ac-PHF6 in PBS at 100 µM (C) and 200 µM (D) peptide concentrations.

2.3.7. Transmission electron microscopy

TEM images reveal long fibrillar structures for both PBS (Figure 2.7A) and water (Figure 2.7B) samples. The morphology of the fibers, however, looks very different. While the PBS sample shows fibrils that are very typical of amyloid fibrils, those observed for the water sample are more like tapes. As the Ac-PHF6 water sample displayed largely unordered conformation in solution (Fig. 2.2A) and no appreciable enhancement in ThT fluorescence intensity when diluted to 100 µM concentration (Fig. 2.5A), The tape-like structures observed in TEM apparently formed during the drying process.

2.3.8. Hydrogel stability

The stability of Ac-PHF6 hydrogel was assessed by monitoring the release of peptide from the hydrogel into the bulk solution. The 100 µl hydrogel was submerged in 1.4 ml PBS, and the

peptide release was estimated by measuring peptide concentration in PBS as a function of time. Less than 5% peptide accumulated in PBS after 2 weeks of incubation, suggesting good hydrogel stability (Fig. 2.7C).

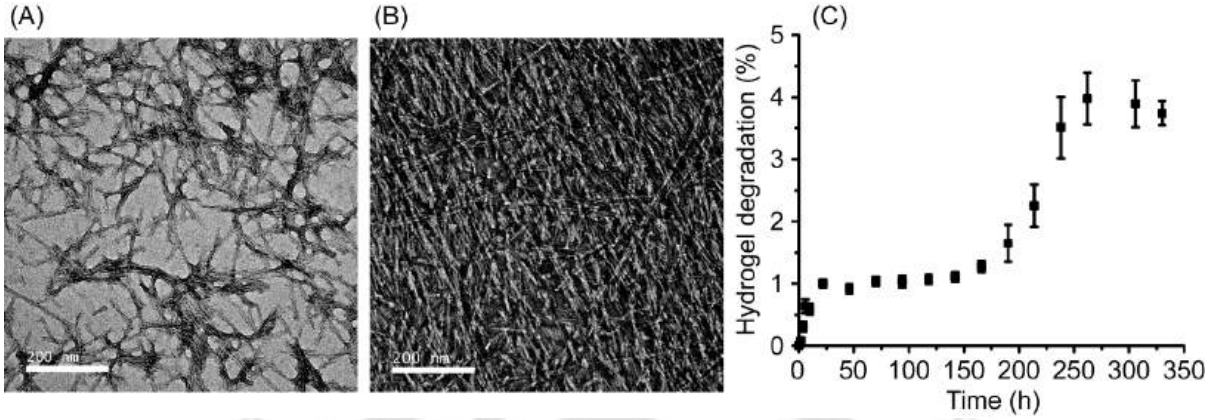

Figure 2.7. Transmission electron microscopy and hydrogel degradation. TEM images for Ac-PHF6 samples in PBS (A) and water (B). Scale bars represent 200 nm. The hydrogel degradation (peptide release from hydrogel) over time (C).

2.3.9. Drug/dye release and cell culture

Small molecule entrapment, followed by subsequent release, was examined using fluorescent dye calcein and anticancer drug doxorubicin. The gels were prepared in the fluorescence cuvette, and these molecules were entrapped during the gelation process. PBS was carefully added on top of the gel, and fluorescence emission intensity was measured as a function of time (Fig. 2.8A and 2.8B). Steady release of the molecules is observed for about 12 hours, beyond which no further enhancement in fluorescence emission intensity was observed. The effect of drug entrapment on the morphology of fibrils underlying hydrogels was investigated. The 24-h-old hydrogel containing 23 µM doxorubicin was investigated by TEM (Fig. 2.8C). No noticeable change in fibril morphology is observed, suggesting that drug entrapment does not adversely affect the Ac-PHF6 fibrils. The doxorubicin loading capacity was determined by layering an equal volume of concentrated (10 mM) doxorubicin solution on top of 20 mM hydrogel and estimating the doxorubicin uptake after 18 h. The doxorubicin concentration in the hydrogel was estimated to be 292.8 ± 19.4 µM. This corresponds to 169.8 ± 11.2 µg doxorubicin/ml hydrogel.

HEK-293 cells were used for cell culture assays. Ac-PHF6 gel prepared in PBS was equilibrated with DMEM and seeded with about 10,000 cells, which were allowed to grow for 48 hours. The cells were stained with calcein acetoxymethyl ester (Calcein-AM). Calcein AM

is a hydrophobic, non-fluorescent compound that readily crosses the cell membrane. Following cellular uptake, it is hydrolyzed by cellular esterases to give fluorescent calcein. Therefore, calcein fluorescence is directly related to the activity of cellular esterases, which in turn is linked to cell viability. HEK-293 cells were found to grow inside the gel (Fig. 2.8D). Besides, the expression of the housekeeping gene GAPDH was analyzed. The cells grown without Ac-PHF6 (positive control), in 10 mM hydrogel, and in 15 mM hydrogel were harvested. The RNA was isolated and amplified into DNA through reverse-transcriptase PCR. The cells grown in the gel were found to express GAPDH (Fig. 2.8E).

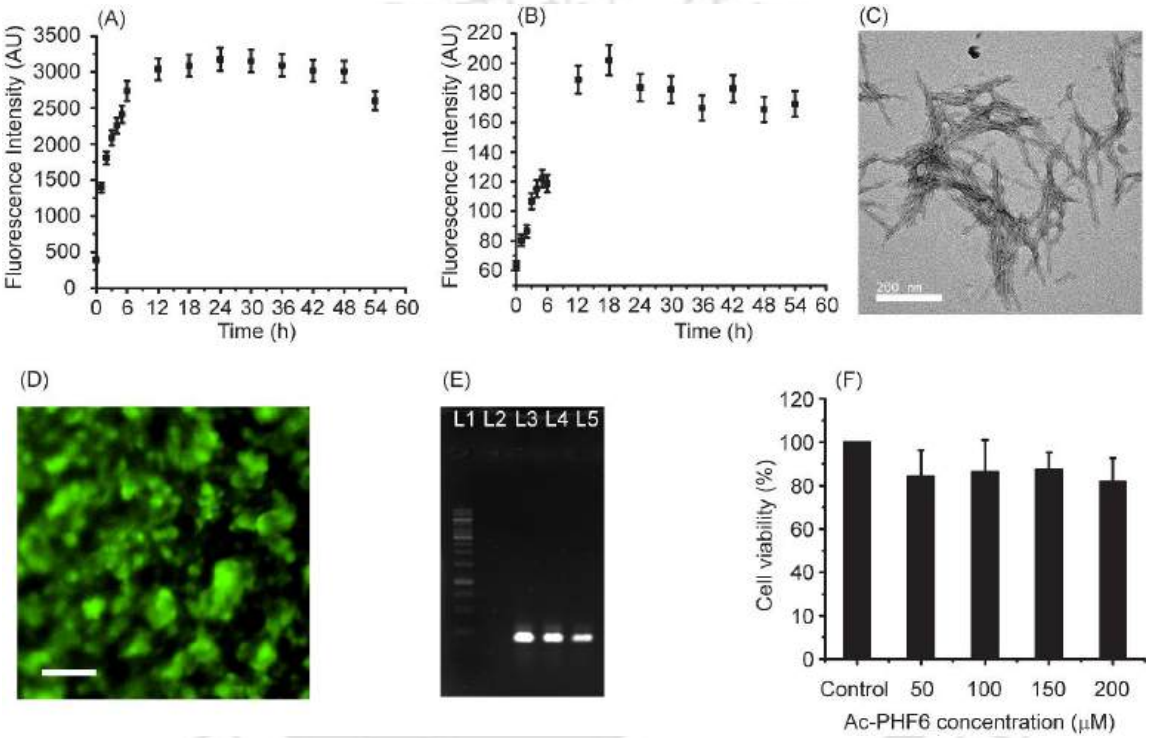

Figure 2.8. Biomedical applications. Release of calcein dye (A) and anticancer drug doxorubicin (B) from PBS hydrogels, (C) morphology of the doxorubicin-harboring hydrogel (scale bar = 200 nm), (D) calcein fluorescence image of HEK-293 cells growing in the hydrogel. The scale bar represents 50 μm (E) Agarose gel electrophoresis showing GAPDH expression. L1 is the marker lane, L2 is negative control, L3 is positive control (HEK-293 cells growing in DMEM, without peptide gel), and L4 and L5 represent the cells growing in 10 mM and 15 mM gels, respectively. (F) HEK-293 cell viability, as assessed using MTT assay.

The biocompatibility of Ac-PHF6 was further assessed through cell viability assay. The metabolically active cells reduce MTT into formazan that absorbs 570 nm light. Dead cells, on the other hand, cannot reduce the MTT, failing to contribute to the signal. The percentage cell viability was calculated with respect to the peptide-untreated cells (Fig. 2.8F). No significant

decrease in cell viability was observed at the peptide concentrations tested, suggesting that the peptide is non-toxic up to at least 200 µM concentration.

2.3.10. Injectability

All the assays discussed above were carried out with gel samples that were 24 h old. An injectable hydrogelator should cause instant gelation of a biological fluid. To assess injectability, a 20 mM peptide stock solution was prepared in water that contained 0.4 mM rhodamine B. The colored solution thus obtained was slowly injected into the PBS while slowly withdrawing the pipette tip. The peptide displayed gelation as soon as it came in contact with the PBS. Withdrawal of the pipette tip from the PBS resulted in a long gel thread. The photographs of the gel thread-containing glass cuvette, taken at different time points, reveal the gradual release of rhodamine B from the gel thread. The release of dye was more or less complete in 2 hours (Fig. 2.9). It is likely that the surface of the string gels quickly, and the internal region gels somewhat slower. When it comes to injectability, the concentration of phosphate plays an important role in pain sensation at the injection site [196]. The recommended phosphate concentration is ≤ 10 mM. The PBS that I used in this study contained 11.8 mM phosphate, a little higher than the recommended concentration. Therefore, I investigated whether phosphate is essential for Ac-PHF6 self-assembly and hydrogelation. I found that 150 mM NaCl was sufficient to cause gelation, confirming that the gelation is a salt-induced effect and phosphate is dispensable.

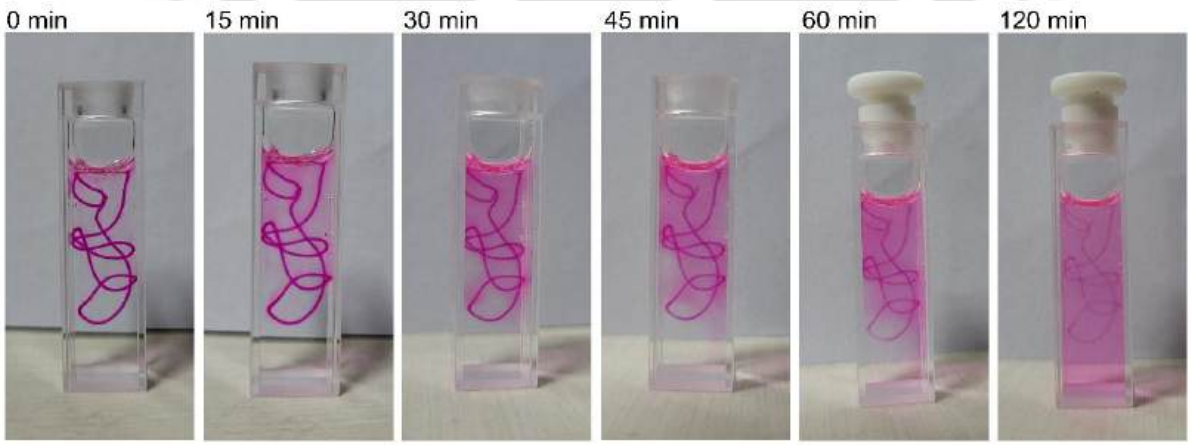

Figure 2.9. The photographs of the glass cuvette containing the gel thread suspended in PBS. The gel thread contains rhodamine B that gradually releases to PBS.

2.4. Conclusion

Amyloidogenic peptides and the short peptide stretches derived from them have a negative connotation attached to them. It is often argued that the peptides derived from amyloidogenic proteins/peptides could possess cytotoxicity. Research in the past few decades has established that the cytotoxicity of amyloids is primarily associated with prefibrillar oligomers, with mature fibrils being the inert species [197]–[202]. The kinetics of self-assembly, therefore, is associated with cytotoxicity. Slow aggregation kinetics implies a longer life span of prefibrillar species that could lead to cytotoxicity [203]. Therefore, the peptides that display rapid self-assembly, preferably without any lag phase, display little or no cytotoxicity. This theory is further supported by many functional amyloids discovered in very diverse organisms, including humans, that show rapid aggregation kinetics [114], [204]. Amyloid fibrils are no longer considered a pathogenic fold. Pituitary peptide hormones are stored in the form of amyloid fibrils [205]. Maji and coworkers have designed peptide hydrogelators based on the amyloidogenic stretches from β-amyloid and α-synuclein. The hydrogels thus obtained could be used for stem cell differentiation [187], [188]. Besides, a vast majority of peptide hydrogelators reported in the literature self-assemble through β-sheet formation [55], [206]. The underlying architecture of these self-assembled structures is a cross-β-sheet, the so-called amyloid fold [207]. Therefore, the concerns about the cytotoxicity of amyloid-derived peptide hydrogelators may be unnecessary, especially when the peptides display rapid self-assembly kinetics. Ac-PHF6 displays rapid self-assembly, wherein mere contact with PBS causes gelation. The simple selection criteria that led me to identify Ac-PHF6 as a potential hydrogelator could be used to identify more such peptides. To conclude, Ac-PHF6 is a promising injectable hydrogelator that forms a viscous solution in water but causes instant gelation of phosphate-buffered saline and cell culture media.

CHAPTER 3

Investigations into the self-assembly and hydrogelation of Ac-PHF6 analogs with electron-deficient aromatic rings

3.1. Introduction

As many functional amyloids have been identified in the past few decades, amyloid fibrils are no longer considered pathogenic fibrils [103], [117], [123], [208]. Amyloidogenic peptides, therefore, have gathered significant attention as biocompatible materials. Compared to a much better understanding of peptide self-assembly in the past two decades, the understanding of peptide hydrogelation remains primitive. Hydrogelating peptides are often discovered serendipitously or through empirical screening rather than rational design. A deeper understanding of the molecular interactions governing self-assembly, such as hydrogen bonding, dipole-dipole forces, hydrophobic effects, and π–π stacking, should enable the prediction of hydrogelating peptides as well as their emergent properties [155], [209], [210]. Aromatic amino acids are crucial in peptide self-assembly, facilitating assembly through π-stacking interactions [211]–[215]. The occurrence of phenylalanine and tyrosine is far more than that of tryptophan in self-assembling peptides [25]. Reches and Gazit reported nanotubes formed by the peptide diphenylalanine [216]. They subsequently investigated the aromatic homodipeptides wherein halogen groups were attached to the phenyl ring [213]. Halogen modification had deterministic effects on the assembly of dipeptides and the emergent superstructures. Fmoc-Phe-OH, Fmoc-Tyr-OH, and Fmoc-Phe-Phe-OH have been reported in the literature to form hydrogels [55], [63], [73], [217]. The self-assembly has been attributed to π–π interactions between the aromatic side chains and the Fmoc moiety.

A subtle perturbation of the aromatic ring's electronic properties, therefore, can dramatically affect self-assembly and hydrogelation. Nilsson and coworkers investigated the self-assembly and hydrogelation of phenyl-ring substituted Fmoc-Phe-OH. Such modifications alter the molecule's hydrophobicity and electronic properties, thereby influencing π–π interactions and self-assembly [56], [67], [218]. Fmoc-Tyr-OH is a better gelator than Fmoc-Phe. The hydroxyl group is an inductively electron-withdrawing group but an electron-donating group through resonance. The resonance effect usually outweighs the inductive effect of the hydroxyl group. Considering this, the phenolic ring in Fmoc-Tyr-OH is expected to be more electron-rich compared to the phenyl group. In contrast, the inductive effect is stronger than the resonance effect for halogens. Interestingly, Fmoc-F_5-Phe (Fmoc-protected pentafluorophenylalanine), an amino acid with depleted electron density in the pentafluorophenyl ring, forms better hydrogel than Fmoc-Tyr [67]. These results indicate that substitutions in the aromatic side chain can dramatically affect self-assembly and hydrogelation. It is important to note that the ring

substitutions also contribute to the size of the aromatic side chain and its hydrophobicity. To understand if the aromatic residues confer aggregation propensity due to their hydrophobicity and β-sheet propensity, the ring electronic effects, or ring geometry, Desamero and coworkers carried out a detailed investigation on $hIAPP_{22-29}$ (NFGAILSS) [219]. They made many analogs by substituting the Phe23 ring with several electron-withdrawing and electron-donating groups. They found that the peptide analogs with electron-donating groups on the phenyl ring displayed poor aggregation, while those with electron-withdrawing groups displayed better self-assembly. Their results establish that aromatic electronic effects influence peptide self-assembly, with electron-withdrawing substituents promoting it.

As described in Chapter 2, Ac-PHF6 forms a viscous solution in water but causes instant gelation of phosphate-buffered saline and the cell culture media. In this chapter, I investigated the self-assembly and hydrogelation of Ac-PHF6 analogs wherein the electronic properties of the sole aromatic residue in Ac-PHF6 are altered. As uncapped VQIVYK is reported in the literature to self-assemble through parallel β-sheet formation where tyrosine residues are involved in aromatic stacking interactions [160], I investigated the peptide analogs wherein Tyr was substituted with Phe and the phenyl moiety was then substituted with various electron-withdrawing groups at the *para* position (Table 3.1). All peptides caused PBS gelation with comparable rheological properties. The structures underlying the hydrogels were β-sheet fibrils. The electron-deficient aromatic moieties improved self-assembly and hydrogelation. Ac-PHF6 and no other aromatic analog except the one having *p*-(trifluoromethyl)phenylalanine caused the gelation of deionized water. Water gelation caused by *p*-(trifluoromethyl)phenylalanine-containing analog is likely hydrophobicity-driven.

3.2. Materials and Methods

3.2.1. Materials

Fmoc-protected non-natural amino acids were purchased from GL Biochem (Shanghai) Ltd. Rink amide resin, Fmoc-protected natural amino acids, HBTU, HOBt, DIPEA, TFA, acetic anhydride, TIPS, and ThT were same as mentioned in section 2.2.1.

3.2.2. Electrostatic charge density mapping

The structure of toluene was downloaded from PubChem, and aromatic moieties were prepared by substituting the *para* hydrogen atom of toluene using Avogadro 1.2 software [220]. Electrostatic charge density maps of toluene and its substituents were generated by creating the

surface in Avogadro. The extended peptide structures (pdb files) were prepared using UCSF Chimera. The electrostatic charge density maps of the peptides in extended conformation were generated using the APBS (Adaptive Poisson-Boltzmann Solver) program in PyMOL.

3.2.3. Peptide synthesis and characterization

The peptides (listed in Table 3.1) were assembled on Rink amide resin by employing Fmoc chemistry with HBTU/HOBt /DIPEA activation. On-resin N-terminal acetylation, peptide cleavage, and precipitation in diethyl ether were carried out exactly as specified in section 2.2.2. Following multiple rounds of washing with diethyl ether, the peptides were air-dried. The peptides were purified using reversed-phase HPLC on a C18 column, employing a linear gradient of acetonitrile with 0.1% TFA. Peptide identities were ascertained using MALDI-TOF mass spectrometry.

Table 3.1. The sequences of peptides employed in this study.

Peptide sequence	Remarks
Ac-VQIVYK-am	Ac-PHF6 (tau$^{306-311}$)
Ac-VQIVFK-am	Tyr → Phe analog
Ac-VQIVF(fl)K-am	Tyr → *p*-fluorophenylalanine analog
Ac-VQIVF(CN)K-am	Tyr → *p*-cyanophenylalanine analog
Ac-VQIVF(NO_2)K-am	Tyr → *p*-nitrophenylalanine analog
Ac-VQIVF(CF_3)K-am	Tyr → *p*-(trifluoromethyl)phenylalanine analog

3.2.4. Peptide dissolution, hydrogelation and rheology

Peptide stock solutions were prepared in water by weighing the peptides, adding water, and vortexing for a few minutes. All peptides, except Ac-VQIVF(CF_3)K-am, dissolved in water to very high concentrations (>20 mM). Ac-VQIVF(CF_3)K-am was heated for about an hour at 70 °C to achieve a dissolution >20 mM. All the peptides remained as viscous solutions in water up to about 25 mM concentration, except Ac-VQIVF(CF_3)K-am, which gels upon cooling to room temperature. Gelation of PBS was attempted by diluting the peptide solutions to achieve 20 mM peptide concentration. As Ac-VQIVF(CF_3)K-am gels upon cooling down to room temperature, it was diluted in PBS instantly after being taken out from 70 °C. All the peptides caused instant gelation of PBS. Rheology of Ac-PHF6 gel reported in Chapter 2 was carried out for a 24-hour-old gel. Therefore, I carried out the oscillatory rheology on the 20 mM peptide

gels that were aged for 24-hours. Rheology measurements were carried out on an Anton Paar Rheometer MCR 102 using 25 cm parallel plates at a 0.5 mm gap. The amplitude sweep tests were carried out at an angular frequency of 10 rad/s by varying shear strain from 0.01% to 10%. All the gels showed a linear regime up to at least 0.1% strain. Frequency sweep data, therefore, were recorded at 0.1% strain from 0.01-100 rad/s of angular frequency.

3.2.5. Thioflavin T (ThT) fluorescence spectroscopy

ThT fluorescence emission spectra were recorded in PBS for the PBS gels. As ThT fluorescence quantum yield strongly depends on pH, the fluorescence emission spectra for water samples were recorded in 10 mM phosphate buffer, pH 7.4, instead of water. The assay was carried out at 200 μM peptide and 10 μM ThT concentrations. The samples were excited at 450 nm, and emission spectra were recorded. The excitation and emission bandwidths were 2.5 and 5 nm, respectively.

3.2.6. Circular dichroism (CD) spectroscopy

Far-UV electronic CD spectra were recorded on a Jasco J-1500 spectropolarimeter. The 24-hour-old samples (20 mM peptide concentration) were diluted in respective dispersant (water or PBS) to 200 μM concentration, and spectra were recorded in a 1 mm path-length quartz cell. The spectra were recorded from 250-195 nm at 1 nm bandwidth with a scanning speed of 100 nm/min. Each spectrum is the average of 8 accumulations. The spectra were corrected by subtracting the respective dispersant spectrum. The data was converted to mean residue ellipticity using the formula specified in equation 2.1.

3.2.7. Fourier transform infrared (FTIR) spectroscopy

The FTIR spectra were recorded exactly as specified in section 2.2.8.

3.2.8. Molecular dynamics simulations

Molecular dynamics (MD) simulations were carried out for the steric zipper structures prepared for the peptides. The steric zipper structure of uncapped PHF6 peptide (VQIVYK.pdb) was obtained from the WALTZ-DB database *(http://waltzdb.switchlab.org/)* [221]. N-terminal acetylation was done in BIOVIA Discovery Studio. The aromatic analogs were generated by substituting the Tyr residue with Phe and ring-substituted-Phe using the SwissSidechain plugin in UCSF-Chimera. MD simulations were carried out using the CHARMM36 force field. The peptide amidation was done by choosing CT2 as the terminal patch when prompted by pdb2gmx command. The steric zippers were placed in a cubic box with a minimum distance

of 1 nm from the box edge, solvated with water (TIP3P), and neutralized with chloride ions. NaCl (150 mM) was added to each system. The systems underwent energy minimization, followed by equilibration under NVT (100 ps) and NPT (200 ps) at 300 K temperature and 1 bar pressure. Subsequently, the production MD simulations were carried out for 200 ns. Trajectory analyses were performed using VMD and UCSF-Chimera. Cluster analysis was done using the *gromos* algorithm with a 0.2 nm cutoff.

3.2.9. Transmission electron microscopy (TEM)

TEM samples were prepared as mentioned in section 2.2.9.

3.3. Results and discussion

Desamero and coworkers investigated $hIAPP_{22-29}$ (NFGAILSS) analogs wherein the phenyl ring was substituted with electron-donating and electron-withdrawing groups [219]. The peptide analogs with electron-deficient aromatic rings favored self-assembly, while those with electron-donating groups exhibited poor aggregation. Nilsson and coworkers found that incorporating a halogen in the phenyl group of Fmoc-Phe-OH promotes self-assembly and hydrogelation [56]. Fmoc-F_5-Phe, an analog with a highly-electron-deficient aromatic ring, displays faster self-assembly and hydrogelation compared to Fmoc-Tyr-OH [67]. These studies propound that electron-withdrawing moieties on aromatic side chains facilitate peptide self-assembly and hydrogelation. Ac-PHF6 contains a Tyr side chain and causes PBS hydrogelation. Here, I investigate the hydrogelation of Ac-PHF6 analogs, wherein Tyr310 is replaced with Phe and its ring-substituted derivatives (Table 3.1).

3.3.1. Electrostatic charge density map

An electrostatic charge density map provides valuable insights into molecular interactions. It helps in predicting electrostatic interactions that include ionic bonds, hydrogen bonds, and dipolar interactions. The charge density maps for the aromatic side chains incorporated in Ac-PHF6 analogs are shown in Fig. 3.1. Toluene was used as the model for the Phe side chain, and its substituents were used as models for other aromatic side chains employed in this study. *Para*-cresol, the model for Tyr side chain, shows the highest electron density in the ring (Fig. 1B). All other aromatic groups display lower electron density in the aromatic ring. The surface charge density maps of the peptides listed in Table 3.1 in extended conformation are shown in Fig. 3.2.

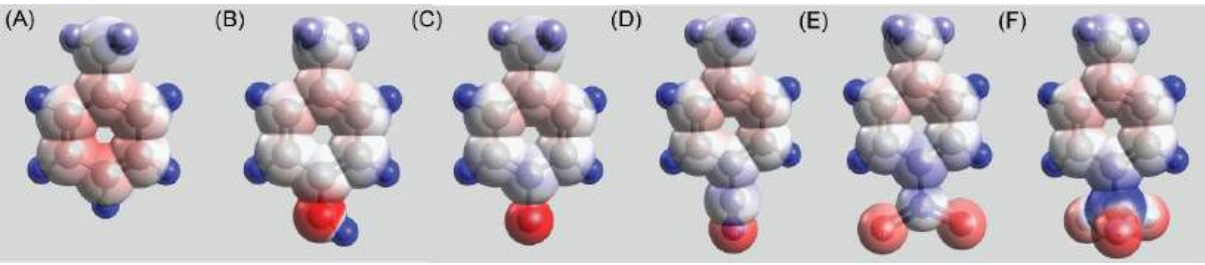

Figure 3.1. Electrostatic charge density maps of toluene (A), *p*-cresol (B), 4-fluorotoluene (C), 4-cyanotoluene (D), 4-nitrotoluene (E), and 4-(trifluoromethyl)toluene (F).

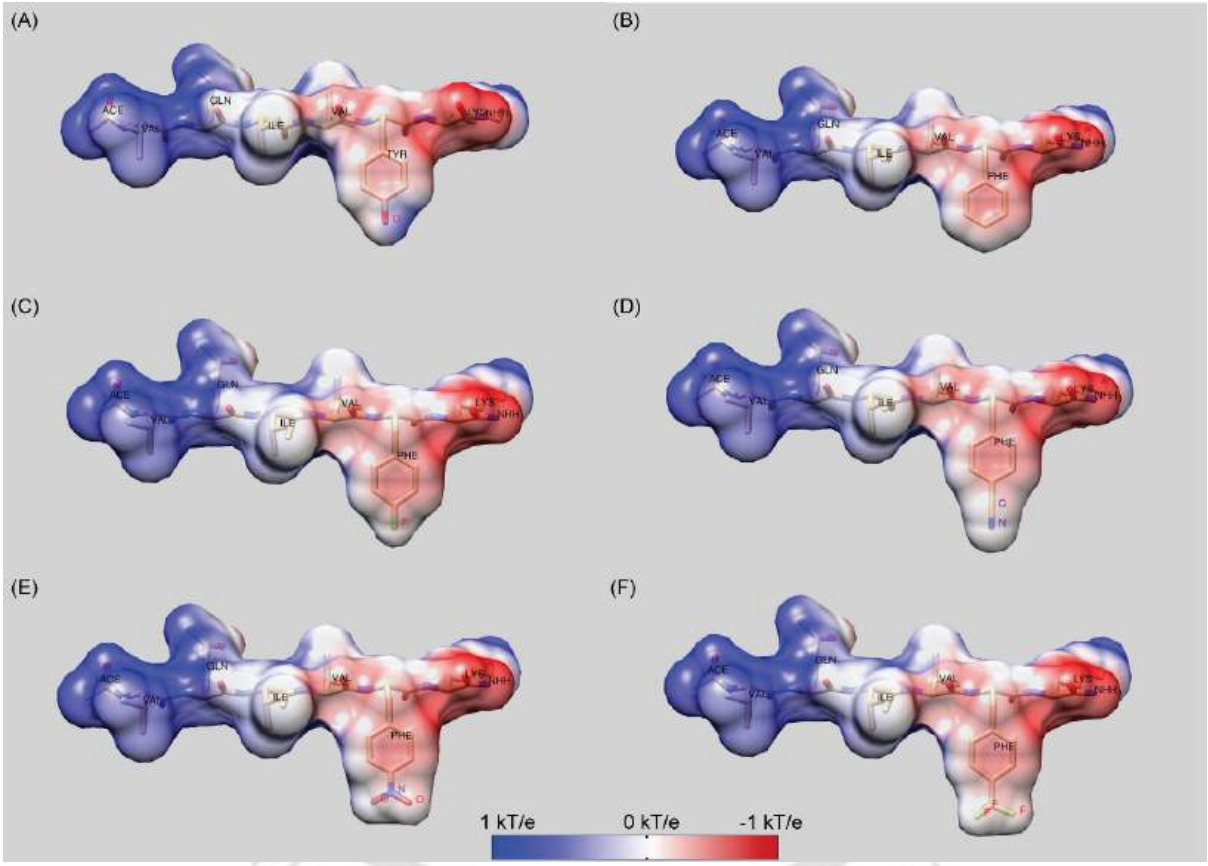

Figure 3.2. Electrostatic surface charge density maps of (A) Ac-PHF6, (B) Ac-VQIVFK-am, (C) Ac-VQIVF(fl)K-am, (D) Ac-VQIVF(CN)K-am, (E) Ac-VQIVF(NO_2)K-am, and (F) Ac-VQIVF(CF_3)K-am.

3.3.2. Hydrogelation

Peptide stock solutions were prepared in water. All peptides, except Ac-VQIVF(CF_3)K-am, readily dissolved in water to >20 mM concentration (Fig. 3.3A-E). Ac-VQIVF(CF_3)K-am displayed lower solubility and had to be heated at 70 °C for an hour to achieve dissolution. Cooling down to room-temperature resulted in hydrogelation (Fig. 3.3F). No other peptide caused water gelation. The uncapped PHF6 (VQIVYK) has been reported in the literature to self-assemble in the presence of high salt concentration *via* parallel in-register β-sheet

formation [160]. Capped peptide (Ac-PHF6) is also expected to assemble similarly. The salt masks the intermolecular electrostatic repulsion between terminal Lys residues in parallel β-sheet arrangement.

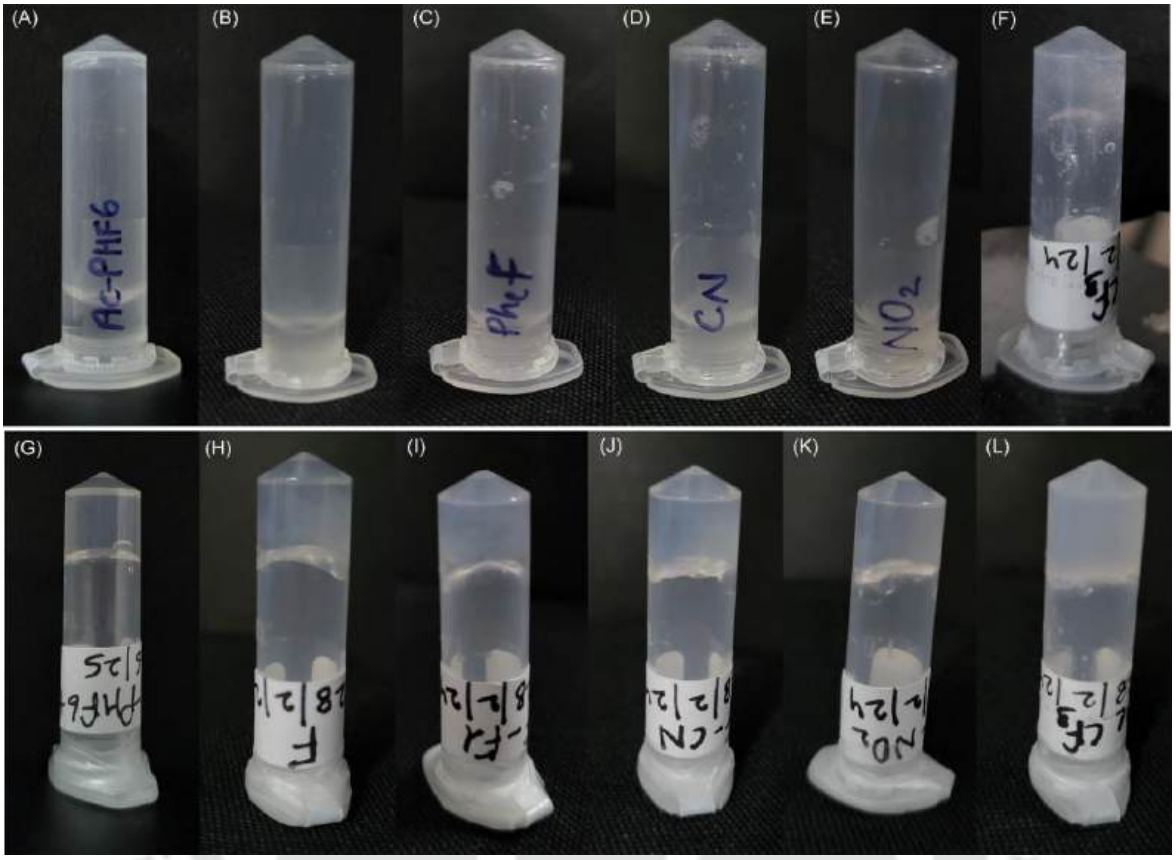

Figure 3.3. Inverted vials of Ac-PHF6 and its analogs showing 20 mM samples in water (top panels) and PBS (bottom panels). (A, G) Ac-PHF6, (B, H) Ac-VQIVFK-am, (C, I) Ac-VQIVF(fl)K-am, (D, J) Ac-VQIVF(CN)K-am, (E, K) Ac-VQIVF(NO_2)K-am, and (F, L) Ac-VQIVF(CF_3)K-am.

The self-assembly and gelation of Ac-VQIVF(CF_3)K-am in water is likely hydrophobicity-driven. Trifluoromethyl is a hydrophobic functional group. The high hydrophobicity of *p*-(trifluoromethyl)phenylalanine renders Ac-VQIVF(CF_3)K-am poorly soluble in water, facilitating its self-assembly through entropic contribution. PBS gelation was set up by diluting the peptide stock solutions in 10× PBS. As Ac-VQIVF(CF_3)K-am causes water gelation at room temperature, it was diluted immediately after taking out from 70 °C. All the peptides caused PBS gelation. The gels formed at 10 and 15 mM peptide concentrations were very fragile. Firm gels were obtained at 20 mM concentration (Fig. 3.3G-L). The gelation was instant, but the inverted tube images shown in Fig. 3.3 were taken for the 24-hour-old samples. As Ac-PHF6 hydrogel (20 mM peptide concentration) reported in chapter 2 was characterized

after 24 hours incubation, the assays with Ac-PHF6 analogs were also carried out with 20 mM gel samples incubated at room temperature for 24 hours.

3.3.3. Rheology

Rheology of a material is determined by its inner structure. As aromatic substitutions could modulate the peptide self-assembly, affecting the hydrogel's inner structure, the hydrogels' viscoelasticity was investigated using bulk rheology. The frequency sweep test was conducted at a strain of 0.1%, the strain that lies in the linear viscoelastic regime. The data is shown in Fig. 3.4. Interestingly, all the gels displayed a comparable storage modulus of about 1-2 × 10^4 Pa. There are small differences in the loss moduli, though. Instant PBS gelation caused by the peptides could lead to some non-uniformity within the gels. Such non-uniformity could contribute to minor differences observed in the loss moduli. The rheology data suggest that Tyr electronic properties do not contribute significantly to Ac-PHF6 hydrogelation. Unlike Fmoc-F_5-Phe-OH, which forms a much stronger hydrogel than Fmoc-Tyr-OH [67], I find that substitution of Tyr in Ac-PHF6 with Phe or its analogs with electron-withdrawing groups has no significant effect on rheology. The only apparent difference to Ac-PHF6 is that Ac-VQIVF(CF_3)K-am displays lower solubility in water due to the high hydrophobicity of the Phe(CF_3) group. The higher hydrophobicity caused the peptide to gel in deionized water as well.

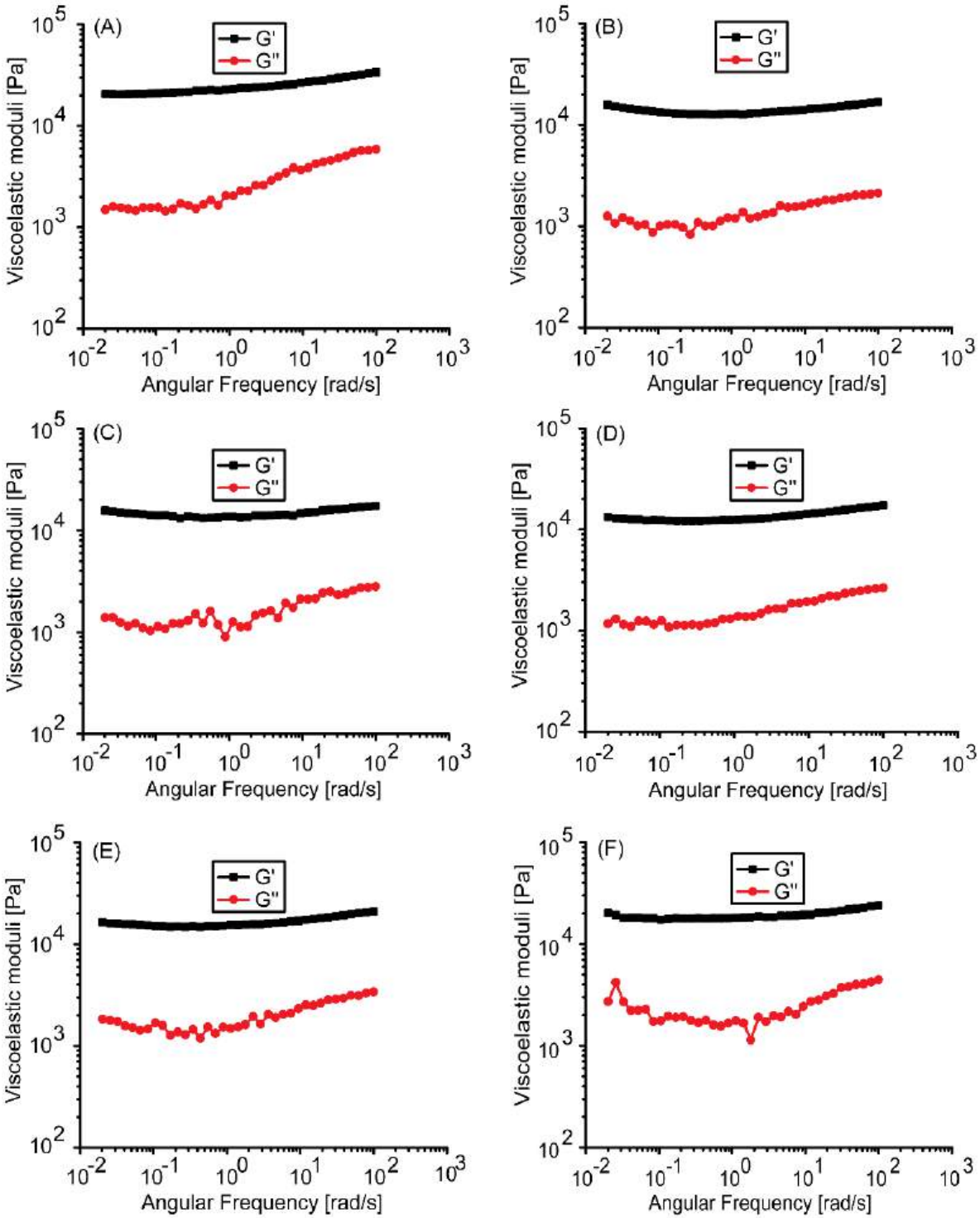

Figure 3.4. Rheology of PBS gels. Plot of G' and G" against angular frequency for 20 mM gels of (A) Ac-PHF6, (B) Ac-VQIVFK-am, (C) Ac-VQIVF(fl)K-am, (D) Ac-VQIVF(CN)K-am, (E) Ac-VQIVF(NO_2)K-am, and (F) Ac-VQIVF(CF_3)K-am.

3.3.4. CD spectroscopy

The secondary structure of Ac-PHF6 analogs was examined in PBS and water samples using far-UV CD spectroscopy. The samples were diluted to a concentration of 200 μM in the respective dispersant (water/PBS) for CD spectroscopy. The spectrum suggests a largely unordered conformation in water with a little contribution from β-sheets (Fig. 3.5A). On the other hand, the peptide displays a distinct β-sheet spectrum in PBS. Ac-VQIVFK-am displays a negative band around 200 nm in water, indicating a largely unordered conformation (Fig. 3.5B). The peptide displays a broad band centered around 215 nm in PBS, suggesting a β-sheet conformation. Ac-VQIVF(fl)K-am also takes up a largely unordered conformation in water, as indicated by the 200 nm negative band (Fig. 3.5C). The spectrum in PBS is characterized by a broad band around 225 nm and a weak positive band around 205 nm. The spectrum is very similar to that for Ac-PHF6 in PBS and is assigned to the β-sheet conformation. Ac-VQIVF(CN)K-am (Fig. 3.5D) and Ac-VQIVF(NO_2)K-am (Fig. 3.5E) display a negative band around 220 nm alongside the band around 200 nm in water. These data indicate that a fraction of the peptide takes up the β-sheet conformation, suggesting a tendency to self-assemble in water. In PBS, both the peptides display distinct β-sheet conformation. Ac-VQIVF(CF_3)K-am displays a very different spectrum in water (Fig. 3.5F). The spectrum is characterized by 200 and ~212 nm negative bands of comparable amplitudes. The spectrum suggests that the peptide takes up a mixture of β-sheet and random coil conformations. In PBS, a typical β-sheet CD spectrum is observed. The CD data show that the peptides with strong electron-withdrawing groups i.e., cyano, nitro, and trifluoromethyl groups, have β-sheet content in water, suggesting their tendency to self-assemble in water itself. Ac-VQIVFK-am and Ac-VQIVF(fl)K-am, i.e., the peptides without an electron-withdrawing group and with a weak electron-withdrawing group, respectively, show largely unordered conformation. The most dramatic effect of the electron-withdrawing group is observed for Ac-VQIVF(CF_3)K-am, which displays lower solubility in deionized water at room temperature and causes gelation upon cooling after being heated.

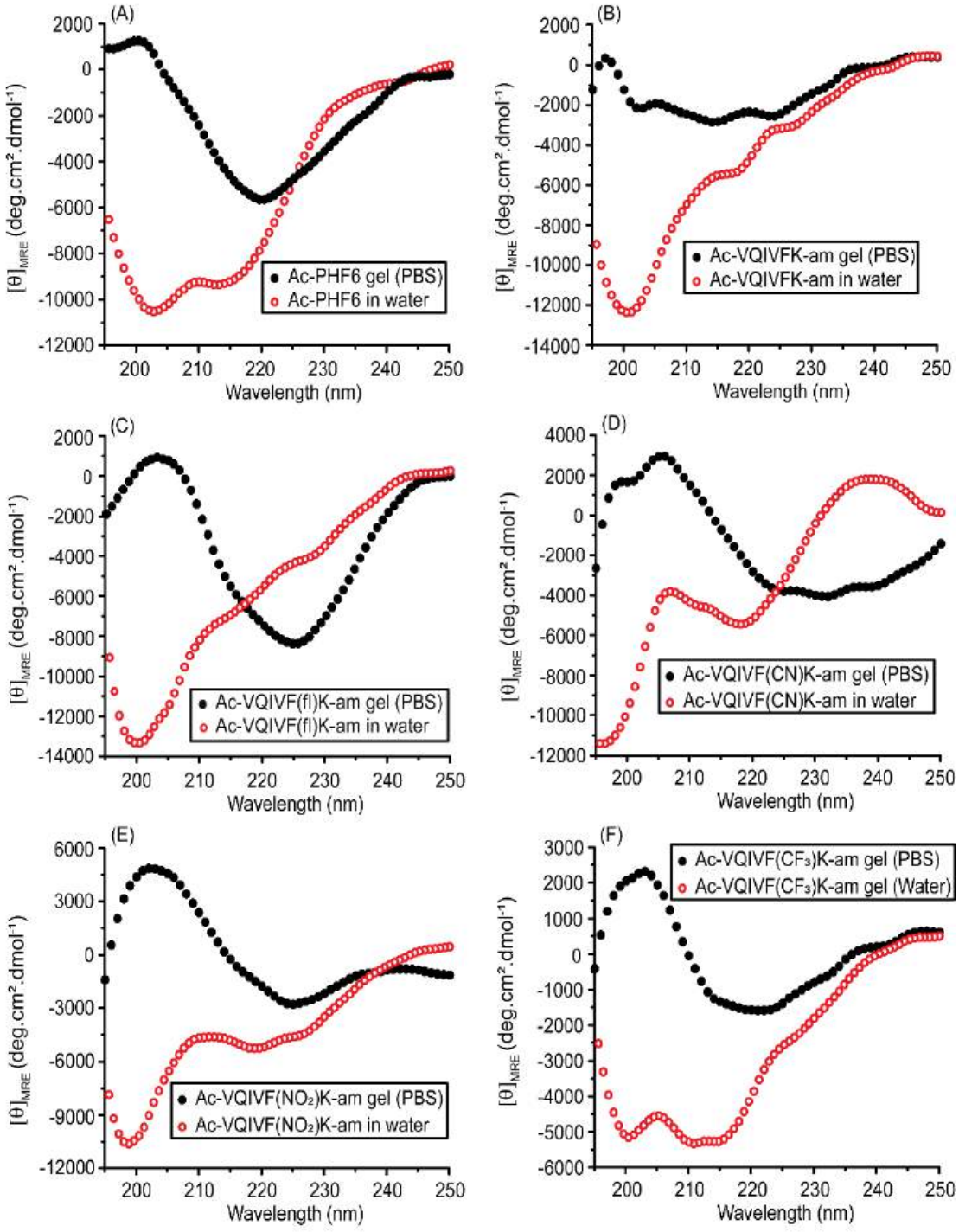

Figure 3.5. CD spectra of Ac-PHF6 analogs, (A) Ac-PHF6, (B) Ac-VQIVFK-am, (C) Ac-VQIVF(fl)K-am, (D) Ac-VQIVF(CN)K-am, (E) Ac-VQIVF(NO_2)K-am, and (F) Ac-VQIVF(CF_3)K-am.

3.3.5. FTIR spectroscopy

CD spectroscopy is an excellent method for investigating the α-helical conformations. However, the huge structural diversity of β-sheets makes CD spectroscopy somewhat less

reliable for accurately estimating the β-sheet conformation [222]. Regarding self-assembling peptides with aromatic residues, contributions from aromatic stacking interactions in far-UV CD spectra further hinder secondary structure prediction. FTIR spectroscopy is particularly suitable for investigating the β-sheets. The position of the amide I band is sensitive to the peptide backbone conformation. The ATR-FTIR spectra of Ac-PHF6 analogs are shown in Fig. 3.6. All the peptides display the amide I band centered between 1624 - 1626 cm^{-1} for both water and PBS samples. ATR-FTIR data unambiguously proves that the peptides take a β-sheet conformation in the hydrogels. Unlike CD spectroscopy, where Ac-VQIVFK-am and Ac-VQIVF(fl)K-am display random coil conformation for water samples, the FTIR spectra indicate β-sheet conformation. This is attributed to the drying of the peptides for ATR-FTIR spectroscopy. The peptide concentration increases during the drying processes, facilitating self-assembly. Such behavior was seen for Ac-PHF6 as well in Chapter 2.

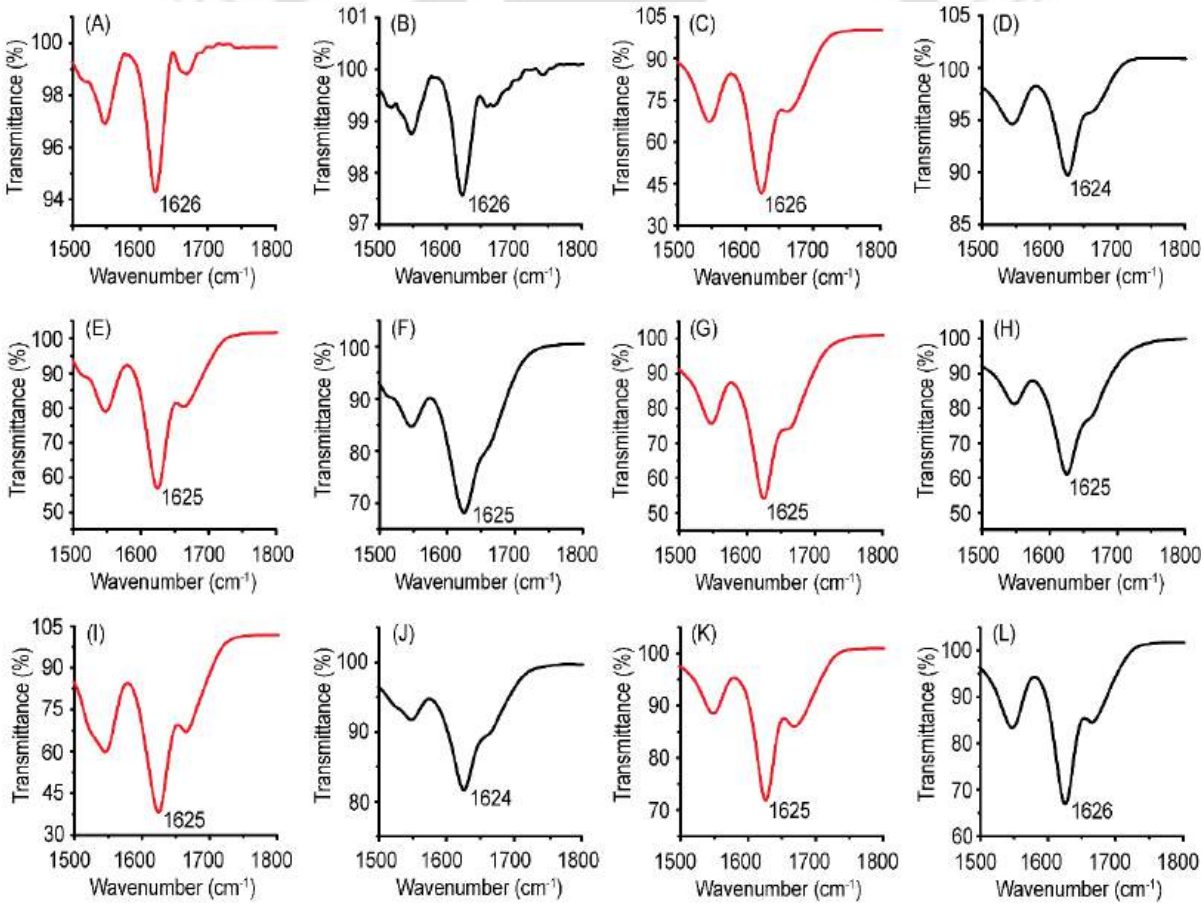

Figure 3.6. ATR-FTIR spectroscopy spectra of Ac-PHF6 and its analogs. The red traces are the spectra recorded for water samples, while the black traces are the spectra recorded for PBS samples. (A, B) Ac-PHF6, (C, D) Ac-VQIVFK-am, (E, F) Ac-VQIVF(fl)K-am, (G, H) Ac-VQIVF(CN)K-am, (I, J) Ac-VQIVF(NO_2)K-am, and (K, L) Ac-VQIVF(CF_3)K-am.

3.3.6. ThT fluorescence

The fluorescence of ThT, a benzothiazole dye that demonstrates a higher quantum yield when bound to amyloid fibrils, is routinely used to characterize amyloid-like fibrils. ThT fluorescence spectra are shown in Fig. 3.7. Ac-PHF6 gel sample caused enhancement in ThT fluorescence emission intensity, while no noticeable enhancement was observed for the water sample (Fig. 3.7A). All the peptides caused a large enhancement in ThT fluorescence intensity, confirming that the superstructures underlying the hydrogels are amyloid-like fibrils. The PBS samples caused a larger enhancement in ThT fluorescence than the water samples. Ac-VQIVFK-am and Ac-VQIVF(fl)K-am display around 4-fold higher intensity for PBS samples compared to water samples (Fig. 3.7B and 3.7C). Interestingly, however, the ThT fluorescence observed for Ac-VQIVF(NO_2)K-am PBS is about 2-fold higher than the water sample (Fig. 3.7E). This difference in intensity further decreases for Ac-VQIVF(CN)K-am and Ac-VQIVF(CF_3)K-am samples (Fig. 3.7D and 3.7F). The PBS samples of these peptides display only about 25% higher ThT fluorescence intensity than the water samples. These data align with the CD spectroscopy data and suggest that the Ac-PHF6 analogs wherein the aromatic residue has a strong electron-withdrawing group, have a higher aggregation propensity.

3.3.7. MD simulations

As all Ac-PHF6 analogs formed hydrogels in PBS with very similar rheological properties, I got curious to investigate the stability of the steric zippers formed by them using MD simulations. The starting structures of the peptides were prepared by modifying the VQIVYK.pdb steric zipper structure (Fig. 3.8A) available in WALTZ-DB database. The simulation data was subjected to cluster analysis to find the most representative structure of the largest cluster. The middle structures of the largest cluster are shown in Fig. 3.8B-G. The largest cluster shows steric zipper structures for all six peptides. The RMSD plot (Fig. 3.8H) also shows no appreciable difference deviation throughout the 200 ns simulation. These data suggest that parallel in-register β-sheet steric zipper is a stable architecture for Ac-PHF6 and its analogs.

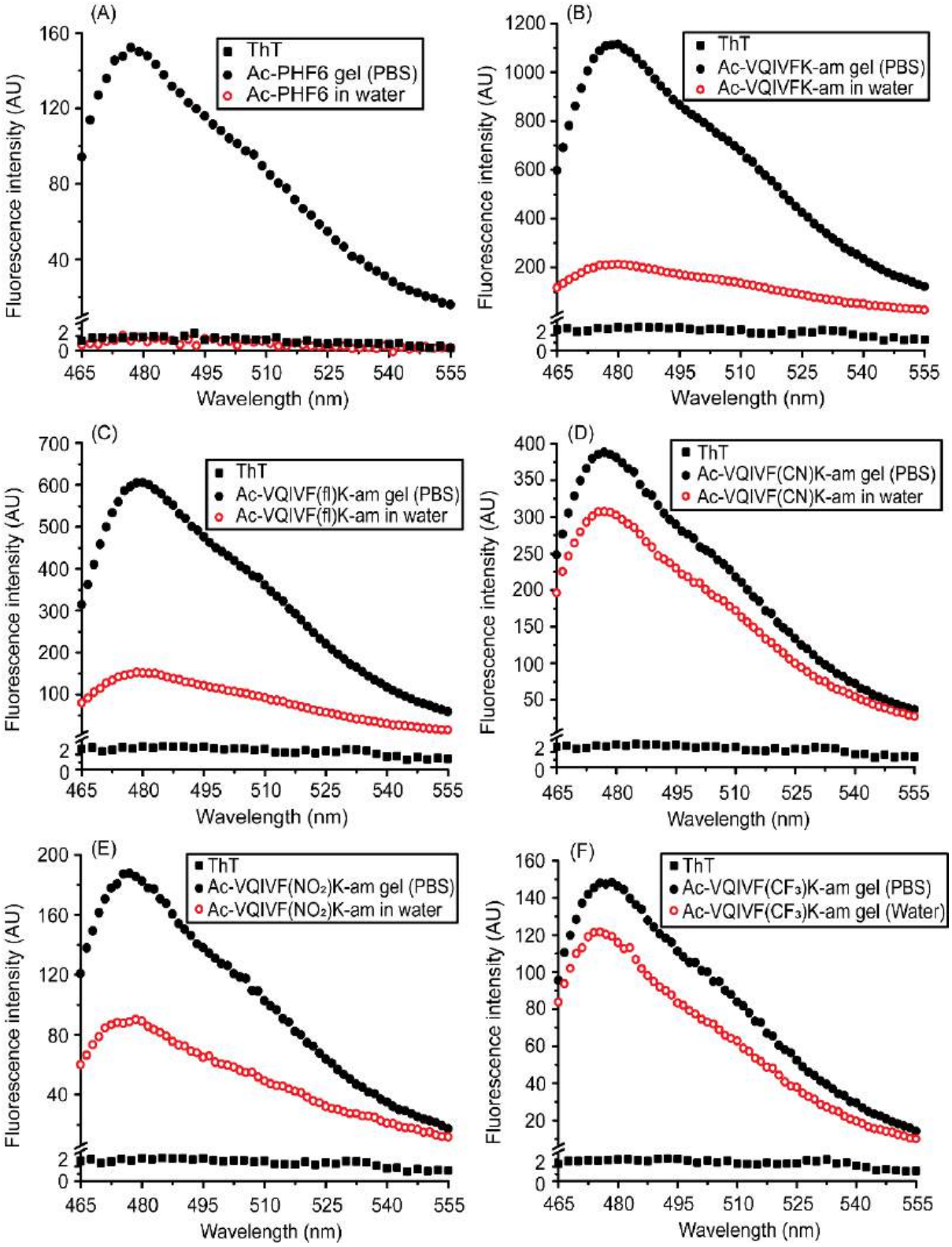

Figure 3.7. ThT fluorescence spectra of Ac-PHF6 analogs. (A) Ac-VQIVFK-am, (B) Ac-VQIVF(fl)K-am, (C) Ac-VQIVF(CN)K-am, (D) Ac-VQIVF(NO_2)K-am, and (E) Ac-VQIVF(CF_3)K-am.

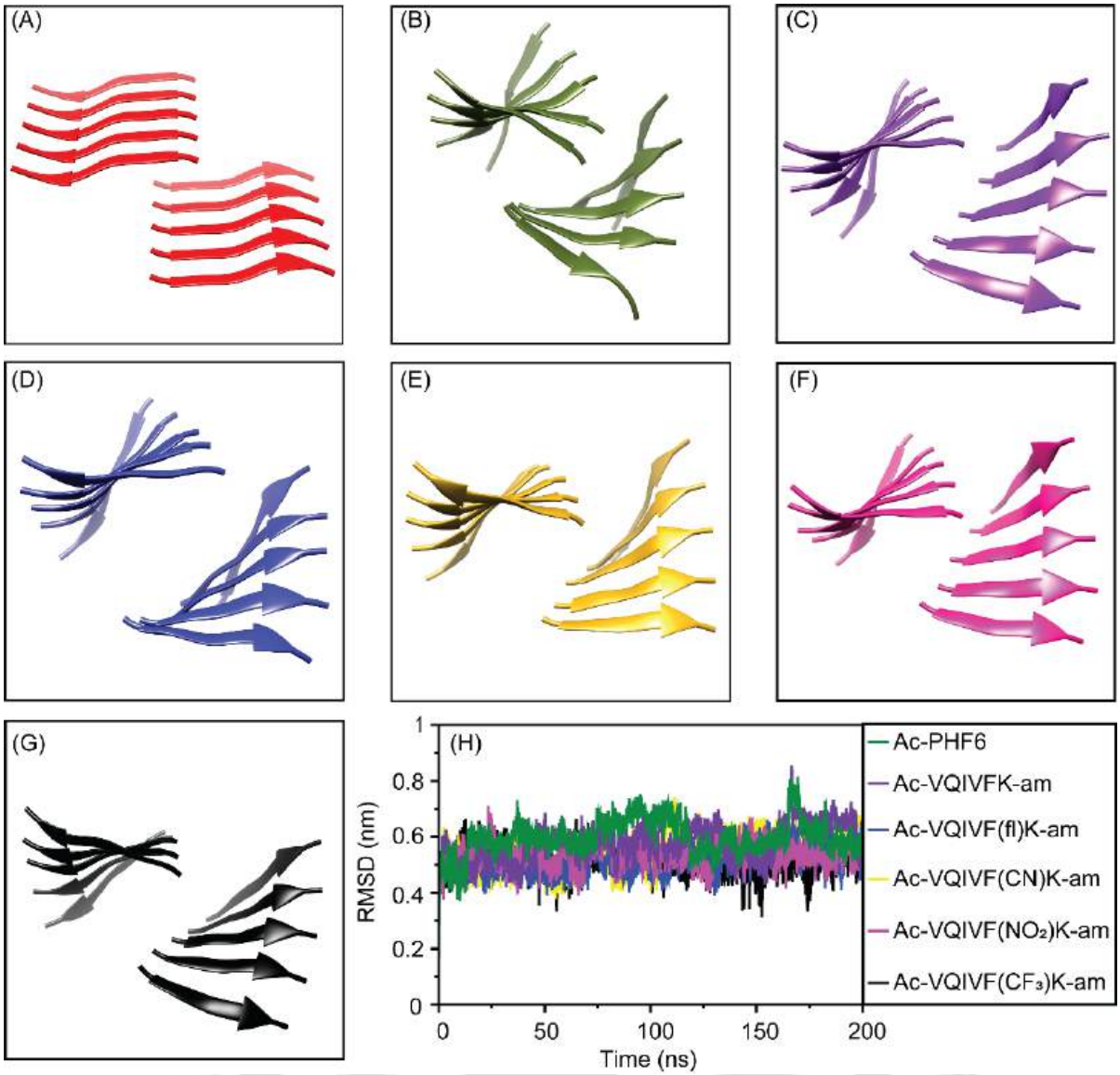

Figure 3.8. MD simulations of the peptide steric zippers. (A) the VQIVYK steric zipper obtained from WALTZ-DB database. The middle structure of the largest cluster for (B) Ac-PHF6, (C) Ac-VQIVFK-am, (D) Ac-VQIVF(fl)K-am, (E) Ac-VQIVF(CN)K-am, (F) Ac-VQIVF(NO_2)K-am, and (G) Ac-VQIVF(CF_3)K-am. (H) The RMSD plots obtained from the trajectory of simulation.

3.3.7. Transmission electron microscopy

The comparable viscoelastic properties observed for all peptides indicate that the inner structure underlying the hydrogels could also be similar. The morphology of the self-assembled structures underlying the hydrogels, therefore, was investigated using TEM. All peptides self-assemble into fibrillar superstructures. Ac-PHF6 formed fibrils similar to those reported in the literature (Fig. 3.9A) [159], [223]. Ac-VQIVFK-am and VQIVF(fl)K-am also self-assemble to form straight fibrils (Fig. 3.9B and 3.9C), similar to Ac-PHF6 [159], [223]. Ac-VQIVF(CN)K-

am and Ac-VQIVF(NO_2)K-am form long straight filaments that show extensive entanglement (Fig. 3.9D and 3.9E). Ac-VQIVF(CF_3)K-am forms fibrils that appear to form clumps, possibly through lateral interactions between individual fibrils (Fig. 3.9F).

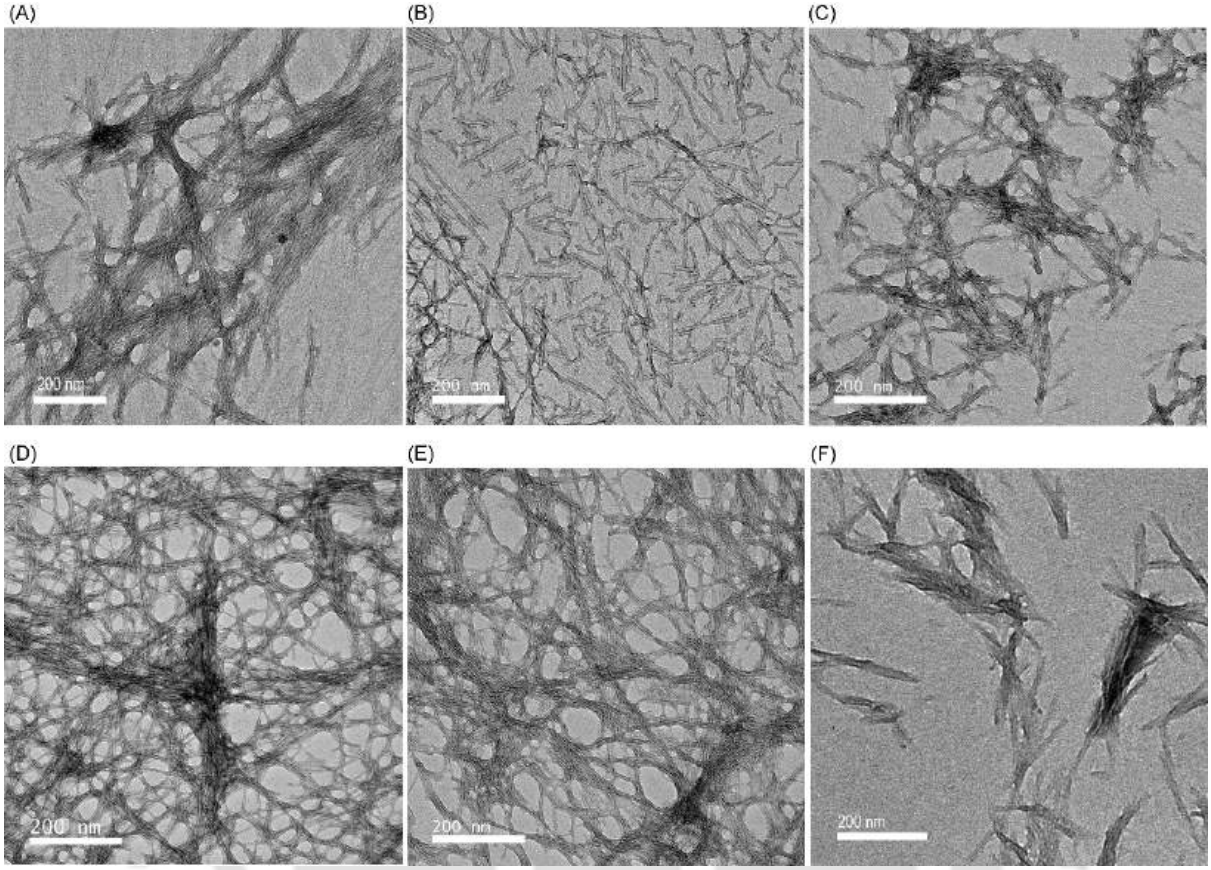

Fig. 3.9. TEM images showing the structures underlying the PBS gels. (A) Ac-PHF6, (B) Ac-VQIVFK-am, (C) Ac-VQIVF(fl)K-am, (D) Ac-VQIVF(CN)K-am, (E) Ac-VQIVF(NO_2)K-am, and (F) Ac-VQIVF(CF_3)K-am.

3.4. Conclusions

As Ac-PHF6 harbors a Tyr residue, and analogs with electron-withdrawing groups in the aromatic rings of self-assembling peptides have been reported in the literature to form stronger gels, I investigated aromatic analogs of Ac-PHF6. The Ac-PHF6 analogs with electron-withdrawing groups in the phenyl ring improve the peptide's self-assembling propensity. The analog with the strongest electron-withdrawing group (trifluoromethyl), *i.e.,* Ac-VQIVF(CF_3)K-am causes gelation of deionized water, an attribute that all other peptide analogs lacked. Notably, among all aromatic amino acids employed in this study, the *p*-(trifluoromethyl)phenylalanine has the highest hydrophobicity. The aromatic amino acids investigated in Ac-PHF6 analogs have very different electronic and steric properties, but all

the peptides formed PBS gels with comparable stiffness. The aromatic moieties' contribution to hydrogelation appears more through their hydrophobicity than the aromatic electronic effects. The role of Tyr residue in Ac-PHF6, therefore, is that of a bulky hydrophobic residue rather than an aromatic one. It would be interesting to investigate if the aliphatic analogs of Ac-PHF6 also cause hydrogelation.

CHAPTER 4

Investigating the hydrogelation of Ac-PHF6 aliphatic analogs

4.1. Introduction

Aromatic moieties have the reputation of driving self-assembly through aromatic stacking interactions. Aromatic residues are also crucial in amyloid peptide self-assembly [213], [214]. Even though the scientific community acknowledges the role of aromatic residues in peptide self-assembly and hydrogelation, the necessity to have them is debated [186], [224]. Many short peptides that lack aromatic moieties have been reported in the literature to form ordered superstructures [225], [226]. The results in Chapter 3 show that the Ac-PHF6 analogs wherein the phenolic moiety of tyrosine was substituted with phenyl, *p*-fluorophenyl, *p*-cyanophenyl, *p*-nitrophenyl, and *p*-(trifluoromethyl)phenyl, formed hydrogels with comparable rheological properties. These data made me speculate that Tyr might be contributing to Ac-PHF6 self-assembly and hydrogelation through its hydrophobicity rather than aromatic electronic effects. In this chapter, I test this hypothesis by investigating the aliphatic analogs of Ac-PHF6. Specifically, Tyr^{310} was substituted with residues having different side-chain hydrophobicities, namely Lys, Ala, Met, Val, and Ile. In addition to these variants, I also investigated the self-assembly of Ac-PHF6* (CH_3CO-VQIINK-NH_2). PHF6* is another peptide motif similar to Ac-PHF6, but without an aromatic residue (refer Fig. 1.4).

4.2. Materials and Methods

4.2.1. Materials

The sources of the reagents used in this chapter are same as specified in section 2.2.1.

4.2.2. Peptide synthesis and characterization

The peptides were assembled on Rink amide resin by employing Fmoc chemistry with HBTU/HOBt/DIPEA activation. The N-terminal acetylation, peptide cleavage from the resin, and precipitation in diethyl ether followed by washing was carried out exactly as carried out for Ac-PHF6 (section 2.2.2). The peptides were air-dried and purified using reversed-phase HPLC on a C18 column by employing a linear gradient of acetonitrile with 0.1% TFA. Peptide identities were ascertained using MALDI-TOF mass spectrometry.

4.2.3. Peptide dissolution, hydrogelation, and rheology

The peptide stock solutions were prepared in water by weighing the peptides, adding deionized water, and vortexing for a few minutes. The concentrations of the stock solutions were estimated using Waddell's method [227]. All Ac-PHF6 analogs readily dissolved in water to

concentrations higher than 20 mM and remained as viscous solutions at room temperature. Ac-PHF6*, however, showed precipitation above ~17 mM concentration. The critical aggregation concentration (CAC) for all peptides was investigated in PBS after incubation for 12 hours. The 90° light scattering was measured at 600 nm. The scattering intensity is plotted against peptide concentration. Linear trend lines are drawn on the data to determine the critical aggregation concentration. The PBS hydrogelation was investigated by diluting the stock solutions prepared in water. As the Ac-PHF6 hydrogel in chapter 2 was prepared at 20 mM concentration, the hydrogels of Ac-PHF6 aliphatic analogs were also set up at 20 mM concentration for direct comparison. Due to the lower water solubility of Ac-PHF6*, the gel could not be set up at 20 mM concentration. Therefore, the hydrogel was set up at 10 mM concentration. Instant gelation was observed for all the peptides, as ascertained by inverting the tubes. Rheology measurements for the 24-hour-old gels were carried out on an Anton Paar Rheometer MCR 102 using 25 cm parallel plates at a 0.5 mm gap. The amplitude sweep tests were carried out at an angular frequency of 10 rad/s by varying shear strain from 0.01% to 10%. As the gels displayed a linear regime up to at least 0.1% strain, the frequency sweep data were collected at 0.1% strain.

The 24-hour-old hydrogels were characterized using various methods. All experiments were conducted in triplicate, and the results are presented as mean values with the corresponding standard deviation. The peptides dissolved in water at the corresponding concentrations *i.e.* 20 mM for Ac-PHF6 analogs and 10 mM for Ac-PHF6*, even though they did not form gels, were also characterized after 24 h of preparation.

4.2.4. Thioflavin T (ThT) fluorescence spectroscopy

The gel samples were sheared through vortexing and diluted using PBS for ThT fluorescence spectroscopy. The peptide samples in water were diluted in 10 mM phosphate buffer pH 7.4 for the ThT fluorescence assay. This ensures that ThT fluorescence is not influenced by the difference in pH between water and PBS samples. The assay was carried out at 200 μM peptide and 10 μM ThT concentrations. The samples were excited at 450 nm with a 2.5 nm bandwidth, and fluorescence emission spectra were recorded using an emission bandwidth of 5 nm.

4.2.5. Congo red (CR) spectral shift assay

Congo red is a dye that binds to amyloid fibrils with high specificity. Binding to amyloid-like fibrils is accompanied by a red shift in the visible region absorption band. A 300 μM CR solution was prepared in 90% PBS and 10% ethanol, as described elsewhere [228]. The

concentration was estimated using a molar absorption coefficient of 59,3000 $M^{-1}cm^{-1}$ at 505 nm. The 24 hour-old peptide gel samples were sheared and CR absorption spectra were recorded at 9 µM concentration with 30 µg/ml peptide concentration.

4.2.6. Circular dichroism (CD) spectroscopy

Far-UV electronic CD spectra were recorded on a Jasco J-1500 spectropolarimeter. The 24-hour-old samples were diluted in the respective dispersant (water or PBS) to 200 µM concentration, and spectra were recorded in a 1 mm path-length quartz cell. The spectra were recorded from 260-195 nm at 1 nm bandwidth with a 100 nm/min scanning speed and 8 accumulations. The spectra were corrected by subtracting the respective dispersant spectrum, and the mean residue ellipticity was calculated as described in chapter 2 (Equation 2.1).

4.2.7. Fourier Transform Infrared (FTIR) spectroscopy

The infrared spectra were recorded as mentioned in section 2.2.8

4.2.8. Transmission Electron Microscopy (TEM)

The samples for TEM imaging were prepared as described in section 2.2.9

4.2.9. Cell culture and viability

Cytocompatibility of the peptides was assessed through MTT assay. Ten thousand HEK-293 cells were seeded in a 96-well plate in complete DMEM and incubated at 37 °C with 5 % CO_2 for 24 h. The wells were then treated with 50, 100, 150, and 200 µM peptide, and further incubated for 24 h. Following incubation, the growth medium was discarded and 100 µl of MTT in plain DMEM (1 mg/ml) was added to each well and incubated for 3 h. Subsequently, MTT solution was removed, and 100 µl DMSO was added. The absorbance of the purple-colored product was recorded at 570 nm using a multi-well plate reader (Multiskan GO, Thermo Scientific).

HEK-293 cells were cultured in a T25 flask using DMEM supplemented with 10% FBS and 1% antibiotic-antimycotic cocktail. The cells were incubated at 37 °C with 5% CO_2 for growth and maintenance. The 10 mM Ac-PHF6* PBS gel was set up in a 96-well plate. The 24-hour-old gel was equilibrated with DMEM for 24 hours. The gel was then seeded with 10,000 HEK-293 cells and incubated for 24 hours. For studying GAPDH expression, the total RNA was isolated using RNAiso Plus reagent, followed by cDNA synthesis with MultiScribe™ Reverse Transcriptase, and PCR (40 cycles) using primers designed for GAPDH amplification. The cell growth on the hydrogel (5mM Ac-PHF6*) was assessed through fluorescence imaging. The

wells were washed with PBS and treated with a 5 µM calcein AM solution prepared in PBS. The plate was incubated at 37 °C with 5% CO_2 for 30 minutes. The cells were washed thrice with PBS, and images were captured using a Nikon Eclipse Ts2R fluorescence microscope.

4.3. Results and discussion

4.3.1. Hydrogelation and rheology

The primary structure of the peptides employed in this study are shown in Fig. 4.1A and 4.1B. The critical aggregation concentration (CAC) of the peptides in PBS was investigated using 90° light scattering (Fig. 4.2). All peptides, except Ac-VQIVAK-am and Ac-VQIVKK-am display CAC below 100 µM. Ac-VQIVAK-am displays a CAC around 200 µM whereas Ac-VQIVKK-am CAC was found to be >1 mM. As the Ac-PHF6 hydrogel reported in the chapters 2 and 3 were prepared at 20 mM concentration, I investigated the aliphatic analogs at the same concentration. Ac-PHF6 analogs readily dissolved in water to concentrations higher than 20 mM. Ac-PHF6*, however, displayed lower solubility. The concentration higher than ~17 mM could not be achieved. Stock solutions prepared in water were diluted in PBS to achieve the desired concentrations (20 mM for Ac-PHF6 analogs, 10 mM for Ac-PHF6*). The samples were left undisturbed at room temperature for 24 hours. All the samples formed hydrogels, as confirmed by inverting the vials (Fig. 4.1C-H). Subsequent experiments were carried out at the aforementioned concentrations for both water and PBS samples. As hydrogels formed by Ac-PHF6 and its aromatic analogs reported in the chapters 2 and 3 were characterized for 24-hour-old samples, all assays reported in this chapter were also carried out after incubating the peptide samples at room temperature for 24 hours. Ac-VQIVVK-am and Ac-VQIVIK-am formed transparent hydrogels (Fig. 4.1C and D), while the gels formed by all other peptides were translucent (Fig. 4.1E-H).

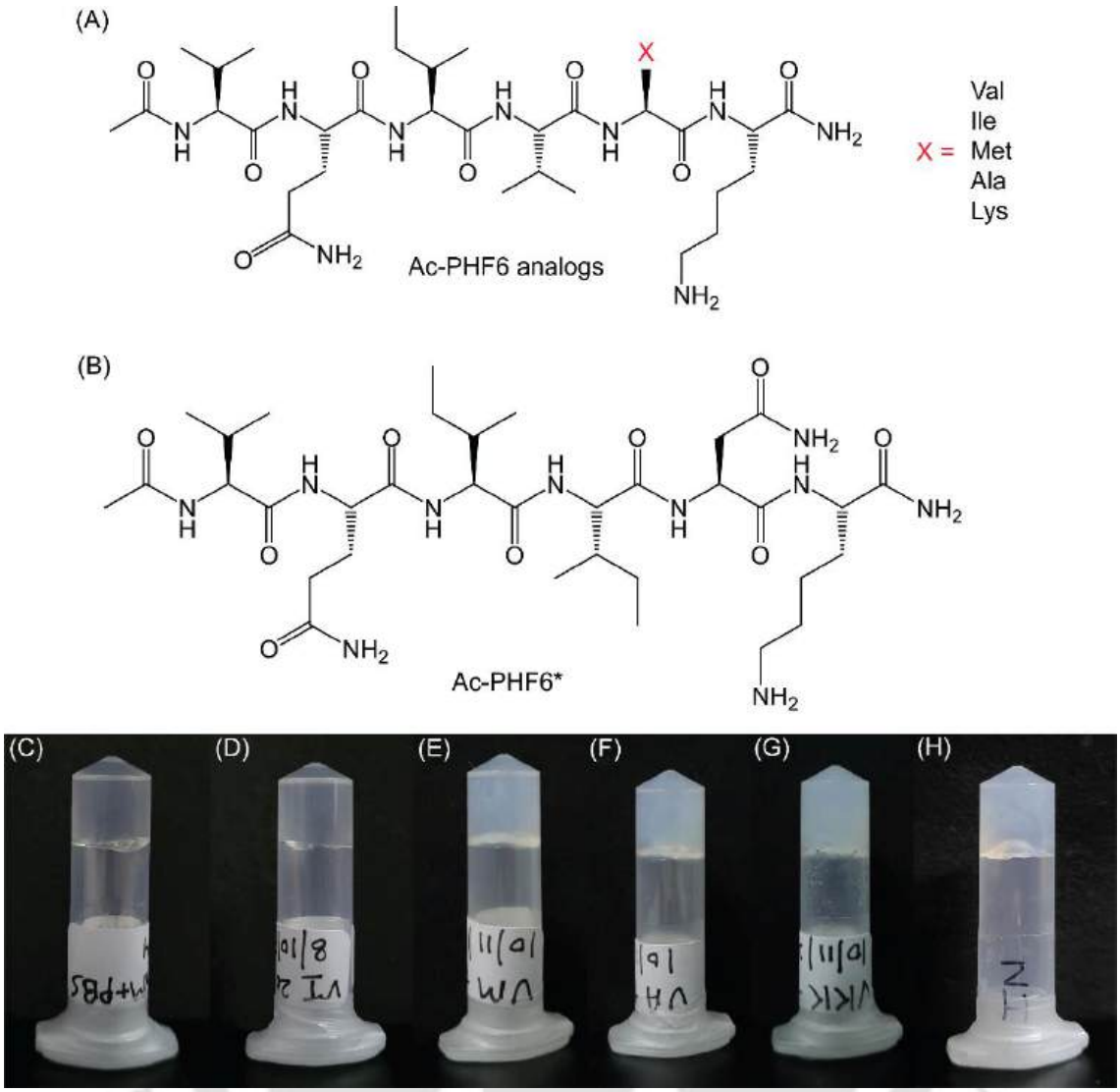

Figure 4.1. The primary structures of the (A) Ac-PHF6 analogs and (B) Ac-PHF6*. 'X' in panel A represents the side chains of Val, Ile, Met, Ala, and Lys. Inverted vials showing hydrogels formed by 20 mM (C) Ac-VQIVVK-am, (D) Ac-VQIVIK-am, (E) Ac-VQIVMK-am, (F) Ac-VQIVAK-am, (G) Ac-VQIVKK-am, and (H) 10 mM Ac-PHF6*.

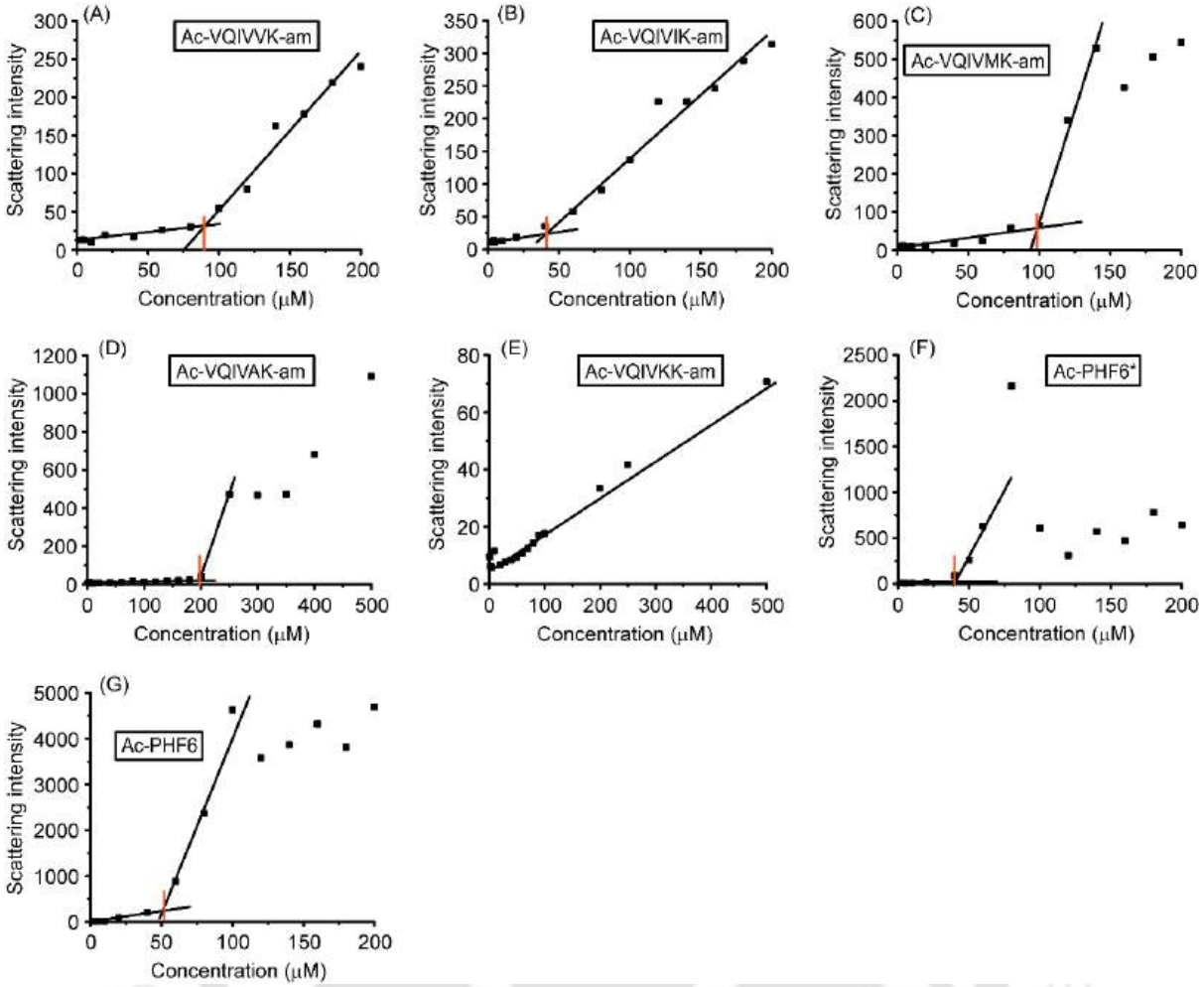

Figure 4.2. The 90° light scattering was measured for (A) Ac-VQIVVK-am, (B) Ac-VQIVIK-am, (C) Ac-VQIVMK-am, (D) Ac-VQIVAK-am, (E) Ac-VQIVKK-am, (F) 10 mM Ac-PHF6*, and (G) Ac-PHF6.

Rheology was carried out to investigate the viscoelasticity of the hydrogels. Ac-VQIVVK-am and Ac-VQIVIK-am formed hydrogels with storage moduli of around 60 kPa from 100 rad/s down to 0.02 rad/s (Fig. 4.3A and 4.3B). The loss moduli were ~6-10 kPa. The rheology data for 20 mM Ac-PHF6 hydrogel is shown in Fig. 4.3G. The hydrogel displays storage and loss moduli of ~20 kPa and ~1-5 kPa, respectively. These rheological characteristics are similar to the 20 mM Ac-PHF6 hydrogel reported in the literature [223]. Substitution of Tyr^{310} in Ac-PHF6 with Val or Ile, therefore, results in stiffer hydrogels. The Ac-VQIVMK-am and Ac-VQIVAK-am formed hydrogels with storage moduli around 30 kPa (Fig. 4.3C and 4.3D). Met and Ala have lower hydrophobicities than those of Val and Ile, and form hydrogels with lower stiffness. Ac-VQIVKK-am formed softer gel with a storage modulus of about 1 kPa (Fig. 4.3E). I previously investigated Ac-PHF6 analogs wherein the Tyr side chain was replaced with several electron-deficient aromatic groups [229]. Interestingly, all analogs formed hydrogels,

prompting me to hypothesize that the sole aromatic residue Tyr^{310} in Ac-PHF6 might contribute to self-assembly and hydrogelation more through its hydrophobicity than the aromaticity. Hydrogelation by Ac-PHF6 aliphatic analogs proves that hypothesis. The Ac-PHF6 analogs wherein Tyr is substituted with Val, Ile, Met, and Ala form hydrogels with higher stiffness than that of the Ac-PHF6 hydrogel. The Y310K analog, on the other hand, forms hydrogel with stiffness lower than Ac-PHF6 hydrogel. Besides, unlike all other peptides, the kinetics of gelation is much slower. Whereas all other peptides cause instant PBS gelation, the Y310K analog takes about 2 hours to form hydrogel. These data made me wonder if Ac-PHF6*, a tau interaction motif very similar to Ac-PHF6 but lacking an aromatic residue, could also form hydrogel. As Ac-PHF6* displayed lower solubility, the hydrogel could not be set up at 20 mM concentration. Ac-PHF6* hydrogel, therefore, was prepared at 10 mM concentration for all the assays. The 10 mM hydrogel exhibited a storage modulus of about 10 kPa in the 0.02 - 100 rad/s frequency range. The loss modulus was around one order of magnitude less (Fig. 4.3F). The viscoelasticity of 10 mM Ac-PHF6 hydrogel is not reported in the literature. Therefore, I prepared 10 mM Ac-PHF6 hydrogel and measured its viscoelasticity to directly compare with that of Ac-PHF6* hydrogel (Fig. 4.3G). Clearly, the Ac-PHF6* displays higher storage and loss moduli at all frequencies. Tyr^{310}, therefore, is superfluous for Ac-PHF6 self-assembly and hydrogelation.

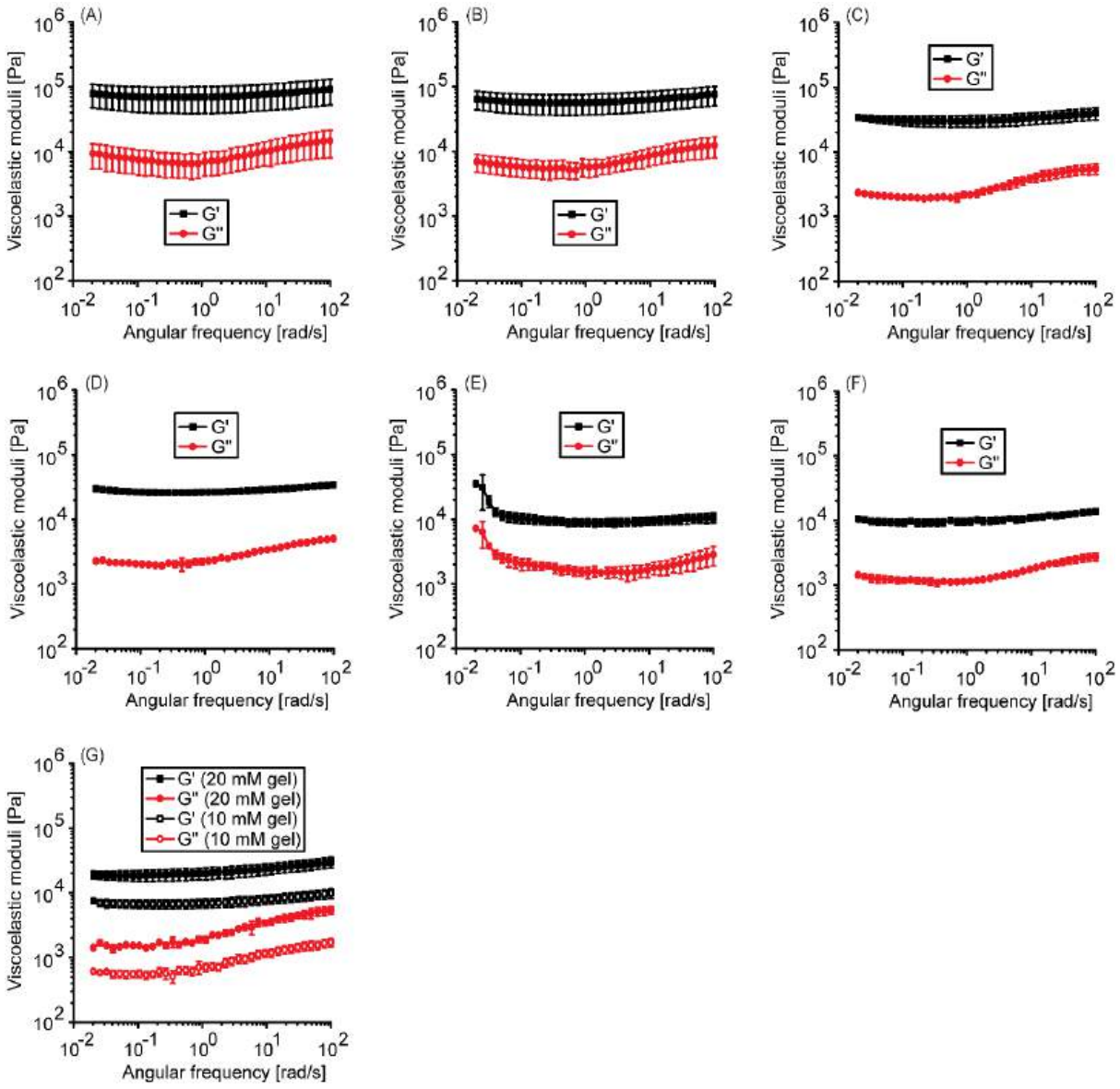

Figure 4.3. Oscillatory rheology data for hydrogels formed by 20 mM (A) Ac-VQIVVK-am, (B) Ac-VQIVIK-am, (C) Ac-VQIVMK-am, (D) Ac-VQIVAK-am, (E) Ac-VQIVKK-am, (F) 10 mM Ac-PHF6*, and (G) 10 mM and 20 mM Ac-PHF6. The data is presented as the mean of three replicates and the error bars represent the standard deviation.

4.3.2. ThT fluorescence

The structures underlying the hydrogels were investigated using ThT fluorescence, an assay routinely employed to identify the amyloid-like aggregates. The binding of ThT to amyloid-like fibrils causes a large enhancement in its fluorescence intensity. All peptides, except for Ac-VQIVKK-am, caused enhancement in ThT fluorescence intensity (Fig. 4.4). The enhancement caused by PBS samples is at least 2 times more than that caused by the water samples. This is consistent with the understanding that charge screening of the terminal lysine

residue facilitates self-assembly. Notably, the PBS sample of Ac-PHF6* exhibited more than 3-fold higher ThT fluorescence compared to the water sample (Fig. 4.4F). Eisenberg and coworkers have investigated the steric-zippers formed by VQIVYK and VQIINK peptides [230]. VQIINK is reported to form steric zippers with higher shape complementarity and a larger steric zipper interface. Using tau K18 constructs wherein R2 and R3 contain identical hexapeptide motifs, i.e. constructs with two PHF6 or two PHF6*, they further show that PHF6* is a better interaction motif in driving self-assembly. The higher ThT fluorescence intensity observed for Ac-PHF6*, therefore, could be due to its higher aggregation propensity.

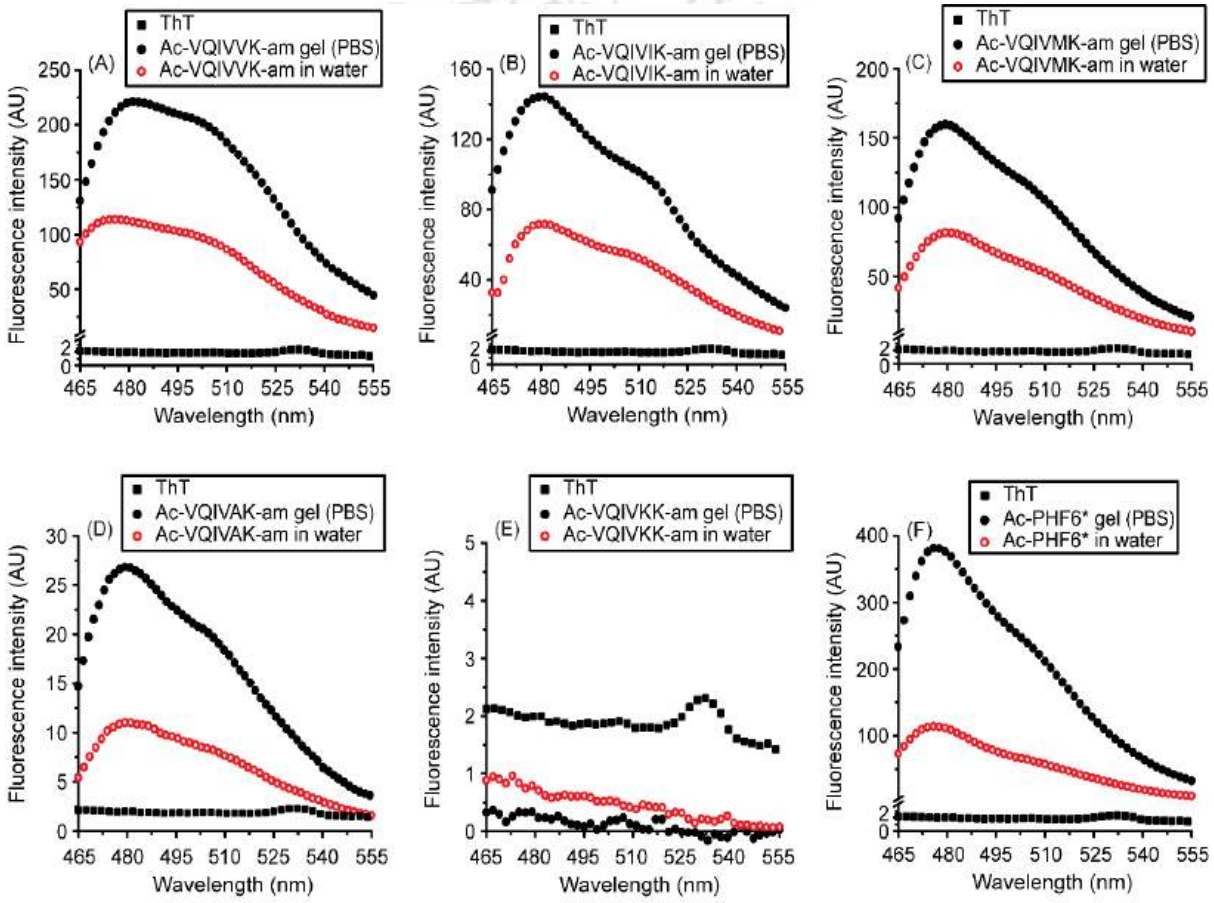

Figure 4.4. ThT fluorescence emission spectra of (A) Ac-VQIVVK-am, (B) Ac-VQIVIK-am, (C) Ac-VQIVMK-am, (D) Ac-VQIVAK-am, (E) Ac-VQIVKK-am, and (F) Ac-PHF6*.

4.3.3. Congo red spectral shift assay

Congo red, a sulfonated diazo dye, displays absorption bands centred around 340 and 496 nm in water. Binding of congo red to amyloid fibrils causes a red-shift in the lower energy band. Fig. 4.5 shows the congo red absorption spectra recorded with the PBS peptide samples. All peptides, except for Ac-VQIVKK-am, exhibit a red shift in the lower energy absorption band.

These data are consistent with the ThT fluorescence data. The hydrogel formed by Ac-VQIVKK-am, therefore, is not made up of amyloid-like fibrillar structures.

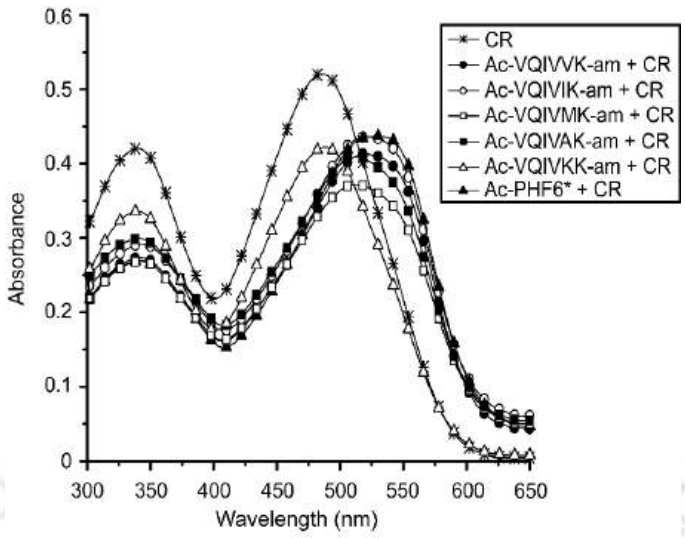

Fig. 4.5. Congo red absorption spectra with peptides obtained after shearing the PBS hydrogels.

4.3.4. CD spectroscopy

The secondary structures of the peptides were analyzed using far-UV CD spectroscopy. The samples were diluted to 200 μM in their respective dispersant for the measurements. In water, CD spectra of all the peptides display a negative band around 198 nm and a lower intensity shoulder around 220 nm (Fig. 4.6). These spectra are suggestive of a mixture of β-sheet and random coil conformations. In PBS, all Ac-PHF6 analogs, except Ac-VQIVKK-am, show a negative band around 220 nm and a positive band around 200 nm (Fig. 4.6A-D). These spectra suggest a predominantly β-sheet structure. Ac-VQIVKK-am in PBS displays a spectrum very similar to that observed in water, albeit with a slightly red-shifted higher energy band (Fig. 4.6E). Ac-PHF6* displays an intense negative band around 202 nm alongside the 220 nm shoulder (Fig. 4.6F). This CD spectrum comes as a surprise as Ac-PHF6* caused the highest enhancement in ThT fluorescence intensity among all the peptides. Manavalan and Johnson found two distinct types of CD spectra for β-sheet proteins. The one that was eventually designated βI shows a classical β-sheet signature with a ~215 – 220 nm negative band and a 195 – 200 nm positive band. The second type of spectrum, known as βII, exhibits a negative band around 200 nm [231], [232].. The Ac-PHF6* CD spectrum in PBS looks similar to that observed in water, but with much higher ellipticity and a slightly red-shifted higher energy band. An ellipticity this large is very atypical of protein CD spectra. Sreerama and Woody assigned such a large ellipticity to poly(Pro)II-like conformation [233]. A large ellipticity

observed for poly(Pro)II implies that a protein with a high poly(Pro)II to β-sheet ratio would give a βII CD signature.

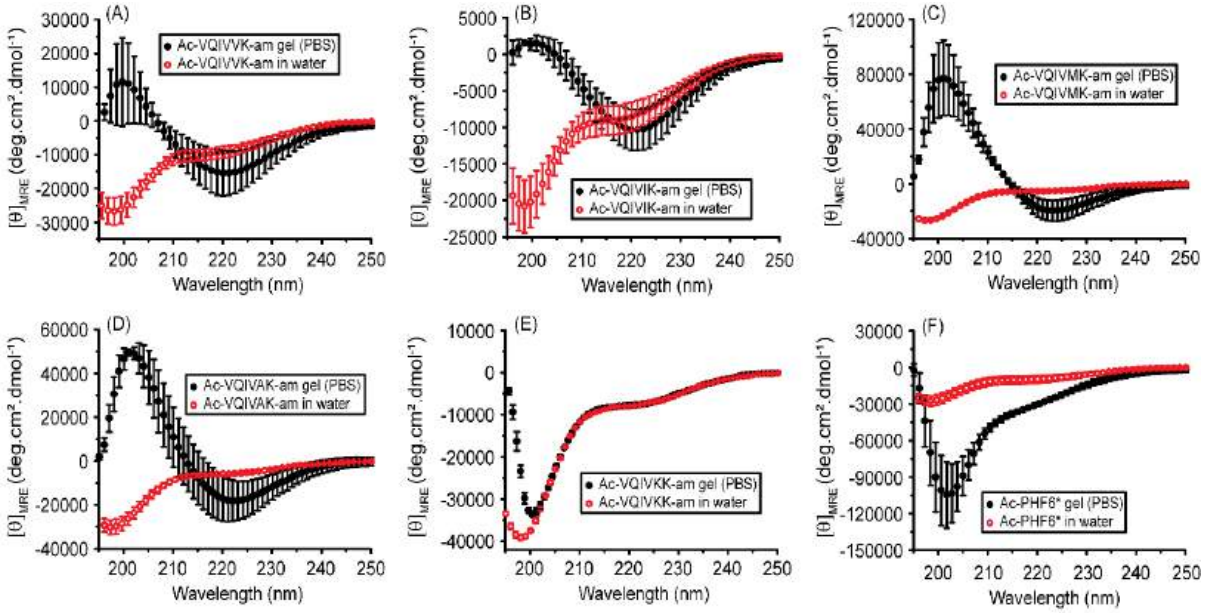

Figure 4.6. CD spectra of (A) Ac-VQIVVK-am, (B) Ac-VQIVIK-am, (C) Ac-VQIVMK-am, (D) Ac-VQIVAK-am, (E) Ac-VQIVKK-am, and (F) Ac-PHF6*. The data is presented as the mean of three replicates and the error bars represent the standard deviation.

4.3.5. FTIR spectroscopy

As the CD spectrum observed for Ac-PHF6* in PBS was atypical, the secondary structures were further validated using infrared spectroscopy. The frequency of the amide I band is sensitive to the polypeptide backbone conformation, and is particularly suitable for β-sheet structure. The amide I band for β-sheet in proteins is observed between 1625 - 1640 cm^{-1} [234]. Aggregated strands display further lower frequencies with the amide I band lying between 1610 - 1635 cm^{-1} [194], [234]. Infrared spectroscopy, therefore, has emerged as a method of choice for investigating the self-assembled proteins and peptides [194], [235]. Dried samples of all peptides exhibited an amide I band near 1626 cm^{-1} in both PBS and water, clearly establishing the β-sheet conformation of the superstructures underlying the hydrogels (Fig. 4.7).

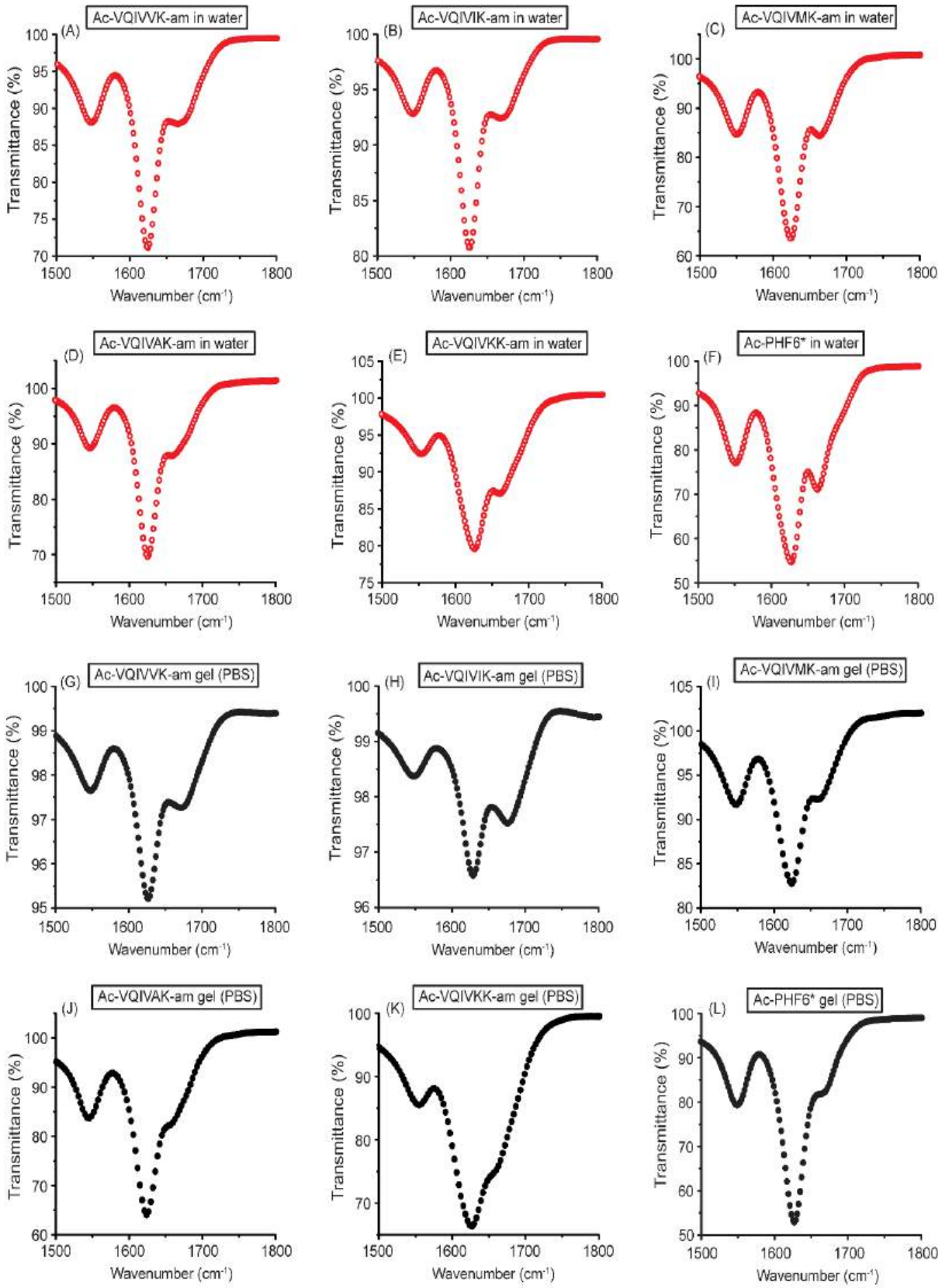

Figure 4.7. The ATR-FTIR spectra of peptide water samples (panels A-F) and PBS samples (panels G-L).

4.3.6. Transmission Electron Microscopy

The morphology of the self-assembled structures forming the hydrogels was analyzed using TEM (Fig. 4.8). Ribbon-like structures were observed for Ac-VQIVVK-am (Fig. 4.8A) and Ac-VQIVIK-am (Fig. 4.8B) water samples. Such ribbon-like structures have been reported in the literature for Ac-PHF6 [223]. Ac-VQIVMK-am and Ac-VQIVAK-am form typical amyloid-like filamentous assemblies in water (Fig. 4.8C and 4.8D). Unlike the other Ac-PHF6 analogs that showed abundant fibrillar structures spread throughout the copper grid used for imaging, very few long filamentous structures were found for Ac-VQIVKK-am (Fig. 4.8E). In PBS, all Ac-PHF6 analogs, except Ac-VQIVKK-am, formed typical amyloid-like fibrils (Fig. 4.8G-J). The fibrils are rod-like, resembling those previously reported for Ac-PHF6 [223], [236]. Ac-VQIVKK-am formed long, straight, and flat ribbon-like structures, suggesting a different mode of assembly (Fig. 4.8K). Ac-PHF6*, unlike Ac-PHF6 analogs, formed very different superstructures. In water, the peptide self-assembled into long ribbon-like structures that laterally assemble to form flat sheets (Fig. 4.8F). Some of these sheets appear to curl near the edges (Inset, Fig. 4.8F). In PBS, Ac-PHF6* formed long, straight but densely entangled fibrous structures (Fig. 4.8L).

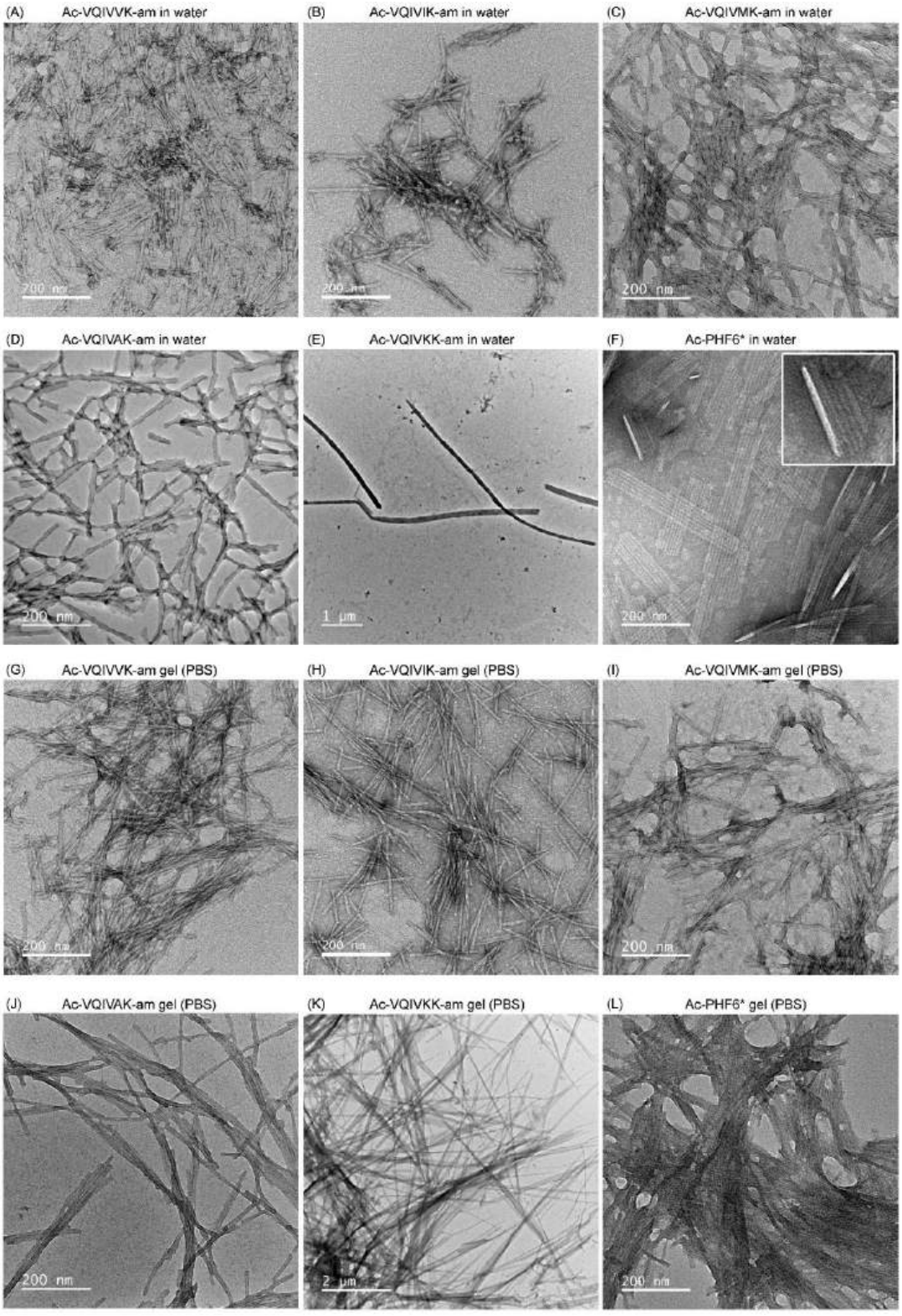

Figure 4.8. TEM images of water samples (upper panels A-F) and PBS hydrogels (lower panels G-L).

4.3.7. Cytocompatibility of Ac-PHF6*

The cytocompatibility of peptides was assessed using an MTT cell viability assay. In this assay, viable cells metabolically reduce MTT to formazan crystals, which absorb light at 570 nm. In contrast, non-viable cells lack this activity and do not contribute to the absorbance signal. The cell viability was normalized to untreated control cells (Fig. 4.9A-F). The cells displayed ~80% viability up to 200 µM peptide concentration for all six peptides.

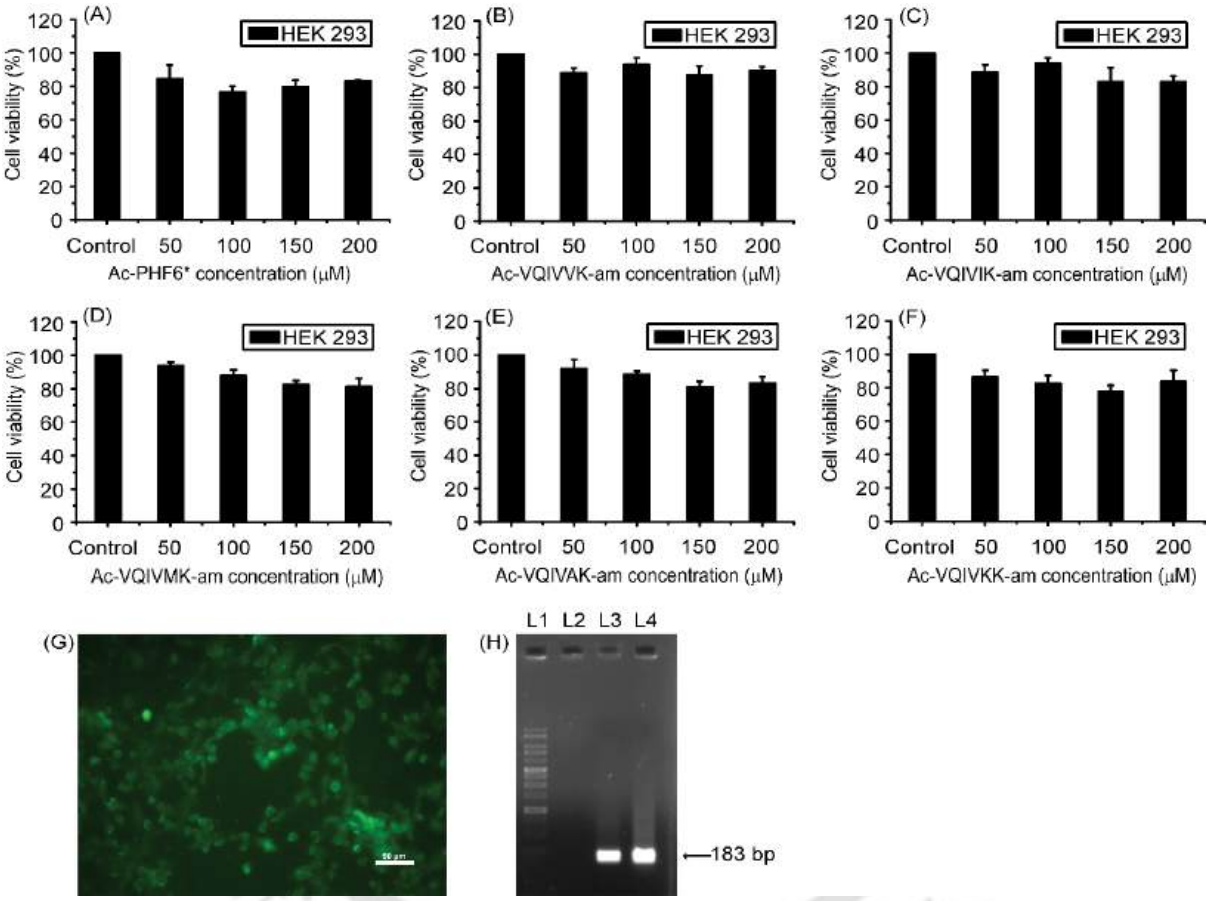

Figure 4.9. HEK-293 cell-viability using MTT assay (A-F). Cells grown on Ac-PHF6* hydrogel (G), and GAPDH expression shown by HEK-293 cells grown on the hydrogel (H). The scale bar represents 50 µm. L1 is the 1 kb (250 – 10,000 bp) DNA molecular weight marker lane, L2 is the negative control, L3 represents the GAPDH amplification from cells cultured in DMEM without peptide (positive control), and L4 represents the GAPDH amplification from cells cultured in Ac-PHF6* hydrogel.

Ac-PHF6 hydrogel has been reported in the literature to support culture of mammalian cells [223]. I wondered if Ac-PHF6* hydrogel could also support cell culture. The HEK-293 cells were cultured on a 24-hour-old hydrogel (5 mM Ac-PHF6*) for 24 hours and then stained with calcein AM, a membrane-permeable, non-fluorescent probe. Intracellular esterases hydrolyze

calcein AM into fluorescent calcein, with fluorescence intensity correlating directly with esterase activity, and therefore, cell viability. Microscopic analysis confirmed HEK-293 cell proliferation in the hydrogel matrix (Fig. 4.9G). The expression of the housekeeping gene GAPDH was also investigated. Cells grown without Ac-PHF6* (positive control), and in 10 mM hydrogel were harvested, followed by RNA extraction and reverse transcription PCR (RT-PCR). The cells grown in the hydrogel were found to express GAPDH (Fig. 4.9H).

4.4. Conclusion

I demonstrated in chapter 2 that Ac-PHF6 (CH_3CO-VQIVYK-NH_2) forms an injectable and biocompatible hydrogel in PBS. The peptide contains a Tyr residue that was believed to facilitate self-assembly through aromatic stacking interactions. In chapter 3, I examined aromatic analogs of Ac-PHF6 bearing electron-withdrawing substituents on the phenyl ring [229]. All the analogs formed hydrogels, leading me to speculate that the Tyr residue may not contribute to self-assembly and gelation due to its aromaticity. Ac-PHF6 analogs wherein Tyr is substituted with amino acids with hydrophobic side chains (Val, Ile, Met, Ala) formed amyloid-like fibrils very similar to those formed by Ac-PHF6. All four peptides caused instant gelation of PBS. The peptide wherein Tyr was substituted with Lys, an amino acid with polar side chain, formed a soft gel with much lower gelation rate. Besides, the assembly of the Y310K analog appears to be different from all other Ac-PHF6 analogs. Ac-PHF6*, a native peptide stretch from the R2 region of tau that lacks an aromatic residue, was also found to form hydrogel. Like Ac-PHF6, Ac-PHF6* also supported HEK-293 cell growth. These findings suggest that the role of aromatic residues in peptide self-assembly and hydrogelation may be overemphasized. It is likely that the aromatic residues in many peptides simply contribute through their size and hydrophobicity.

CHAPTER 5

Hydrogelation by Ac-PHF6 and Ac-PHF6* analogs with cationic N-terminus

5.1. Introduction

The amino acid composition and sequence can be strategically designed to fine-tune key properties, including gelation behavior, mechanical strength, and biodegradation profiles. The subtle modifications to the sequence or termini chemistry can have marked effects on self-assembly and hydrogelation, highlighting the sensitive dependence of hydrogelation on subtle molecular features [121]. Hauser and coworkers explored how subtle structural changes in ultrashort peptides affect their self-assembly, nanostructure formation, hydrogelation, and phase transition, revealing a high sensitivity to molecular variations with implications for designing novel peptide nanostructures for biomedical applications [237]. Webber and coworkers developed amphiphilic tripeptides with sequence-controlled nanostructure, allowing for the production of diverse nanostructures by altering a single amino acid [238]. Their design strategy involved incorporating a hydrophobic Phe at the N-terminus, followed by a variable aliphatic residue (Val, Leu, Ile), and a hydrophilic Asp at the C-terminus. These peptides can form hydrogels with high aspect-ratio structures that support cell viability in culture, even at low concentrations. Muller and coworkers have demonstrated that the sequence and size of non-polar amino acids significantly affect the self-assembly properties of amphiphilic peptides, leading to variations in secondary structures and matrix morphology, with potential applications in drug delivery and tissue engineering [239].

Tuttle and coworkers investigated the complete tripeptide sequence space (peptides with free termini) to understand the features that direct hydrogelation. One of the defining features is the charge coupling i.e. having a cationic residue at N-terminus and/or an anionic residue at C-terminus. For tripeptides with free termini, a cationic N-terminal residue and/or an anionic C-terminal residue contribute to hydrogelation propensity. As Ac-PHF6 and Ac-PHF6* harbour a lysine residue at C-terminus, I sought to investigate its analogs wherein lysine is at the N-terminus. For this study, two strategies were chosen, namely (i) shifting the C-terminal lysine to N-terminus, and (ii) investigating the retropeptide. I also included the end-capped boaamphiphilic peptides CH_3CO-KVQIVYK-NH_2 and CH_3CO-KVQIINK-NH_2 in this study. It is worth noting that the two analogs of Ac-PHF6* i.e. CH_3CO-KVQIIN-NH_2 ($tau^{274-279}$) and CH_3CO-KVQIINK-NH_2 ($tau^{275-280}$) happen to be the native sequences within the tau. The peptides investigated are shown in Table 1.

5.2. Materials and methods

5.2.1. Materials

The sources of the reagents used in this chapter are same as specified in section 2.2.1.

5.2.2. Peptide synthesis and characterization

The peptide amides were assembled on Rink amide resin while peptide acids were assembled on Wang resin preloaded with Fmoc-Lys(Boc)-OH by employing Fmoc chemistry with HBTU/HOBt/DIPEA activation. N-terminal acetylation, cleavage of peptide and precipitation was carried out with same process mentioned in section 2.2.2. Purification was carried out using reversed-phase high-performance liquid chromatography on a C18 column using a linear gradient of acetonitrile in water. The identity of the purified peptides was confirmed using MALDI-TOF mass spectrometry using HCCA as the matrix.

Table 1. The Ac-PHF6 (CH_3CO-VQIVYK-NH_2) and Ac-PHF6* (CH_3CO-VQIINK-NH_2) analogs investigated in this study.

Peptide sequence	Remarks	Charge on N-terminal residue	Charge on peptide
KVQIVY-am	Ac-PHF6 analog with Lys at N-terminus, uncapped N-terminus.	+2	+2
Ac-KVQIVY-am	Ac-PHF6 analog with Lys at N-terminus, both ends capped.	+1	+1
KYVIQV-am	PHF6 retropeptide; uncapped N-terminus, amidated C-terminus	+2	+2
Ac-KVQIVYK-am	Bolaamphiphilic analog of Ac-PHF6 with both ends capped	+1	+2
Ac-KVQIIN-am	Ac-PHF6* analog with Lys at N-terminus, both ends capped	+1	+1
Ac-KVQIINK-am	Bolaamphiphilic analog of Ac-PHF6* with both ends capped	+1	+2

5.2.3. Peptide dissolution, hydrogelation and rheology

All synthesized peptides except Ac-KVQIVY-am exhibited good aqueous solubility, and stock solutions were prepared in water. Peptide concentrations for Ac-PHF6 analogs were

determined spectrophotometrically by measuring absorbance at 280 nm, using the molar extinction coefficient of Tyr (1280 $M^{-1}cm^{-1}$). Up to approximately 25 mM, all the peptides except Ac-KVQIVY-am remained as thick viscous solutions. As Ac-PHF6* analogs lack aromatic residues, their concentration was estimated using Wadell's method [227]. Ac-KVQIVY-am resulted in a turbid suspension in water at 20 mM concentration. Therefore, the stock solutions for Ac-KVQIVY-am were prepared at lower concentrations, mostly between 17-19 mM. Within this concentration range, the peptide formed clear viscous solutions. None of the peptide stock solutions in water, except Ac-KVQIIN-am, formed gel. Gelation in PBS was attempted by diluting the stock solutions prepared in water. The 24 hour-old PBS hydrogels were subjected to oscillatory rheology on an Anton Paar MCR 102 rheometer equipped with 25 mm parallel plate geometry and a gap of 0.5 mm. Amplitude sweep tests were carried out at a constant angular frequency of 10 rad/s, with shear strain varied from 0.01% to 10%. All gel samples displayed a well-defined linear viscoelastic regime (LVR) extending up to at least 0.1% strain. Consequently, frequency sweep experiments were conducted at 0.1% strain to ensure measurements remained within the LVR.

5.2.4. Intrinsic fluorescence spectroscopy

Intrinsic tyrosine fluorescence spectra were acquired on a Jasco FP-8500 spectrofluorometer by diluting the PBS and water samples in respective dispersants to 200 µM concentration. The fluorescence emission spectra were recorded by exciting at 280 nm with 2.5 nm bandwidth, and recording emission intensities from 290 - 400 nm with 5 nm bandwidth. The spectra were corrected by subtracting the respective dispersant spectra.

5.2.5. ThT fluorescence spectroscopy

The ThT fluorescence emission spectra for PBS gel samples were recorded in PBS. Given the pH sensitivity of ThT fluorescence quantum yield, spectra for the water samples were not collected in water, but in 10 mM phosphate buffer (pH 7.4). The assay was carried out at 200 µM peptide concentration and 10 µM ThT concentration. The samples were excited at 450 nm with a 2.5 nm bandwidth, and emission spectra were collected using a 5 nm emission bandwidth.

5.2.6. Circular dichroism (CD) spectroscopy

Far-UV CD spectra were acquired on a Jasco J-1500 CD spectropolarimeter. The 24-hour-old samples were diluted to 200 µM in the respective dispersant. Measurements were performed using a 1 mm path length quartz cell. The spectra were recorded over the wavelength range of

195-250 nm, with a bandwidth of 1 nm, a scan speed of 100 nm/min, and eight accumulations. All spectra were corrected by subtracting the spectra of the corresponding solvent blanks.

5.2.7. Fourier Transform Infrared (FTIR) spectroscopy

The FTIR measurements were carried out as described in Section 2.2.8.

5.2.8. Transmission Electron Microscopy

The TEM samples were prepared as per the protocol provided in Section 2.2.9.

5.2.9. Cell culture assay

Human embryonic kidney (HEK-293) cells were maintained in T25 flasks using Dulbecco's Modified Eagle's Medium (DMEM) supplemented with 10% fetal bovine serum (FBS) and 1% antibiotic-antimycotic solution. Cells were cultured at 37 °C in a humidified 5% CO_2 incubator and passaged using trypsin for detachment. Hydrogels of Ac-KVQIVYK-am and KYVIQV-am (10 mM, 70 µL) were prepared in PBS and allowed to set in a 96-well plate. After 24 hours, 200 µL of complete DMEM was added to each well containing the gel, and the plate was incubated for another 24 hours at 37 °C with 5% CO_2. The medium was removed, and gels were equilibrated with fresh DMEM for 10 minutes before cell seeding. Subsequently, the gels were seeded with HEK-293 cells (10^4 cells/well), and incubated under the same conditions for 24 hours. Following incubation, the wells were gently washed with PBS to remove unattached cells. Total RNA was extracted using RNAiso Plus reagent (Takara Bio, Shiga, Japan), and complementary DNA (cDNA) was synthesized using MultiScribe™ Reverse Transcriptase (Applied Biosystems, Waltham, MA, USA). PCR was performed for 40 cycles using GAPDH-specific primers as described elsewhere [121].

5.2.10. Cell viability assay

The cytocompatibility of Ac-KVQIVYK-am and KYVIQV-am was evaluated using the MTT assay [149]. A 96-well plate containing complete DMEM (100 µl) was seeded with HEK-293 cells (10^4 cells per well) and incubated at 37 °C in 5% CO_2 for 24 hours. Following incubation, the cells were treated with varying concentrations (50, 100, 150, and 200 µM) of Ac-PHF6 analogs, and the plate was returned to the incubator for an additional 24 hours. Subsequently, the culture medium was carefully aspirated, and 100 µl of MTT solution (1 mg/mL in serum-free DMEM) was added to each well. The plate was incubated for 3 hours at 37 °C, allowing viable cells to metabolize MTT into insoluble formazan crystals. The MTT solution was then discarded, and 100 µl of DMSO was added to solubilize the formazan product. Absorbance

was measured at 570 nm using a Multiskan GO microplate reader (Thermo Scientific), with cell viability expressed relative to untreated control wells.

5.3. Results and discussion

5.3.1. Hydrogelation and rheology

The peptides exhibited good solubility in water. Except Ac-KVQIVY-am, all other peptides could be dissolved up to about 25 mM concentration. Ac-KVQIVY-am could be dissolved up to around 18 mM concentration. Except Ac-KVQIIN-am, not other peptide stock solutions exhibited gelation up to at least 24 hours, as ascertained by tilting and inverting the tubes. Ac-KVQIIN-am formed very soft gel of water after keeping undisturbed for 24 h. The stock solutions prepared in water were diluted in PBS. Ac-KVQIVY-am, Ac-KVQIIN-am, and Ac-KVQIINK-am were diluted to 15 mM concentration while the other peptides were diluted to 20 mM concentrations. All peptides, except KVQIVY-am caused instant gelation of PBS. The samples were allowed to stand for 24 h at room temperature. No gelation was observed for KVQIVY-am even after 24 h. These two peptides, therefore, were not investigated any further. Ac-KVQIVYK-am and KYVIQV-am formed transparent hydrogel (Fig. 5.1A and 5.1B). Ac-KVQIVY-am, Ac-KVQIIN-am, and Ac-KVQIINK-am on the other hand, formed turbid gels (Fig. 5.1C-E).

The gelation results highlight the critical influence of subtle sequence modifications on peptide self-assembly and hydrogel formation. This observation aligns with prior findings by Hauser and coworkers, who demonstrated that even minimal structural alterations in tripeptides can dramatically impact their ability to self-assemble, form nanostructures, and undergo hydrogelation and phase transitions [237]. A consistent trend emerging from our study is that C-terminal amidation significantly enhances the propensity for gelation, likely by minimizing electrostatic repulsion and promoting intermolecular hydrogen bonding. Similarly, N-terminal acetylation facilitates gelation. Ac-KVQIVY-am forms a hydrogel, whereas its N-terminal uncapped analog KVQIVY-am does not. Interestingly, KYVIQV-am, the retropeptide with free amino terminus also causes PBS gelation. These data parallel our previous findings with PHF6, where Ac-PHF6 (Ac-VQIVYK-am) caused instant gelation of PBS, while the uncapped peptide VQIVYK failed to gel under identical conditions even after several days of incubation [223]. Together, these results underscore the importance of terminal modifications and residue positioning in controlling peptide self-assembly and hydrogelation through modulating electrostatics and hydrogen bonding.

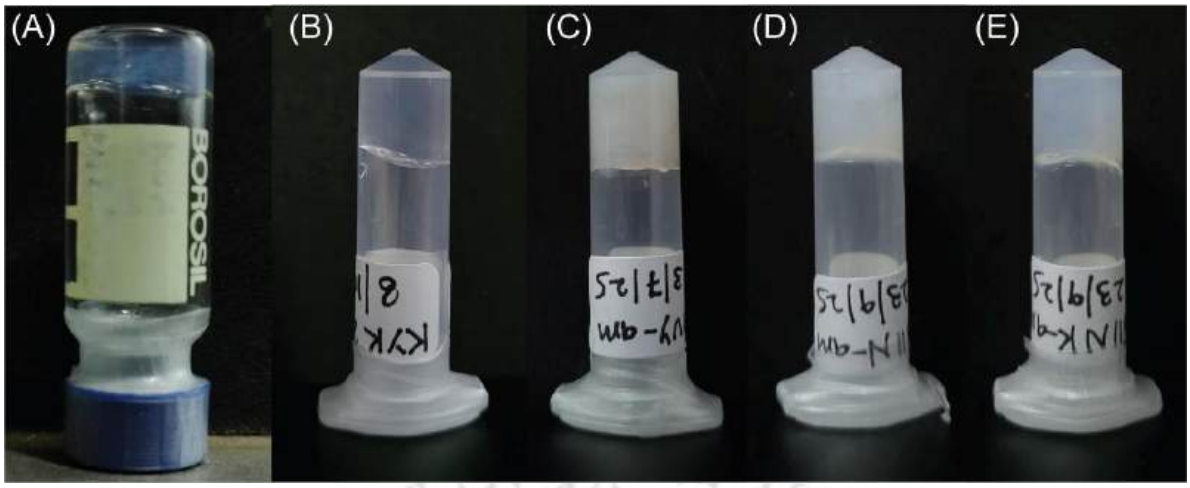

Figure 5.1. Inverted tubes showing hydrogels formed by (A) KYVIQV-am, (B) Ac-KVQIVYK-am, (C) Ac-KVQIVY-am, (D) Ac-KVQIIN-am, and (E) Ac-KVQIINK-am.

Given that subtle modifications in peptide sequences can modulate self-assembly, potentially altering the internal architecture of the resulting hydrogels, I investigated the viscoelastic properties of the hydrogels using oscillatory rheology. Rheological measurements were performed on 24-hour-old hydrogels to ensure direct comparison with our previously reported hydrogels [223]. The 24-hour-old 20 mM Ac-PHF6 hydrogel reported in Chapter 2 exhibited a storage modulus (G′) of approximately 20 kPa over a frequency range of 0.01-624 rad/s [223]. Ac-KVQIVYK-am hydrogel exhibited higher complex modulus compared to that reported for Ac-PHF6 hydrogel (Fig. 5.2C). The retropeptide KYVIQV-am, on the other hand, exhibited lower complex modulus. The storage modulus is around 2-fold lesser than that reported for Ac-PHF6 hydrogel (Fig. 5.2A). This reduced mechanical strength may be attributed to electrostatic repulsion at the uncapped N-terminus, which likely disrupts efficient packing and network formation, an effect not observed in the fully capped analogs. Ac-KVQIVY-am hydrogel (15 mM peptide concentration), intuitively, exhibited a relatively low mechanical strength, with a storage modulus of ~6-8 kPa (Fig. 5.2B). Ac-KVQIIN-am and Ac-KVQIINK-am hydrogels, even though prepared at 15 mM concentration, exhibited a storage modulus of ~20 kPa, similar to that observed for 20 mM Ac-PHF6 hydrogel (Fig. 5.2D and 5.2E). The Ac-PHF6* analogs, therefore, are better gelators than the Ac-PHF6 analogs. These results suggest that small alterations in peptide sequence and terminal capping can substantially influence the mechanical rigidity of hydrogels, thereby offering a tunable approach to design peptide-based materials with tailored viscoelastic properties.

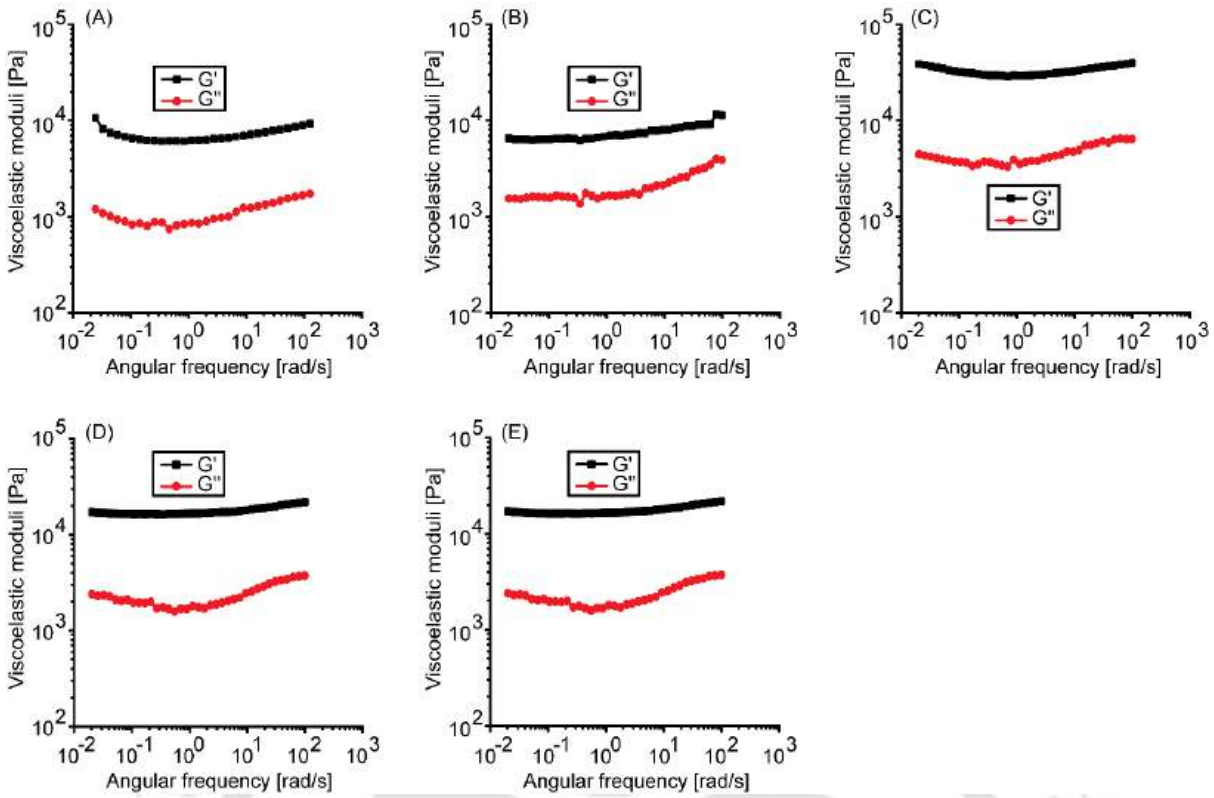

Figure 5.2. Rheological assessment of peptide hydrogels obtained from (A) KYVIQV-am, (B) Ac-KVQIVY-am, (C) Ac-KVQIVYK-am, (D) Ac-KVQIIN-am, and (E) Ac-KVQIINK-am.

5.3.2. Intrinsic tyrosine fluorescence

As Ac-PHF6 analogs have a tyrosine residue, tyrosine fluorescence was measured. To minimize the impact of concentration-dependent artefacts such as the inner-filter effect, intrinsic tyrosine fluorescence emission spectra were recorded by diluting the samples to 200 µM concentration. Upon excitation at 280 nm, all water samples exhibited emission maxima centered around 303 nm (Fig. 5.3), a characteristic of Tyr fluorescence. The PBS samples of all three peptides displayed lower emission intensity. This attenuation likely reflects differences in the local microenvironment surrounding the Tyr residues in the self-assembled structures. Several factors may contribute to this decreased emission, including increased local chromophore density within aggregates, which can flatten absorbance and reduce effective excitation, quenching effects arising from π–π stacking of Tyr residues during peptide aggregation, and the presence of Cl^- ions in PBS. These results suggest that the peptides display pronounced self-assembly in PBS than in water. imply that the peptides adopt more tightly packed or quenched conformations in PBS, consistent with an aggregation-driven fluorescence suppression mechanism. In addition to lower emission intensity, a slight (~3 nm) blue shift is also observed in Ac-KVQIVY-am in PBS (Fig. 5.3B). Unlike the other two peptides, the

tyrosine residue in Ac-KVQIVY-am is at the terminus and therefore more accessible to the solvent and the ions present in PBS. Metal ions have been reported in the literature to cause shifts in the tyrosine emission spectra [240]. Sodium ion is known to cause blue shift in tyrosine emission spectrum.

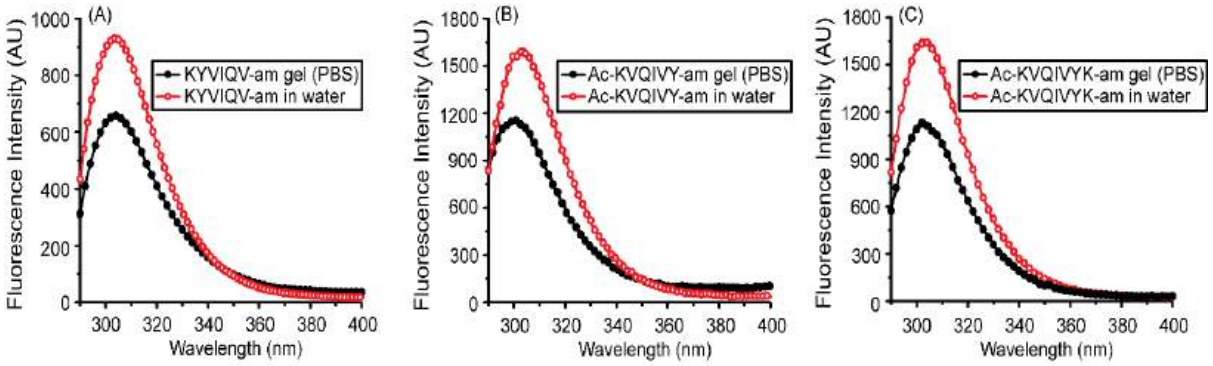

Figure 5.3. Intrinsic Tyr spectra of (A) KYVIQV-am, (B) Ac-KVQIVY-am, and (C) Ac-KVQIVYK-am.

5.3.3. ThT fluorescence

ThT is a benzothiazole-based fluorescent dye that is widely used to detect amyloid fibrils. Binding to amyloid fibrils causes a marked enhancement in its quantum yield. The ThT fluorescence spectra for the Ac-PHF6 analogs are presented in Fig. 5.4A-C. KYVIQV-am and Ac-KVQIVY-am display distinct enhancement in ThT fluorescence emission, with PBS samples showing notably higher ThT fluorescence signal compared to the samples prepared in water (Fig. 5.4A and 5.4B). KYVIQV-am in PBS caused around 7-fold enhancement in ThT fluorescence emission intensity, whereas water sample caused only around 3-fold enhancement (Fig. 5.4A). This data suggests that the peptide displays far better self-assembly in PBS than in water. This property is attributed to the double-charged N-terminal residue. The peptide molecules would experience stronger electrostatic repulsion in water than in PBS. Masking of the charges by salt in PBS would facilitate self-assembly. The ThT fluorescence emission enhancement caused by Ac-KVQIVY-am is higher than that caused by KYVIQV-am, and difference between the water and PBS samples is modest (Fig. 5.4B). No appreciable enhancement in ThT fluorescence intensity was observed for bolaamphiphile peptide Ac-KVQIVYK-am (Fig. 5.4C). These data indicate a lack of canonical amyloid fibrils. The Ac-PHF6* analogs demonstrated a markedly higher ThT fluorescence compared to the Ac-PHF6 analogs. Ac-KVQIIN-am showed a little higher fluorescence intensity in PBS than in water (Fig. 5.4D). The ThT fluorescence emission intensity observed for Ac-KVQIINK-am in PBS is comparable to that observed for Ac-KVQIIN-am (Fig. 5.4E). However, the fluorescence

intensity in water is lower, probably due to the presence of lysine residue at both the termini. In the absence of salt, the electrostatic repulsion between peptide chains would adversely affect the self-assembly.

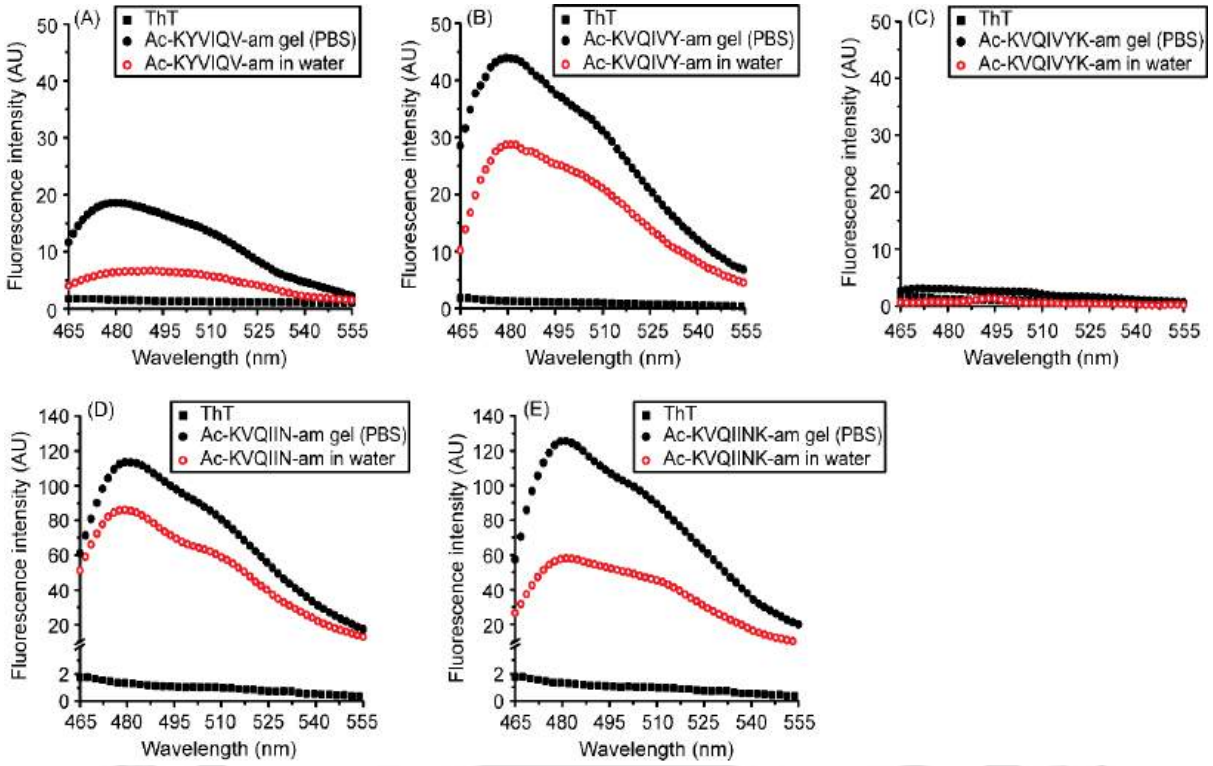

Figure 5.4. ThT fluorescence emission spectra for (A) KYVIQV-am, (B) Ac-KVQIVY-am, (C) Ac-KVQIVYK-am, (D) Ac-KVQIIN-am, and (E) Ac-KVQIINK-am.

5.3.4. CD spectroscopy

The secondary structures of the peptides in the self-assembled structures were investigated using far-UV CD spectroscopy. The peptide samples were diluted to 200 μM in their respective dispersants prior to CD measurements. In water, KYVIQV-am exhibited a prominent negative band near 200 nm, accompanied by minor shoulders at 210 and 215 nm, indicative of a predominantly unordered conformation (Fig. 5.5A). In PBS, the peptide displayed a negative band around 220 nm with a very weak positive band around 207 nm, and another weak negative band around 200 nm. The spectrum is suggestive of a mixture of β-sheet and random coil conformations. Ac-KVQIVY-am, in water, displayed a spectrum with the negative bands around 218 and 198 nm. The spectrum is suggestive of a mixture of β-sheet and random coil conformations (Fig. 5.5B). In PBS, the spectrum is that of typical β-sheets, with a broad negative band around 220 nm and a positive band near 200 nm. The CD profile closely resembles that reported for Ac-PHF6 in PBS, supporting the formation of amyloid-like β-sheet

assemblies under physiological ionic strength. Ac-KVQIVYK-am in water displayed a negative band around 200 nm with a shoulder 218 nm. The spectral signature is suggestive of a largely disordered conformation (Fig. 5.5C). In PBS, the peptide displayed a slightly red-shifted high energy band and a more pronounced 218 nm, indicating a mixture of random coil and β-sheet conformations. Ac-KVQIIN-am exhibited negative bands near 200 and 220 nm in water, indicating a combination of β-sheet and random coil conformations (Fig. 5.5D). In PBS, the peptide displayed a very high ellipticity positive band around 202 nm alongside a much less intense negative band around 225 nm. This CD signature is assigned to β-sheet structures. The CD spectrum of Ac-KVQIINK-am in water is very similar that that observed for Ac-KVQIIN-am in water (Fig. 5.5E). In PBS, however, the spectrum is dramatically different, instead of an intense band positive band around 202 nm, an intense negative band is observed. Such band in the literature has been assigned to β_{II} proteins [233]. Spectrum with similar features has also been reported for Ac-PHF6* in PBS. These results highlight the sensitivity of peptide self-assembly and secondary structure to minor sequence modifications.

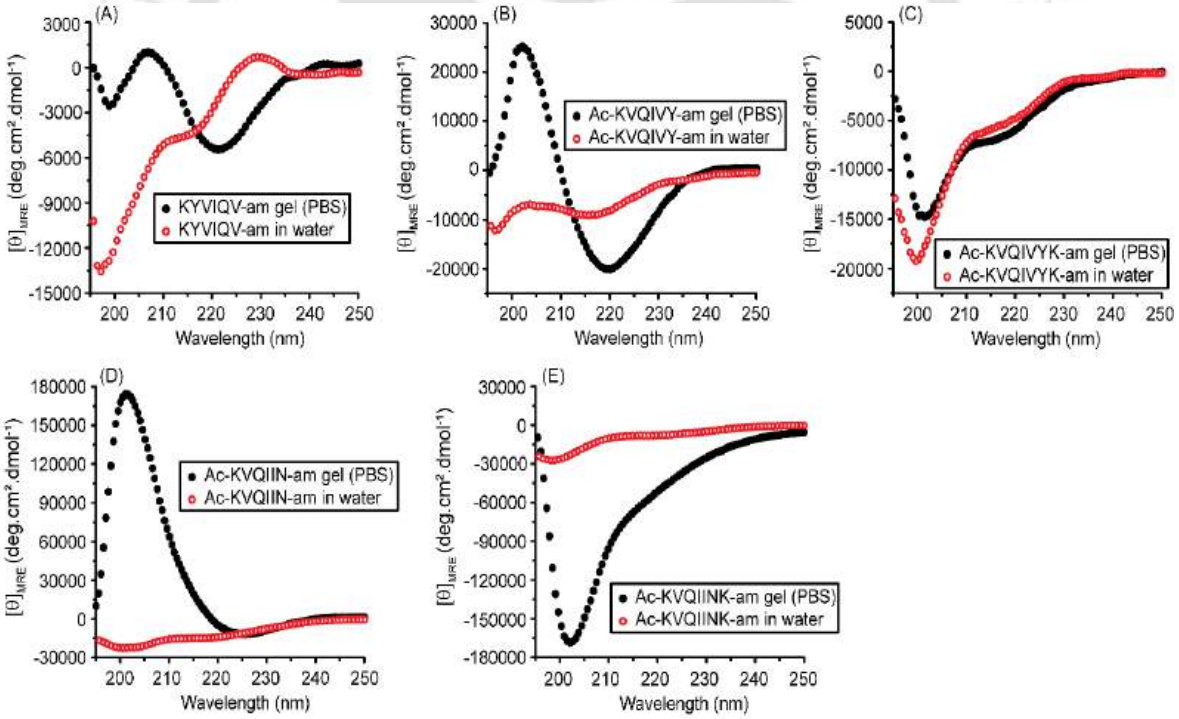

Figure 5.5. CD spectra of (A) KYVIQV-am, (B) Ac-KVQIVY-am, (C) Ac-KVQIVYK-am, (D) Ac-KVQIIN-am, and (E) Ac-KVQIINK-am.

5.3.5. FTIR spectroscopy

Infrared spectroscopy is a powerful tool to investigate the secondary structures of proteins and peptides. The frequency of amide I band, in particular, is very sensitive to the conformation of the polypeptide backbone. The secondary structure of the peptide hydrogels was further examined using ATR-FTIR spectroscopy. Spectra were acquired for both PBS and water samples after air-drying them on the diamond ATR crystal. All the samples displayed amide I band centred around 1626 cm^{-1} (Fig. 5.6). This band validates the presence of β-sheet conformation. The disagreement between CD and FTIR data is attributed to the differences in the experimental conditions. The peptide samples were diluted 2-fold for FTIR spectroscopy, and dried after depositing on the ATR crystal. Drying is accompanied with an increase in concentration. Therefore, the peptide samples were barely diluted for the assay. CD spectroscopy, unfortunately, cannot be carried out at high concentrations. The samples were diluted to 200 μM concentration for the assay, *i.e.* a 75-fold dilution for 15 mM samples, and a 100-fold dilution for the 20 mM samples. Such large dilutions can shift the equilibrium towards breakdown of self-assembled structures, thereby contributing to the unordered conformation.

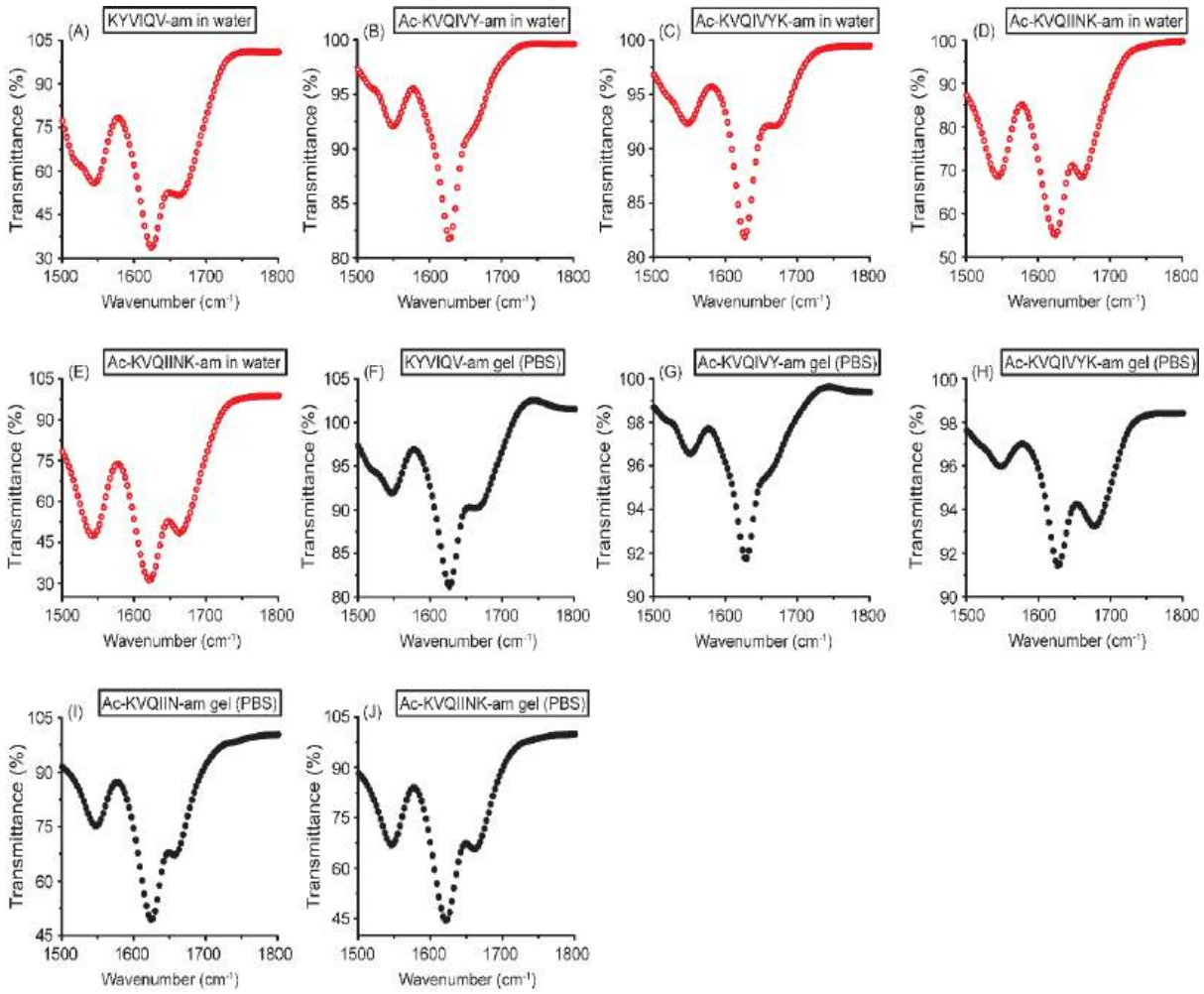

Figure 5.6. FTIR spectra of (A, F) KYVIQV-am, (B, G) Ac-KVQIVY-am, (C, H) Ac-KVQIVYK-am, (D, I) Ac-KVQIIN-am, and (E, J) Ac-KVQIINK-am. The red traces represent water samples, while black traces are for PBS samples.

5.3.6. Transmission Electron Microscopy

The morphology of the self-assembled nanostructures underlying the hydrogels was examined using TEM. All peptide gel samples revealed the presence of elongated fibrillar structures, although the fiber thickness and length varied significantly among the peptides. The KYVIQV-am, Ac-KVQIIN-am, and Ac-KVQIINK-am exhibited long, straight fibrils that closely resemble the morphology previously reported in the literature for Ac-PHF6 (Fig. 5.7A, 5.7D and 5.7E) [159]. In contrast, the Ac-KVQIVY-am formed long and rather straight fibrils, whereas Ac-KVQIVYK-am peptide formed distinctly thinner, more flexible elongated fibrils (Fig. 5.7C). These data indicate that subtle variations in self-assembled peptides can have dramatic effects on their mode of assembly. Such effects can also define the emergent properties of the self-assembled structures.

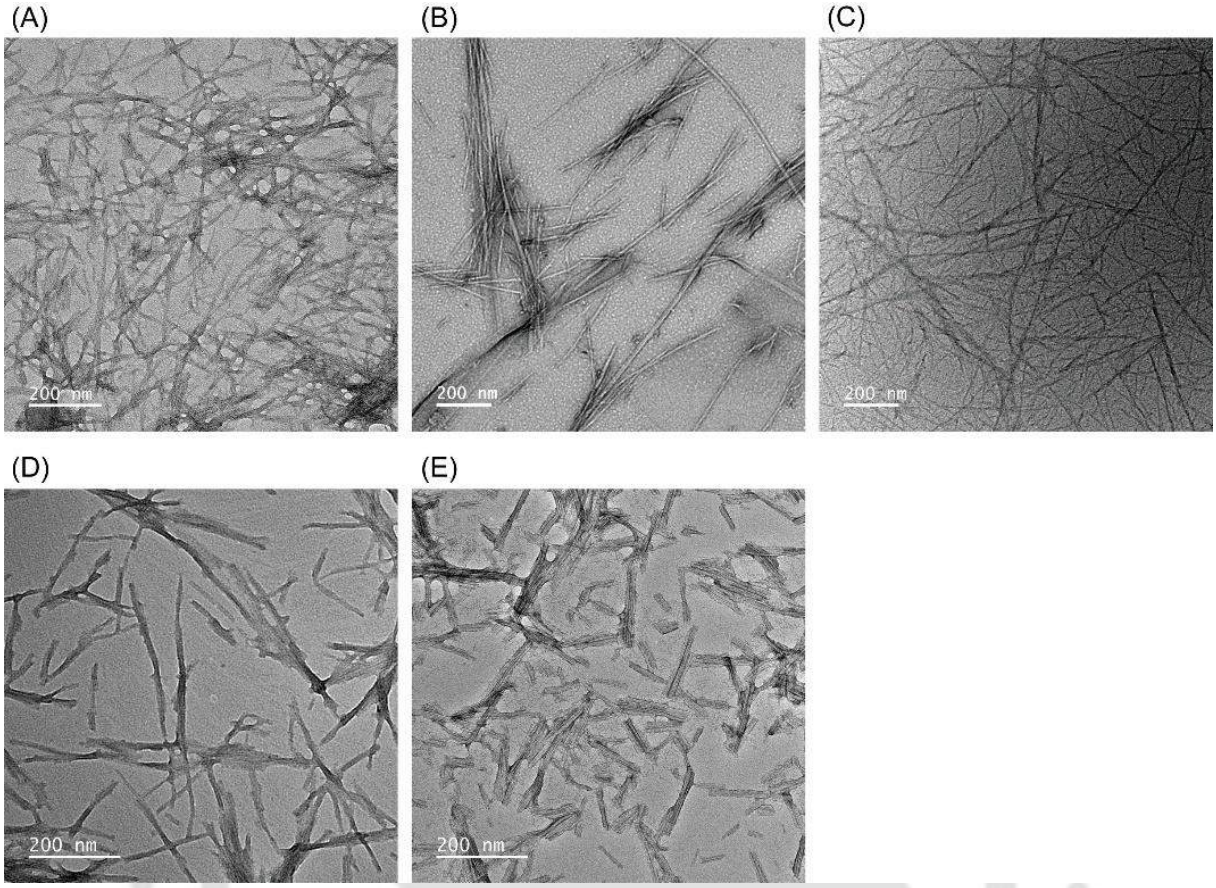

Figure 5.7. TEM images of (A) KYVIQV-am, (B) Ac-KVQIVY-am, (C) Ac-KVQIVYK-am, (D) Ac-KVQIIN-am, and (E) Ac-KVQIINK-am.

5.3.7. Cytocompatibility of hydrogels

The cytocompatibility of hydrogels derived from KYVIQV-am and Ac-KVQIVYK-am was evaluated using HEK-293 cells. Cells were cultured on 24-hour-old hydrogels for 24 hours, after which the expression of the housekeeping gene GAPDH was assessed. The cells grown in the absence of hydrogels served as the positive control. Following incubation, the total RNA was extracted from both the positive control and hydrogel-treated cells, and reverse transcription PCR (RT-PCR) was performed. The expression of GAPDH in cells cultured on hydrogels suggests that the hydrogels are compatible for cell culture (Fig. 5.8A). The biocompatibility was further assessed using MTT assay, an assay that is routinely employed to measure cell viability. This colorimetric assay relies on the ability of metabolically active cells to reduce MTT to formazan, which exhibits absorbance at 570 nm. Non-viable cells, lacking this metabolic activity, do not contribute to the signal. Cell viability was expressed as a percentage relative to untreated control cells. The results demonstrated no significant decrease in cell viability across the tested concentrations, indicating that both KYVIQV-am and Ac-KVQIVYK-am hydrogels are non-cytotoxic up to 200 μM concentration (Fig. 5.8B, and 5.8C).

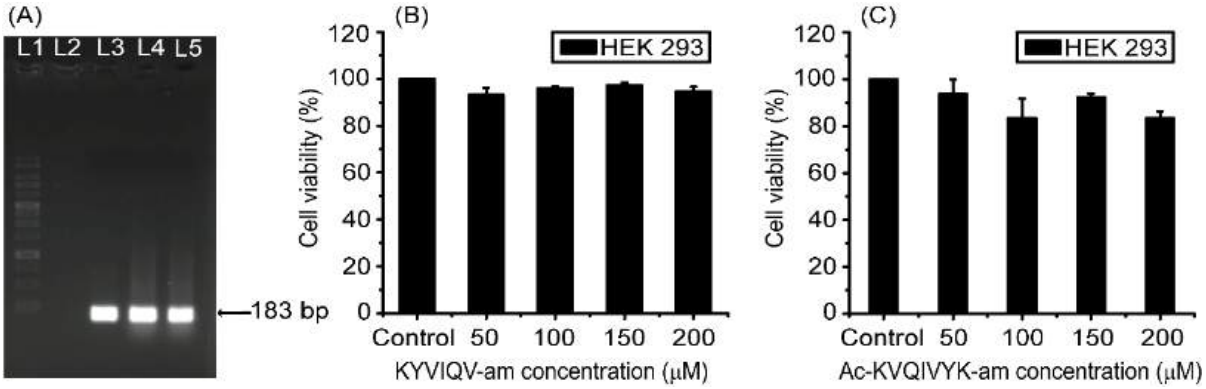

Figure 5.8. Cytocompatibility evaluation of peptide hydrogels. (A) GAPDH expression analyzed via RT-PCR. Lane L1: molecular weight marker; L2: negative control; L3: positive control (HEK-293 cells cultured without peptide hydrogel); L4 and L5: HEK-293 cells grown on 10 mM KYVIQV-am and Ac-KVQIVYK-am hydrogels, respectively. MTT assay results showing cell viability of HEK-293 cells cultured on (B) KYVIQV-am and (C) Ac-KVQIVYK-am hydrogels.

5.4. Conclusions

Ac-PHF6 and Ac-PHF6* harbour a lysine residue at C-terminus. I investigated their analogs by placing the lysine residue at N-terminus. KVQIVY-am, though has a pair of charges at N-terminus residue, failed to cause hydrogelation. N-terminal acetylation of the peptide, turned it into a hydrogelator. Interestingly, however, the retropeptide with free amino terminus also turned out to be a gelator, albeit with lower stiffness than that reported for Ac-PHF6. Out of curiosity, I also employed a bolaamphilic analog having a lysine residue at both N and C termini. The bolaamphile of Ac-PHF6 turned out to be a strong gelator with complex modulus higher than that reported for Ac-PHF6 at identical (20 mM) concentration. The Ac-PHF6* analogs (Ac-KVQIIN-am and Ac-KVQIINK-am), that also happen to be native sequences in tau protein, formed 15 mM hydrogels with storage moduli comparable to 20 mM Ac-PHF6 hydrogel. To conclude, the guidelines drawn about hydrogelation from the tripeptide sequence space do not directly translate to longer sequences.

CHAPTER 6

Conclusions and Future Directions

6.1 Conclusions

The diverse applications that the hydrogels promise to offer in healthcare are one of the major driving forces of the hydrogel research. Among the various classes of materials that form hydrogels, peptides have gained special attention. Peptides, especially the short ones, are straightforward to synthesize. They offer high chemical diversity, and they are native to living organism. A large number of peptide and peptide-based hydrogels have been reported in the literature. Of particular note are the ones that harbour a bulky non-native aromatic moiety at their N-terminus. Fluorenyl, followed by naphthyl, happen to be the most widely employed aromatic moiety in dipeptide and tripeptide hydrogels. Such aromatic moieties drive self-assembly through aromatic stacking interactions. The self-assembled structures then form 3-dimensional matrices that may cause gelation. Even though such structures have shown promising results as far as their applications in healthcare are concerned, the concern about their safety persist. For instance, degradation of Fmoc-protected peptide can cause release of highly-reactive dibenzofulvene moiety that can cause cytotoxicity [153]. Besides, the Fmoc-decorated superstructures underlying the hydrogels could have immunogenicity concerns.

The aim of this doctoral thesis was to identify native peptide sequences that cause hydrogelation at physiological ionic strength or can be engineered through minimal modifications to do so. Amyloid forming proteins and peptides are well-studied systems in the context of diseases. However, they have also been explored as promising materials in past few decades. They form β-sheet rich fibrils that can also cause gelation. I, therefore, focused on well-studied short (<10 residues) amyloidogenic peptides. As aromatic residues have been reported in the literature to facilitate the self-assembly of short peptide sequences, I surveyed short aromatic amino acid-containing amyloid peptides. It is imperative that a peptide that resists self-assembly in water, but self-assembles under high salt conditions must have a net charge. Therefore, the peptides having no net charge were rejected. If the charged residues are juxtaposed in the self-assembled structures, the assembly would be further inhibited. I, therefore, focused on peptide(s) that self-assemble through parallel β-sheet formation. Out criteria led me to PHF6. The uncapped peptide self-assembles through parallel β-sheet formation [160]. Even though the uncapped peptide PHF6 failed to cause hydrogelation, the end-capped peptide Ac-PHF6 turned out to be a promising injectable hydrogelator. The peptide remained as viscous solution in water, but caused hydrogelation of PBS and cell culture media. The gels were found to be cytocompatible that allowed cell culture. Further investigations

revealed that substitution of Tyr with electron-withdrawing aromatic and aliphatic amino acids does improve self-assembly but aromaticity is not essential for self-assembly and hydrogelation. The Ac-PHF6* was also found to be a gelator.

6.2 Future scopes

The self-assembly and hydrogelation of Ac-PHF6 and Ac-PHF6* suggest that short, native peptide stretches can turn out to be promising hydrogelators or could be engineered into hydrogelators through minimal modifications. I showed that the Ac-PHF6 and Ac-PHF6* hydrogels are cytocompatible and can be used for cell culture. It would be interesting to see if the hydrogel matrix could support growth of primary cells and organoids. The sequences could be tagged with bioactive motifs such as RGD to support organoid culture or tissue-specific applications. At the applications front, there are many applications that could not be taken up, but could be explored in future. For instance, substitutions of the tyrosine residue in Ac-PHF6 did not adversely affect its hydrogelation. This implies that tyrosine could be used to tag the drugs with carboxylate groups through an ester linkage, without affecting its hydrogelation propensity. The release would depend on the esterase activity in a biological system as well as diffusion through the hydrogel matrix. Such drugs are expected to exhibit sustained release for longer during. were irrespective of the results. The other aspect that could not be taken up as part of this thesis is the entrapment/release of large entities such as proteins, nucleic acids, and nanoparticles or even the cells. As biologics are rapidly shaping up the medicine, entrapment/release of such entities is of high therapeutic value. Another promising direction involves leveraging the Tyr residue of Ac-PHF6 for photo-crosslinking *via* dityrosine formation, which could modulate both self-assembly and hydrogelation. I assumed that a peptide stretch that is native to humans would be biocompatible without any immune reactions. However, this aspect has not been explicitly established. Immunogenicity, inflammatory responses, serum stability, and *in vivo* clearance/degradation of the hydrogels have also not been assessed.

It is important to note that I have explored only a couple of related native peptide sequences that were selected by manually surveying the short amyloidogenic sequences that I came across. I have completely overlooked the native protein/protein interactions. The native proteins could harbour short stretches that drive their interaction, and could be explored for self-assembly and hydrogelation. I believe that the existing peptide hydrogelation data and the

interaction databases could be used to train the artificial intelligence models. Such artificial intelligence tools could mine the yet hidden hydrogelating gems.

References

[1] D. Mandal, A. Nasrolahi Shirazi, and K. Parang, "Self-assembly of peptides to nanostructures," *Org. Biomol. Chem.*, vol. 12, no. 22, pp. 3544–3561, 2014, doi: 10.1039/c4ob00447g.

[2] L. Ruan *et al.*, "Designed amphiphilic peptide forms stable nanoweb , slowly releases encapsulated hydrophobic drug , and accelerates animal hemostasis," vol. 106, no. 13, pp. 1–6, 2009, doi: 10.1073/pnas.0900026106.

[3] A. Altunbas, S. J. Lee, S. A. Rajasekaran, J. P. Schneider, and D. J. Pochan, "Encapsulation of curcumin in self-assembling peptide hydrogels as injectable drug delivery vehicles," *Biomaterials*, vol. 32, no. 25, pp. 5906–5914, 2011, doi: https://doi.org/10.1016/j.biomaterials.2011.04.069.

[4] P. Worthington, S. Langhans, and D. Pochan, "β-hairpin peptide hydrogels for package delivery," *Adv. Drug Deliv. Rev.*, vol. 110–111, pp. 127–136, 2017, doi: https://doi.org/10.1016/j.addr.2017.02.002.

[5] J. B. Matson and S. I. Stupp, "Self-assembling peptide scaffolds for regenerative medicine," *Chem. Commun.*, vol. 48, no. 1, pp. 26–33, 2012, doi: 10.1039/c1cc15551b.

[6] N. Changsan *et al.*, "BrSPR-20-P1 peptide isolated from Brevibacillus sp. developed into liposomal hydrogel as a potential topical antimicrobial agent," *RSC Adv.*, vol. 14, no. 37, pp. 27394–27411, 2024, doi: 10.1039/D4RA03722G.

[7] N. Özbek, E. L. Vilarrocha, B. V. Jover, E. F. Ventura, and B. Escuder, "Lysine-based non-cytotoxic ultrashort self-assembling peptides with antimicrobial activity," *RSC Adv.*, vol. 14, no. 21, pp. 15120–15128, 2024, doi: 10.1039/D3RA08883A.

[8] K. Basu *et al.*, "Peptide based hydrogels for cancer drug release: modulation of stiffness, drug release and proteolytic stability of hydrogels by incorporating d-amino acid residue(s)," *Chem. Commun.*, vol. 52, no. 28, pp. 5045–5048, 2016, doi: 10.1039/C6CC01744D.

[9] A. Dasgupta, J. H. Mondal, and D. Das, "Peptide hydrogels," *RSC Adv.*, vol. 3, no. 24, pp. 9117–9149, 2013, doi: 10.1039/c3ra40234g.

[10] D. A. Salick, D. J. Pochan, and J. P. Schneider, "Design of an Injectable β-Hairpin

Peptide Hydrogel That Kills Methicillin-Resistant Staphylococcus aureus," *Adv. Mater.*, vol. 21, no. 41, pp. 4120–4123, Nov. 2009, doi: https://doi.org/10.1002/adma.200900189.

[11] V. Jayawarna *et al.*, "Nanostructured Hydrogels for Three-Dimensional Cell Culture Through Self-Assembly of Fluorenylmethoxycarbonyl–Dipeptides," *Adv. Mater.*, vol. 18, no. 5, pp. 611–614, Mar. 2006, doi: https://doi.org/10.1002/adma.200501522.

[12] A. Baral *et al.*, "Assembly of an Injectable Noncytotoxic Peptide-Based Hydrogelator for Sustained Release of Drugs," *Langmuir*, vol. 30, no. 3, pp. 929–936, Jan. 2014, doi: 10.1021/la4043638.

[13] J. Naskar, G. Palui, and A. Banerjee, "Tetrapeptide-Based Hydrogels: for Encapsulation and Slow Release of an Anticancer Drug at Physiological pH," *J. Phys. Chem. B*, vol. 113, no. 35, pp. 11787–11792, Sep. 2009, doi: 10.1021/jp904251j.

[14] D. A. Salick, J. K. Kretsinger, D. J. Pochan, and J. P. Schneider, "Inherent Antibacterial Activity of a Peptide-Based β-Hairpin Hydrogel," *J. Am. Chem. Soc.*, vol. 129, no. 47, pp. 14793–14799, Nov. 2007, doi: 10.1021/ja076300z.

[15] J. D. Hartgerink, E. Beniash, and S. I. Stupp, "Self-Assembly and Mineralization of Peptide-Amphiphile Nanofibers," *Science (80-.).*, vol. 294, no. 5547, pp. 1684–1688, Nov. 2001, doi: 10.1126/science.1063187.

[16] L. Haines-Butterick *et al.*, "Controlling hydrogelation kinetics by peptide design for three-dimensional encapsulation and injectable delivery of cells," *Proc. Natl. Acad. Sci.*, vol. 104, no. 19, pp. 7791–7796, May 2007, doi: 10.1073/pnas.0701980104.

[17] D. Datta and N. Chaudhary, "Chapter 8 - Peptide-based hydrogels for biomedical applications," Y. B. T.-T. B. Hasija, Ed. Academic Press, 2021, pp. 203–232.

[18] X. D. Xu *et al.*, "Peptide hydrogel as an intraocular drug delivery system for inhibition of postoperative scarring formation," *ACS Appl. Mater. Interfaces*, vol. 2, no. 9, pp. 2663–2671, 2010, doi: 10.1021/am100484c.

[19] A. Baral, S. Roy, S. Ghosh, D. Hermida-Merino, I. W. Hamley, and A. Banerjee, "A Peptide-Based Mechano-sensitive, Proteolytically Stable Hydrogel with Remarkable Antibacterial Properties," *Langmuir*, vol. 32, no. 7, pp. 1836–1845, Feb. 2016, doi: 10.1021/acs.langmuir.5b03789.

[20] B. Hansda *et al.*, "Histidine-Containing Amphiphilic Peptide-Based Non-Cytotoxic Hydrogelator with Antibacterial Activity and Sustainable Drug Release," *Langmuir*, vol. 39, no. 21, pp. 7307–7316, May 2023, doi: 10.1021/acs.langmuir.3c00235.

[21] C. A. E. Hauser and S. Zhang, "Designer self-assembling peptide nanofiber biological materials," *Chem. Soc. Rev.*, vol. 39, no. 8, pp. 2780–2790, 2010, doi: 10.1039/b921448h.

[22] M. Rizwan *et al.*, "pH sensitive hydrogels in drug delivery: Brief history, properties, swelling, and release mechanism, material selection and applications," *Polymers (Basel).*, vol. 9, no. 4, 2017, doi: 10.3390/polym9040137.

[23] D. Seliktar, "Designing Cell-Compatible Hydrogels," vol. 336, no. June, pp. 1124–1129, 2012.

[24] J. Y. Sun *et al.*, "Highly stretchable and tough hydrogels," *Nature*, vol. 489, no. 7414, pp. 133–136, 2012, doi: 10.1038/nature11409.

[25] S. Loic, "Amino Acids Modification to Improve and Fine-Tune Peptide- Based Hydrogels," *Amin. Acid - New Insights Roles Plant Anim.*, 2017, doi: 10.5772/intechopen.68705.

[26] T. Vijayakanth *et al.*, "Peptide hydrogen-bonded organic frameworks," *Chem. Soc. Rev.*, vol. 53, no. 8, pp. 3640–3655, 2024, doi: 10.1039/D3CS00648D.

[27] P. Chakraborty *et al.*, "Unusual Two-Step Assembly of a Minimalistic Dipeptide-Based Functional Hypergelator," *Adv. Mater.*, vol. 32, no. 9, p. 1906043, Mar. 2020, doi: https://doi.org/10.1002/adma.201906043.

[28] M.-M. Guy and N. Voyer, "Structure and hydrogel formation studies on homologs of a lactoglobulin-derived peptide," *Biophys. Chem.*, vol. 163–164, pp. 1–10, 2012, doi: https://doi.org/10.1016/j.bpc.2011.12.005.

[29] R. Bischoff and H. Schlüter, "Amino acids: Chemistry, functionality and selected non-enzymatic post-translational modifications," *J. Proteomics*, vol. 75, no. 8, pp. 2275–2296, 2012, doi: 10.1016/j.jprot.2012.01.041.

[30] L. M. De Leon Rodriguez, Y. Hemar, J. Cornish, and M. A. Brimble, "Structure-mechanical property correlations of hydrogel forming β-sheet peptides," *Chem. Soc. Rev.*, vol. 45, no. 17, pp. 4797–4824, 2016, doi: 10.1039/c5cs00941c.

[31] C. Diaferia, G. Morelli, and A. Accardo, “Fmoc-diphenylalanine as a suitable building block for the preparation of hybrid materials and their potential applications,” *J. Mater. Chem. B*, vol. 7, no. 34, pp. 5142–5155, 2019, doi: 10.1039/c9tb01043b.

[32] D. T. Eddington and D. J. Beebe, “Flow control with hydrogels,” *Adv. Drug Deliv. Rev.*, vol. 56, no. 2, pp. 199–210, 2004, doi: 10.1016/j.addr.2003.08.013.

[33] H. Wang and W. Zhao, “Application of hydrogel for energy storage and conversion,” *Next Mater.*, vol. 1, no. 4, p. 100049, 2023, doi: https://doi.org/10.1016/j.nxmate.2023.100049.

[34] N. Kaur, Hamid, P. Choudhary, and A. K. Jaiswal, “Recent progress in bioactive loaded hydrogels for food applications,” *J. Agric. Food Res.*, vol. 20, p. 101756, 2025, doi: https://doi.org/10.1016/j.jafr.2025.101756.

[35] L. Li, P. Wu, F. Yu, and J. Ma, “Double network hydrogels for energy/environmental applications: challenges and opportunities,” *J. Mater. Chem. A*, vol. 10, no. 17, pp. 9215–9247, 2022, doi: 10.1039/D2TA00540A.

[36] L. Tang *et al.*, “A sequential light-harvesting system with thermosensitive colorimetric emission in both aqueous solution and hydrogel,” *Chem. Commun.*, vol. 60, no. 35, pp. 4719–4722, 2024, doi: 10.1039/D4CC00616J.

[37] L. Hu *et al.*, “Hydrogel-Based Flexible Electronics,” *Adv. Mater.*, vol. 35, no. 14, p. 2205326, Apr. 2023, doi: https://doi.org/10.1002/adma.202205326.

[38] A. S. Hoffman, “Hydrogels for biomedical applications,” *Adv. Drug Deliv. Rev.*, vol. 64, no. SUPPL., pp. 18–23, 2012, doi: 10.1016/j.addr.2012.09.010.

[39] K. Na, K. H. Lee, and Y. H. Bae, “pH-sensitivity and pH-dependent interior structural change of self-assembled hydrogel nanoparticles of pullulan acetate/oligo-sulfonamide conjugate,” *J. Control. Release*, vol. 97, no. 3, pp. 513–525, 2004, doi: 10.1016/j.jconrel.2004.04.005.

[40] K. S. De, N. R. Aluru, B. Johnson, W. C. Crone, D. J. Beebe, and J. Moore, “Equilibrium swelling and kinetics of pH-responsive hydrogels: Models, experiments, and simulations,” *J. Microelectromechanical Syst.*, vol. 11, no. 5, pp. 544–555, 2002, doi: 10.1109/JMEMS.2002.803281.

[41] R. Zheng *et al.*, “Assembly of short amphiphilic peptoids into nanohelices with

controllable supramolecular chirality," *Nat. Commun.*, vol. 15, no. 1, pp. 1–9, 2024, doi: 10.1038/s41467-024-46839-y.

[42] H. Yan, A. Saiani, J. E. Gough, and A. F. Miller, "Thermoreversible protein hydrogel as cell scaffold," *Biomacromolecules*, vol. 7, no. 10, pp. 2776–2782, 2006, doi: 10.1021/bm0605560.

[43] D. E. Owens, Y. Jian, J. E. Fang, B. V. Slaughter, Y. H. Chen, and N. A. Peppas, "Thermally responsive swelling properties of polyacrylamide/poly(acrylic acid) interpenetrating polymer network nanoparticles," *Macromolecules*, vol. 40, no. 20, pp. 7306–7310, 2007, doi: 10.1021/ma071089x.

[44] J. Naskar, G. Palui, and A. Banerjee, "Tetrapeptide-based hydrogels: For encapsulation and slow release of an anticancer drug at physiological ph," *J. Phys. Chem. B*, vol. 113, no. 35, pp. 11787–11792, 2009, doi: 10.1021/jp904251j.

[45] M. A. Ward and T. K. Georgiou, "Thermoresponsive polymers for biomedical applications," *Polymers (Basel).*, vol. 3, no. 3, pp. 1215–1242, 2011, doi: 10.3390/polym3031215.

[46] L. A. Haines, K. Rajagopal, B. Ozbas, D. A. Salick, D. J. Pochan, and J. P. Schneider, "Light-activated hydrogel formation via the triggered folding and self-assembly of a designed peptide," *J. Am. Chem. Soc.*, vol. 127, no. 48, pp. 17025–17029, 2005, doi: 10.1021/ja054719o.

[47] Y. Ding, Y. Li, M. Qin, Y. Cao, and W. Wang, "Photo-cross-linking approach to engineering small tyrosine-containing," *Langmuir*, vol. 29, no. 43, pp. 13299–13306, 2013, doi: 10.1021/la4029639.

[48] M. Choi, J. W. Choi, S. Kim, S. Nizamoglu, S. K. Hahn, and S. H. Yun, "Light-guiding hydrogels for cell-based sensing and optogenetic synthesis in vivo," *Nat. Photonics*, vol. 7, no. 12, pp. 987–994, 2013, doi: 10.1038/nphoton.2013.278.

[49] J. Li, R. Xing, S. Bai, and X. Yan, "Recent advances of self-assembling peptide-based hydrogels for biomedical applications," *Soft Matter*, vol. 15, no. 8, pp. 1704–1715, 2019, doi: 10.1039/C8SM02573H.

[50] C. Diaferia *et al.*, "Bi-functional peptide-based 3D hydrogel-scaffolds," *Soft Matter*, vol. 16, no. 30, pp. 7006–7017, 2020, doi: 10.1039/D0SM00825G.

[51] C. Liu, Q. Zhang, S. Zhu, H. Liu, and J. Chen, "Preparation and applications of peptide-based injectable hydrogels," *RSC Adv.*, vol. 9, no. 48, pp. 28299–28311, 2019, doi: 10.1039/C9RA05934B.

[52] Q. Chai, Y. Jiao, and X. Yu, "Hydrogels for biomedical applications: Their characteristics and the mechanisms behind them," *Gels*, vol. 3, no. 1, 2017, doi: 10.3390/gels3010006.

[53] T. P. J. Knowles and M. J. Buehler, "Nanomechanics of functional and pathological amyloid materials," *Nat. Nanotechnol.*, vol. 6, no. 8, pp. 469–479, 2011, doi: 10.1038/nnano.2011.102.

[54] H. Arakawa, K. Takeda, S. L. Higashi, A. Shibata, Y. Kitamura, and M. Ikeda, "Self-assembly and hydrogel formation ability of Fmoc-dipeptides comprising α-methyl-L-phenylalanine," *Polym. J.*, vol. 52, no. 8, pp. 923–930, 2020, doi: 10.1038/s41428-019-0301-5.

[55] A. M. Smith *et al.*, "Fmoc-Diphenylalanine Self Assembles to a Hydrogel via a Novel Architecture Based on π–π Interlocked β-Sheets," *Adv. Mater.*, vol. 20, no. 1, pp. 37–41, Jan. 2008, doi: https://doi.org/10.1002/adma.200701221.

[56] D. M. Ryan, S. B. Anderson, and B. L. Nilsson, "The influence of side-chain halogenation on the self-assembly and hydrogelation of Fmoc-phenylalanine derivatives," *Soft Matter*, vol. 6, no. 14, pp. 3220–3231, 2010, doi: 10.1039/c0sm00018c.

[57] S. Fleming, S. Debnath, P. W. J. M. Frederix, T. Tuttle, and R. V Ulijn, "Aromatic peptide amphiphiles: significance of the Fmoc moiety," *Chem. Commun.*, vol. 49, no. 90, pp. 10587–10589, 2013, doi: 10.1039/C3CC45822A.

[58] K. Tao, A. Levin, L. Adler-Abramovich, and E. Gazit, "Fmoc-modified amino acids and short peptides: Simple bio-inspired building blocks for the fabrication of functional materials," *Chem. Soc. Rev.*, vol. 45, no. 14, pp. 3935–3953, 2016, doi: 10.1039/c5cs00889a.

[59] J. P. Jung, J. Z. Gasiorowski, and J. H. Collier, "Fibrillar peptide gels in biotechnology and biomedicine.," *Biopolymers*, vol. 94, no. 1, pp. 49–59, 2010, doi: 10.1002/bip.21326.

[60] R. Vegners, I. Shestakova, I. Kalvinsh, R. M. Ezzell, and P. A. Janmey, “Use of a gel-forming dipeptide derivative as a carrier for antigen presentation,” *J. Pept. Sci.*, vol. 1, no. 6, pp. 371–378, 1995, doi: 10.1002/psc.310010604.

[61] Y. Zhang, H. Gu, Z. Yang, and B. Xu, “Supramolecular Hydrogels Respond to Ligand-Receptor Interaction,” *J. Am. Chem. Soc.*, vol. 125, no. 45, pp. 13680–13681, 2003, doi: 10.1021/ja036817k.

[62] Z. Yang, H. Gu, D. Fu, P. Gao, J. K. Lam, and B. Xu, “Enzymatic formation of supramolecular hydrogels,” *Adv. Mater.*, vol. 16, no. 16, pp. 1440–1444, 2004, doi: 10.1002/adma.200400340.

[63] S. Sutton, N. L. Campbell, A. I. Cooper, M. Kirkland, W. J. Frith, and D. J. Adams, “Controlled release from modified amino acid hydrogels governed by molecular size or network dynamics,” *Langmuir*, vol. 25, no. 17, pp. 10285–10291, 2009, doi: 10.1021/la9011058.

[64] V. Jayawarna *et al.*, “Introducing chemical functionality in Fmoc-peptide gels for cell culture,” *Acta Biomater.*, vol. 5, no. 3, pp. 934–943, 2009, doi: 10.1016/j.actbio.2009.01.006.

[65] R. Orbach *et al.*, “The rheological and structural properties of Fmoc-peptide-based hydrogels: The effect of aromatic molecular architecture on self-assembly and physical characteristics,” *Langmuir*, vol. 28, no. 4, pp. 2015–2022, 2012, doi: 10.1021/la204426q.

[66] M. Zhou *et al.*, “Self-assembled peptide-based hydrogels as scaffolds for anchorage-dependent cells,” *Biomaterials*, vol. 30, no. 13, pp. 2523–2530, 2009, doi: 10.1016/j.biomaterials.2009.01.010.

[67] D. M. Ryan, S. B. Anderson, F. T. Senguen, R. E. Youngman, and B. L. Nilsson, “Self-assembly and hydrogelation promoted by F5-phenylalanine,” *Soft Matter*, vol. 6, no. 3, pp. 475–479, 2010, doi: 10.1039/b916738b.

[68] G. Cheng, V. Castelletto, C. M. Moulton, G. E. Newby, and I. W. Hamley, “Hydrogelation and self-assembly of Fmoc-tripeptides: Unexpected influence of sequence on self-assembled fibril structure, and hydrogel modulus and anisotropy,” *Langmuir*, vol. 26, no. 7, pp. 4990–4998, 2010, doi: 10.1021/la903678e.

[69] R. Huang, W. Qi, L. Feng, R. Su, and Z. He, “Self-assembling peptide-polysaccharide hybrid hydrogel as a potential carrier for drug delivery,” *Soft Matter*, vol. 7, no. 13, pp. 6222–6230, 2011, doi: 10.1039/c1sm05375b.

[70] J. Nanda and A. Banerjee, “β-Amino acid containing proteolitically stable dipeptide based hydrogels: Encapsulation and sustained release of some important biomolecules at physiological pH and temperature,” *Soft Matter*, vol. 8, no. 12, pp. 3380–3386, 2012, doi: 10.1039/c2sm07168a.

[71] L. Chronopoulou *et al.*, “Biosynthesis and characterization of cross-linked fmoc peptide-based hydrogels for drug delivery applications,” *Gels*, vol. 1, no. 2, pp. 179–193, 2015, doi: 10.3390/gels1020179.

[72] R. Das Mahapatra, J. Dey, and R. G. Weiss, “L -Carnosine-Derived Fmoc-Tripeptides Forming pH-Sensitive and Proteolytically Stable Supramolecular Hydrogels,” *Langmuir*, vol. 33, no. 45, pp. 12989–12999, 2017, doi: 10.1021/acs.langmuir.7b03018.

[73] C. Diaferia, E. Rosa, G. Morelli, and A. Accardo, “Fmoc-Diphenylalanine Hydrogels: Optimization of Preparation Methods and Structural Insights,” *Pharmaceuticals*, vol. 15, no. 9, 2022, doi: 10.3390/ph15091048.

[74] E. Rosa *et al.*, “Multicomponent Hydrogel Matrices of Fmoc-FF and Cationic Peptides for Application in Tissue Engineering,” *Macromol. Biosci.*, vol. 22, no. 7, p. 2200128, Jul. 2022, doi: https://doi.org/10.1002/mabi.202200128.

[75] M. Criado-Gonzalez, M. I. Peñas, F. Barbault, A. J. Müller, F. Boulmedais, and R. Hernández, “Salt-induced Fmoc-tripeptide supramolecular hydrogels: a combined experimental and computational study of the self-assembly,” *Nanoscale*, vol. 16, no. 20, pp. 9887–9898, 2024, doi: 10.1039/d4nr00335g.

[76] J. D. Hartgerink, E. Beniash, and S. I. Stupp, “Peptide-amphiphile nanofibers: A versatile scaffold for the preparation of self-assembling materials,” *Proc. Natl. Acad. Sci. U. S. A.*, vol. 99, no. 8, pp. 5133–5138, 2002, doi: 10.1073/pnas.072699999.

[77] K. L. Niece, J. D. Hartgerink, J. J. J. M. Donners, and S. I. Stupp, “Self-Assembly Combining Two Bioactive Peptide-Amphiphile Molecules into Nanofibers by Electrostatic Attraction,” *J. Am. Chem. Soc.*, vol. 125, no. 24, pp. 7146–7147, Jun. 2003, doi: 10.1021/ja028215r.

[78] M. P. Hendricks, K. Sato, L. C. Palmer, and S. I. Stupp, “Supramolecular Assembly of Peptide Amphiphiles,” *Acc. Chem. Res.*, vol. 50, no. 10, pp. 2440–2448, 2017, doi: 10.1021/acs.accounts.7b00297.

[79] W. Sun, D. A. Gregory, and X. Zhao, “Designed peptide amphiphiles as scaffolds for tissue engineering,” *Adv. Colloid Interface Sci.*, vol. 314, no. February, p. 102866, 2023, doi: 10.1016/j.cis.2023.102866.

[80] C. Wu, W. Liao, Y. Zhang, and Y. Yan, “Peptide-based supramolecular hydrogels and their biotherapeutic applications,” *Biomater. Sci.*, vol. 12, no. 19, pp. 4855–4874, 2024, doi: 10.1039/d4bm00865k.

[81] N. Nandi *et al.*, “Amphiphilic Peptide-Based Supramolecular, Noncytotoxic, Stimuli-Responsive Hydrogels with Antibacterial Activity,” *Biomacromolecules*, vol. 18, no. 11, pp. 3621–3629, 2017, doi: 10.1021/acs.biomac.7b01006.

[82] B. F. Lin *et al.*, “PH-responsive branched peptide amphiphile hydrogel designed for applications in regenerative medicine with potential as injectable tissue scaffolds,” *J. Mater. Chem.*, vol. 22, no. 37, pp. 19447–19454, 2012, doi: 10.1039/c2jm31745a.

[83] F. Wang *et al.*, “Supramolecular Tubustecan Hydrogel as Chemotherapeutic Carrier to Improve Tumor Penetration and Local Treatment Efficacy,” *ACS Nano*, vol. 14, no. 8, pp. 10083–10094, 2020, doi: 10.1021/acsnano.0c03286.

[84] V. Y. Ho-Wook Jun and and J. D. H. Sergey E. Paramonov, “Advanced Materials - 2005 - Jun - Enzyme-Mediated Degradation of Peptide-Amphiphile Nanofiber Networks.pdf.” .

[85] K. Yamada, H. Ihara, T. Ide, T. Fukumoto, and C. Hirayama, “Formation of Helical Super Structure From Single-Walled Bilayers By Amphiphiles With Oligo-L-Glutamic Acid-Head Group,” *Chem. Lett.*, vol. 13, no. 10, pp. 1713–1716, 1984, doi: 10.1246/cl.1984.1713.

[86] T. J. Mitchison *et al.*, “Self-Assembly and Mineralization of Peptide-Amphiphile Nanofibers,” vol. 294, no. November, pp. 1684–1689, 2001.

[87] M. O. Guler, L. Hsu, S. Soukasene, D. A. Harrington, J. F. Hulvat, and S. I. Stupp, “Presentation of RGDS epitopes on self-assembled nanofibers of branched peptide amphiphiles,” *Biomacromolecules*, vol. 7, no. 6, pp. 1855–1863, 2006, doi:

10.1021/bm060161g.

[88] M. O. Guler and S. I. Stupp, “A self-assembled nanofiber catalyst for ester hydrolysis,” *J. Am. Chem. Soc.*, vol. 129, no. 40, pp. 12082–12083, 2007, doi: 10.1021/ja075044n.

[89] M. A. Greenfield, J. R. Hoffman, M. O. De La Cruz, and S. I. Stupp, “Tunable mechanics of peptide nanofiber gels,” *Langmuir*, vol. 26, no. 5, pp. 3641–3647, 2010, doi: 10.1021/la9030969.

[90] K. Shroff, E. L. Rexeisen, M. A. Arunagirinathan, and E. Kokkoli, “Fibronectin-mimetic peptide-amphiphile nanofiber gels support increased cell adhesion and promote ECM production,” *Soft Matter*, vol. 6, no. 20, pp. 5064–5072, 2010, doi: 10.1039/c0sm00321b.

[91] S. Dutta, A. Shome, T. Kar, and P. K. Das, “Counterion-induced modulation in the antimicrobial activity and biocompatibility of amphiphilic hydrogelators: Influence of in-situ-synthesized ag-nanoparticle on the bactericidal property,” *Langmuir*, vol. 27, no. 8, pp. 5000–5008, 2011, doi: 10.1021/la104903z.

[92] E. Sleep *et al.*, “Injectable biomimetic liquid crystalline scaffolds enhance muscle stem cell transplantation,” *Proc. Natl. Acad. Sci. U. S. A.*, vol. 114, no. 38, pp. E7919–E7928, 2017, doi: 10.1073/pnas.1708142114.

[93] “2014 - Dehsorkhi - Self-assembling amphiphilic peptides.pdf.” .

[94] S. Zhang, T. Holmes, C. Lockshin, and A. Rich, “Spontaneous assembly of a self-complementary oligopeptide to form a stable macroscopic membrane,” *Proc. Natl. Acad. Sci. U. S. A.*, vol. 90, no. 8, pp. 3334–3338, 1993, doi: 10.1073/pnas.90.8.3334.

[95] C. J. Bowerman and B. L. Nilsson, “Charles J. Bowerman, Bradley L. Nilsson,” vol. 98, no. 3, 2012, doi: 10.1002/bip.22058.

[96] S. Zhang, C. Lockshin, A. Herbert, E. Winter, and A. Rich, “Zuotin, a putative Z-DNA binding protein in Saccharomyces cerevisiae.,” *EMBO J.*, vol. 11, no. 10, pp. 3787–3796, Oct. 1992, doi: https://doi.org/10.1002/j.1460-2075.1992.tb05464.x.

[97] T. C. Holmes, S. De Lacalle, X. Su, G. Liu, A. Rich, and S. Zhang, “Extensive neurite outgrowth and active synapse formation on self-assembling peptide scaffolds,” 2000, doi: 10.1073/pnas.97.12.6728.

[98] N. Komuro, N. Nakajima, M. Hamada, and Y. Koyama, “Design and synthesis of amphiphilic alternating peptides with lower critical solution temperature behaviors,” *Polym. J.*, vol. 54, no. 7, pp. 903–912, 2022, doi: 10.1038/s41428-022-00639-7.

[99] W. Y. Seow, G. Salgado, E. B. Lane, and C. A. E. Hauser, “Transparent crosslinked ultrashort peptide hydrogel dressing with high shape-fidelity accelerates healing of full-thickness excision wounds,” *Sci. Rep.*, vol. 6, no. September, pp. 1–12, 2016, doi: 10.1038/srep32670.

[100] J. Bai *et al.*, “Enzymatic Regulation of Self-Assembling Peptide A9K2 Nanostructures and Hydrogelation with Highly Selective Antibacterial Activities,” *ACS Appl. Mater. Interfaces*, vol. 8, no. 24, pp. 15093–15102, 2016, doi: 10.1021/acsami.6b03770.

[101] T. Kiyota, S. Lee, and G. Sugihara, “Design and Synthesis of Amphiphilic α-Helical Model Peptides with Systematically Varied Hydrophobic−Hydrophilic Balance and Their Interaction with Lipid- and Bio-Membranes,” *Biochemistry*, vol. 35, no. 40, pp. 13196–13204, Jan. 1996, doi: 10.1021/bi961289t.

[102] D. Datta, A. Harikrishna, R. Nagaraj, and N. Chaudhary, “Self-assembly of β-turn motif-connected tandem repeats of Aβ16-22 and its aromatic analogs,” *Pept. Sci.*, vol. 111, no. 3, p. e24099, May 2019, doi: https://doi.org/10.1002/pep2.24099.

[103] V. K. Belwal and N. Chaudhary, “Amyloids and their untapped potential as hydrogelators,” *Soft Matter*, vol. 16, no. 44, pp. 10013–10028, 2020, doi: 10.1039/d0sm01578d.

[104] E. H. Koo, P. T. Lansbury, and J. W. Kelly, “Amyloid diseases: Abnormal protein aggregation in neurodegeneration,” *Proc. Natl. Acad. Sci.*, vol. 96, no. 18, pp. 9989–9990, Aug. 1999, doi: 10.1073/pnas.96.18.9989.

[105] P. D. Gorevic and E. C. Franklin, “Amyloidosis,” *Annu. Rev. Med.*, vol. 32, no. Volume 32, 1981, pp. 261–271, 1981, doi: https://doi.org/10.1146/annurev.me.32.020181.001401.

[106] E. D. Roberson and L. Mucke, “100 Years and Counting: Prospects for Defeating Alzheimer’s Disease,” *Science (80-.).*, vol. 314, no. 5800, pp. 781–784, Nov. 2006, doi: 10.1126/science.1132813.

[107] T. D. Vaden, S. A. N. Gowers, T. S. J. A. De Boer, J. D. Steill, J. Oomens, and L. C.

Snoek, “Conformational preferences of an amyloidogenic peptide: IR spectroscopy of Ac-VQIVYK-NHMe,” *J. Am. Chem. Soc.*, vol. 130, no. 44, pp. 14640–14650, 2008, doi: 10.1021/ja804213s.

[108] E. D EANES and G. G GLENNER, “X-RAY DIFFRACTION STUDIES ON AMYLOID FILAMENTS,” *J. Histochem. Cytochem.*, vol. 16, no. 11, pp. 673–677, Nov. 1968, doi: 10.1177/16.11.673.

[109] R. Kayed *et al.*, “Common Structure of Soluble Amyloid Oligomers Implies Common Mechanism of Pathogenesis,” *Science (80-.).*, vol. 300, no. 5618, pp. 486–489, Apr. 2003, doi: 10.1126/science.1079469.

[110] M. Sakono and T. Zako, “Amyloid oligomers: formation and toxicity of Aβ oligomers,” *FEBS J.*, vol. 277, no. 6, pp. 1348–1358, Mar. 2010, doi: https://doi.org/10.1111/j.1742-4658.2010.07568.x.

[111] P. H. Nguyen *et al.*, “Amyloid Oligomers: A Joint Experimental/Computational Perspective on Alzheimer’s Disease, Parkinson’s Disease, Type II Diabetes, and Amyotrophic Lateral Sclerosis,” *Chem. Rev.*, vol. 121, no. 4, pp. 2545–2647, Feb. 2021, doi: 10.1021/acs.chemrev.0c01122.

[112] M. R. Chapman *et al.*, “Role of Escherichia coli curli operons in directing amyloid fiber formation,” *Science (80-.).*, vol. 295, no. 5556, pp. 851–855, 2002, doi: 10.1126/science.1067484.

[113] C. P. J. Maury, “The emerging concept of functional amyloid,” *J. Intern. Med.*, vol. 265, no. 3, pp. 329–334, 2009, doi: 10.1111/j.1365-2796.2008.02068.x.

[114] D. M. Fowler, A. V. Koulov, C. Alory-Jost, M. S. Marks, W. E. Balch, and J. W. Kelly, “Functional amyloid formation within mammalian tissue,” *PLoS Biol.*, vol. 4, no. 1, pp. 0100–0107, 2006, doi: 10.1371/journal.pbio.0040006.

[115] D. M. Fowler, A. V Koulov, C. Alory-Jost, M. S. Marks, W. E. Balch, and J. W. Kelly, “Functional Amyloid Formation within Mammalian Tissue,” *PLOS Biol.*, vol. 4, no. 1, p. e6, Nov. 2005, [Online]. Available: https://doi.org/10.1371/journal.pbio.0040006.

[116] T. Fukuma, A. S. Mostaert, and S. P. Jarvis, “Explanation for the mechanical strength of amyloid fibrils,” *Tribol. Lett.*, vol. 22, no. 3, pp. 233–237, 2006, doi: 10.1007/s11249-006-9086-8.

[117] S. K. Maji *et al.*, "Functional amyloids as natural storage of peptide hormones in pituitary secretory granules," *Science (80-.).*, vol. 325, no. 5938, pp. 328–332, 2009, doi: 10.1126/science.1173155.

[118] J. Li and F. Zhang, "Amyloids as Building Blocks for Macroscopic Functional Materials: Designs, Applications and Challenges," *International Journal of Molecular Sciences*, vol. 22, no. 19. 2021, doi: 10.3390/ijms221910698.

[119] G. Tyagi and S. Sengupta, "Unveiling the multifaceted potential of amyloid fibrils: from pathogenic myths to biotechnological marvels," *Biophys. Rev.*, vol. 16, no. 6, pp. 737–751, 2024, doi: 10.1007/s12551-024-01232-3.

[120] S. Das *et al.*, "Implantable amyloid hydrogels for promoting stem cell differentiation to neurons," *NPG Asia Mater.*, vol. 8, no. 9, pp. 1–14, 2016, doi: 10.1038/am.2016.116.

[121] D. Datta, V. Kumar, S. Kumar, R. Nagaraj, and N. Chaudhary, "Hydrogel Formation by an Aromatic Analogue of a β-Amyloid Fragment, Aβ16-22: A Scaffold for 3D Cell Culture," *ACS Omega*, vol. 4, no. 1, pp. 620–627, 2019, doi: 10.1021/acsomega.8b02771.

[122] D. Datta, V. Kumar, S. Kumar, R. Nagaraj, and N. Chaudhary, "Limpid hydrogels from β-turn motif-connected tandem repeats of Aβ16-22," *Soft Matter*, vol. 15, no. 24, pp. 4827–4835, 2019, doi: 10.1039/c9sm00343f.

[123] L. Yang, H. Li, L. Yao, Y. Yu, and G. Ma, "Amyloid-Based Injectable Hydrogel Derived from Hydrolyzed Hen Egg White Lysozyme," *ACS Omega*, vol. 4, no. 5, pp. 8071–8080, 2019, doi: 10.1021/acsomega.8b03492.

[124] R. S. Jacob *et al.*, "Self healing hydrogels composed of amyloid nano fibrils for cell culture and stem cell differentiation," *Biomaterials*, vol. 54, pp. 97–105, 2015, doi: 10.1016/j.biomaterials.2015.03.002.

[125] L. Jean, C. F. Lee, P. Hodder, N. Hawkins, and D. J. Vaux, "Dynamics of the formation of a hydrogel by a pathogenic amyloid peptide: Islet amyloid polypeptide," *Sci. Rep.*, vol. 6, no. April, pp. 1–10, 2016, doi: 10.1038/srep32124.

[126] A. Kumari, B. Ahmad, and B. Ahmad, "The physical basis of fabrication of amyloid-based hydrogels by lysozyme," *RSC Adv.*, vol. 9, no. 64, pp. 37424–37435, 2019, doi: 10.1039/c9ra07179b.

[127] L. J. Juszczak, “Comparative Vibrational Spectroscopy of Intracellular Tau and Extracellular Collagen I Reveals Parallels of Gellation and Fibrillar Structure,” *J. Biol. Chem.*, vol. 279, no. 9, pp. 7395–7404, 2004, doi: 10.1074/jbc.M309971200.

[128] M. J. Krysmann, V. Castelletto, A. Kelarakis, I. W. Hamley, R. A. Hule, and D. J. Pochan, “Self-assembly and hydrogelation of an amyloid peptide fragment,” *Biochemistry*, vol. 47, no. 16, pp. 4597–4605, 2008, doi: 10.1021/bi8000616.

[129] G. Bhak, S. Lee, J. W. Park, S. Cho, and S. R. Paik s, “Amyloid hydrogel derived from curly protein fibrils of α-synuclein,” *Biomaterials*, vol. 31, no. 23, pp. 5986–5995, 2010, doi: 10.1016/j.biomaterials.2010.03.080.

[130] D. N. Woolfson, “Building fibrous biomaterials from α-helical and collagen-like coiled-coil peptides,” *Pept. Sci.*, vol. 94, no. 1, pp. 118–127, Jan. 2010, doi: https://doi.org/10.1002/bip.21345.

[131] W. Y. Seow and C. A. E. Hauser, “Short to ultrashort peptide hydrogels for biomedical uses,” *Mater. Today*, vol. 17, no. 8, pp. 381–388, 2014, doi: 10.1016/j.mattod.2014.04.028.

[132] J. Liu, L. Zhang, Z. Yang, and X. Zhao, “Controlled release of paclitaxel from a self-assembling peptide hydrogel formed in situ and antitumor study in vitro.,” *Int. J. Nanomedicine*, vol. 6, pp. 2143–2153, 2011, doi: 10.2147/ijn.s24038.

[133] C. Hu *et al.*, “Regulating cancer associated fibroblasts with losartan-loaded injectable peptide hydrogel to potentiate chemotherapy in inhibiting growth and lung metastasis of triple negative breast cancer,” *Biomaterials*, vol. 144, pp. 60–72, 2017, doi: 10.1016/j.biomaterials.2017.08.009.

[134] M. Delgado, K. J. Lee, L. Altobell, C. Spanka, P. Wentworth, and K. D. Janda, “A parallel approach to the discovery of carrier delivery vehicles to enhance antigen immunogenicity,” *J. Am. Chem. Soc.*, vol. 124, no. 18, pp. 4946–4947, 2002, doi: 10.1021/ja025715b.

[135] H. Yan *et al.*, “Thermo-reversible protein fibrillar hydrogels as cell scaffolds,” *Faraday Discuss.*, vol. 139, pp. 71–84, 2008, doi: 10.1039/b717748h.

[136] S. Chowdhuri, M. Ghosh, L. Adler-Abramovich, and D. Das, “The effects of a short self-assembling peptide on the physical and biological properties of biopolymer

hydrogels," *Pharmaceutics*, vol. 13, no. 10, pp. 1–15, 2021, doi: 10.3390/pharmaceutics13101602.

[137] Y. Loo, A. Lakshmanan, M. Ni, L. L. Toh, S. Wang, and C. A. E. Hauser, "Peptide Bioink: Self-Assembling Nanofibrous Scaffolds for Three-Dimensional Organotypic Cultures," *Nano Lett.*, vol. 15, no. 10, pp. 6919–6925, 2015, doi: 10.1021/acs.nanolett.5b02859.

[138] S. Woerly, "Porous hydrogels for neural tissue engineering," *Mater. Sci. Forum*, vol. 250, pp. 53–68, 1997, doi: 10.4028/www.scientific.net/msf.250.53.

[139] Y. Tabata, M. Miyao, M. Ozeki, and Y. Ikada, "Controlled release of vascular endothelial growth factor by use of collagen hydrogels," *J. Biomater. Sci. Polym. Ed.*, vol. 11, no. 9, pp. 915–930, 2000, doi: 10.1163/156856200744101.

[140] X. Liu *et al.*, "Functionalized self-assembling peptide nanofiber hydrogels mimic stem cell niche to control human adipose stem cell behavior in vitro," *Acta Biomater.*, vol. 9, no. 6, pp. 6798–6805, 2013, doi: 10.1016/j.actbio.2013.01.027.

[141] Z. Li *et al.*, "Bone marrow enriched graft, modified by self-assembly peptide, repairs critically-sized femur defects in goats," *Int. Orthop.*, vol. 38, no. 11, pp. 2391–2398, 2014, doi: 10.1007/s00264-014-2388-9.

[142] F. Paladini, S. T. Meikle, I. R. Cooper, J. Lacey, V. Perugini, and M. Santin, "Silver-doped self-assembling di-phenylalanine hydrogels as wound dressing biomaterials," *J. Mater. Sci. Mater. Med.*, vol. 24, no. 10, pp. 2461–2472, 2013, doi: 10.1007/s10856-013-4986-2.

[143] Y. Loo *et al.*, "Ultrashort peptide nanofibrous hydrogels for the acceleration of healing of burn wounds," *Biomaterials*, vol. 35, no. 17, pp. 4805–4814, 2014, doi: 10.1016/j.biomaterials.2014.02.047.

[144] N. C. Carrejo *et al.*, "Multidomain Peptide Hydrogel Accelerates Healing of Full-Thickness Wounds in Diabetic Mice," *ACS Biomater. Sci. Eng.*, vol. 4, no. 4, pp. 1386–1396, 2018, doi: 10.1021/acsbiomaterials.8b00031.

[145] C. C. Zhao, L. Zhu, Z. Wu, R. Yang, N. Xu, and L. Liang, "Resveratrol-loaded peptide-hydrogels inhibit scar formation in wound healing through suppressing inflammation," *Regen. Biomater.*, vol. 7, no. 1, pp. 99–107, 2019, doi: 10.1093/rb/rbz041.

[146] S. Wu *et al.*, "Dextran and peptide-based pH-sensitive hydrogel boosts healing process in multidrug-resistant bacteria-infected wounds," *Carbohydr. Polym.*, vol. 278, no. December 2021, p. 118994, 2022, doi: 10.1016/j.carbpol.2021.118994.

[147] M. Guerrero *et al.*, "Hydrogel-antimicrobial peptide association: A novel and promising strategy to combat resistant infections," *Colloids Surfaces B Biointerfaces*, vol. 247, no. September 2024, 2025, doi: 10.1016/j.colsurfb.2024.114451.

[148] Q. Zhao, Y. Zhao, Z. Lu, and Y. Tang, "Amino Acid-Modified Conjugated Oligomer Self-Assembly Hydrogel for Efficient Capture and Specific Killing of Antibiotic-Resistant Bacteria," *ACS Appl. Mater. Interfaces*, vol. 11, no. 18, pp. 16320–16327, 2019, doi: 10.1021/acsami.9b02643.

[149] B. Hansda *et al.*, "Histidine-Containing Amphiphilic Peptide-Based Non-Cytotoxic Hydrogelator with Antibacterial Activity and Sustainable Drug Release," *Langmuir*, vol. 39, no. 21, pp. 7307–7316, 2023, doi: 10.1021/acs.langmuir.3c00235.

[150] A. Adak, S. Ghosh, V. Gupta, and S. Ghosh, "Biocompatible Lipopeptide-Based Antibacterial Hydrogel," *Biomacromolecules*, vol. 20, no. 5, pp. 1889–1898, 2019, doi: 10.1021/acs.biomac.8b01836.

[151] A. D'souza *et al.*, "Nine-Residue Peptide Self-Assembles in the Presence of Silver to Produce a Self-Healing, Cytocompatible, Antimicrobial Hydrogel," *ACS Appl. Mater. Interfaces*, vol. 12, no. 14, pp. 17091–17099, 2020, doi: 10.1021/acsami.0c01154.

[152] Y. Y. Xie *et al.*, "Structure-Dependent Antibacterial Activity of Amino Acid-Based Supramolecular Hydrogels," *Colloids Surfaces B Biointerfaces*, vol. 193, no. May, p. 111099, 2020, doi: 10.1016/j.colsurfb.2020.111099.

[153] W. T. Truong, Y. Su, D. Gloria, F. Braet, and P. Thordarson, "Dissolution and degradation of Fmoc-diphenylalanine self-assembled gels results in necrosis at high concentrations in vitro," *Biomater. Sci.*, vol. 3, no. 2, pp. 298–307, 2015, doi: 10.1039/c4bm00244j.

[154] J. P. Schneider, D. J. Pochan, B. Ozbas, K. Rajagopal, L. Pakstis, and J. Kretsinger, "Responsive hydrogels from the intramolecular folding and self-assembly of a designed peptide," *J. Am. Chem. Soc.*, vol. 124, no. 50, pp. 15030–15037, 2002, doi: 10.1021/ja027993g.

[155] P. W. J. M. Frederix *et al.*, "Exploring the sequence space for (tri-)peptide self-assembly to design and discover new hydrogels," *Nat. Chem.*, vol. 7, no. 1, pp. 30–37, 2015, doi: 10.1038/nchem.2122.

[156] M. Margittai and R. Langen, *Fibrils with parallel in-register structure constitute a major class of amyloid fibrils: Molecular insights from electron paramagnetic resonance spectroscopy*, vol. 41, no. 3–4. 2008.

[157] M. Von Bergen, P. Friedhoff, J. Biernat, J. Heberle, E. M. Mandelkow, and E. Mandelkow, "Assembly of τ protein into Alzheimer paired helical filaments depends on a local sequence motif (306VQIVYK311) forming β structure," *Proc. Natl. Acad. Sci. U. S. A.*, vol. 97, no. 10, pp. 5129–5134, 2000, doi: 10.1073/pnas.97.10.5129.

[158] M. von Bergen *et al.*, "Mutations of Tau Protein in Frontotemporal Dementia Promote Aggregation of Paired Helical Filaments by Enhancing Local β-Structure*," *J. Biol. Chem.*, vol. 276, no. 51, pp. 48165–48174, 2001, doi: https://doi.org/10.1074/jbc.M105196200.

[159] W. J. Goux *et al.*, "The formation of straight and twisted filaments from short tau peptides," *J. Biol. Chem.*, vol. 279, no. 26, pp. 26868–26875, 2004, doi: 10.1074/jbc.M402379200.

[160] M. R. Sawaya *et al.*, "Atomic structures of amyloid cross-β spines reveal varied steric zippers," *Nature*, vol. 447, no. 7143, pp. 453–457, 2007, doi: 10.1038/nature05695.

[161] I. Stroganova, H. Willenberg, T. Tente, A. Depraz Depland, S. Bakels, and A. M. Rijs, "Exploring the Aggregation Propensity of PHF6 Peptide Segments of the Tau Protein Using Ion Mobility Mass Spectrometry Techniques," *Anal. Chem.*, vol. 96, no. 13, pp. 5115–5124, Apr. 2024, doi: 10.1021/acs.analchem.3c04974.

[162] E. Pretti, M. S. Shell, and J. A. Mccammon, "Mapping the configurational landscape and aggregation phase behavior of the tau protein fragment PHF6," vol. 120, no. 48, 2023, doi: 10.1073/pnas.2309995120/-/DCSupplemental.Published.

[163] I. Stroganova, Z. Toprakcioglu, H. Willenberg, T. P. J. Knowles, and A. M. Rijs, "Unraveling the Structure and Dynamics of Ac-PHF6-NH2 Tau Segment Oligomers," *ACS Chem. Neurosci.*, vol. 15, no. 18, pp. 3391–3400, Sep. 2024, doi: 10.1021/acschemneuro.4c00404.

[164] S. Paul and P. Biswas, “Molecular Dynamics Simulation Study of the Self-Assembly of Tau-Derived PHF6 and Its Inhibition by Oleuropein Aglycone from Extra Virgin Olive Oil,” *J. Phys. Chem. B*, vol. 128, no. 23, pp. 5630–5641, Jun. 2024, doi: 10.1021/acs.jpcb.4c02393.

[165] S. J. A. Shah, Q. Zhang, J. Guo, H. Liu, H. Liu, and J. Villà-Freixa, “Identification of Aggregation Mechanism of Acetylated PHF6* and PHF6 Tau Peptides Based on Molecular Dynamics Simulations and Markov State Modeling,” *ACS Chem. Neurosci.*, vol. 14, no. 21, pp. 3959–3971, 2023, doi: 10.1021/acschemneuro.3c00578.

[166] H. Kadavath *et al.*, “Tau stabilizes microtubules by binding at the interface between tubulin heterodimers,” *Proc. Natl. Acad. Sci.*, vol. 112, no. 24, pp. 7501–7506, Jun. 2015, doi: 10.1073/pnas.1504081112.

[167] E. Mandelkow, M. von Bergen, J. Biernat, and E.-M. Mandelkow, “Structural principles of tau and the paired helical filaments of Alzheimer’s disease.,” *Brain Pathol.*, vol. 17, no. 1, pp. 83–90, Jan. 2007, doi: 10.1111/j.1750-3639.2007.00053.x.

[168] K. Iqbal, F. Liu, C.-X. Gong, and I. Grundke-Iqbal, “Tau in Alzheimer disease and related tauopathies.,” *Curr. Alzheimer Res.*, vol. 7, no. 8, pp. 656–664, Dec. 2010, doi: 10.2174/156720510793611592.

[169] F. Hernµndez and J. Avila, “Cellular and Molecular Life Sciences,” vol. 64, pp. 2219–2233, 2007, doi: 10.1007/s00018-007-7220-x.

[170] A. del C. Alonso, T. Zaidi, M. Novak, I. Grundke-Iqbal, and K. Iqbal, “Hyperphosphorylation induces self-assembly of τ into tangles of paired helical filaments/straight filaments,” *Proc. Natl. Acad. Sci.*, vol. 98, no. 12, pp. 6923–6928, Jun. 2001, doi: 10.1073/pnas.121119298.

[171] S. Barghorn, P. Davies, and E. Mandelkow, “Tau Paired Helical Filaments from Alzheimer’s Disease Brain and Assembled in Vitro Are Based on β-Structure in the Core Domain,” *Biochemistry*, vol. 43, no. 6, pp. 1694–1703, Feb. 2004, doi: 10.1021/bi0357006.

[172] M. KIDD, “Paired Helical Filaments in Electron Microscopy of Alzheimer’s Disease,” *Nature*, vol. 197, no. 4863, pp. 192–193, 1963, doi: 10.1038/197192b0.

[173] K. A. Butner and M. W. Kirschner, “Tau protein binds to microtubules through a flexible

array of distributed weak sites.," *J. Cell Biol.*, vol. 115, no. 3, pp. 717–730, Nov. 1991, doi: 10.1083/jcb.115.3.717.

[174] N. Gustke, B. Trinczek, J. Biernat, E.-M. Mandelkow, and E. Mandelkow, "Domains of tau Protein and Interactions with Microtubules," *Biochemistry*, vol. 33, no. 32, pp. 9511–9522, Oct. 1994, doi: 10.1021/bi00198a017.

[175] B. L. Goode *et al.*, "Functional interactions between the proline-rich and repeat regions of tau enhance microtubule binding and assembly.," *Mol. Biol. Cell*, vol. 8, no. 2, pp. 353–365, Feb. 1997, doi: 10.1091/mbc.8.2.353.

[176] S. F. Levy, A. C. LeBoeuf, M. R. Massie, M. A. Jordan, L. Wilson, and S. C. Feinstein, "Three- and Four-repeat Tau Regulate the Dynamic Instability of Two Distinct Microtubule Subpopulations in Qualitatively Different Manners: IMPLICATIONS FOR NEURODEGENERATION*," *J. Biol. Chem.*, vol. 280, no. 14, pp. 13520–13528, 2005, doi: https://doi.org/10.1074/jbc.M413490200.

[177] K. Tomoo *et al.*, "Possible Role of Each Repeat Structure of the Microtubule-Binding Domain of the Tau Protein in In Vitro Aggregation," *J. Biochem.*, vol. 138, no. 4, pp. 413–423, Oct. 2005, doi: 10.1093/jb/mvi142.

[178] P. Friedhoff, M. von Bergen, E.-M. Mandelkow, and E. Mandelkow, "Structure of tau protein and assembly into paired helical filaments," *Biochim. Biophys. Acta - Mol. Basis Dis.*, vol. 1502, no. 1, pp. 122–132, 2000, doi: https://doi.org/10.1016/S0925-4439(00)00038-7.

[179] S. Ambadipudi, J. Biernat, D. Riedel, E. Mandelkow, and M. Zweckstetter, "Liquid-liquid phase separation of the microtubule-binding repeats of the Alzheimer-related protein Tau," *Nat. Commun.*, vol. 8, no. 1, pp. 1–13, 2017, doi: 10.1038/s41467-017-00480-0.

[180] S. Wegmann *et al.*, "Tau protein liquid–liquid phase separation can initiate tau aggregation," *EMBO J.*, vol. 37, no. 7, pp. 1–21, 2018, doi: 10.15252/embj.201798049.

[181] D. J. Pochan, J. P. Schneider, J. Kretsinger, B. Ozbas, K. Rajagopal, and L. Haines, "Thermally Reversible Hydrogels via Intramolecular Folding and Consequent Self-Assembly of a de Novo Designed Peptide," *J. Am. Chem. Soc.*, vol. 125, no. 39, pp. 11802–11803, Oct. 2003, doi: 10.1021/ja0353154.

[182] B. Ozbas, J. Kretsinger, K. Rajagopal, J. P. Schneider, and D. J. Pochan, "Salt-Triggered Peptide Folding and Consequent Self-Assembly into Hydrogels with Tunable Modulus," *Macromolecules*, vol. 37, no. 19, pp. 7331–7337, Sep. 2004, doi: 10.1021/ma0491762.

[183] M. Juković, I. Ratkaj, D. Kalafatovic, and N. J. Bradshaw, "Amyloids, amorphous aggregates and assemblies of peptides – Assessing aggregation," *Biophys. Chem.*, vol. 308, p. 107202, 2024, doi: https://doi.org/10.1016/j.bpc.2024.107202.

[184] P. Dey and P. Biswas, "Exploring the aggregation of amyloid-β 42 through Monte Carlo simulations," *Biophys. Chem.*, vol. 297, p. 107011, 2023, doi: https://doi.org/10.1016/j.bpc.2023.107011.

[185] P. C. Ke *et al.*, "Chem Soc Rev future †," pp. 5473–5509, 2020, doi: 10.1039/c9cs00199a.

[186] A. Lakshmanan, D. W. Cheong, A. Accardo, E. Di Fabrizio, C. Riekel, and C. A. E. Hauser, "Aliphatic peptides show similar self-assembly to amyloid core sequences, challenging the importance of aromatic interactions in amyloidosis," *Proc. Natl. Acad. Sci.*, vol. 110, no. 2, pp. 519–524, Jan. 2013, doi: 10.1073/pnas.1217742110.

[187] R. S. Jacob *et al.*, "Self healing hydrogels composed of amyloid nano fibrils for cell culture and stem cell differentiation," *Biomaterials*, vol. 54, pp. 97–105, 2015, doi: https://doi.org/10.1016/j.biomaterials.2015.03.002.

[188] S. Das *et al.*, "Implantable amyloid hydrogels for promoting stem cell differentiation to neurons," *NPG Asia Mater.*, vol. 8, no. 9, pp. e304–e304, 2016, doi: 10.1038/am.2016.116.

[189] S. Moktan, E. Perkins, F. Kratz, and D. Raucher, "Thermal Targeting of an Acid-Sensitive Doxorubicin Conjugate of Elastin-like Polypeptide Enhances the Therapeutic Efficacy Compared with the Parent Compound In Vivo," *Mol. Cancer Ther.*, vol. 11, no. 7, pp. 1547–1556, Jul. 2012, doi: 10.1158/1535-7163.MCT-11-0998.

[190] P. Bjelkmar, P. Larsson, M. A. Cuendet, B. Hess, and E. Lindahl, "Implementation of the CHARMM Force Field in GROMACS: Analysis of Protein Stability Effects from Correction Maps, Virtual Interaction Sites, and Water Models," *J. Chem. Theory Comput.*, vol. 6, no. 2, pp. 459–466, Feb. 2010, doi: 10.1021/ct900549r.

[191] S. Pronk *et al.*, "GROMACS 4.5: a high-throughput and highly parallel open source

molecular simulation toolkit," *Bioinformatics*, vol. 29, no. 7, pp. 845–854, Apr. 2013, doi: 10.1093/bioinformatics/btt055.

[192] K. Vanommeslaeghe *et al.*, "CHARMM general force field: A force field for drug-like molecules compatible with the CHARMM all-atom additive biological force fields," *J. Comput. Chem.*, vol. 31, no. 4, pp. 671–690, Mar. 2010, doi: https://doi.org/10.1002/jcc.21367.

[193] M. H. Chen, L. L. Wang, J. J. Chung, Y.-H. Kim, P. Atluri, and J. A. Burdick, "Methods To Assess Shear-Thinning Hydrogels for Application As Injectable Biomaterials," *ACS Biomater. Sci. Eng.*, vol. 3, no. 12, pp. 3146–3160, Dec. 2017, doi: 10.1021/acsbiomaterials.7b00734.

[194] R. Sarroukh, E. Goormaghtigh, J.-M. Ruysschaert, and V. Raussens, "ATR-FTIR: A 'rejuvenated' tool to investigate amyloid proteins," *Biochim. Biophys. Acta - Biomembr.*, vol. 1828, no. 10, pp. 2328–2338, 2013, doi: https://doi.org/10.1016/j.bbamem.2013.04.012.

[195] H. Naiki, K. Higuchi, M. Hosokawa, and T. Takeda, "Fluorometric determination of amyloid fibrils in vitro using the fluorescent dye, thioflavine T," *Anal. Biochem.*, vol. 177, no. 2, pp. 244–249, 1989, doi: https://doi.org/10.1016/0003-2697(89)90046-8.

[196] I. Usach, R. Martinez, T. Festini, and J.-E. Peris, "Subcutaneous Injection of Drugs: Literature Review of Factors Influencing Pain Sensation at the Injection Site," *Adv. Ther.*, vol. 36, no. 11, pp. 2986–2996, 2019, doi: 10.1007/s12325-019-01101-6.

[197] M. Bucciantini *et al.*, "Inherent toxicity of aggregates implies a common mechanism for protein misfolding diseases," *Nature*, vol. 416, no. 6880, pp. 507–511, 2002, doi: 10.1038/416507a.

[198] G. Bitan, E. A. Fradinger, S. M. Spring, and D. B. Teplow, "Neurotoxic protein oligomers—what you see is not always what you get," *Amyloid*, vol. 12, no. 2, pp. 88–95, Jun. 2005, doi: 10.1080/13506120500106958.

[199] S. W. Chen *et al.*, "Structural characterization of toxic oligomers that are kinetically trapped during α-synuclein fibril formation," *Proc. Natl. Acad. Sci.*, vol. 112, no. 16, pp. E1994–E2003, Apr. 2015, doi: 10.1073/pnas.1421204112.

[200] C. G. Glabe, "Common mechanisms of amyloid oligomer pathogenesis in degenerative

disease," *Neurobiol. Aging*, vol. 27, no. 4, pp. 570–575, 2006, doi: https://doi.org/10.1016/j.neurobiolaging.2005.04.017.

[201] C. G. Glabe, "Structural Classification of Toxic Amyloid Oligomers*," *J. Biol. Chem.*, vol. 283, no. 44, pp. 29639–29643, 2008, doi: https://doi.org/10.1074/jbc.R800016200.

[202] A. Laganowsky *et al.*, "Atomic View of a Toxic Amyloid Small Oligomer," *Science (80-.).*, vol. 335, no. 6073, pp. 1228–1231, Mar. 2012, doi: 10.1126/science.1213151.

[203] A. Brown and M. Török, "Functional amyloids in the human body," *Bioorg. Med. Chem. Lett.*, vol. 40, p. 127914, 2021, doi: https://doi.org/10.1016/j.bmcl.2021.127914.

[204] D. M. Fowler, A. V Koulov, W. E. Balch, and J. W. Kelly, "Functional amyloid – from bacteria to humans," *Trends Biochem. Sci.*, vol. 32, no. 5, pp. 217–224, 2007, doi: https://doi.org/10.1016/j.tibs.2007.03.003.

[205] S. K. Maji *et al.*, "Functional Amyloids As Natural Storage of Peptide Hormones in Pituitary Secretory Granules," *Science (80-.).*, vol. 325, no. 5938, pp. 328–332, Jul. 2009, doi: 10.1126/science.1173155.

[206] K. Fu, H. Wu, and Z. Su, "Self-assembling peptide-based hydrogels: Fabrication, properties, and applications," *Biotechnol. Adv.*, vol. 49, p. 107752, 2021, doi: https://doi.org/10.1016/j.biotechadv.2021.107752.

[207] R. Gallardo, N. A. Ranson, and S. E. Radford, "Amyloid structures: much more than just a cross-β fold," *Curr. Opin. Struct. Biol.*, vol. 60, pp. 7–16, 2020, doi: https://doi.org/10.1016/j.sbi.2019.09.001.

[208] D. Otzen and R. Riek, "Functional Amyloids," 2025, doi: 10.1101/cshperspect.a033860.

[209] J. Wang, K. Liu, R. Xing, and X. Yan, "Peptide self-assembly: thermodynamics and kinetics," *Chem. Soc. Rev.*, vol. 45, no. 20, pp. 5589–5604, 2016, doi: 10.1039/C6CS00176A.

[210] F. Li *et al.*, "Design of self-assembly dipeptide hydrogels and machine learning via their chemical features," *Proc. Natl. Acad. Sci.*, vol. 116, no. 23, pp. 11259–11264, Jun. 2019, doi: 10.1073/pnas.1903376116.

[211] A. Banerjee, G. Palui, and A. Banerjee, "Pentapeptide based organogels: the role of adjacently located phenylalanine residues in gel formation," *Soft Matter*, vol. 4, no. 7,

pp. 1430–1437, 2008, doi: 10.1039/B802205B.

[212] W. Li *et al.*, "Unraveling the influence of aromatic endcaps in peptide self-assembly," *Polymer (Guildf).*, vol. 302, p. 127090, 2024, doi: https://doi.org/10.1016/j.polymer.2024.127090.

[213] M. Reches and E. Gazit, "Designed aromatic homo-dipeptides: formation of ordered nanostructures and potential nanotechnological applications," *Phys. Biol.*, vol. 3, no. 1, p. S10, 2006, doi: 10.1088/1478-3975/3/1/S02.

[214] E. Gazit, "A possible role for π-stacking in the self-assembly of amyloid fibrils," *FASEB J.*, vol. 16, no. 1, pp. 77–83, Jan. 2002, doi: https://doi.org/10.1096/fj.01-0442hyp.

[215] S. K. Pachahara and R. Nagaraj, "Probing the role of aromatic residues in the self-assembly of Aβ(16–22) in fluorinated alcohols and their aqueous mixtures," *Biochem. Biophys. Reports*, vol. 2, pp. 1–13, 2015, doi: https://doi.org/10.1016/j.bbrep.2015.04.005.

[216] M. Reches and E. Gazit, "Casting Metal Nanowires Within Discrete Self-Assembled Peptide Nanotubes," *Science (80-.).*, vol. 300, no. 5619, pp. 625–627, Apr. 2003, doi: 10.1126/science.1082387.

[217] A. Mahler, M. Reches, M. Rechter, S. Cohen, and E. Gazit, "Rigid, Self-Assembled Hydrogel Composed of a Modified Aromatic Dipeptide," *Adv. Mater.*, vol. 18, no. 11, pp. 1365–1370, Jun. 2006, doi: https://doi.org/10.1002/adma.200501765.

[218] D. M. Ryan, T. M. Doran, S. B. Anderson, and B. L. Nilsson, "Effect of C-terminal modification on the self-assembly and hydrogelation of fluorinated Fmoc-Phe derivatives," *Langmuir*, vol. 27, no. 7, pp. 4029–4039, 2011, doi: 10.1021/la1048375.

[219] A. A. Profit, J. Vedad, M. Saleh, and R. Z. B. Desamero, "Aromaticity and amyloid formation: Effect of π-electron distribution and aryl substituent geometry on the self-assembly of peptides derived from hIAPP22–29," *Arch. Biochem. Biophys.*, vol. 567, pp. 46–58, 2015, doi: https://doi.org/10.1016/j.abb.2014.12.008.

[220] M. D. Hanwell, D. E. Curtis, D. C. Lonie, T. Vandermeersch, E. Zurek, and G. R. Hutchison, "Avogadro: an advanced semantic chemical editor, visualization, and analysis platform," *J. Cheminform.*, vol. 4, no. 1, p. 17, 2012, doi: 10.1186/1758-2946-4-17.

[221] N. Louros, K. Konstantoulea, M. De Vleeschouwer, M. Ramakers, J. Schymkowitz, and F. Rousseau, "WALTZ-DB 2.0: an updated database containing structural information of experimentally determined amyloid-forming peptides," *Nucleic Acids Res.*, vol. 48, no. D1, pp. D389–D393, Jan. 2020, doi: 10.1093/nar/gkz758.

[222] A. Micsonai *et al.*, "Accurate secondary structure prediction and fold recognition for circular dichroism spectroscopy," *Proc. Natl. Acad. Sci.*, vol. 112, no. 24, pp. E3095–E3103, Jun. 2015, doi: 10.1073/pnas.1500851112.

[223] S. S. Verma, S. Bhattacharya, S. Kumar, and N. Chaudhary, "The amyloidogenic peptide stretch in human tau, tau306–311 is a promising injectable hydrogelator," *Biophys. Chem.*, vol. 322, no. December 2024, 2025, doi: 10.1016/j.bpc.2025.107438.

[224] C. A. E. Hauser *et al.*, "Natural tri- to hexapeptides self-assemble in water to amyloid β-type fiber aggregates by unexpected α-helical intermediate structures," *Proc. Natl. Acad. Sci. U. S. A.*, vol. 108, no. 4, pp. 1361–1366, Sep. 2011, [Online]. Available: http://www.jstor.org/stable/41001866.

[225] H. Erdogan *et al.*, "Morphological Versatility in the Self-Assembly of Val-Ala and Ala-Val Dipeptides," *Langmuir*, vol. 31, no. 26, pp. 7337–7345, Jul. 2015, doi: 10.1021/acs.langmuir.5b01406.

[226] C. Subbalakshmi, P. Basak, and R. Nagaraj, "Self-assembly of t-butyloxycarbonyl protected dipeptide methyl esters composed of leucine, isoleucine, and valine into highly organized structures from alcohol and aqueous alcohol mixtures," *Pept. Sci.*, vol. 108, no. 6, p. e23033, Nov. 2017, doi: https://doi.org/10.1002/bip.23033.

[227] P. Wolf, "A critical reappraisal of Waddell's technique for ultraviolet spectrophotometric protein estimation," *Anal. Biochem.*, vol. 129, no. 1, pp. 145–155, 1983, doi: https://doi.org/10.1016/0003-2697(83)90062-3.

[228] W. E. Klunk, R. F. Jacob, and R. P. B. T.-M. in E. Mason, "[19] Quantifying amyloid by congo red spectral shift assay," in *Amyloid, Prions, and Other Protein Aggregates*, vol. 309, Academic Press, 1999, pp. 285–305.

[229] S. S. Verma and N. Chaudhary, "Substitution of tyrosine with electron-deficient aromatic amino acids improves Ac-PHF6 self-assembly and hydrogelation," *RSC Adv.*, vol. 15, no. 28, pp. 22216–22227, 2025, doi: 10.1039/D5RA03251B.

[230] P. M. Seidler *et al.*, "Structure-based inhibitors of tau aggregation," *Nat. Chem.*, vol. 10, no. 2, pp. 170–176, 2018, doi: 10.1038/nchem.2889.

[231] P. Manavalan and W. C. Johnson, "Sensitivity of circular dichroism to protein tertiary structure class," *Nature*, vol. 305, no. 5937, pp. 831–832, 1983, doi: 10.1038/305831a0.

[232] J. Wu, J. T. Yang, and C.-S. C. Wu, "β-II conformation of all-β proteins can be distinguished from unordered form by circular dichroism," *Anal. Biochem.*, vol. 200, no. 2, pp. 359–364, 1992, doi: https://doi.org/10.1016/0003-2697(92)90479-Q.

[233] N. Sreerama and R. W. Woody, "Structural composition of βI- and βII-proteins," *Protein Sci.*, vol. 12, no. 2, pp. 384–388, Feb. 2003, doi: https://doi.org/10.1110/ps.0235003.

[234] M. Jackson and H. H. Mantsch, "The Use and Misuse of FTIR Spectroscopy in the Determination of Protein Structure," *Crit. Rev. Biochem. Mol. Biol.*, vol. 30, no. 2, pp. 95–120, Jan. 1995, doi: 10.3109/10409239509085140.

[235] P. Sassi, A. Giugliarelli, M. Paolantoni, A. Morresi, and G. Onori, "Unfolding and aggregation of lysozyme: A thermodynamic and kinetic study by FTIR spectroscopy," *Biophys. Chem.*, vol. 158, no. 1, pp. 46–53, 2011, doi: https://doi.org/10.1016/j.bpc.2011.05.002.

[236] N. Chaudhary, S. Singh, and R. Nagaraj, "Morphology of self-assembled structures formed by short peptides from the amyloidogenic protein tau depends on the solvent in which the peptides are dissolved," *J. Pept. Sci.*, vol. 15, no. 10, pp. 675–684, Sep. 2009, doi: https://doi.org/10.1002/psc.1172.

[237] K. H. Chan, B. Xue, R. C. Robinson, and C. A. E. Hauser, "Systematic Moiety Variations of Ultrashort Peptides Produce Profound Effects on Self-Assembly, Nanostructure Formation, Hydrogelation, and Phase Transition," *Sci. Rep.*, vol. 7, no. 1, p. 12897, 2017, doi: 10.1038/s41598-017-12694-9.

[238] J. K. Sahoo, C. Nazareth, M. A. VandenBerg, and M. J. Webber, "Self-assembly of amphiphilic tripeptides with sequence-dependent nanostructure," *Biomater. Sci.*, vol. 5, no. 8, pp. 1526–1530, 2017, doi: 10.1039/C7BM00304H.

[239] K. Wang, J. D. Keasling, and S. J. Muller, "Effects of the sequence and size of non-polar residues on self-assembly of amphiphilic peptides," *Int. J. Biol. Macromol.*, vol. 36, no.

4, pp. 232–240, 2005, doi: https://doi.org/10.1016/j.ijbiomac.2005.06.006.

[240] J. M. Antosiewicz and D. Shugar, “UV–Vis spectroscopy of tyrosine side-groups in studies of protein structure. Part 2: selected applications,” *Biophys. Rev.*, vol. 8, no. 2, pp. 163–177, 2016, doi: 10.1007/s12551-016-0197-7.

Biophysical Chemistry 322 (2025) 107438

Contents lists available at ScienceDirect

Biophysical Chemistry

journal homepage: www.elsevier.com/locate/biophyschem

The amyloidogenic peptide stretch in human tau, tau$^{306–311}$ is a promising injectable hydrogelator

Shubhangini Singh Verma, Shinjini Bhattacharya, Sachin Kumar, Nitin Chaudhary *

Department of Biosciences and Bioengineering, Indian Institute of Technology Guwahati, Guwahati 781 039, India

ARTICLE INFO

Keywords:
Native
Peptide
Tau
PHF6
Injectable
Hydrogel

ABSTRACT

A vast majority of peptide hydrogelators harbor a bulky, non-native aromatic moiety. Such foreign moieties raise safety concerns as far as biomedical applications of hydrogels are concerned. The hydrogel research, therefore, has branched to another dimension – to identify native or native-like short peptide stretches that could cause the gelation of biological fluids. Using well-defined criteria to identify native peptide stretches that could form a viscous solution in water but cause gelation of phosphate-buffered saline (PBS), we identified the hexapeptide stretch from human tau, *viz.* tau$^{306–311}$, as a promising injectable hydrogelator. The peptide causes instant gelation of PBS and the cell culture media. Such hydrogels find applications as drug delivery vehicles, scaffolds for mammalian cell culture, wound-dressing material, *etc.*

1. Introduction

Hydrogels constitute a class of soft materials with very high water content. Hydrogelators, the molecules that cause hydrogelation, belong to a diverse class of molecules. As hydrogels find many applications in medicine, biocompatible hydrogelators have drawn considerable attention. [1,2] Peptides, owing to the diversity of the monomers that constitute them, their ease of synthesis, and the well-understood principles underlying their folding and self-assembly, are excellent candidates for biocompatible hydrogelators. [3] A large number of peptides have been reported in the literature that self-assemble to form β-sheet-rich fibrils, eventually causing hydrogelation. A vast majority of these peptides, however, employ bulky non-native aromatic moieties, such as fluorene and naphthalene. [4] Aromatic moieties facilitate self-assembly through stacking interactions and therefore serve as self-assembly platforms for hydrogels. [5–13] Incorporation of foreign aromatic moieties, however, raises safety concerns as far as biomedical applications are concerned. For instance, the degradation of Fmoc-FF hydrogel causes cell death through necrosis. [14] Therefore, the peptides that lack foreign moieties have gained considerable attention as biocompatible hydrogelators. Schneider and coworkers designed peptides with a β-turn-inducing motif that self-assembled under specific cues, causing hydrogelation. [15–17]. Stupp and coworkers designed a peptide amphiphile wherein a palmitoyl chain was attached to the N-terminus of the peptidic moiety. [18] The peptide self-assembles at acidic pH, forming hydrogels that direct the hydroxyapatite mineralization when treated with calcium chloride and dibasic sodium phosphate. Peptide amphiphile is an interesting template for designing self-assembling peptides with different properties and applications. [19–22] Native peptides are attractive gelators for biomedical applications as concerns about toxicity and immunogenicity are not there. Amyloid fibrils constitute an important class of self-assembling peptides. [23–25] Hauser and coworkers have reported hydrogelation by several short native *N*-acetylated amyloidogenic peptides. [26] Banerjee and coworkers reported hydrogel formed by a tetrapeptide from human amylin, hIAPP$_{24–27}$. [27] Maji and coworkers have also reported several amyloid peptide hydrogelators. [28,29] The potential of amyloid peptides as hydrogelators has been reviewed elsewhere. [30]

Hydrogelators with foreign aromatic moieties are usually very small in size. Unfortunately, peptide hydrogelators lacking foreign aromatic moieties are generally much larger. [15,19] The large size of the designed peptides raises concerns about immune response when it comes to applications such as drug delivery or scaffolds in regenerative medicine. An interesting approach, therefore, could be identifying short native peptide stretches that can undergo hydrogelation under physiological conditions or be engineered into hydrogelators through minimal modifications. We have previously investigated the hydrogelation of Aβ$_{16–22}$ (CH_3CO-KLVFFAE-NH_2). [31] The peptide does not cause hydrogelation up to 20 mM concentration. Substitution of Phe20 with Tyr turns it into a potent hydrogelator, where hydrogelation is observed

* Corresponding author.
E-mail address: chaudhary@iitg.ac.in (N. Chaudhary).

https://doi.org/10.1016/j.bpc.2025.107438
Received 6 December 2024; Received in revised form 10 March 2025; Accepted 22 March 2025
Available online 24 March 2025

at 2 mM peptide concentration. The peptide stock solutions, however, were required to be prepared in 1,1,1,3,3,3-hexofluoro-2-propanol (HFIP). We subsequently showed that the peptide wherein two $A\beta_{16-22}$ repeats are connected *via* β-turn supporting motifs is a gelator. [32] However, the stock solution was still required to be prepared in HFIP.

Our quest continued for native sequence(s) that could be dissolved in water to a very high concentration without gelation and diluted in PBS to obtain the gel. We surveyed short self-assembling native peptide sequences that could be salt-triggered to self-assemble. The following three criteria were applied to shortlist the peptides: (i) the peptide has one or more charged residues, (ii) there is at least one aromatic residue, and (iii) the peptide self-assembles through parallel β-sheet formation, preferably the in-register β-sheet. Parallel in-register β-sheet has been observed for many amyloidogenic proteins/peptides. [33] Such an arrangement places the identical residues juxtaposed in the strands of the β-sheet. If a peptide contains charged residues, electrostatic repulsion between juxtaposed residues discourages self-assembly. However, self-assembly can be facilitated through the shielding of charges by salt. These selection criteria led us to the peptide VQIVYK ($tau^{306-311}$). Mandelkow and coworkers first identified this peptide as the minimal interaction motif for tau self-assembly. [34,35] The hexapeptide, termed PHF6, was shown to form fibrils in the presence of heparin. Kirschner and coworkers investigated the end-capped $tau^{306-311}$, where the N-terminus of the peptide was acetylated while the C-terminus was an amide (CH_3CO-VQIVYK-NH_2). The peptide rapidly forms amyloid fibrils in the presence of 150 mM salt. [36] Eisenberg and coworkers subsequently investigated the microcrystals formed by VQIVYK, the peptide with free termini. They find that the peptide self-assembles through parallel in-register β-sheets. [37] These two studies convinced us that VQIVYK could be a promising salt-triggered gelator. $Tau^{306-311}$ self-assembly has been extensively investigated using theoretical as well as various experimental methods. [38–42] Despite a large volume of literature on the $tau^{306-311}$ self-assembly, there is no report on its hydrogelation. Here, we report that the peptide forms hydrogel as soon as it encounters the salt, an attribute that makes it a promising injectable hydrogelator.

We investigated the uncapped (VQIVYK) and the end-capped (CH_3CO-VQIVYK-NH_2) peptides. The uncapped peptide remained a clear solution in water as well as in PBS (137 mM NaCl, 2.7 mM KCl, 10 mM Na_2HPO_4, and 1.8 mM KH_2PO_4, pH 7.4). The end-capped peptide CH_3CO-VQIVYK-NH_2 (Ac-PHF6), on the other hand, formed a clear solution in water but caused instant gelation of PBS as well as the cell culture media DMEM and RPMI.

2. Materials and methods

2.1. Materials

Rink amide resin, Fmoc-protected amino acids, 1-Hydroxybenzotriazole hydrate (HOBt), and *N,N,N′,N′*-tetramethyl-*O*-(1*H*-benzotriazol-1-yl)uronium hexafluorophosphate (HBTU) were acquired from Novabiochem. Fmoc-Lys(Boc)-Wang resin was purchased from GL Biochem (Shanghai) Ltd., China. *N,N*-dimethylformamide, *N,N*-diisopropylethylamine (DIPEA), trifluoroacetic acid (TFA), acetic anhydride, thioflavin T (ThT), calcein, calcein-AM, diethyl ether, triisopropylsilane (TIPS), and rhodamine B were procured from Merck. Doxorubicin hydrochloride was purchased from Tokyo Chemical Industry (India) Pvt. Ltd. HEK cell line was obtained from the National Centre for Cell Science (NCCS), Pune, India. Dulbecco's Modified Eagle Medium (DMEM) and fetal bovine serum (FBS) for cell culture were procured from HiMedia, while RPMI 1640 medium and antibiotic-antimycotic cocktail were procured from Gibco. RNAiso Plus reagent was purchased from Takara Bio, Shiga, Japan, while MultiScribe™ Reverse Transcriptase was purchased from Applied Biosystems, Waltham, Massachusetts, USA. 3-(4,5-Dimethylthiazol-2-yl)-2,5-diphenyltetrazolium bromide (MTT) was procured from Sisco Research Laboratories Pvt. Ltd. (India).

2.2. Peptide synthesis and characterization

The peptides were synthesized by employing Fmoc chemistry with HBTU/HOBt/DIPEA activation. The uncapped peptide (VQIVYK) was assembled on Fmoc-Lys(Boc)-Wang resin, while Ac-PHF6 was assembled on Rink amide resin. N-terminal acetylation for Ac-PHF6 was carried out on-resin using 10-equivalents each of acetic anhydride and DIPEA. The peptides were cleaved from the resins using a cleavage cocktail containing 95 % TFA, 2.5 % TIPS, and 2.5 % water. The peptides were precipitated in ice-chilled diethyl ether, followed by multiple rounds of washing with diethyl ether. The peptides were air-dried and dissolved in water for analytical reversed-phase HPLC and purification. The identities of the peptides were ascertained using MALDI-TOF mass spectrometry on a Bruker Autoflex Speed MALDI-TOF mass spectrometer.

2.3. Peptide dissolution, hydrogelation, and rheology

Both peptides readily dissolved in water to very high concentrations (>20 mM). The concentrations were estimated using Tyr molar absorption coefficient of 1280 M^{-1} cm^{-1} at 280 nm. Both peptides formed clear, viscous solutions up to about 25 mM concentration. Gelation of PBS was attempted by diluting the peptide solutions to achieve 5, 10, 15, and 20 mM concentrations. Hydrogelation was established by gently inverting the 24-h-old tubes. Rheology measurements of 20 mM gel were carried on an Anton Paar Rheometer MCR 102 using 25 cm parallel plates at 0.5 mm gap. The amplitude sweep test was carried out at an angular frequency of 10 rad/s by varying shear strain from 0.01 % to 10 %. The gel showed a linear regime up to at least 0.2 % strain. Frequency sweep data was recorded with 0.1 % strain. Unless mentioned otherwise, all subsequent studies were carried out with 20 mM Ac-PHF6 samples prepared in water or PBS that were incubated at room temperature for 24 h.

2.4. Intrinsic tyrosine fluorescence spectroscopy

Intrinsic tyrosine fluorescence spectra were recorded for the 20 mM Ac-PHF6 samples prepared in water and PBS on a Jasco FP-8500 spectrofluorometer. As 20 mM is a very high concentration, the spectra were recorded by diluting the samples in respective dispersants (water or PBS) to 100 μM concentration. Fluorescence emission spectra were recorded from 290 to 400 nm with 5 nm slit width by exciting the samples at 280 nm (2.5 nm slit width).

2.5. Tyrosine fluorescence quenching

Tyrosine fluorescence quenching assay was carried out for the water and PBS samples at 100 and 200 μM concentrations. As ionic strength plays a critical role in the self-assembly of Ac-PHF6, acrylamide was used as the collisional quencher. The samples were excited at 280 nm, and fluorescence emission spectra were recorded. An increasing amount of acrylamide was added, and fluorescence emission spectra were recorded. The fluorescence intensities were taken at the emission λ_{max} corresponding to the unquenched samples, and data are presented as Stern-Volmer plots.

2.6. Thioflavin T (ThT) fluorescence spectroscopy

The ThT fluorescence emission spectrum for the Ac-PHF6 gel sample was recorded in PBS. As ThT fluorescence quantum yield strongly depends on pH, the fluorescence emission spectrum for the water sample was not recorded in water but in 10 mM phosphate buffer, pH 7.4, to enable direct comparison with the gel sample. The assay was carried out at 100 μM peptide concentration and 10 μM ThT concentration. The samples were excited at 450 nm (slit width = 2.5 nm), and emission spectra were recorded from 465 to 555 nm with 5 nm slit width.

2.7. Circular dichroism (CD) spectroscopy

Far-UV electronic CD spectra were recorded on a Jasco J-1500 spectropolarimeter. The 24-h-old 20 mM peptide samples were diluted to the desired concentrations in respective dispersants, and spectra were recorded in a 1 mm path-length quartz cell. The spectra were recorded from 250 to 195 nm at 1 nm bandwidth with a 100 nm/min scanning speed. Each spectrum is the average of 8 accumulations. The spectra were corrected by subtracting the respective dispersant's spectrum.

2.8. Fourier transform infrared (FTIR) spectroscopy

FTIR spectra were recorded on a Shimadzu IRAffinity-1S Fourier transform infrared spectrometer equipped with a diamond ATR crystal. The samples were diluted 2-fold, and ~ 5 μl volume of the diluted sample was deposited on the diamond crystal and allowed to dry. Each spectrum is the average of 40 scans recorded at 4 cm^{-1} resolution.

2.9. Transmission electron microscopy

The samples were diluted 2-fold in water and deposited on the carbon-coated copper grids. After 10 min, the excess solvent was removed using lint-free tissue paper, and grids were stained with uranyl acetate for 10 min. The grids were air-dried, and the images were captured at 200 kV using a JEM-2100F transmission electron microscope (JEOL, Japan).

2.10. Hydrogel stability

The stability/degradation of Ac-PHF6 hydrogel was investigated by monitoring the release of peptide molecules from hydrogel to the bulk solution. The 20 mM Ac-PHF6 hydrogel (100 μl) was prepared in PBS. The gel was washed once with 100 μl PBS, and 1.4 ml PBS was carefully added on top of the hydrogel. The concentration of Ac-PHF6, released into PBS from the hydrogel, was estimated using Tyr molar absorption coefficient of 1280 M^{-1} cm^{-1} at 280 nm. The hydrogel was subsequently sheared by vigorous vortexing and diluted 10-fold in PBS to measure the absorbance. The concentration of the sheared hydrogel was considered to be 100 % degradation.

2.11. Calcein release assay

Calcein at 500 μM concentration was trapped inside the gel. Briefly, 5 μl of 5 mM calcein stock solution prepared in 10× PBS was added to the cuvette. 45 μl of 22 mM peptide stock solution in water was subsequently added. The cuvette was left undisturbed for 24 h, resulting in a colored gel. The release of calcein was studied by gently adding 700 μl of PBS on top of the dye-containing gel and monitoring fluorescence emission intensity at 520 nm after exciting at 490 nm. The excitation and emission slit widths were 2.5 and 5 nm, respectively.

2.12. Doxorubicin release assay

Doxorubicin (23 μM) was trapped inside the Ac-PHF6 gel. Briefly, 5 μl of 0.23 mM doxorubicin stock solution prepared in 10× PBS was added to a quartz fluorescence cuvette. Subsequently, 45 μl of 22 mM peptide stock solution in water was added, and the cuvette was left undisturbed for 24 h at room temperature. After 24 h, 700 μl of PBS was gently added on top of the doxorubicin-loaded gel. Doxorubicin release was monitored by recording fluorescence emission intensity at 560 nm over time by exciting at 490 nm. The excitation and emission slit widths were 2.5 and 5 nm, respectively.

2.13. Drug loading efficiency

The drug loading efficiency of Ac-PHF6 hydrogel was assessed using doxorubicin as the representative drug. A 20 mM Ac-PHF6 hydrogel was prepared (100 μl volume). A 10 mM doxorubicin stock solution was prepared in PBS, 100 μl volume was carefully added on top of the gel, and incubated for 18 h. After 18 h incubation, the doxorubicin solution was removed, and the hydrogel was quickly washed once with 100 μl PBS. PBS (1.4 ml) was then added to the hydrogel, and the gel was sheared by vortexing. The sheared sample was 10-fold diluted, and absorbance was recorded at 495 nm. The concentration of doxorubicin was estimated using a molar absorption coefficient of 9250 M^{-1} cm^{-1} at 495 nm. [43]

2.14. Injectability

A 20 mM Ac-PHF6 stock solution was prepared in water that contained 0.4 mM rhodamine B. The peptide was carefully injected into a glass cuvette containing 3 ml PBS. While injecting the peptide, the pipette tip was gently withdrawn from the cuvette. Instant gelation resulted in a colored thread of peptide hydrogel dispersed in PBS. The video of the procedure can be found in the supplementary data (Movie M1). Images of the glass cuvette containing the hydrogel thread were captured at different times to see the rhodamine B release from the gel thread.

2.15. Cell culture assay

Human embryonic kidney (HEK-293) cells were cultured in a T25 flask using Dulbecco's Modified Eagle's Medium (DMEM) supplemented with 10 % fetal bovine serum (FBS) and 1 % antibiotic-antimycotic cocktail. The cells were incubated at 37 °C with 5 % CO_2 for growth and maintenance. The cells were harvested using trypsin. The 10 and 15 mM PBS gels (70 μl volume) were set up in a 96-well plate. After 24 h, 200 μl complete DMEM was added to the wells having gels, and the gels were incubated at 37 °C with 5 % CO_2 for 24 h. The medium was removed, and the gels were equilibrated with fresh complete medium for 10 min. Finally, the medium was removed, and the gels were seeded with HEK-293 cells (10^4 cells/well) and kept at 37 °C with 5 % CO_2 for 48 h. The wells were subsequently washed with PBS. A 5 μM calcein-AM solution was prepared in incomplete DMEM, and 200 μl volume was added to the wells for staining the cells. After 30 min of incubation, the cells were washed with PBS thrice, and images were recorded using a Nikon Eclipse Ts2R fluorescence microscope.

2.16. RNA isolation and polymerase chain reaction

The total RNA was isolated from HEK-293 cells using RNAiso Plus reagent (Takara Bio, Shiga, Japan). The cDNA was synthesized using MultiScribe™ Reverse Transcriptase (Applied Biosystems, Waltham, Massachusetts, USA). PCR (40 cycles) was carried out using primers designed for GAPDH amplification as described elsewhere. [31]

2.17. Cell viability assay

The biocompatibility of Ac-PHF6 was assessed through MTT assay. [21] Briefly, 10,000 HEK-293 cells in complete DMEM were seeded in a 96-well plate and incubated at 37 °C with 5 % CO_2 for 24 h. The cells were then treated with Ac-PHF6 (50, 100, 150, 200 μM), and further incubated for 24 h. Subsequently, the growth medium was discarded, and 100 μl of MTT (1 mg/ml in plain DMEM) was added to each well and incubated for 3 h. The MTT solution was then removed, and 100 μl dimethylsulfoxide was added to each well. The absorbance was recorded at 570 nm in a multiwell plate reader (Multiskan GO, Thermo Scientific).

2.18. Molecular dynamics simulation

The extended conformation ($\phi = \psi = 180^o$) of VQIVYK was created using UCSF Chimera. N-terminal acetylation and C-terminal amidation

were carried out using BIOVIA Discovery Studio. The self-assembly was investigated by including 216 randomly oriented peptide molecules in a cubic box having 8157.38 nm^3 volume. NaCl (150 mM) was subsequently added to the box. This setup corresponds to a peptide concentration of about 44 mM, a concentration much higher than the concentration at which gelation was experimentally observed. The C-terminal lysine residue contributes a positive charge to the peptide chain. Therefore, a chloride ion per peptide molecule was added to achieve an electrically-neutral system. Molecular dynamics simulation was performed with the GROMACS software package utilizing the CHARMM27 force field and a TIP3P water model. [44,45] The modeled system was subjected to energy minimization using the steepest descent algorithm and was equilibrated through NVT and NPT ensembles (500 ns each) before a 200 ns production MD run. The simulation employed the leap-frog integration method along with the Verlet cutoff scheme. Long-range electrostatic interactions were handled using the Particle Mesh Ewald (PME) method, while bond lengths were constrained with the LINCS algorithm. Periodic boundary conditions were applied throughout the simulation. The results were analyzed using VMD, UCSF-Chimera, and Gromacs built-in tools.

3. Results

The synthesized peptides were characterized using analytical HPLC and MALDI-TOF mass spectrometry. The peptides were found to be ≥ 95 % pure, as ascertained by the areas under the peaks in the chromatograms (Figure S1). The MALDI-TOF mass spectra confirmed the identity of the peptides (Figure S2).

3.1. Hydrogelation and rheology

Both peptides (VQIVYK and CH_3CO-VQIVYK-NH_2) readily dissolved in deionized water to >20 mM concentration, giving clear, viscous solutions that could be easily pipetted out. The peptides were diluted to achieve 5, 10, 15, and 20 mM concentrations in PBS. Instant gelation was observed for Ac-PHF6 at 20 mM concentration. All the samples were kept undisturbed for 24 h and assessed visually for gelation by gently inverting the vials. Ac-PHF6 formed soft and fragile gels at 10 and 15 mM concentrations but a much stronger gel at 20 mM (~1.6 wt%) concentration. The 10 and 20 mM gels in inverted tubes are shown in Fig. 1. The peptide caused instant gelation of cell culture media DMEM and RPMI 1640 as well at 20 mM concentration. The inverted tube showing DMEM gel is shown in Fig. 1D. The stock solution prepared in water remained viscous for at least a week and could also be stored at 4 °C without gelation. These attributes make Ac-PHF6 a promising injectable hydrogelator. The uncapped peptide VQIVYK, on the other hand, failed to cause gelation. Both water and PBS samples of VQIVYK remained as solutions up to at least 20 mM peptide concentration. VQIVYK, therefore, was not further investigated. Unless mentioned otherwise, all investigations were carried out for 20 mM Ac-PHF6 samples that were incubated for 24 h at room temperature. The 20 mM Ac-PHF6 hydrogel was subjected to rheological characterization. An oscillatory strain sweep was carried out to identify the linear viscoelastic region, *i.e.,* the oscillatory strain through which the complex stress varies linearly. [46] The gel displays a linear relationship for at least up to 0.2 % strain. Frequency sweep, therefore, was carried out at a strain of 0.1 % (Fig. 1E). The gel exhibits a storage modulus of around 20 kPa in the entire frequency range (624–0.01 rad/s).

3.2. Secondary structure characterization

The CD spectra were recorded by diluting the 20 mM samples to 100 μM concentration (Fig. 2A). The CD spectrum of the water sample suggests a largely unstructured peptide. On the other hand, the PBS sample displays a negative band around 225 nm and a positive band around 200 nm, suggesting a distinct β-sheet conformation. Interestingly,

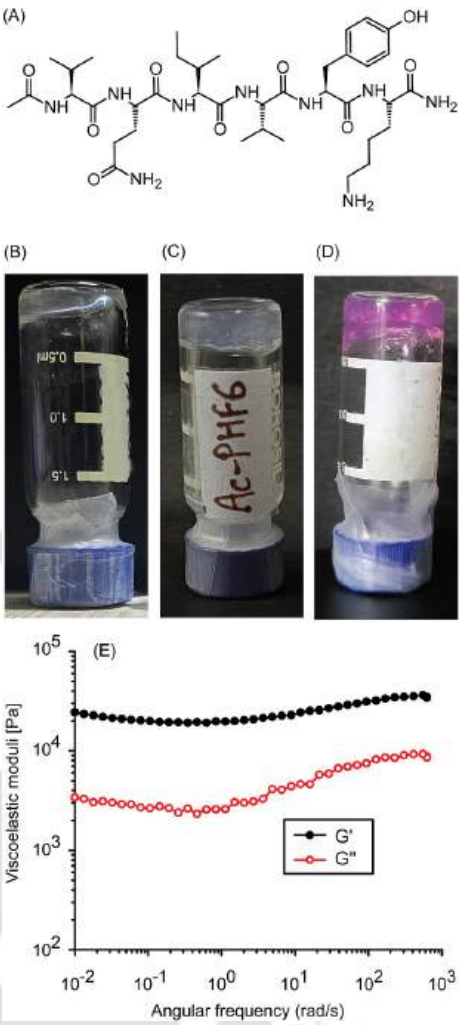

Fig. 1. Hydrogelation caused by Ac-PHF6. (A) Chemical structure of Ac-PHF6, (B) PBS gel formed by 10 mM peptide, (C) PBS gel formed by 20 mM peptide, (D) DMEM gel formed by 20 mM peptide, and (E) frequency sweep rheological characterization of 20 mM PBS gel.

however, attenuated total reflectance-Fourier transform infrared (ATR-FTIR) spectra of the dried peptide exhibit amide I band ~1626 cm^{-1} for both the samples, indicating β-sheet structure (Fig. 2B). [47] At first, the infrared spectroscopy data may appear to contradict the CD data. However, it is important to note that ATR-FTIR spectra were recorded in the dried form, while CD spectra were recorded in solution. Drying is associated with a gradual increase in peptide concentration that can facilitate self-assembly in water as well, eventually showing the amide I band around 1626 cm^{-1}. To validate this interpretation, we recorded the CD spectra for 20 mM water sample by diluting it to 400 and 200 μM concentrations (Figure S3). The spectrum recorded at 400 μM concentration shows distinct bands around 219 and 206 nm, suggesting a mixture of β-sheet and random coil conformations. At 200 μM concentration, these bands are blue-shifted. Besides, the intensity of the 214 nm band is much smaller than the 198 nm band, suggesting a larger contribution from random coil conformation. These data indicate that the peptide takes up a β-sheet conformation at high concentrations, and dilution shifts the equilibrium towards unordered conformation.

3.3. Molecular dynamics simulation

MD simulation of 216 Ac-PHF6 molecules in 150 mM NaCl was carried out for 200 ns. The peptide molecules in extended conformation

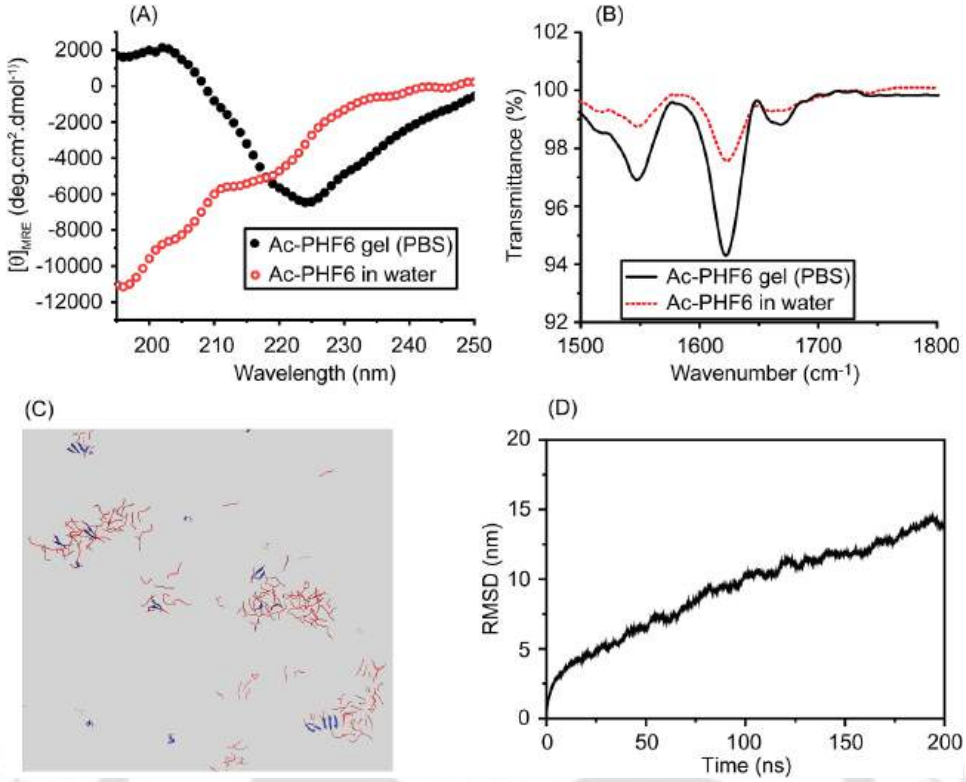

Fig. 2. Characterization of self-assembled structures underlying the hydrogel. (A) CD spectra, (B) FTIR spectra, (C) Snapshot after 200 ns molecular dynamics simulation, showing clustering of peptide molecules. (D) RMSD plotted against time, showing that the system has not reached equilibrium.

were randomly oriented in the box. The 200 ns snapshot is shown in Fig. 2C, where peptide molecules can be seen forming clusters, some of them elongated. The simulation time (200 ns), however, was insufficient to attain the equilibrium, as suggested by the increasing root mean squared deviation throughout the 200 ns simulation (Fig. 2D).

3.4. ThT fluorescence

ThT fluorescence spectra were recorded to investigate the nature of self-assembled structures. ThT is a benzothiazole dye that displays enhanced fluorescence emission intensity when bound to cross-β sheet-rich fibrillar structures, the structure that forms the core of amyloid fibrils. [48] As ThT fluorescence emission quantum yield is sensitive to pH, the spectrum for the water sample was recorded in low ionic strength buffer (10 mM phosphate buffer, pH 7.4) instead of water. The PBS sample causes a large enhancement in ThT fluorescence intensity, whereas no significant enhancement is observed for the water sample (Fig. 3A).

3.5. Intrinsic tyrosine fluorescence

As very high concentration brings in the inner-filter effect, intrinsic tyrosine fluorescence spectra for 20 mM samples were recorded by diluting them to 100 μM concentration in the respective dispersant. Excitation at 280 nm resulted in emission spectra with λ_{max} around 303 nm for both samples (Fig. 3B). The PBS sample, however, displays a much lower quantum yield than the water sample. The lower quantum yield could be multifactorial. These factors include absorption flattening due to self-assembly-induced local increase in chromophore (Tyr) concentration, the self-quenching of the stacked tyrosine side chains, and quenching by 150 mM chloride ions present in PBS.

Tyrosine fluorescence quenching data are presented as Stern-Volmer plots (Fig. 3C-F). The data for both water and PBS samples could be fit linearly. The Stern-Volmer constants (K_{SV}) observed for water samples at 100 and 200 μM peptide concentrations were 15.6 ± 3.1 M^{-1} (Fig. 3C) and 15.11 ± 2.77 M^{-1} (Fig. 3D), respectively. The K_{SV} values obtained for PBS samples, on the other hand, were lower. The 100 and 200 μM PBS samples displayed K_{SV} values of 11.4 ± 2.96 M^{-1} (Fig. 3E) and 10.6 ± 2.44 M^{-1} (Fig. 3F), respectively. The lower K_{SV} values observed for PBS samples suggest that the peptide self-assembly in PBS shields the tyrosine residues from the aqueous quencher.

3.6. Transmission electron microscopy

TEM images reveal long fibrillar structures for both PBS (Fig. 4A) and water (Fig. 4B) samples. The morphology of the fibers, however, looks very different. While the PBS sample shows fibrils that are very typical of amyloid fibrils, those observed for the water sample are more like tapes. As the Ac-PHF6 water sample displayed largely unordered conformation in solution (Fig. 2A) and no appreciable enhancement in ThT fluorescence intensity when diluted to 100 μM concentration (Fig. 3A), we conclude that the tape-like structures observed in TEM are formed at high concentrations or during the drying process.

3.7. Hydrogel stability

The stability of Ac-PHF6 hydrogel was assessed by monitoring the release of peptide from the hydrogel into the bulk solution. The 100 μl hydrogel was submerged in 1.4 ml PBS, and the peptide release was estimated by measuring peptide concentration in PBS as a function of time. Less than 5 % peptide accumulated in PBS after 2 weeks of incubation, suggesting good hydrogel stability (Fig. 4C).

3.8. Drug/dye release and cell culture

Small molecule entrapment, followed by subsequent release, was examined using fluorescent dye calcein and anticancer drug doxorubicin. The gels were prepared in the fluorescence cuvette, and these

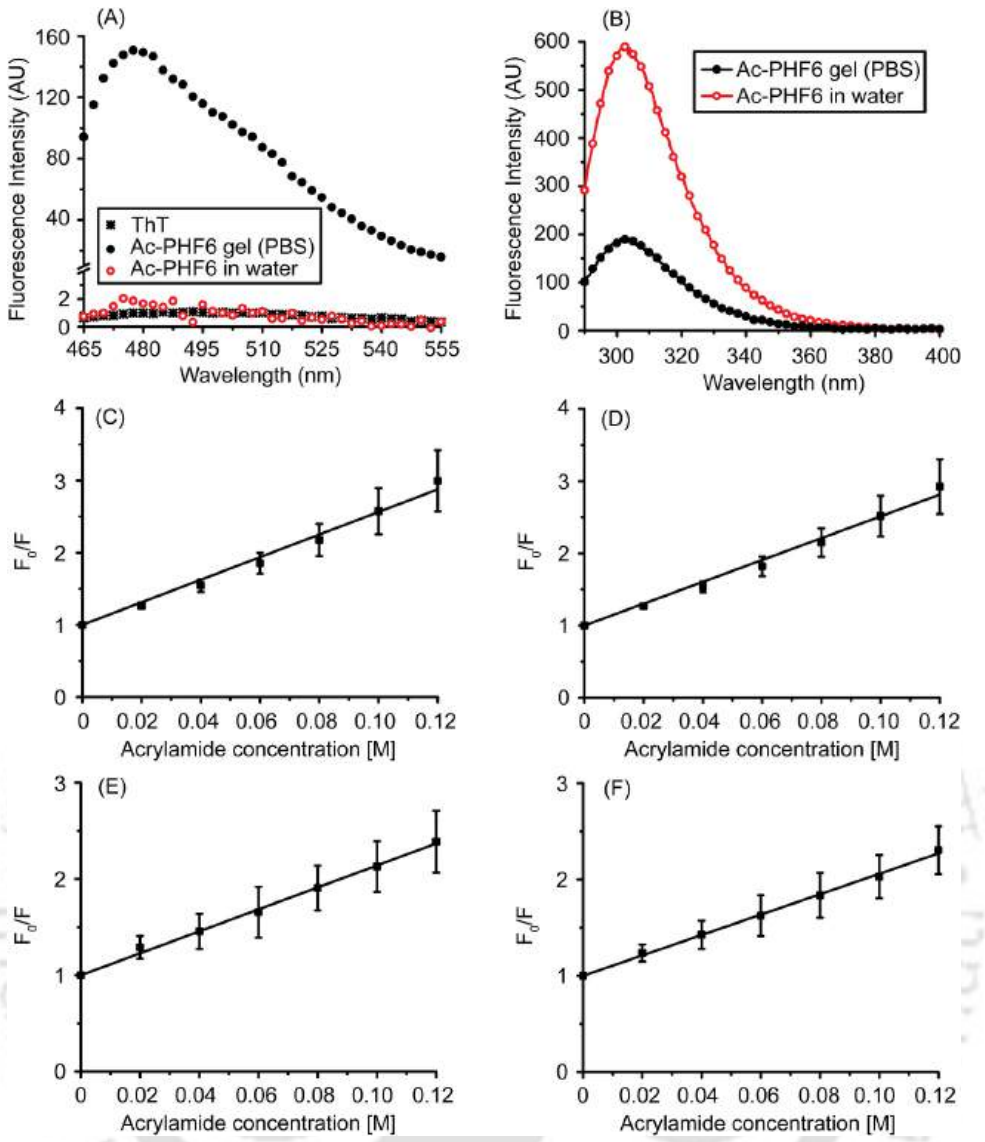

Fig. 3. Fluorescence spectroscopy. ThT fluorescence spectra of Ac-PHF6 samples in water and PBS (A). Intrinsic tyrosine fluorescence emission spectra (B), Stern-Volmer plots for Ac-PHF6 in water at 100 μM (C) and 200 μM (D) peptide concentrations, and Stern-Volmer plots for Ac-PHF6 in PBS at 100 μM (E) and 200 μM (F) peptide concentrations.

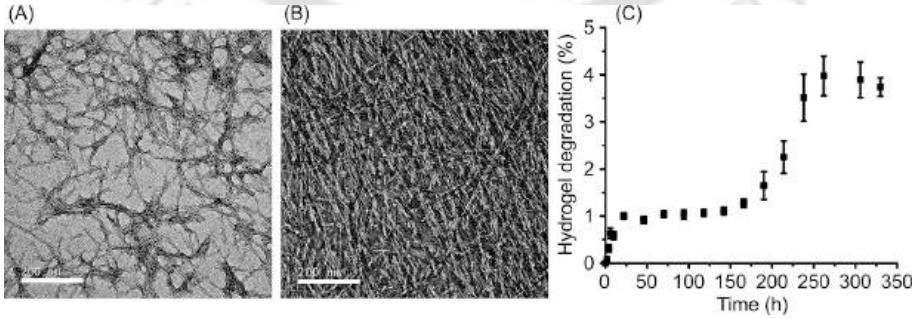

Fig. 4. Transmission electron microscopy and hydrogel degradation. TEM images for Ac-PHF6 samples in PBS (A) and water (B). Scale bars represent 200 nm. The hydrogel degradation (peptide release from hydrogel) over time (C).

molecules were entrapped during the gelation process. PBS was carefully added on top of the gel, and fluorescence emission intensity was measured as a function of time (Fig. 5A and B). Steady release of the molecules is observed for about 12 h, beyond which no further enhancement in fluorescence emission intensity was observed. The effect of drug entrapment on the morphology of fibrils underlying hydrogels was investigated. The 24-h-old hydrogel containing 23 μM doxorubicin was investigated by TEM (Fig. 5C). No noticeable change in fibril morphology is observed, suggesting that drug entrapment does not adversely affect the Ac-PHF6 fibrils. The doxorubicin loading capacity

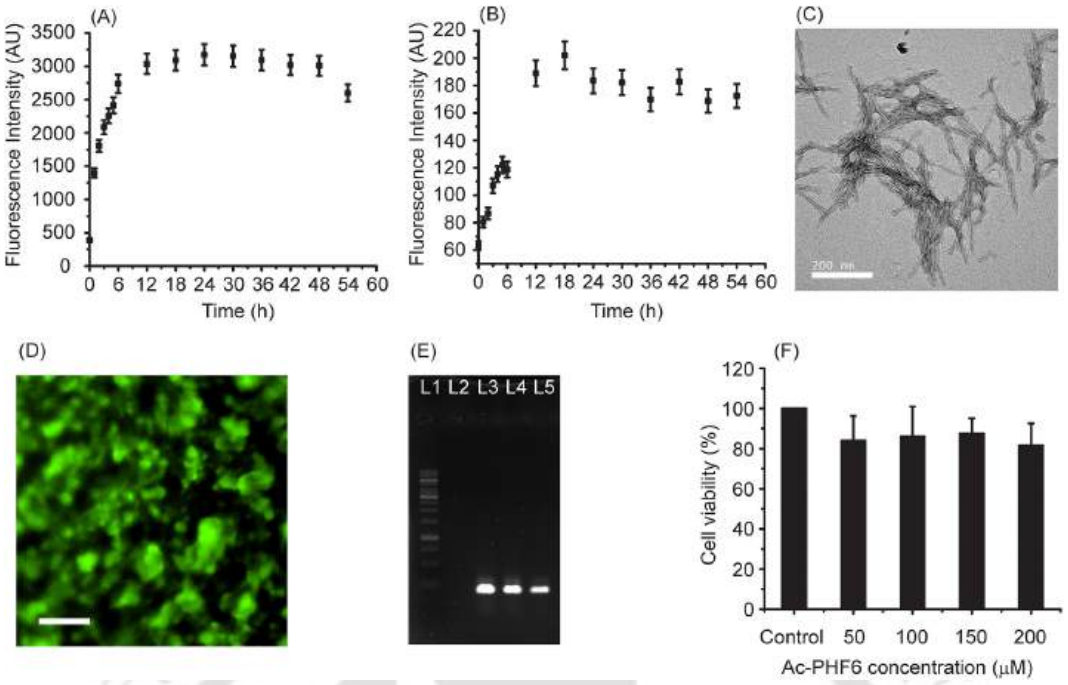

Fig. 5. Biomedical applications. Release of calcein dye (A) and anticancer drug doxorubicin (B) from PBS hydrogels, (C) morphology of the doxorubicin-harboring hydrogel (scale bar = 200 nm), (D) calcein fluorescence image of HEK-293 cells growing in the hydrogel. The scale bar represents 50 μm (E) Agarose gel electrophoresis showing GAPDH expression. L1 is the marker lane, L2 is negative control, L3 is positive control (HEK-293 cells growing in DMEM, without peptide gel), and L4 and L5 represent the cells growing in 10 mM and 15 mM gels, respectively. (F) HEK-293 cell viability, as assessed using MTT assay.

was determined by layering an equal volume of concentrated (10 mM) doxorubicin solution on top of 20 mM hydrogel and estimating the doxorubicin uptake after 18 h. The doxorubicin concentration in the hydrogel was estimated to be 292.8 ± 19.4 μM. This corresponds to 169.8 ± 11.2 μg doxorubicin/ml hydrogel.

HEK-293 cells were used for cell culture assays. Ac-PHF6 gel prepared in PBS was equilibrated with DMEM and seeded with about 10,000 cells, which were allowed to grow for 48 h. The cells were stained with calcein acetoxymethyl ester (Calcein-AM). Calcein AM is a hydrophobic, non-fluorescent compound that readily crosses the cell membrane. Following cellular uptake, it is hydrolyzed by cellular esterases to give fluorescent calcein. Therefore, calcein fluorescence is directly related to the activity of cellular esterases, which in turn is linked to cell viability. HEK-293 cells were found to grow inside the gel (Fig. 5D). Besides, the expression of the housekeeping gene GAPDH was analyzed. The cells grown without Ac-PHF6 (positive control), in 10 mM hydrogel, and in 15 mM hydrogel were harvested. The RNA was isolated and amplified into DNA through reverse-transcriptase PCR. The cells grown in the gel were found to express GAPDH (Fig. 5E).

The biocompatibility of Ac-PHF6 was further assessed through cell viability assay. The metabolically active cells reduce MTT into formazan that absorbs 570 nm light. Dead cells, on the other hand, cannot reduce the MTT, failing to contribute to the signal. The percentage cell viability was calculated with respect to the peptide-untreated cells (Fig. 5F). No significant decrease in cell viability was observed at the peptide concentrations tested, suggesting that the peptide is non-toxic up to at least 200 μM concentration.

3.9. Injectability

All the assays discussed above were carried out with gel samples that were 24 h old. An injectable hydrogelator should cause instant gelation of a biological fluid. To assess injectability, a 20 mM peptide stock solution was prepared in water that contained 0.4 mM rhodamine B. The colored solution thus obtained was slowly injected into the PBS while slowly withdrawing the pipette tip. The peptide displayed gelation as soon as it came in contact with the PBS. Withdrawal of the pipette tip from the PBS resulted in a long gel thread (Movie M1). The photographs of the gel thread-containing glass cuvette, taken at different time points, reveal the gradual release of rhodamine B from the gel thread. The release of dye was more or less complete in 2 h (Figure S4). It is likely that the surface of the string observed in the movie M1 gels quickly, and the internal region gels somewhat slower. When it comes to injectability, the concentration of phosphate plays an important role in pain sensation at the injection site. [49] The recommended phosphate concentration is ≤10 mM. The PBS that we used in this study contained 11.8 mM phosphate, a little higher than the recommended concentration. Therefore, we investigated whether phosphate is essential for Ac-PHF6 self-assembly and hydrogelation. We found that 150 mM NaCl was sufficient to cause gelation (data not shown), confirming that the gelation is a salt-induced effect and phosphate is dispensable.

4. Conclusion

Amyloidogenic peptides and the short peptide stretches derived from them have a negative connotation attached to them. It is often argued that the peptides derived from amyloidogenic proteins/peptides could possess cytotoxicity. Research in the past few decades has established that the cytotoxicity of amyloids is primarily associated with prefibrillar oligomers, with mature fibrils being the inert species. [50–55] The kinetics of self-assembly, therefore, is associated with cytotoxicity. Slow aggregation kinetics implies a longer life span of prefibrillar species that could lead to cytotoxicity. [56] Therefore, the peptides that display rapid self-assembly, preferably without any lag phase, display little or no cytotoxicity. This theory is further supported by many functional amyloids discovered in very diverse organisms, including humans, that show rapid aggregation kinetics. [57,58] Amyloid fibrils are no longer considered a pathogenic fold. Pituitary peptide hormones are stored in the form of amyloid fibrils. [59] Maji and coworkers have designed peptide hydrogelators based on the amyloidogenic stretches from β-amyloid and α-synuclein. The hydrogels thus obtained could be used for stem cell differentiation. [28,29]. Besides, a vast majority of peptide

hydrogelators reported in the literature self-assemble through β-sheet formation. [60,61] The underlying architecture of these self-assembled structures is a cross-β-sheet, the so-called amyloid fold. [62] Therefore, the concerns about the cytotoxicity of amyloid-derived peptide hydrogelators may be unnecessary, especially when the peptides display rapid self-assembly kinetics. Ac-PHF6 displays rapid self-assembly, wherein mere contact with PBS causes gelation. The simple selection criteria that led us to identify Ac-PHF6 as a potential hydrogelator could be used to identify more such peptides. To conclude, Ac-PHF6 is a promising injectable hydrogelator that forms a viscous solution in water but causes instant gelation of phosphate-buffered saline and cell culture media.

4.1. Future directions

We establish Ac-PHF6, a native peptide stretch from human tau, as a promising injectable hydrogelator. Injectable hydrogels are particulary suitable as drug delivery vehicles. Using doxorubicin and calcein, we have shown that the gel can entrap small molecules that are slowly released from the gel into the bulk solution. As calcein and doxorubicin are almost completely released from the gel within 12 h, it would be interesting to investigate if chemical cross-linking of the gel improves drug retention for a longer duration. Ac-PHF6 hydrogel stability assay shows that at least 95 % of peptide remains inside the hydrogel for up to two weeks. This is a valuable attribute of a wound-dressing material that can keep the wound moist, supporting regular cellular activity and promoting healing. However, a hydrogel should eventually degrade when it comes to non-topical biomedical applications. Therefore, the hydrogel degradability for such applications should be assessed in serum as well. As our focus was to identify a native, biocompatible hydrogelator, we did not attempt to engineer the peptide for better hydrogelators. Ac-PHF6 contains tyrosine as the sole aromatic residue. Considering the far greater prevalence of Phe over Tyr in short peptide hydrogelators, it would be worth investigating if substituting Tyr to Phe improves the hydrogelation propensity and other gel attributes. Tuttle and coworkers investigated the tripeptide sequence space with free termini and proposed certain guidelines that promote tripeptide gelation. [63] They proposed that a positively charged residue is preferred at N-terminus, while aromatic residues are more favourable at positions 2 and 3 in the tripeptide. Position 3 of a tripeptide is the C-terminal residue. It is interesting to note that transferring the C-terminal lysine to the N-terminus would render the tyrosine residue to be at the C-terminus. Even though Tuttle's guidelines may not be applicable to longer peptide sequences, it would be interesting to investigate if transferring the C-terminal lysine to N-terminus improves the hydrogel.

Supplementary data to this article can be found online at https://doi.org/10.1016/j.bpc.2025.107438.

CRediT authorship contribution statement

Shubhangini Singh Verma: Writing – original draft, Investigation. **Shinjini Bhattacharya:** Investigation. **Sachin Kumar:** Writing – review & editing, Supervision, Resources. **Nitin Chaudhary:** Writing – review & editing, Supervision, Resources, Funding acquisition, Conceptualization.

Funding

Funding from the DBT Twinning project BT/PR15921/NER/95/140/2015, Department of Biotechnology, Ministry of Science and Technology, India is acknowledged.

Declaration of competing interest

The authors declare that they have no known competing financial interests or personal relationships that could have appeared to influence the work reported in this paper.

Acknowledgements

SSV and SB acknowledge the Ministry of Education, Govt. of India for fellowship. The authors thank Central Instruments Facility, IIT Guwahati, for transmission electron microscopy imaging and MALDI-TOF mass spectrometry.

References

[1] Q. Chai, Y. Jiao, X. Yu, Hydrogels for biomedical applications: their characteristics and the mechanisms behind them, Gels 3 (2017).
[2] M. Rostamipoor, A. Farsinejad, M. Amiri, A. Fatemi, P. Khazaeli, S. Anvari, Topical ocular administration using thermosensitive chitosan-glycerophosphate-PRP hydrogels for improved ocular bioavailability, Biophys. Chem. 305 (2024) 107141.
[3] D. Datta, N. Chaudhary, Chapter 8 - peptide-based hydrogels for biomedical applications, in: Y. Hasija (Ed.), Translational Biotechnology, Academic Press, 2021, pp. 203–232.
[4] S. Loic, Amino acids modification to improve and fine-tune peptide- based hydrogels, in: T. Asao (Ed.), Amino Acid, InTech, Rijeka, 2017.
[5] Dassault Systèmes BIOVIA, Discovery Studio Modeling Environment, Release 2017, Dassault Systèmes, San Diego, 2016.
[6] R. Orbach, L. Adler-Abramovich, S. Zigerson, I. Mironi-Harpaz, D. Seliktar, E. Gazit, Self-assembled Fmoc-peptides as a platform for the formation of nanostructures and hydrogels, Biomacromolecules 10 (2009) 2646–2651.
[7] V. Jayawarna, S.M. Richardson, A.R. Hirst, N.W. Hodson, A. Saiani, J.E. Gough, R. V. Ulijn, Introducing chemical functionality in Fmoc-peptide gels for cell culture, Acta Biomater. 5 (2009) 934–943.
[8] S. Fleming, S. Debnath, P.W.J.M. Frederix, T. Tuttle, R.V. Ulijn, Aromatic peptide amphiphiles: significance of the Fmoc moiety, Chem. Commun. 49 (2013) 10587–10589.
[9] A.D. Martin, P. Thordarson, Beyond Fmoc: a review of aromatic peptide capping groups, J. Mater. Chem. B 8 (2020) 863–877.
[10] T. Vijayakanth, S. Dasgupta, P. Ganatra, S. Rencus-Lazar, A.V. Desai, S. Nandi, R. Jain, S. Bera, A.I. Nguyen, E. Gazit, R. Misra, Peptide hydrogen-bonded organic frameworks, Chem. Soc. Rev. 53 (2024) 3640–3655.
[11] P. Chakraborty, Y. Tang, T. Yamamoto, Y. Yao, T. Guterman, S. Zilberzwige-Tal, N. Adadi, W. Ji, T. Dvir, A. Ramamoorthy, G. Wei, E. Gazit, Unusual two-step assembly of a minimalistic dipeptide-based functional Hypergelator, Adv. Mater. 32 (2020) 1906043.
[12] S. Bera, X. Dong, B. Krishnarjuna, S.A. Raab, D.A. Hales, W. Ji, Y. Tang, L.J. W. Shimon, A. Ramamoorthy, D.E. Clemmer, G. Wei, E. Gazit, Solid-state packing dictates the unexpected solubility of aromatic peptides, Cell Report. Phys. Sci. 2 (2021) 100391.
[13] G. Fichman, T. Guterman, J. Damron, L. Adler-Abramovich, J. Schmidt, E. Kesselman, L.J.W. Shimon, A. Ramamoorthy, Y. Talmon, E. Gazit, Spontaneous structural transition and crystal formation in minimal supramolecular polymer model, Sci. Adv. 2 (2025) e1500827.
[14] W.T. Truong, Y. Su, D. Gloria, F. Braet, P. Thordarson, Dissolution and degradation of Fmoc-diphenylalanine self-assembled gels results in necrosis at high concentrations in vitro, biomaterials, Science 3 (2015) 298–307.
[15] J.P. Schneider, D.J. Pochan, B. Ozbas, K. Rajagopal, L. Pakstis, J. Kretsinger, Responsive hydrogels from the intramolecular folding and self-assembly of a designed peptide, J. Am. Chem. Soc. 124 (2002) 15030–15037.
[16] D.J. Pochan, J.P. Schneider, J. Kretsinger, B. Ozbas, K. Rajagopal, L. Haines, Thermally reversible hydrogels via intramolecular folding and consequent self-assembly of a de novo designed peptide, J. Am. Chem. Soc. 125 (2003) 11802–11803.
[17] B. Ozbas, J. Kretsinger, K. Rajagopal, J.P. Schneider, D.J. Pochan, Salt-triggered peptide folding and consequent self-assembly into hydrogels with tunable Modulus, Macromolecules 37 (2004) 7331–7337.
[18] J.D. Hartgerink, E. Beniash, S.I. Stupp, Self-assembly and mineralization of peptide-amphiphile nanofibers, Science 294 (2001) 1684–1688.
[19] J.D. Hartgerink, E. Beniash, S.I. Stupp, Peptide-amphiphile nanofibers: a versatile scaffold for the preparation of self-assembling materials, Proc. Natl. Acad. Sci. USA 99 (2002) 5133–5138.
[20] K.L. Niece, J.D. Hartgerink, J.J. Donners, S.I. Stupp, Self-assembly combining two bioactive peptide-amphiphile molecules into nanofibers by electrostatic attraction, J. Am. Chem. Soc. 125 (2003) 7146–7147.
[21] B. Hansda, J. Majumder, B. Mondal, A. Chatterjee, S. Das, S. Kumar, R. Gachhui, V. Castelletto, I.W. Hamley, P. Sen, A. Banerjee, Histidine-containing amphiphilic peptide-based non-cytotoxic Hydrogelator with antibacterial activity and sustainable drug release, Langmuir 39 (2023) 7307–7316.
[22] A. Baral, S. Roy, A. Dehsorkhi, I.W. Hamley, S. Mohapatra, S. Ghosh, A. Banerjee, Assembly of an injectable noncytotoxic peptide-based Hydrogelator for sustained release of drugs, Langmuir 30 (2014) 929–936.
[23] P.C. Ke, R. Zhou, L.C. Serpell, R. Riek, T.P.J. Knowles, H.A. Lashuel, E. Gazit, I. W. Hamley, T.P. Davis, M. Fändrich, D.E. Otzen, M.R. Chapman, C.M. Dobson, D. S. Eisenberg, R. Mezzenga, Half a century of amyloids: past, present and future, Chem. Soc. Rev. 49 (2020) 5473–5509.

[24] M. Juković, I. Ratkaj, D. Kalafatovic, N.J. Bradshaw, Amyloids, amorphous aggregates and assemblies of peptides – assessing aggregation, Biophys. Chem. 308 (2024) 107202.
[25] P. Dey, P. Biswas, Exploring the aggregation of amyloid-β 42 through Monte Carlo simulations, Biophys. Chem. 297 (2023) 107011.
[26] A. Lakshmanan, D.W. Cheong, A. Accardo, E. Di Fabrizio, C. Riekel, C.A. Hauser, Aliphatic peptides show similar self-assembly to amyloid core sequences, challenging the importance of aromatic interactions in amyloidosis, Proc. Natl. Acad. Sci. USA 110 (2013) 519–524.
[27] J. Naskar, G. Palui, A. Banerjee, Tetrapeptide-based hydrogels: for encapsulation and slow release of an anticancer drug at physiological pH, J. Phys. Chem. B 113 (2009) 11787–11792.
[28] R.S. Jacob, D. Ghosh, P.K. Singh, S.K. Basu, N.N. Jha, S. Das, P.K. Sukul, S. Patil, S. Sathaye, A. Kumar, A. Chowdhury, S. Malik, S. Sen, S.K. Maji, Self healing hydrogels composed of amyloid nano fibrils for cell culture and stem cell differentiation, Biomaterials 54 (2015) 97–105.
[29] S. Das, K. Zhou, D. Ghosh, N.N. Jha, P.K. Singh, R.S. Jacob, C.C. Bernard, D. I. Finkelstein, J.S. Forsythe, S.K. Maji, Implantable amyloid hydrogels for promoting stem cell differentiation to neurons, NPG Asia Mater. 8 (2016) e304.
[30] V.K. Belwal, N. Chaudhary, Amyloids and their untapped potential as hydrogelators, Soft Matter 16 (2020) 10013–10028.
[31] D. Datta, V. Kumar, S. Kumar, R. Nagaraj, N. Chaudhary, Hydrogel formation by an aromatic analogue of a β-amyloid fragment, Aβ16–22: a scaffold for 3D cell culture, ACS Omega 4 (2019) 620–627.
[32] D. Datta, V. Kumar, S. Kumar, R. Nagaraj, N. Chaudhary, Limpid hydrogels from β-turn motif-connected tandem repeats of Aβ16–22, Soft Matter 15 (2019) 4827–4835.
[33] M. Margittai, R. Langen, Fibrils with parallel in-register structure constitute a major class of amyloid fibrils: molecular insights from electron paramagnetic resonance spectroscopy, Q. Rev. Biophys. 41 (2008) 265–297.
[34] M. von Bergen, P. Friedhoff, J. Biernat, J. Heberle, E.M. Mandelkow, E. Mandelkow, Assembly of tau protein into Alzheimer paired helical filaments depends on a local sequence motif ((306)VQIVYK(311)) forming beta structure, Proc. Natl. Acad. Sci. USA 97 (2000) 5129–5134.
[35] M. von Bergen, S. Barghorn, L. Li, A. Marx, J. Biernat, E.-M. Mandelkow, E. Mandelkow, Mutations of tau protein in frontotemporal dementia promote aggregation of paired helical filaments by enhancing local β-structure*, J. Biol. Chem. 276 (2001) 48165–48174.
[36] W.J. Goux, L. Kopplin, A.D. Nguyen, K. Leak, M. Rutkofsky, V. D. Shanmuganandam, D. Sharma, H. Inouye, D.A. Kirschner, The formation of straight and twisted filaments from short tau peptides, J. Biol. Chem. 279 (2004) 26868–26875.
[37] M.R. Sawaya, S. Sambashivan, R. Nelson, M.I. Ivanova, S.A. Sievers, M.I. Apostol, M.J. Thompson, M. Balbirnie, J.J. Wiltzius, H.T. McFarlane, A.O. Madsen, C. Riekel, D. Eisenberg, Atomic structures of amyloid cross-beta spines reveal varied steric zippers, Nature 447 (2007) 453–457.
[38] S.J.A. Shah, Q. Zhang, J. Guo, H. Liu, H. Liu, J. Villà-Freixa, Identification of aggregation mechanism of acetylated PHF6* and PHF6 tau peptides based on molecular dynamics simulations and Markov state modeling, ACS Chem. Neurosci. 14 (2023) 3959–3971.
[39] E. Pretti, M.S. Shell, Mapping the configurational landscape and aggregation phase behavior of the tau protein fragment PHF6, Proc. Natl. Acad. Sci. 120 (2023) e2309995120.
[40] S. Paul, P. Biswas, Molecular dynamics simulation study of the self-assembly of tau-derived PHF6 and its inhibition by Oleuropein Aglycone from extra virgin olive oil, J. Phys. Chem. B 128 (2024) 5630–5641.
[41] I. Stroganova, Z. Toprakcioglu, H. Willenberg, T.P.J. Knowles, A.M. Rijs, Unraveling the structure and dynamics of ac-PHF6-NH2 tau segment oligomers, ACS Chem. Neurosci. 15 (2024) 3391–3400.
[42] I. Stroganova, H. Willenberg, T. Tente, A. Depraz Depland, S. Bakels, A.M. Rijs, Exploring the aggregation propensity of PHF6 peptide segments of the tau protein using ion mobility mass spectrometry techniques, Anal. Chem. 96 (2024) 5115–5124.
[43] S. Moktan, E. Perkins, F. Kratz, D. Raucher, Thermal targeting of an acid-sensitive doxorubicin conjugate of elastin-like polypeptide enhances the therapeutic efficacy compared with the parent compound in vivo, Mol. Cancer Ther. 11 (2012) 1547–1556.
[44] S. Pronk, S. Pall, R. Schulz, P. Larsson, P. Bjelkmar, R. Apostolov, M.R. Shirts, J. C. Smith, P.M. Kasson, D. van der Spoel, B. Hess, E. Lindahl, GROMACS 4.5: a high-throughput and highly parallel open source molecular simulation toolkit, Bioinformatics 29 (2013) 845–854.
[45] P. Bjelkmar, P. Larsson, M.A. Cuendet, B. Hess, E. Lindahl, Implementation of the CHARMM force field in GROMACS: analysis of protein stability effects from correction maps, virtual interaction sites, and water models, J. Chem. Theory Comput. 6 (2010) 459–466.
[46] M.H. Chen, L.L. Wang, J.J. Chung, Y.H. Kim, P. Atluri, J.A. Burdick, Methods to assess shear-thinning hydrogels for application as injectable biomaterials, ACS Biomater. Sci. Eng. 3 (2017) 3146–3160.
[47] R. Sarroukh, E. Goormaghtigh, J.M. Ruysschaert, V. Raussens, ATR-FTIR: a "rejuvenated" tool to investigate amyloid proteins, Biochim. Biophys. Acta 2013 (1828) 2328–2338.
[48] H. Naiki, K. Higuchi, M. Hosokawa, T. Takeda, Fluorometric determination of amyloid fibrils in vitro using the fluorescent dye, thioflavin T, Anal. Biochem. 177 (1989) 244–249.
[49] I. Usach, R. Martinez, T. Festini, J.-E. Peris, Subcutaneous injection of drugs: literature review of factors influencing pain sensation at the injection site, Adv. Ther. 36 (2019) 2986–2996.
[50] M. Bucciantini, E. Giannoni, F. Chiti, F. Baroni, L. Formigli, J. Zurdo, N. Taddei, G. Ramponi, C.M. Dobson, M. Stefani, Inherent toxicity of aggregates implies a common mechanism for protein misfolding diseases, Nature 416 (2002) 507–511.
[51] G. Bitan, E.A. Fradinger, S.M. Spring, D.B. Teplow, Neurotoxic protein oligomers–what you see is not always what you get, Amyloid 12 (2005) 88–95.
[52] S.W. Chen, S. Drakulic, E. Deas, M. Ouberai, F.A. Aprile, R. Arranz, S. Ness, C. Roodveldt, T. Guilliams, E.J. De-Genst, D. Klenerman, N.W. Wood, T.P. Knowles, C. Alfonso, G. Rivas, A.Y. Abramov, J.M. Valpuesta, C.M. Dobson, N. Cremades, Structural characterization of toxic oligomers that are kinetically trapped during alpha-synuclein fibril formation, Proc. Natl. Acad. Sci. USA 112 (2015) E1994–E2003.
[53] C.G. Glabe, Common mechanisms of amyloid oligomer pathogenesis in degenerative disease, Neurobiol. Aging 27 (2006) 570–575.
[54] C.G. Glabe, Structural classification of toxic amyloid oligomers, J. Biol. Chem. 283 (2008) 29639–29643.
[55] A. Laganowsky, C. Liu, M.R. Sawaya, J.P. Whitelegge, J. Park, M. Zhao, A. Pensalfini, A.B. Soriaga, M. Landau, P.K. Teng, D. Cascio, C. Glabe, D. Eisenberg, Atomic view of a toxic amyloid small oligomer, Science 335 (2012) 1228–1231.
[56] A. Brown, M. Török, Functional amyloids in the human body, Bioorg. Med. Chem. Lett. 40 (2021) 127914.
[57] D.M. Fowler, A.V. Koulov, C. Alory-Jost, M.S. Marks, W.E. Balch, J.W. Kelly, Functional amyloid formation within mammalian tissue, PLoS Biol. 4 (2006) e6.
[58] D.M. Fowler, A.V. Koulov, W.E. Balch, J.W. Kelly, Functional amyloid–from bacteria to humans, Trends Biochem. Sci. 32 (2007) 217–224.
[59] S.K. Maji, M.H. Perrin, M.R. Sawaya, S. Jessberger, K. Vadodaria, R.A. Rissman, P. S. Singru, K.P. Nilsson, R. Simon, D. Schubert, D. Eisenberg, J. Rivier, P. Sawchenko, W. Vale, R. Riek, Functional amyloids as natural storage of peptide hormones in pituitary secretory granules, Science 325 (2009) 328–332.
[60] A.M. Smith, R.J. Williams, C. Tang, P. Coppo, R.F. Collins, M.L. Turner, A. Saiani, R.V. Ulijn, Fmoc-diphenylalanine self assembles to a hydrogel via a novel architecture based on π–π interlocked β-sheets, Adv. Mater. 20 (2008) 37–41.
[61] K. Fu, H. Wu, Z. Su, Self-assembling peptide-based hydrogels: fabrication, properties, and applications, Biotechnol. Adv. 49 (2021) 107752.
[62] R. Gallardo, N.A. Ranson, S.E. Radford, Amyloid structures: much more than just a cross-β fold, Curr. Opin. Struct. Biol. 60 (2020) 7–16.
[63] P.W.J.M. Frederix, G.G. Scott, Y.M. Abul-Haija, D. Kalafatovic, C.G. Pappas, N. Javid, N.T. Hunt, R.V. Ulijn, T. Tuttle, Exploring the sequence space for (tri-) peptide self-assembly to design and discover new hydrogels, Nat. Chem. 7 (2015) 30–37.

RSC Advances

PAPER

View Article Online
View Journal | View Issue

Cite this: *RSC Adv.*, 2025, **15**, 22216

Substitution of tyrosine with electron-deficient aromatic amino acids improves Ac-PHF6 self-assembly and hydrogelation†

Shubhangini Singh Verma and Nitin Chaudhary *

The hexapeptide PHF6 (VQIVYK), an amyloidogenic peptide stretch from human tau, self-assembles *via* parallel in-register β-sheet formation, wherein Tyr residues are involved in aromatic stacking interactions. Ac-PHF6 (CH_3CO-VQIVYK-NH_2) forms a viscous solution in water but causes instant gelation of PBS and cell culture media. Aromatic substitutions have been reported in the literature to modulate the self-assembly of peptides. In this study, we perturbed the electronic properties of the sole aromatic residue in Ac-PHF6 and studied hydrogelation. The Tyr residue was substituted with Phe, and the phenyl moiety was then substituted with various electron-withdrawing groups at the *para* position. All peptides caused PBS gelation with comparable rheological properties. The structures underlying the hydrogels were β-sheet fibrils. The electron-deficient aromatic moieties improved self-assembly and hydrogelation. Ac-PHF6 and no other aromatic analog except the one having *p*-(trifluoromethyl)phenylalanine caused the gelation of deionized water. Water gelation caused by the *p*-(trifluoromethyl)phenylalanine-containing analog is likely hydrophobicity-driven.

Received 8th May 2025
Accepted 23rd June 2025

DOI: 10.1039/d5ra03251b

rsc.li/rsc-advances

Introduction

Hydrogels have emerged as promising soft materials in recent years. Their applications span very diverse areas.[1–6] Peptides constitute an important class of self-assembling polymers.[7–12] Hydrogels formed by self-assembling peptides have emerged as promising biomaterials.[13–32] Hydrogels formed by native peptides offer significant advantages as they circumvent concerns related to toxicity and immunogenicity. Most peptide hydrogelators reported in the literature self-assemble to form β-sheet-rich fibrils. Such fibrils are long known to be associated with amyloid diseases. Amyloid fibrils, therefore, were considered pathogenic structures. As many functional amyloids have been identified in the past few decades, amyloid fibrils are no longer considered pathogenic fibrils.[33,34] Amyloidogenic peptides, therefore, have gathered significant attention as biocompatible materials.

Amyloid peptides self-assemble *via* cross-β-sheet architecture to form fibrillar structures. Under appropriate conditions, such fibrillar structures can form robust three-dimensional hydrogels.[35,36] Hauser and coworkers demonstrated hydrogel formation by short, *N*-acetylated amyloidogenic peptides.[37] Banerjee and coworkers reported thermoreversible, pH-sensitive hydrogel formed by a human amylin tetrapeptide, $hIAPP_{24-27}$.[17] Maji and coworkers have reported several amyloid hydrogelators with promising biomedical applications.[38,39] Not all amyloid peptides cause hydrogelation. Mere self-assembly into fibrillar structures, therefore, does not necessitate hydrogelation. Subtle modifications, however, can dramatically affect the hydrogelation propensity.[40]

Compared to a much better understanding of peptide self-assembly in the past two decades, the understanding of peptide hydrogelation remains primitive. Hydrogelating peptides are often discovered serendipitously or through empirical screening rather than rational design. A deeper understanding of the molecular interactions governing self-assembly, such as hydrogen bonding, dipole–dipole forces, hydrophobic effects, and π–π stacking, should enable the prediction of hydrogelating peptides as well as their emergent properties.[10,41,42] Aromatic amino acids are crucial in peptide self-assembly, facilitating assembly through π-stacking interactions.[43–47] The occurrence of phenylalanine and tyrosine is far more than that of tryptophan in self-assembling peptides.[48] Reches and Gazit reported nanotubes formed by the peptide diphenylalanine.[49] They subsequently investigated the aromatic homodipeptides wherein halogen groups were attached to the phenyl ring.[44] Halogen modification had deterministic effects on the assembly of dipeptides and the emergent superstructures. Fmoc-Phe-OH, Fmoc-Tyr-OH, and Fmoc-Phe-Phe-OH have been reported in the literature to form hydrogels.[50–52] The self-assembly has been attributed to π–π interactions between the aromatic side chains and the Fmoc moiety.

a, Department of Biosciences and Bioengineering, Indian Institute of Technology Guwahati, Guwahati 781 039, India. E-mail: chaudhary@iitg.ac.in; Fax: +91-361-2582249; Tel: +91-361-2582224

† Electronic supplementary information (ESI) available. See DOI: https://doi.org/10.1039/d5ra03251b

$A\beta_{16-22}$, a well-studied amyloidogenic peptide from β-amyloid, harbors a pair of Phe residues that facilitate self-assembly.[53] The end-capped $A\beta_{16-22}$ (CH_3CO-KLVFFAE-NH_2) self-assembles to form antiparallel β-sheets. We have previously investigated the hydrogelation propensity of end-capped $A\beta_{16-22}$. The peptide fails to form hydrogel up to at least 20 mM concentration.[40] However, the peptide wherein Phe20 is substituted with Tyr forms hydrogel at as low as 2 mM concentration. A subtle perturbation of the aromatic ring's electronic properties, therefore, can dramatically affect self-assembly and hydrogelation. Nilsson and coworkers investigated the self-assembly and hydrogelation of phenyl-ring substituted Fmoc-Phe-OH. Such modifications alter the molecule's hydrophobicity and electronic properties, thereby influencing π–π interactions and self-assembly.[54–56] Fmoc-Tyr-OH is a better gelator than Fmoc-Phe. The hydroxyl group is an inductively electron-withdrawing group but an electron-donating group through resonance. The resonance effect usually outweighs the inductive effect of the hydroxyl group. Considering this, the phenolic ring in Fmoc-Tyr-OH is expected to be more electron-rich compared to the phenyl group. In contrast, the inductive effect is stronger than the resonance effect for halogens. Interestingly, Fmoc-F_5-Phe (Fmoc-protected pentafluorophenylalanine), an amino acid with depleted electron density in the pentafluorophenyl ring, forms better hydrogel than Fmoc-Tyr.[55] These results indicate that substitutions in the aromatic side chain can dramatically affect self-assembly and hydrogelation. It is important to note that the ring substitutions also contribute to the size of the aromatic side chain and its hydrophobicity. To understand if the aromatic residues confer aggregation propensity through their hydrophobicity and β-sheet propensity, the ring electronic effects, or ring geometry, Desamero and coworkers carried out a detailed investigation on $hIAPP_{22-29}$ (NFGAILSS).[57] They made many analogs by substituting the Phe23 ring with several electron-withdrawing and electron-donating groups. They found that the peptide analogs with electron-donating groups on the phenyl ring displayed poor aggregation, while those with electron-withdrawing groups displayed better self-assembly. Their results establish that aromatic electronic effects influence peptide self-assembly, with electron-withdrawing substituents promoting it.

We have recently reported $tau^{306-311}$ (CH_3CO-VQIVYK-NH_2), an amyloidogenic stretch from human tau, as a promising biocompatible hydrogelator.[58] Tau is a microtubule-associated protein that gets aggregated in several neurodegenerative diseases, collectively called tauopathies.[59,60] Mandelkow identified a couple of hexapeptide stretches ($tau^{306-311}$ and $tau^{275-280}$) that act as interaction motifs, facilitating tau self-assembly.[61,62] $Tau^{306-311}$ self-assembly has been investigated in great detail.[63–68] CH_3CO-VQIVYK-NH_2, known as Ac-PHF6 in the literature, forms a viscous solution in water but causes instant gelation of phosphate-buffered saline and the cell culture media DMEM and RPMI.[58] The peptide harbors a tyrosine residue. As uncapped VQIVYK is reported in the literature to self-assemble through parallel β-sheet formation where tyrosine residues are involved in aromatic stacking interactions,[69] we investigated the peptide analogs wherein Tyr was substituted with Phe or ring-substituted Phe (Table 1).

Table 1 The sequences of peptides employed in this study

Peptide sequence	Remarks
Ac-VQIVYK-am	Ac-PHF6 ($tau^{306-311}$)
Ac-VQIVFK-am	Tyr → Phe analog
Ac-VQIVF(fl)K-am	Tyr → *p*-fluorophenylalanine analog
Ac-VQIVF(CN)K-am	Tyr → *p*-cyanophenylalanine analog
Ac-VQIVF(NO_2)K-am	Tyr → *p*-nitrophenylalanine analog
Ac-VQIVF(CF_3)K-am	Tyr → *p*-(trifluoromethyl)phenylalanine analog

Materials and methods

Materials

Rink amide resin, Fmoc-protected natural amino acids, 1-hydroxybenzotriazole hydrate (HOBt), and *N*,*N*,*N*′,*N*′-tetramethyl-*O*-(1*H*-benzotriazol-1-yl)uronium hexafluorophosphate (HBTU) were acquired from Novabiochem. Fmoc-protected non-natural amino acids were purchased from GL Biochem (Shanghai) Ltd. *N*,*N*-Dimethylformamide, *N*,*N*-diisopropylethylamine (DIPEA), trifluoroacetic acid (TFA), acetic anhydride, thioflavin T (ThT), diethyl ether, triisopropylsilane (TIPS), and acetonitrile were procured from Merck.

Electrostatic charge density mapping

The structure of toluene was downloaded from PubChem, and aromatic moieties were prepared by substituting the *para* hydrogen atom of toluene using Avogadro 1.2 software.[70] Electrostatic charge density maps of toluene and its substituents were generated by creating the surface in Avogadro. The extended peptide structures (pdb files) were prepared using UCSF Chimera. The electrostatic charge density maps of the peptides in extended conformation were generated using the APBS (Adaptive Poisson-Boltzmann Solver) program in PyMOL.

Peptide synthesis and characterization

The peptides (listed in Table 1) were assembled on Rink amide resin by employing Fmoc chemistry with HBTU/HOBt/DIPEA activation. N-terminal acetylation was carried out on-resin using 10 equivalents each of acetic anhydride and DIPEA. The peptides were cleaved from the resin using a cleavage cocktail containing 95% TFA, 2.5% TIPS, and 2.5% water. The peptides were precipitated in ice-chilled diethyl ether. Following multiple rounds of washing with diethyl ether, the peptides were air-dried. The peptides were purified using reversed-phase HPLC on a C18 column, employing a linear gradient of acetonitrile with 0.1% TFA. Peptide identities were ascertained using MALDI-TOF mass spectrometry.

Peptide dissolution, hydrogelation and rheology

Peptide stock solutions were prepared in water by weighing the peptides, adding water, and vortexing for a few minutes. All

TH-3931_206106020

peptides, except Ac-VQIVF(CF_3)K-am, dissolved in water to very high concentrations (>20 mM). Ac-VQIVF(CF_3)K-am was heated for about an hour at 70 °C to achieve a dissolution >20 mM. All the peptides remained as viscous solutions in water up to about 25 mM concentration, except Ac-VQIVF(CF_3)K-am, which gels upon cooling to room temperature. Gelation of PBS was attempted by diluting the peptide solutions to achieve 20 mM peptide concentration. As Ac-VQIVF(CF_3)K-am gels upon cooling down to room temperature, it was diluted in PBS instantly after being taken out from 70 °C. All the peptides caused instant gelation of PBS. Rheology of Ac-PHF6 gel is reported in the literature for a 24-hour-old gel.[58] The 20 mM gel has a storage modulus around 20 kPa from 624 rad s^{-1} down to 0.01 rad s^{-1} frequency. Therefore, we carried out the oscillatory rheology on the 20 mM peptide gels that were aged for 24-hours. Rheology measurements were carried out on an Anton Paar Rheometer MCR 102 using 25 cm parallel plates at a 0.5 mm gap. The amplitude sweep tests were carried out at an angular frequency of 10 rad s^{-1} by varying shear strain from 0.01% to 10%. All the gels showed a linear regime up to at least 0.1% strain. Frequency sweep data, therefore, were recorded at 0.1% strain.

Thioflavin T (ThT) fluorescence spectroscopy

ThT fluorescence emission spectra were recorded in PBS for the PBS gels. As ThT fluorescence quantum yield strongly depends on pH, the fluorescence emission spectra for water samples were recorded in 10 mM phosphate buffer, pH 7.4, instead of water. The assay was carried out at 200 μM peptide and 10 μM ThT concentrations. The samples were excited at 450 nm, and emission spectra were recorded. The excitation and emission bandwidths were 2.5 and 5 nm, respectively.

Circular dichroism (CD) spectroscopy

Far-UV electronic CD spectra were recorded on a Jasco J-1500 spectropolarimeter. The 24-hour-old samples (20 mM peptide concentration) were diluted in respective dispersant (water or PBS) to 200 μM concentration, and spectra were recorded in a 1 mm path-length quartz cell. The spectra were recorded from 250–195 nm at 1 nm bandwidth with a scanning speed of 100 nm min^{-1}. Each spectrum is the average of 8 accumulations. The spectra were corrected by subtracting the respective dispersant spectrum. The data was converted to mean residue ellipticity using the following formula:

$$\theta_{MRE}\ (\text{deg cm}^2\ \text{dmol}^{-1}) = \frac{\theta\ (\text{mdeg}) \times 10^6}{\text{pathlength (mm)} \times \text{peptide (μM)} \times (n-1)},$$

where n is the number of amino acids in the peptide.

Fourier transform infrared (FTIR) spectroscopy

The FTIR spectra were recorded for 24-hour-old samples on a Shimadzu IRAffinity-1S Fourier transform infrared spectrometer equipped with a diamond ATR crystal. The samples were diluted 2-fold, and ~5 μL volume of the diluted samples was deposited on the diamond crystal and allowed to dry. The spectra were recorded with 4 cm^{-1} resolution and 40 scans.

Molecular dynamics (MD) simulations

MD simulations were carried out for the steric zipper structures prepared for the peptides. The steric zipper structure of uncapped PHF6 peptide (VQIVYK.pdb) was obtained from the WALTZ-DB database (http://waltzdb.switchlab.org/).[71] N-terminal acetylation was done in BIOVIA Discovery Studio. The aromatic analogs were generated by substituting the Tyr residue with Phe and ring-substituted-Phe using the SwissSidechain plugin in UCSF-Chimera. MD simulations were carried out using the CHARMM36 force field. The peptide amidation was done by choosing CT2 as the terminal patch when prompted by pdb2gmx command. The steric zippers were placed in a cubic box with a minimum distance of 1 nm from the box edge, solvated with water (TIP3P), and neutralized with chloride ions. NaCl (150 mM) was added to each system. The systems underwent energy minimization, followed by equilibration under NVT (100 ps) and NPT (200 ps) at 300 K temperature and 1 bar pressure. Subsequently, the production MD simulations were carried out for 200 ns. Trajectory analyses were performed using VMD and UCSF-Chimera. Cluster analysis was done using the gromos algorithm with a 0.2 nm cutoff.

Transmission electron microscopy (TEM)

The gel samples were diluted 2-fold in PBS and deposited on the carbon-coated copper grids. After 10 minutes, the excess solvent was removed using lint-free tissue paper, and the grids were stained with uranyl acetate for 10 minutes before being left to

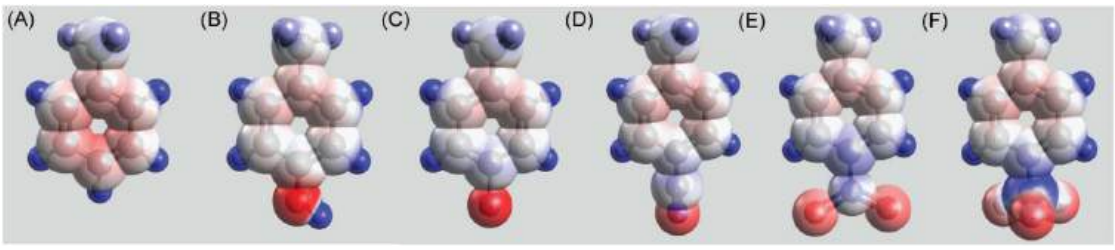

Fig. 1 Electrostatic charge density maps of toluene (A), *p*-cresol (B), 4-fluorotoluene (C), 4-cyanotoluene (D), 4-nitrotoluene (E), and 4-(trifluoromethyl)toluene (F).

TH-3931_206106020

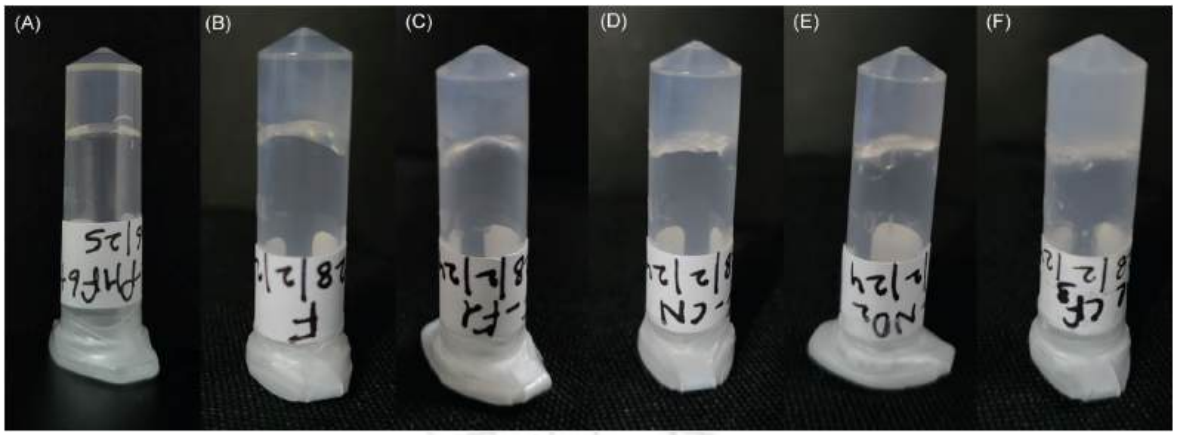

Fig. 2 Inverted vials of Ac-PHF6 and its analogs showing PBS gelation. (A) Ac-PHF6, (B) Ac-VQIVFK-am, (C) Ac-VQIVF(fl)K-am, (D) Ac-VQIVF(CN)K-am, (E) Ac-VQIVF(NO_2)K-am, and (F) Ac-VQIVF(CF_3)K-am.

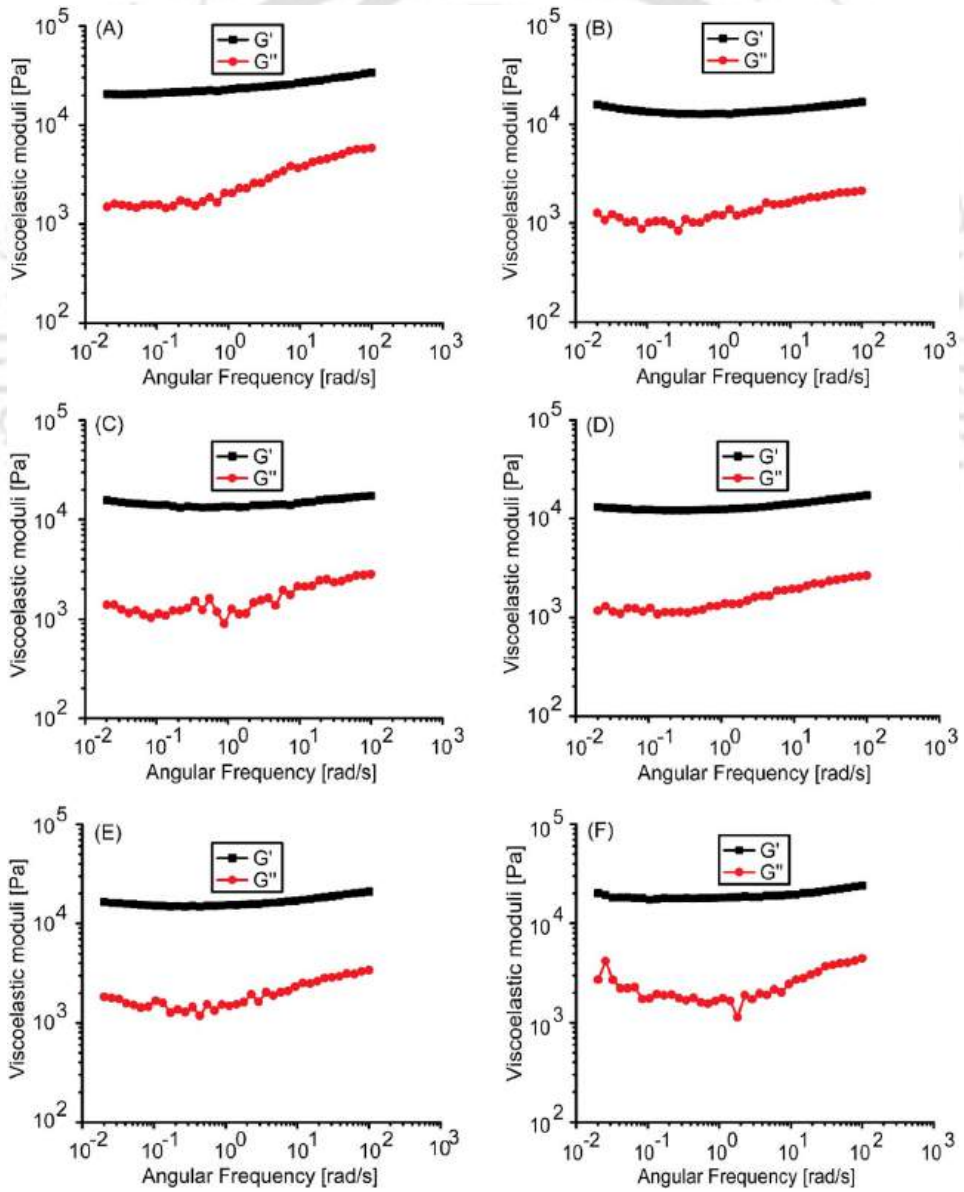

Fig. 3 Rheology of PBS gels. Plot of G' and G'' against angular frequency for 20 mM gels of (A) Ac-PHF6, (B) Ac-VQIVFK-am, (C) Ac-VQIVF(fl)K-am, (D) Ac-VQIVF(CN)K-am, (E) Ac-VQIVF(NO_2)K-am, and (F) Ac-VQIVF(CF_3)K-am.

air dry. The images were acquired at 200 kV using a JEM-2100F (JEOL, Japan) transmission electron microscope.

Results and discussion

Desamero and coworkers investigated $hIAPP_{22-29}$ (NFGAILSS) analogs wherein the phenyl ring was substituted with electron-donating and electron-withdrawing groups.[57] The peptide analogs with electron-deficient aromatic rings favored self-assembly, while those with electron-donating groups exhibited poor aggregation. Nilsson and coworkers found that incorporating a halogen in the phenyl group of Fmoc-Phe-OH promotes self-assembly and hydrogelation.[54] Fmoc-F_5-Phe, an analog with a highly-electron-deficient aromatic ring, displays faster self-assembly and hydrogelation compared to Fmoc-Tyr-OH.[55] These studies propound that electron-withdrawing moieties on aromatic side chains facilitate peptide self-assembly and hydrogelation. Ac-PHF6 contains a Tyr side chain and causes

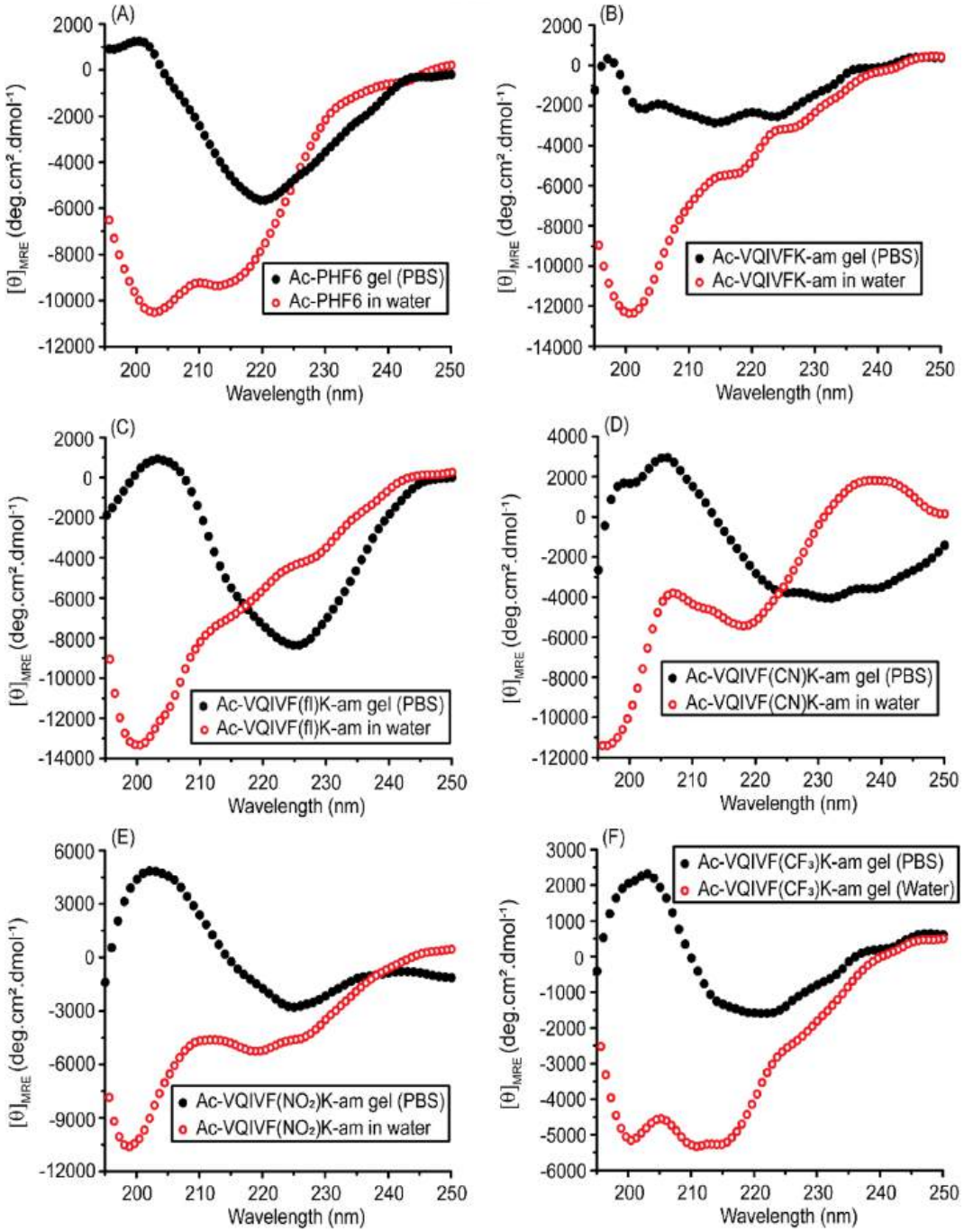

Fig. 4 CD spectra of Ac-PHF6 analogs, (A) Ac-PHF6, (B) Ac-VQIVFK-am, (C) Ac-VQIVF(fl)K-am, (D) Ac-VQIVF(CN)K-am, (E) Ac-VQIVF(NO_2)K-am, and (F) Ac-VQIVF(CF_3)K-am.

PBS hydrogelation. Here, we report the hydrogelation of Ac-PHF6 analogs, wherein Tyr310 is replaced with Phe and its ring-substituted derivatives (Table 1).

Electrostatic charge density map

An electrostatic charge density map provides valuable insights into molecular interactions. It helps in predicting electrostatic interactions that include ionic bonds, hydrogen bonds, and dipolar interactions. The charge density maps for the aromatic side chains incorporated in Ac-PHF6 analogs are shown in Fig. 1. Toluene was used as the model for the Phe side chain, and its substituents were used as models for other aromatic side chains employed in this study. *Para*-cresol, the model for Tyr side chain, shows the highest electron density in the ring (Fig. 1B). All other aromatic groups display lower electron density in the aromatic ring. The surface charge density maps of the peptides listed in Table 1 in their extended conformation are shown in Fig. S1.†

Hydrogelation

Peptide stock solutions were prepared in water. All peptides, except Ac-VQIVF(CF_3)K-am, readily dissolved in water to >20 mM concentration. Ac-VQIVF(CF_3)K-am displayed lower solubility and had to be heated at 70 °C for an hour to achieve dissolution. Cooling down to room temperature resulted in hydrogelation. No other peptide caused water gelation. The uncapped PHF6 (VQIVYK) has been reported in the literature to self-assemble in the presence of high salt concentration *via* parallel in-register β-sheet formation.[69] Capped peptide (Ac-PHF6) is also expected to assemble similarly. The salt masks the intermolecular electrostatic repulsion between terminal Lys residues in parallel β-sheet arrangement. The self-assembly and gelation of Ac-VQIVF(CF_3)K-am in water is likely hydrophobicity-driven. Trifluoromethyl is a hydrophobic functional group. The high hydrophobicity of *p*-(trifluoromethyl)phenylalanine renders Ac-VQIVF(CF_3)K-am poorly soluble in water, facilitating its self-assembly through entropic contribution. PBS gelation was set up by diluting the peptide stock solutions in 10× PBS. As Ac-VQIVF(CF_3)K-am causes water gelation at room temperature, it was diluted immediately after taking out from 70 °C. All the peptides caused PBS gelation. The gels formed at 10 and 15 mM peptide concentrations were very fragile. Firm gels were obtained at 20 mM concentration (Fig. 2). The gelation was instant, but the inverted tube images shown in Fig. 2 were taken for the 24-hour-old samples. As 24-hour-old Ac-PHF6 hydrogel (20 mM peptide concentration) is reported in the literature, the assays with Ac-PHF6 analogs were also carried out with 20 mM gel samples that were incubated at room temperature for 24 hours.

Rheology

Rheology of a material is determined by its inner structure. As aromatic substitutions could modulate the peptide self-

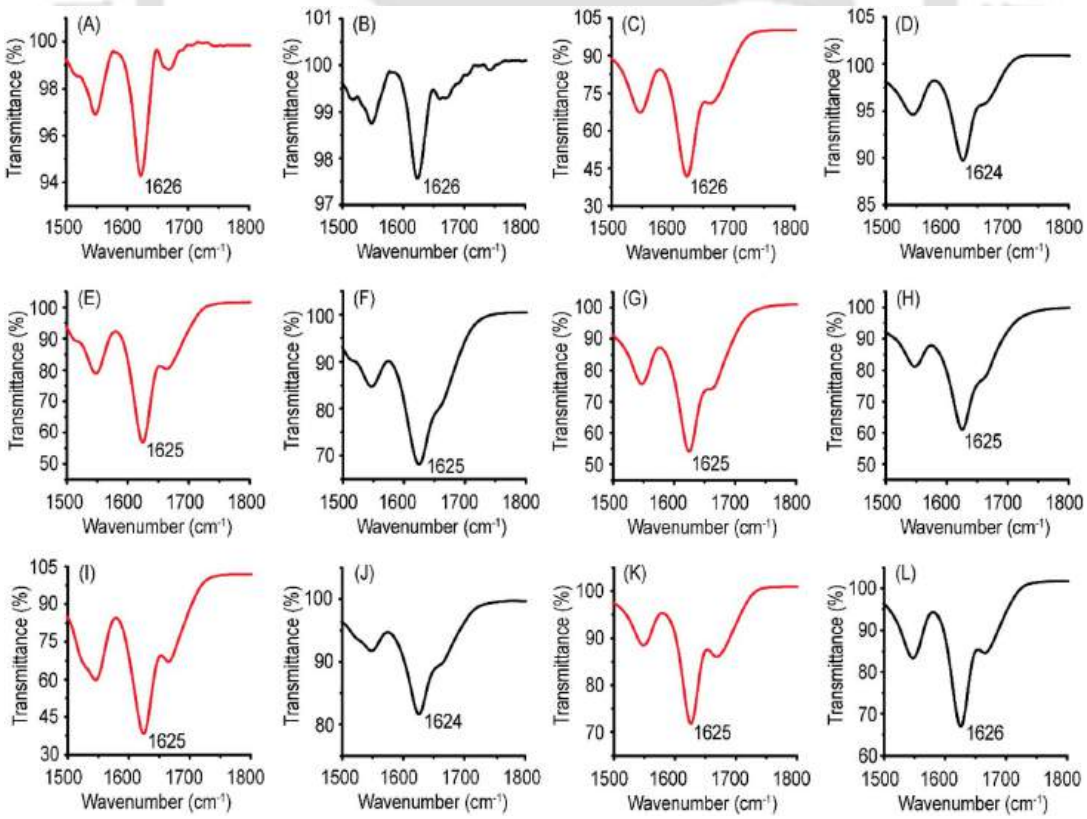

Fig. 5 ATR-FTIR spectra of Ac-PHF6 and its analogs. The red traces are the spectra recorded for water samples, while the black traces are the spectra recorded for PBS samples. (A and B) Ac-PHF6, (C and D) Ac-VQIVFK-am, (E and F) Ac-VQIVF(fl)K-am, (G and H) Ac-VQIVF(CN)K-am, (I and J) Ac-VQIVF(NO_2)K-am, and (K and L) Ac-VQIVF(CF_3)K-am.

TH-3931_206106020

assembly, affecting the hydrogel's inner structure, the hydrogels' viscoelasticity was investigated using bulk rheology. The frequency sweep test was conducted at a strain of 0.1%, the strain that lies in the linear viscoelastic regime. The data is shown in Fig. 3. Interestingly, all the gels displayed a comparable storage modulus of about $1 - 2 \times 10^4$ Pa. There are small differences in the loss moduli, though. Instant PBS gelation caused by the peptides could lead to some non-uniformity within the gels. Such non-uniformity could contribute to minor differences observed in the loss moduli. The rheology data suggest that Tyr electronic properties do not contribute significantly to Ac-PHF6 hydrogelation. Unlike Fmoc-F_5-Phe-OH, which forms a much stronger hydrogel than Fmoc-Tyr-OH,[55] we find that substitution of Tyr in Ac-PHF6 with Phe or its analogs with electron-withdrawing groups has no significant effect on rheology. The only apparent difference to Ac-PHF6 is that Ac-VQIVF(CF_3)K-am displays lower solubility in water due to the high hydrophobicity of the Phe(CF_3) group. The higher hydrophobicity caused the peptide to gel in deionized water as well.

CD spectroscopy

The secondary structures of PBS and water samples were examined using far-UV CD spectroscopy. The samples were

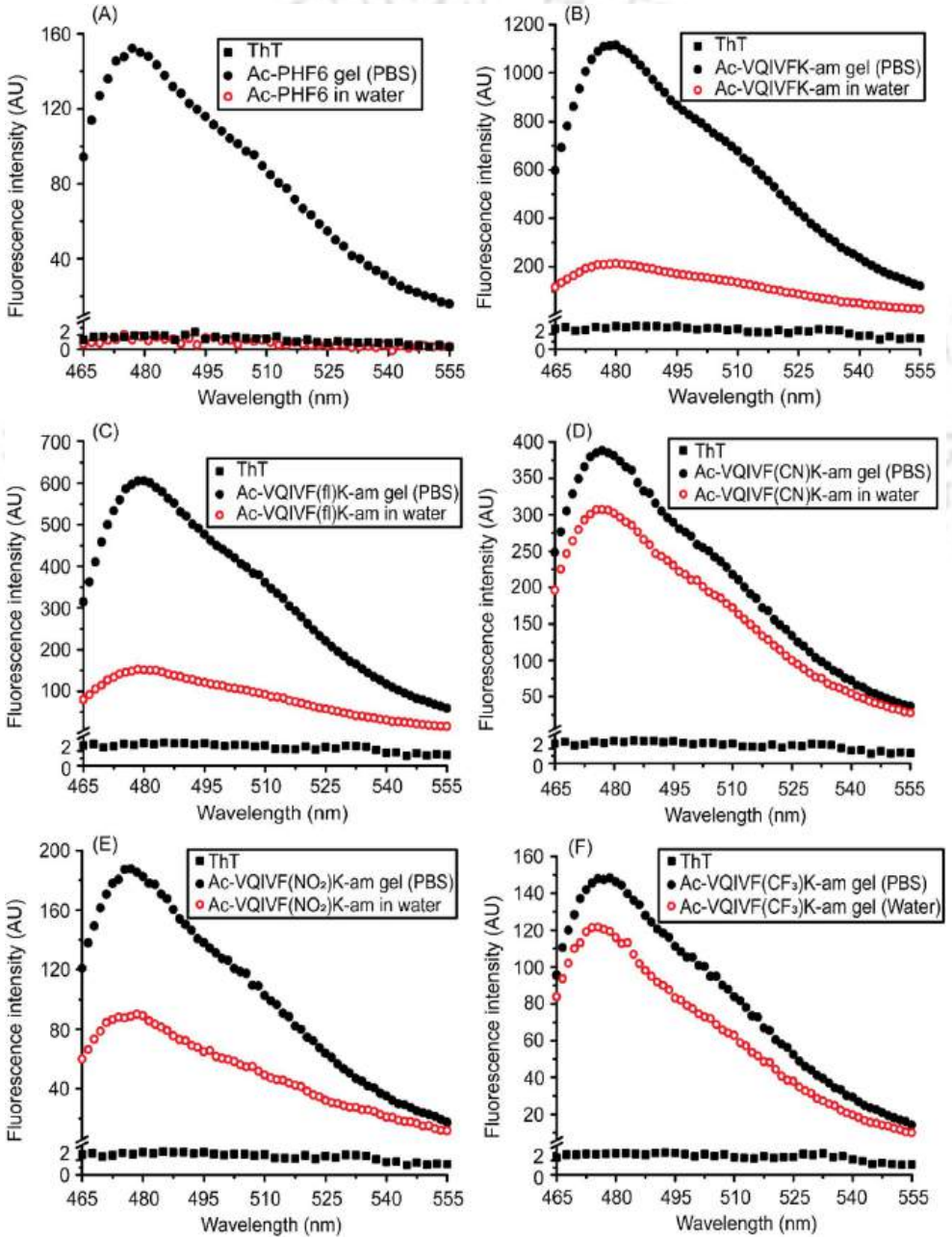

Fig. 6 ThT fluorescence spectra of Ac-PHF6 and its analogs. (A) Ac-PHF6, (B) Ac-VQIVFK-am, (C) Ac-VQIVF(fl)K-am, (D) Ac-VQIVF(CN)K-am, (E) Ac-VQIVF(NO_2)K-am, and (F) Ac-VQIVF(CF_3)K-am.

diluted to a concentration of 200 μM in the respective dispersant (water/PBS) for CD spectroscopy. Ac-PHF6 displays a spectrum very similar to that reported in the literature (Fig. 4A). The spectrum suggests a largely unordered conformation in water with a little contribution from β-sheets. On the other hand, the peptide displays a distinct β-sheet spectrum in PBS. Ac-VQIVFK-am displays a negative band around 200 nm in water, indicating a largely unordered conformation (Fig. 4B). The peptide displays a broad band centered around 215 nm in PBS, suggesting a β-sheet conformation. Ac-VQIVF(fl)K-am also takes up a largely unordered conformation in water, as indicated by the 200 nm negative band (Fig. 4C). The spectrum in PBS is characterized by a broad band around 225 nm and a weak positive band around 205 nm. The spectrum is very similar to that reported for Ac-PHF6 in PBS and is assigned to the β-sheet conformation. Ac-VQIVF(CN)K-am (Fig. 4D) and Ac-VQIVF(NO_2)K-am (Fig. 4E) display a negative band around 220 nm alongside the band around 200 nm in water. These data indicate that a fraction of the peptide takes up the β-sheet conformation, suggesting a tendency to self-assemble in water. In PBS, both the peptides display distinct β-sheet conformation. Ac-VQIVF(CF_3)K-am displays a very different spectrum in water (Fig. 4F). The spectrum is characterized by 200 and ~212 nm negative bands of comparable amplitudes. The spectrum suggests that the peptide takes up a mixture of β-sheet and random coil conformations. In PBS, a typical β-sheet CD spectrum is observed. The CD data show that the peptides with strong electron-withdrawing groups *i.e.*, cyano, nitro, and trifluoromethyl groups, have β-sheet content in water, suggesting their tendency to self-assemble in water itself. Ac-VQIVFK-am and Ac-VQIVF(fl)K-am, *i.e.*, the peptides without an electron-withdrawing group and with a weak electron-withdrawing group, respectively, show largely unordered conformation. The most dramatic effect of the electron-withdrawing group is observed for Ac-VQIVF(CF_3)K-am, which displays lower solubility in deionized water at room temperature and causes gelation upon cooling after being heated.

FTIR spectroscopy

CD spectroscopy is an excellent method for investigating the α-helical conformations. However, the huge structural diversity of β-sheets makes CD spectroscopy somewhat less reliable for accurately estimating the β-sheet conformation.[72] Regarding

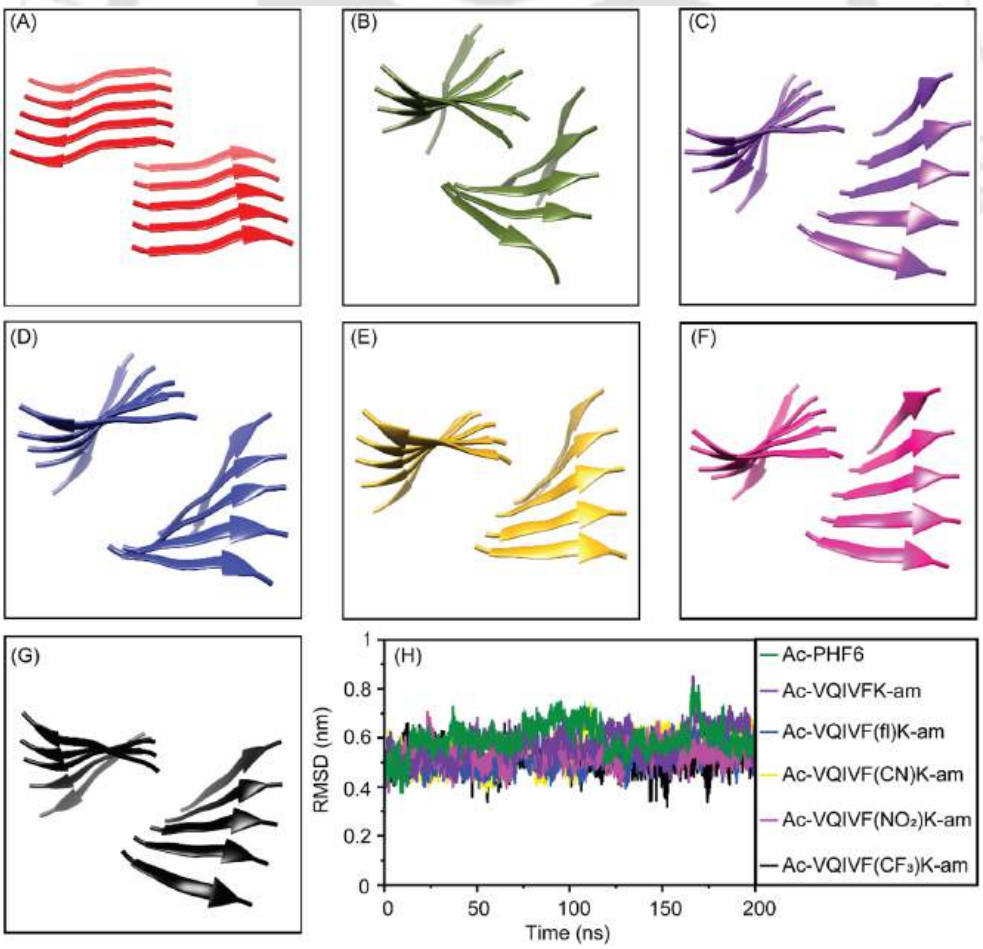

Fig. 7 MD simulations of the peptide steric zippers. (A) The VQIVYK steric zipper obtained from WALTZ-DB database. The middle structure of the largest cluster for (B) Ac-PHF6, (C) Ac-VQIVFK-am, (D) Ac-VQIVF(fl)K-am, (E) Ac-VQIVF(CN)K-am, (F) Ac-VQIVF(NO_2)K-am, and (G) Ac-VQIVF(CF_3)K-am. (H) The RMSD plots obtained from the trajectories of simulations.

TH-3931_206106020

self-assembling peptides with aromatic residues, contributions from aromatic stacking interactions in far-UV CD spectra further hinder secondary structure prediction. FTIR spectroscopy is particularly suitable for investigating the β-sheets. The position of the amide I band is sensitive to the peptide backbone conformation. The ATR-FTIR spectra of Ac-PHF6 and its analogs are shown in Fig. 5. All the peptides display the amide I band centered between 1624–1626 cm^{-1} for both water and PBS samples. ATR-FTIR data unambiguously proves that the peptides take a β-sheet conformation in the hydrogels. Unlike CD spectroscopy, where Ac-VQIVFK-am and Ac-VQIVF(fl)K-am display random coil conformation for water samples, the FTIR spectra indicate β-sheet conformation. This is attributed to the drying of the peptides for ATR-FTIR spectroscopy. The peptide concentration increases during the drying processes, facilitating self-assembly. Such behavior has been reported for Ac-PHF6 in the literature.[58]

ThT fluorescence

The fluorescence of ThT, a benzothiazole dye that demonstrates a higher quantum yield when bound to amyloid fibrils, is routinely used to characterize amyloid-like fibrils. ThT fluorescence spectra are shown in Fig. 6. Ac-PHF6 gel sample caused enhancement in ThT fluorescence emission intensity, while no noticeable enhancement was observed for the water sample (Fig. 6A). This data is similar to that reported in the literature.[58] All the peptides caused a large enhancement in ThT fluorescence intensity, confirming that the superstructures underlying the hydrogels are amyloid-like fibrils. The PBS samples caused a larger enhancement in ThT fluorescence than the water samples. Ac-VQIVFK-am and Ac-VQIVF(fl)K-am display around 4–6 times higher intensity for PBS samples compared to water samples (Fig. 6B and C). Interestingly, however, the ThT fluorescence observed for Ac-VQIVF(NO_2)K-am PBS is about 2-fold higher than the water sample (Fig. 6E). This difference in intensity further decreases for Ac-VQIVF(CN)K-am and Ac-VQIVF(CF_3)K-am samples (Fig. 6D and F). The PBS samples of these peptides display only about 25% higher ThT fluorescence intensity than the water samples. These data align with the CD spectroscopy data and suggest that the Ac-PHF6 analogs wherein the aromatic residue has a strong electron-withdrawing group, have a higher aggregation propensity.

MD simulations

As all Ac-PHF6 analogs formed hydrogels in PBS with very similar rheological properties, we got curious to investigate the stability of the steric zippers formed by them using MD simulations. The starting structures of the peptides were prepared by modifying the VQIVYK.pdb steric zipper structure (Fig. 7A) available in WALTZ-DB database. The simulation data was subjected to cluster analysis to find the most representative structure of the largest cluster. The middle structures of the

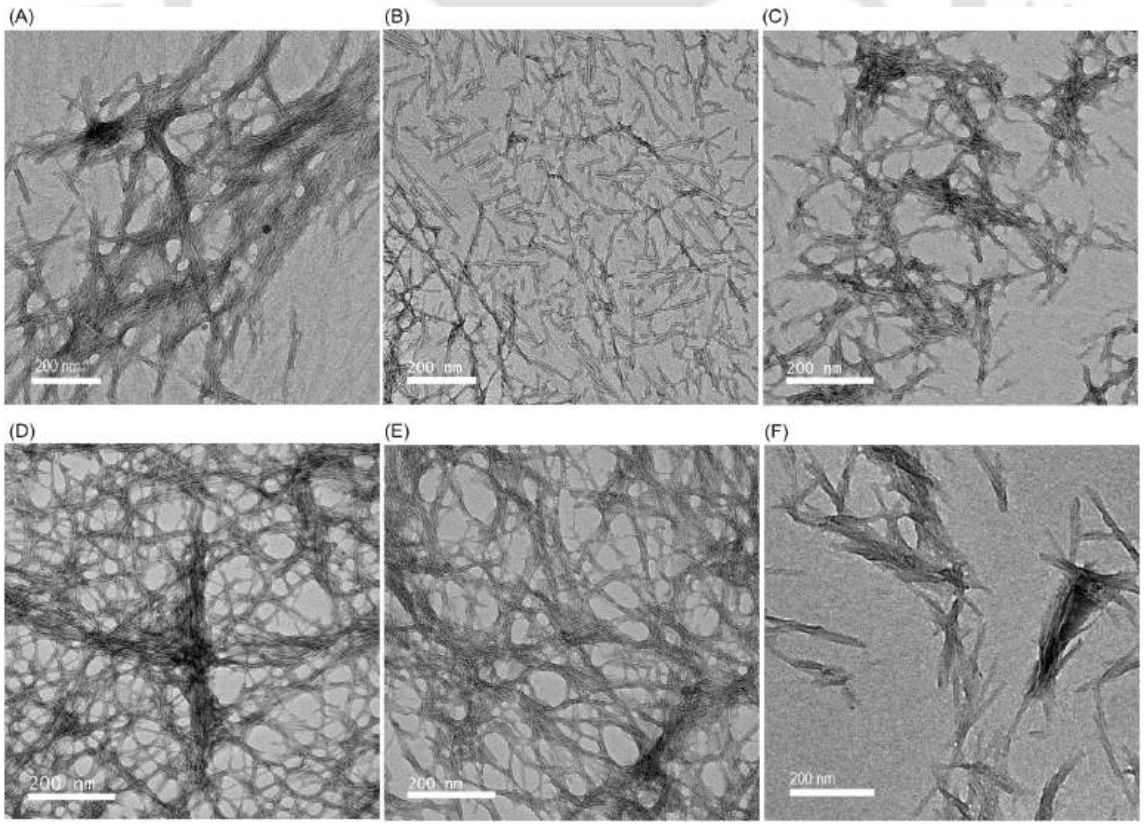

Fig. 8 TEM images showing the structures underlying the PBS gels. (A) Ac-PHF6, (B) Ac-VQIVFK-am, (C) Ac-VQIVF(fl)K-am, (D) Ac-VQIVF(CN)K-am, (E) Ac-VQIVF(NO_2)K-am, and (F) Ac-VQIVF(CF_3)K-am. The scale bars represent 200 nm.

largest cluster are shown in Fig. 7B–G. The largest cluster shows steric zipper arrangement for all six peptides. The RMSD plots (Fig. 7H) also show no appreciable deviation throughout the 200 ns simulation. These data suggest that parallel in-register β-sheet steric zipper is a stable architecture for Ac-PHF6 and its analogs.

Transmission electron microscopy

The comparable viscoelastic properties observed for all peptides indicate that the inner structure underlying the hydrogels could also be similar. The morphology of the self-assembled structures underlying the hydrogels, therefore, was investigated using TEM. All peptides self-assemble into fibrillar superstructures. Ac-PHF6 formed fibrils similar to those reported in the literature (Fig. 8A).[58,63] Ac-VQIVFK-am and VQIVF(fl)K-am also self-assemble to form straight fibrils (Fig. 8B and C), similar to Ac-PHF6.[58,63] Ac-VQIVF(CN)K-am and Ac-VQIVF(NO_2)K-am form long straight filaments that show extensive entanglement (Fig. 8D and E). Ac-VQIVF(CF_3)K-am forms fibrils that appear to form clumps, possibly through lateral interactions between individual fibrils (Fig. 8F).

Conclusions

Ac-PHF6, an amyloidogenic stretch from human tau, is a promising biocompatible hydrogelator. As the peptide harbors a Tyr residue, and analogs with electron-withdrawing groups in the aromatic rings of self-assembling peptides have been reported in the literature to form stronger gels, we investigated aromatic analogs of Ac-PHF6. The Ac-PHF6 analogs with electron-withdrawing groups in the phenyl ring improve the peptide's self-assembling propensity. The analog with the strongest electron-withdrawing group (trifluoromethyl), *i.e.*, Ac-VQIVF(CF_3)K-am causes gelation of deionized water, an attribute that all other peptide analogs lacked. Notably, among all aromatic amino acids employed in this study, the *p*-(trifluoromethyl)phenylalanine has the highest hydrophobicity. The aromatic amino acids incorporated in Ac-PHF6 analogs have very different electronic and steric properties, but all the peptides formed PBS gels with comparable stiffness. The aromatic moieties' contribution to hydrogelation appears more through their hydrophobicity than the aromatic electronic effects. The role of Tyr residue in Ac-PHF6, therefore, is that of a bulky hydrophobic residue rather than an aromatic one. It would be interesting to investigate if the aliphatic analogs of Ac-PHF6 also cause hydrogelation.

Data availability

All data generated in this study are available in the article and the ESI.†

Author contributions

Shubhangini Singh Verma: methodology, validation, formal analysis, investigation, writing – original draft, visualization. Nitin Chaudhary: conceptualization, resources, writing – review & editing, supervision, formal analysis, project administration, funding acquisition.

Conflicts of interest

There are no conflicts of interest to declare.

Acknowledgements

Funding from the DBT Twinning project BT/PR15921/NER/95/140/2015 is acknowledged. SSV acknowledges the Ministry of Education, Govt. of India for fellowship. The authors thank Central Instruments Facility, IIT Guwahati, for transmission electron microscopy imaging and MALDI-TOF mass spectrometry. Param-Ishan, the High-Performance Computing facility at IIT Guwahati is acknowleged for MD simulations.

References

1 A. S. Hoffman, *Adv. Drug Delivery Rev.*, 2012, **64**, 18–23.
2 L. Li, P. Wu, F. Yu and J. Ma, *J. Mater. Chem. A*, 2022, **10**, 9215–9247.
3 L. Hu, P. L. Chee, S. Sugiarto, Y. Yu, C. Shi, R. Yan, Z. Yao, X. Shi, J. Zhi, D. Kai, H.-D. Yu and W. Huang, *Adv. Mater.*, 2023, **35**, 2205326.
4 H. Wang and W. Zhao, *Next Mater.*, 2023, **1**, 100049.
5 L. Tang, Z. Wu, Q. Zhang, Q. Hu, X. Dang, F. Cui, L. Tang and T. Xiao, *Chem. Commun.*, 2024, **60**, 4719–4722.
6 N. Kaur, Hamid, P. Choudhary, A. K. Jaiswal and J. Agr, *Food Res.*, 2025, **20**, 101756.
7 I. W. Hamley, *Soft Matter*, 2011, **7**, 4122–4138.
8 D. Mandal, A. Nasrolahi Shirazi and K. Parang, *Org. Biomol. Chem.*, 2014, **12**, 3544–3561.
9 A. Rawat and R. Nagaraj, *Curr. Top. Med. Chem.*, 2014, **14**, 740–746.
10 J. Wang, K. Liu, R. Xing and X. Yan, *Chem. Soc. Rev.*, 2016, **45**, 5589–5604.
11 S. K. Pachahara, S. Chivukula and N. Ramakrishnan, *Curr. Protein Pept. Sci.*, 2017, **18**, 920–938.
12 C. Subbalakshmi, P. Basak and R. Nagaraj, *Pept. Sci.*, 2017, **108**, e23033.
13 J. D. Hartgerink, E. Beniash and S. I. Stupp, *Science*, 2001, **294**, 1684–1688.
14 V. Jayawarna, M. Ali, T. A. Jowitt, A. F. Miller, A. Saiani, J. E. Gough and R. V. Ulijn, *Adv. Mater.*, 2006, **18**, 611–614.
15 L. Haines-Butterick, K. Rajagopal, M. Branco, D. Salick, R. Rughani, M. Pilarz, M. S. Lamm, D. J. Pochan and J. P. Schneider, *Proc. Natl. Acad. Sci. U. S. A.*, 2007, **104**, 7791–7796.
16 D. A. Salick, J. K. Kretsinger, D. J. Pochan and J. P. Schneider, *J. Am. Chem. Soc.*, 2007, **129**, 14793–14799.
17 J. Naskar, G. Palui and A. Banerjee, *J. Phys. Chem. B*, 2009, **113**, 11787–11792.
18 D. A. Salick, D. J. Pochan and J. P. Schneider, *Adv. Mater.*, 2009, **21**, 4120–4123.

19 X.-D. Xu, L. Liang, C.-S. Chen, B. Lu, N.-l. Wang, F.-G. Jiang, X.-Z. Zhang and R.-X. Zhuo, *ACS Appl. Mater. Interfaces*, 2010, **2**, 2663–2671.
20 A. Altunbas, S. J. Lee, S. A. Rajasekaran, J. P. Schneider and D. J. Pochan, *Biomaterials*, 2011, **32**, 5906–5914.
21 J. Liu, L. Zhang, Z. Yang and X. Zhao, *Int. J. Nanomed.*, 2011, **6**, 2143–2153.
22 Y. Li, F. Wang and H. Cui, *Bioeng. Transl. Med.*, 2016, **1**, 306–322.
23 P. Worthington, S. Langhans and D. Pochan, *Adv. Drug Delivery Rev.*, 2017, **110–111**, 127–136.
24 D. Datta and N. Chaudhary, in *Translational Biotechnology*, ed. Y. Hasija, Academic Press, 2021, pp. 203–232, DOI: 10.1016/B978-0-12-821972-0.00003-4.
25 J. B. Matson and S. I. Stupp, *Chem. Commun.*, 2012, **48**, 26–33.
26 A. Dasgupta, J. H. Mondal and D. Das, *RSC Adv.*, 2013, **3**, 9117–9149.
27 A. Baral, S. Roy, A. Dehsorkhi, I. W. Hamley, S. Mohapatra, S. Ghosh and A. Banerjee, *Langmuir*, 2014, **30**, 929–936.
28 A. Baral, S. Roy, S. Ghosh, D. Hermida-Merino, I. W. Hamley and A. Banerjee, *Langmuir*, 2016, **32**, 1836–1845.
29 K. Basu, A. Baral, S. Basak, A. Dehsorkhi, J. Nanda, D. Bhunia, S. Ghosh, V. Castelletto, I. W. Hamley and A. Banerjee, *Chem. Commun.*, 2016, **52**, 5045–5048.
30 B. Hansda, J. Majumder, B. Mondal, A. Chatterjee, S. Das, S. Kumar, R. Gachhui, V. Castelletto, I. W. Hamley, P. Sen and A. Banerjee, *Langmuir*, 2023, **39**, 7307–7316.
31 N. Özbek, E. L. Vilarrocha, B. V. Jover, E. F. Ventura and B. Escuder, *RSC Adv.*, 2024, **14**, 15120–15128.
32 N. Changsan, A. Atipairin, P. Sakdiset, P. Muenraya, N. Balekar, T. Srichana, R. Sritharadol, S. Phanapithakkun and S. Sawatdee, *RSC Adv.*, 2024, **14**, 27394–27411.
33 S. K. Maji, M. H. Perrin, M. R. Sawaya, S. Jessberger, K. Vadodaria, R. A. Rissman, P. S. Singru, K. P. Nilsson, R. Simon, D. Schubert, D. Eisenberg, J. Rivier, P. Sawchenko, W. Vale and R. Riek, *Science*, 2009, **325**, 328–332.
34 D. Otzen and R. Riek, *Cold Spring Harbor Perspect. Biol.*, 2019, **11**, a033860.
35 L. Yang, H. Li, L. Yao, Y. Yu and G. Ma, *ACS Omega*, 2019, **4**, 8071–8080.
36 V. K. Belwal and N. Chaudhary, *Soft Matter*, 2020, **16**, 10013–10028.
37 A. Lakshmanan, D. W. Cheong, A. Accardo, E. Di Fabrizio, C. Riekel and C. A. Hauser, *Proc. Natl. Acad. Sci. U. S. A.*, 2013, **110**, 519–524.
38 R. S. Jacob, D. Ghosh, P. K. Singh, S. K. Basu, N. N. Jha, S. Das, P. K. Sukul, S. Patil, S. Sathaye, A. Kumar, A. Chowdhury, S. Malik, S. Sen and S. K. Maji, *Biomaterials*, 2015, **54**, 97–105.
39 S. Das, K. Zhou, D. Ghosh, N. N. Jha, P. K. Singh, R. S. Jacob, C. C. Bernard, D. I. Finkelstein, J. S. Forsythe and S. K. Maji, *NPG Asia Mater.*, 2016, **8**, e304.
40 D. Datta, V. Kumar, S. Kumar, R. Nagaraj and N. Chaudhary, *ACS Omega*, 2019, **4**, 620–627.
41 P. W. J. M. Frederix, G. G. Scott, Y. M. Abul-Haija, D. Kalafatovic, C. G. Pappas, N. Javid, N. T. Hunt, R. V. Ulijn and T. Tuttle, *Nat. Chem.*, 2015, **7**, 30–37.
42 F. Li, J. Han, T. Cao, W. Lam, B. Fan, W. Tang, S. Chen, K. L. Fok and L. Li, *Proc. Natl. Acad. Sci. U. S. A.*, 2019, **116**, 11259.
43 E. Gazit, *FASEB J.*, 2002, **16**, 77–83.
44 M. Reches and E. Gazit, *Phys. Biol.*, 2006, **3**, S10–S19.
45 W. Li, Z. Tang, M. Zhang, J. Wang, Y. Liu, M. Ding, D. Zhou and H. Su, *Polymer*, 2024, **302**, 127090.
46 S. K. Pachahara and R. Nagaraj, *Biochem. Biophys. Rep.*, 2015, **2**, 1–13.
47 A. Banerjee, G. Palui and A. Banerjee, *Soft Matter*, 2008, **4**, 1430–1437.
48 S. Loic, in *Amino Acid*, ed. T. Asao, InTech, Rijeka, 2017, ch. 3, DOI: 10.5772/intechopen.68705.
49 M. Reches and E. Gazit, *Science*, 2003, **300**, 625–627.
50 S. Sutton, N. L. Campbell, A. I. Cooper, M. Kirkland, W. J. Frith and D. J. Adams, *Langmuir*, 2009, **25**, 10285–10291.
51 A. Mahler, M. Reches, M. Rechter, S. Cohen and E. Gazit, *Adv. Mater.*, 2006, **18**, 1365–1370.
52 A. M. Smith, R. J. Williams, C. Tang, P. Coppo, R. F. Collins, M. L. Turner, A. Saiani and R. V. Ulijn, *Adv. Mater.*, 2008, **20**, 37–41.
53 J. J. Balbach, Y. Ishii, O. N. Antzutkin, R. D. Leapman, N. W. Rizzo, F. Dyda, J. Reed and R. Tycko, *Biochemistry*, 2000, **39**, 13748–13759.
54 D. M. Ryan, S. B. Anderson and B. L. Nilsson, *Soft Matter*, 2010, **6**, 3220–3231.
55 D. M. Ryan, S. B. Anderson, F. T. Senguen, R. E. Youngman and B. L. Nilsson, *Soft Matter*, 2010, **6**, 475–479.
56 D. M. Ryan, T. M. Doran, S. B. Anderson and B. L. Nilsson, *Langmuir*, 2011, **27**, 4029–4039.
57 A. A. Profit, J. Vedad, M. Saleh and R. Z. B. Desamero, *Arch. Biochem. Biophys.*, 2015, **567**, 46–58.
58 S. S. Verma, S. Bhattacharya, S. Kumar and N. Chaudhary, *Biophys. Chem.*, 2025, **322**, 107438.
59 V. M. Lee, M. Goedert and J. Q. Trojanowski, *Annu. Rev. Neurosci.*, 2001, **24**, 1121–1159.
60 N. Chaudhary and R. Nagaraj, in *Protein Aggregation and Fibrillogenesis in Cerebral and Systemic Amyloid Disease*, ed. J. R. Harris, Springer Netherlands, Dordrecht, 2012, pp. 75–90, DOI: 10.1007/978-94-007-5416-4_4.
61 M. von Bergen, P. Friedhoff, J. Biernat, J. Heberle, E. M. Mandelkow and E. Mandelkow, *Proc. Natl. Acad. Sci. U. S. A.*, 2000, **97**, 5129–5134.
62 M. von Bergen, S. Barghorn, L. Li, A. Marx, J. Biernat, E. M. Mandelkow and E. Mandelkow, *J. Biol. Chem.*, 2001, **276**, 48165–48174.
63 W. J. Goux, L. Kopplin, A. D. Nguyen, K. Leak, M. Rutkofsky, V. D. Shanmuganandam, D. Sharma, H. Inouye and D. A. Kirschner, *J. Biol. Chem.*, 2004, **279**, 26868–26875.
64 N. Chaudhary, S. Singh and R. Nagaraj, *J. Pept. Sci.*, 2009, **15**, 675–684.
65 S. J. A. Shah, Q. Zhang, J. Guo, H. Liu, H. Liu and J. Villà-Freixa, *ACS Chem. Neurosci.*, 2023, **14**, 3959–3971.

66 E. Pretti and M. S. Shell, *Proc. Natl. Acad. Sci. U. S. A.*, 2023, **120**, e2309995120.
67 I. Stroganova, Z. Toprakcioglu, H. Willenberg, T. P. J. Knowles and A. M. Rijs, *ACS Chem. Neurosci.*, 2024, **15**, 3391–3400.
68 I. Stroganova, H. Willenberg, T. Tente, A. Depraz Depland, S. Bakels and A. M. Rijs, *Anal. Chem.*, 2024, **96**, 5115–5124.
69 M. R. Sawaya, S. Sambashivan, R. Nelson, M. I. Ivanova, S. A. Sievers, M. I. Apostol, M. J. Thompson, M. Balbirnie, J. J. Wiltzius, H. T. McFarlane, A. O. Madsen, C. Riekel and D. Eisenberg, *Nature*, 2007, **447**, 453–457.
70 M. D. Hanwell, D. E. Curtis, D. C. Lonie, T. Vandermeersch, E. Zurek and G. R. Hutchison, *J. Cheminf.*, 2012, **4**, 17.
71 N. Louros, K. Konstantoulea, M. De Vleeschouwer, M. Ramakers, J. Schymkowitz and F. Rousseau, *Nucleic Acids Res.*, 2020, **48**, D389–D393.
72 A. Micsonai, F. Wien, L. Kernya, Y.-H. Lee, Y. Goto, M. Réfrégiers and J. Kardos, *Proc. Natl. Acad. Sci. U. S. A.*, 2015, **112**, E3095–E3103.

International Journal of Peptide Research and Therapeutics (2026) 32:21
https://doi.org/10.1007/s10989-026-10803-9

Tyr^{310} is Superfluous for Ac-PHF6 Hydrogelation: Ac-PHF6* is also a Hydrogelator

Shubhangini Singh Verma[1] · Shinjini Bhattacharya[1] · Sachin Kumar[1] · Nitin Chaudhary[1]

Received: 10 September 2025 / Accepted: 3 January 2026

Abstract

Purpose Tau$^{306-311}$, also known as Ac-PHF6 (CH_3CO-VQIVYK-NH_2), is a short peptide that forms a viscous solution in water but causes instant gelation of PBS and cell culture media. Ac-PHF6 analogs wherein tyrosine's phenolic group is substituted with phenyl or electron-deficient aromatic rings, also form hydrogels. These data indicate that the aromatic residues in these peptides may not contribute to self-assembly through their ring electronic effects, but through their hydrophobicity. We test this hypothesis by investigating Ac-PHF6 analogs wherein Tyr is substituted with several aliphatic amino acids with different side-chain hydrophobicities, *viz*. Lys, Ala, Met, Val, and Ile. Ac-PHF6* (tau$^{275-280}$: CH_3CO-VQIINK-NH_2), an aliphatic tau hexapeptide motif similar to Ac-PHF6, was also investigated.

Methods The peptides were synthesized via solid-phase peptide synthesis using Fmoc chemistry. Peptide stock solutions were prepared in water and diluted in PBS. The resulting PBS hydrogels were characterized using oscillatory rheology, ThT fluorescence, CD, and IR spectroscopy, while their supramolecular architectures were examined using TEM. The cytocompatibility of the peptides was evaluated using HEK-293 cells.

Results All peptides, except for the Y310K analog, caused instant gelation of PBS. The Y310K analog formed a gel after approximately 2 h of incubation. Additionally, the Y310K hydrogel exhibited significantly lower stiffness compared to the other hydrogels. The other peptides formed hydrogels with stiffness higher than that of Ac-PHF6 hydrogel. Except for Ac-VQIVKK-am, all peptides formed amyloid-like fibrils, as revealed by ThT fluorescence spectroscopy and congo red spectral shift assay. All peptides were found to be cytocompatible with HEK-293 cells.

Conclusion Tyr residue is not essential for Ac-PHF6 hydrogelation. Tyrosine's contribution to Ac-PHF6 self-assembly and hydrogelation is through its hydrophobicity rather than aromaticity.

Keywords Peptide · Hydrogel · Ac-PHF6 · Ac-PHF6* · Aliphatic · Aromatic

Introduction

Hydrogels are soft material formed by 3-dimensional network of polymers that absorb a large amount of water. They have gained considerable attention in the past few decades for various biomedical applications (Brøndsted and Kopeček 1991; Woerly 1993; Liu et al. 2018; Li et al. 2023; Chatterjee et al. 2020; Hoffman 2012; Datta and Chaudhary 2021; Fichman et al. 2016). Their attribute of closely mimicking the natural extracellular matrix makes them attractive candidates for tissue engineering, drug delivery, and regenerative medicine (Li et al. 2019; Diaferia et al. 2020; Liu et al. 2019; Rosa et al. 2022; Taief et al. 2025). Largely due to their inherent biocompatibility, well-understood folding principles, tunable properties, and ease of synthesis, peptides constitute a highly promising class of hydrogelators (Vijayakanth et al. 2024; Chakraborty et al. 2020; Guy and Voyer 2012). Hydrogels have been reported in the literature from a very diverse classes of peptides. Aromatic moieties have the reputation of driving self-assembly through aromatic stacking interactions. Peptide that are end-capped with bulky aromatic moieties happen to be the most abundant class of peptide hydrogelators. A large number of Fmoc (9-fluorenylmethyloxycarbonyl)-capped peptides have been reported in the literature to cause hydrogelation (Taief et al. 2025; Smith et al. 2008; Ryan et al. 2010; Fleming et al.

✉ Nitin Chaudhary
chaudhary@iitg.ac.in

[1] Department of Biosciences and Bioengineering, Indian Institute of Technology Guwahati, Guwahati 781 039, India

Published online: 13 January 2026

2013; Tao et al. 2016; Loic 2017). Schneider, Pochan, and coworkers devised a design strategy wherein folding of a peptide into an amphiphilic β-hairpin directs its self-assembly and hydrogelation (Schneider et al. 2002). The designed peptide, termed MAX1, formed pH responsive hydrogel. Further intervention on the β-hairpin designs led to novel thermoreversible (MAX3) and light-activable hydrogelators (Pochan et al. 2003; Haines et al. 2005). Stupp and coworkers designed amphiphilic peptides wherein hydrophobicity is conferred by an alkyl chain attached to the peptidic moiety (Hartgerink et al. 2001). Such peptides, termed as peptide amphiphiles, have been reported to form biocompatible gels (Hartgerink et al. 2002; Hendricks et al. 2017). We have previously reported water/alcohol bigels formed by fatty-acylated dipeptides (Datta et al. 2020). The solvents used for initial peptide dissolution can have dramatic effects on peptide self-assembly and hydrogelation (Chaudhary et al. 2009). Solvent switch methodology, therefore, could be an interesting strategy to modulate the self-assembly and gelation of peptides. Gazit and coworkers demonstrated the hydrogelation caused by Fmoc–diphenylalanine upon transferring its hexafluoroisopropanol (HFIP) stock solution into water (Mahler et al. 2006). Perrier, Peltier, and coworkers investigated whether end-to-end cyclized syndiotactic octapeptides could also form gels (Shaikh et al. 2018). They designed cyclic peptides that could form pH-dependent and pH-independent gels. The peptide molecules stack on top of each other to form nanotubes, that eventually entangle to form a 3D network that entraps the solvent molecules. Another class of peptides that has been extensively studied for self-assembly and hydrogelation is amyloids (Datta et al. 2018; Belwal and Chaudhary 2020). Amyloidogenic peptides self-assemble into β-sheet-rich fibrils (Sunde et al. 1997; Juković et al. 2024). While amyloids were once primarily associated with pathological protein aggregation and neurodegenerative diseases, numerous studies have now established the existence of functional amyloids that serve diverse physiological roles and exhibit remarkable structural and mechanical properties (Maji et al. 2009; Fowler et al. 2006; Otzen et al. 2019; Fukuma et al. 2006). The cytotoxicity of amyloids is largely caused by the prefibrillar amyloid oligomers (Kayed et al. 2003; Sakono and Zako 2010; Nguyen et al. 2021). Amyloid fibrils are now recognized as promising building blocks for advanced biomaterials rather than solely disease-related entities (Li and Zhang 2021; Tyagi and Sengupta 2024). Many amyloid peptides have been reported in the literature that form robust 3D hydrogel matrices (Belwal and Chaudhary 2020; Das et al. 2016; Datta et al. 2019a, b; Yang et al. 2019). We have previously reported hydrogelation by an aromatic analog of β-amyloid fragment $A\beta_{16-22}$. The peptide $A\beta_{16-22}$(F20Y) was dissolved in HFIP; dilution into water resulted in transparent hydrogel (Datta et al. 2019a, b).

Aromatic residues play crucial role in amyloid peptide self-assembly (Gazit 2002; Reches and Gazit 2006). Even though the scientific community acknowledges the role of aromatic residues in peptide self-assembly and hydrogelation, the necessity to have them is debated (Lakshmanan et al. 2013; Hauser et al. 2011). Many short peptides that lack aromatic moieties have been reported in the literature to form ordered superstructures (Erdogan et al. 2015; Subbalakshmi et al. 2017). Ac-PHF6 (CH_3CO-VQIVYK-NH_2), a tau-derived peptide, causes gelation of phosphate-buffered saline (PBS) and cell culture media (Verma et al. 2025). We recently reported hydrogelation by five aromatic analogs of Ac-PHF6, the analogs wherein the phenolic moiety of tyrosine was substituted with phenyl, *p*-fluorophenyl, *p*-cyanophenyl, *p*-nitrophenyl, and *p*-(trifluoromethyl)phenyl (Verma and Chaudhary 2025). All Ac-PHF6 analogs formed hydrogels with comparable rheological properties. These data made us speculate that Tyr might be contributing to Ac-PHF6 self-assembly and hydrogelation through its hydrophobicity rather than aromatic electronic effects. In this study, we test this hypothesis by investigating several aliphatic analogs of Ac-PHF6. Tyr^{310} was substituted with residues with different side-chain hydrophobicities, namely Lys, Ala, Met, Val, and Ile. In addition to these variants, we also investigated the self-assembly of Ac-PHF6* (CH_3CO-VQIINK-NH_2). PHF6* is another hexapeptide stretch in the human tau protein that facilitates tau self-assembly. Unlike PHF6, the PHF6* lacks aromatic residues.

Materials and Methods

Materials

Rink amide resin, Fmoc-protected amino acids, 1-Hydroxybenzotriazole hydrate (HOBt), and *N*, *N*,*N*′*N*′-tetramethyl-*O*-(1*H*-benzotriazol-1-yl)uronium hexafluorophosphate (HBTU) were acquired from Novabiochem. *N*, *N*-dimethylformamide, *N*, *N*-diisopropylethylamine (DIPEA), trifluoroacetic acid (TFA), acetic anhydride, thioflavin T (ThT), diethyl ether, isopropanol, triisopropylsilane (TIPS), and acetonitrile were procured from Merck. Dimethyl sulfoxide (DMSO) and 3-(4,5-dimethylthiazol-2-yl)−2,5-diphenyltetrazolium bromide (MTT) were obtained from SRL. Congo red was procured from Sigma-Aldrich. Dulbecco's Modified Eagle's Medium (DMEM) and fetal bovine serum (FBS) were purchased from Invitrogen, while the antibiotic-antimycotic cocktail was sourced from Gibco. Calcein AM was sourced from Thermo Scientific. HEK-293 cell lines were provided by the National Centre

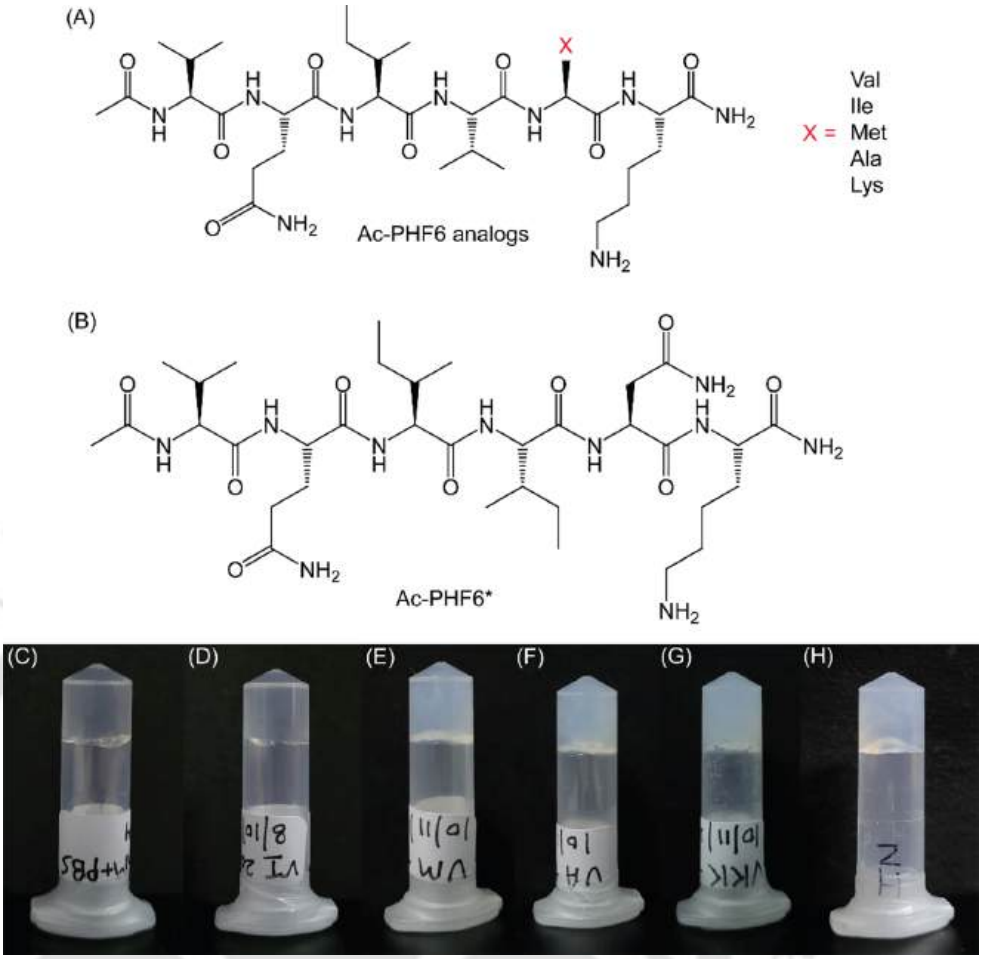

Fig. 1 PBS gelation. The primary structures of the **A** Ac-PHF6 analogs and **B** Ac-PHF6*. 'X' in panel A represents the side chains of Val, Ile, Met, Ala, and Lys. Inverted vials showing hydrogels formed by **C** 20 mM Ac-VQIVVK-am, **D** 20 mM Ac-VQIVIK-am, **E** 20 mM Ac-VQIVMK-am, **F** 20 mM Ac-VQIVAK-am, **G** 20 mM Ac-VQIVKK-am, and **H** 10 mM Ac-PHF6*

for Cell Science, Pune. RNAiso Plus reagent was obtained from Takara Bio (Shiga, Japan), and MultiScribe™ Reverse Transcriptase was sourced from Applied Biosystems, Thermo Fisher Scientific (Waltham, MA, USA).

Peptide Synthesis and Characterization

The peptides were assembled on Rink amide resin by employing Fmoc chemistry with HBTU/HOBt/DIPEA activation. N-terminal acetylation was carried out on-resin using 10 equivalents each of acetic anhydride and DIPEA. The peptides were cleaved from the resin using a cleavage cocktail containing 95% TFA, 2.5% TIPS, and 2.5% water. The synthesized peptides were precipitated in ice-cold diethyl ether, followed by multiple rounds of washing and precipitation. The peptides were air-dried and purified using reversed-phase HPLC on a C18 column by employing a linear gradient of acetonitrile with 0.1% TFA. Peptide identities were ascertained using MALDI-TOF mass spectrometry (Fig. S1).

Peptide Dissolution, Hydrogelation and Rheology

The peptide stock solutions were prepared in water by weighing the peptides, adding deionized water, and vortexing for a few minutes. The concentrations of the stock solutions were estimated using Waddell's method (Wolf 1983). All Ac-PHF6 analogs readily dissolved in water to concentrations higher than 20 mM and remained as viscous solutions at room temperature. Ac-PHF6*, however, showed precipitation above ~ 17 mM concentration. The gelation of PBS was investigated by diluting the stock solutions prepared in water. As characterization of Ac-PHF6 hydrogel reported in the literature was carried out at 20 mM concentration, the hydrogels of Ac-PHF6 analogs were set up at 20 mM concentration. Due to the lower solubility of Ac-PHF6*, the gel could not be set up at 20 mM concentration. Therefore, the hydrogel was set up at 10 mM concentration. Rheology measurements for the 24-hour-old gels were carried out on an Anton Paar Rheometer MCR 102 using 25 cm parallel plates at a 0.5 mm gap. The amplitude sweep tests were carried out at an angular frequency of 10 rad/s by varying shear strain from 0.01% to 10%. As the gels displayed a

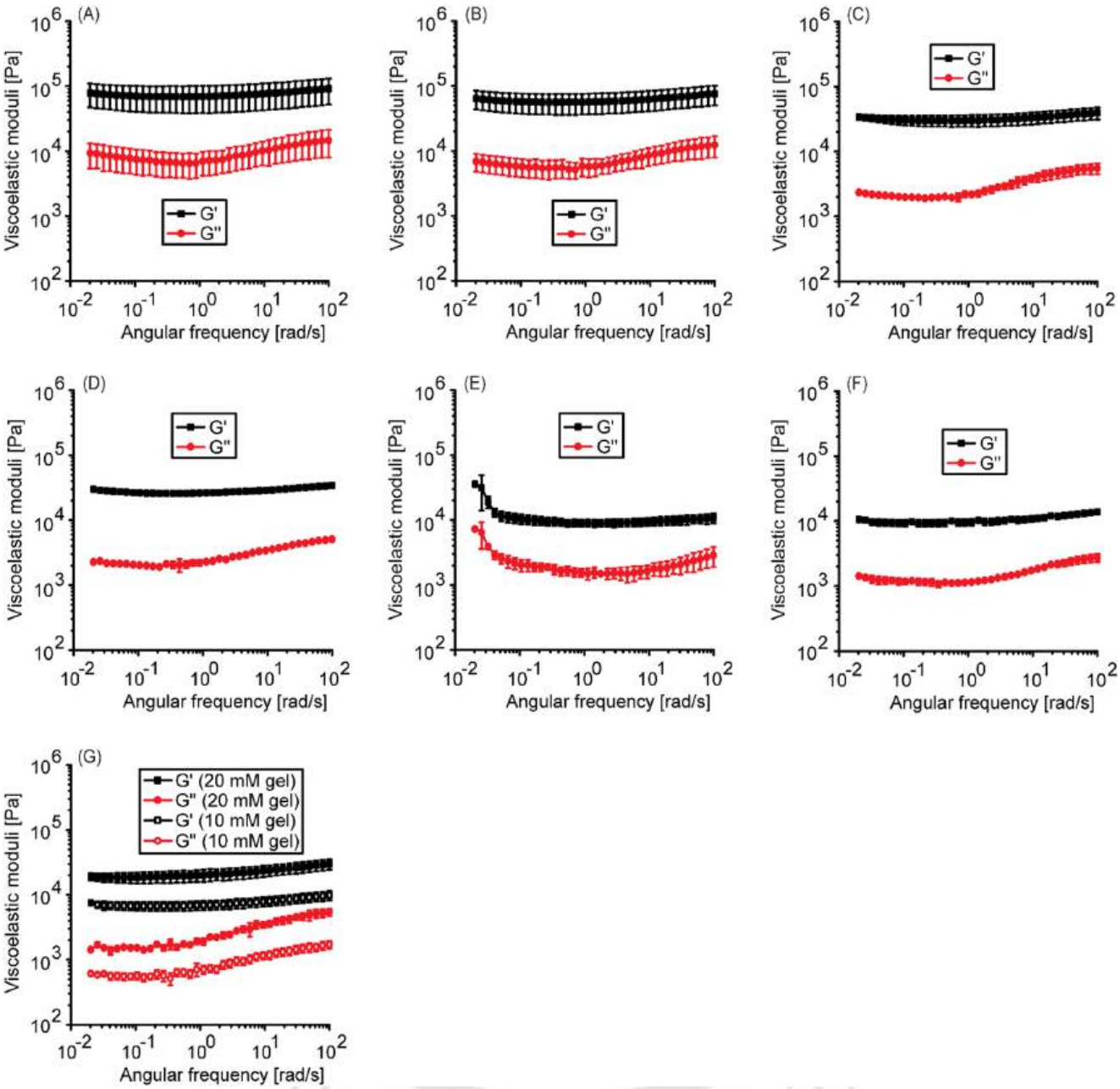

Fig. 2 Rheology. Oscillatory rheology data for hydrogels formed by **A** 20 mM Ac-VQIVVK-am, **B** 20 mM Ac-VQIVIK-am, **C** 20 mM Ac-VQIVMK-am, **D** 20 mM Ac-VQIVAK-am, **E** 20 mM Ac-VQIVKK-am, **F** 10 mM Ac-PHF6*, and **G** 10 and 20 mM Ac-PHF6. The data is presented as the mean of three replicates and the error bars represent the standard deviation

linear regime up to at least 0.1% strain, the frequency sweep data were collected at 0.1% strain. The rheology data were recorded with three replicates, and the data is presented as mean with standard deviations.

The 24-hour-old hydrogels were characterized using various methods. The peptides dissolved in water at the corresponding concentrations i.e. 20 mM for Ac-PHF6 analogs and 10 mM for Ac-PHF6*, even though they did not form gels, were also characterized after 24 h of preparation.

Thioflavin T (ThT) Fluorescence Spectroscopy

The gel samples were sheared through vortexing and diluted using PBS for ThT fluorescence spectroscopy. ThT fluorescence quantum yield is pH-dependent (Naiki et al. 1989). The peptide samples in water, therefore, were diluted in 10 mM phosphate buffer pH 7.4 for the ThT fluorescence assay. This ensures that ThT fluorescence is not influenced by the difference in pH between water and PBS samples. The assay was carried out at 200 µM peptide and 10 µM

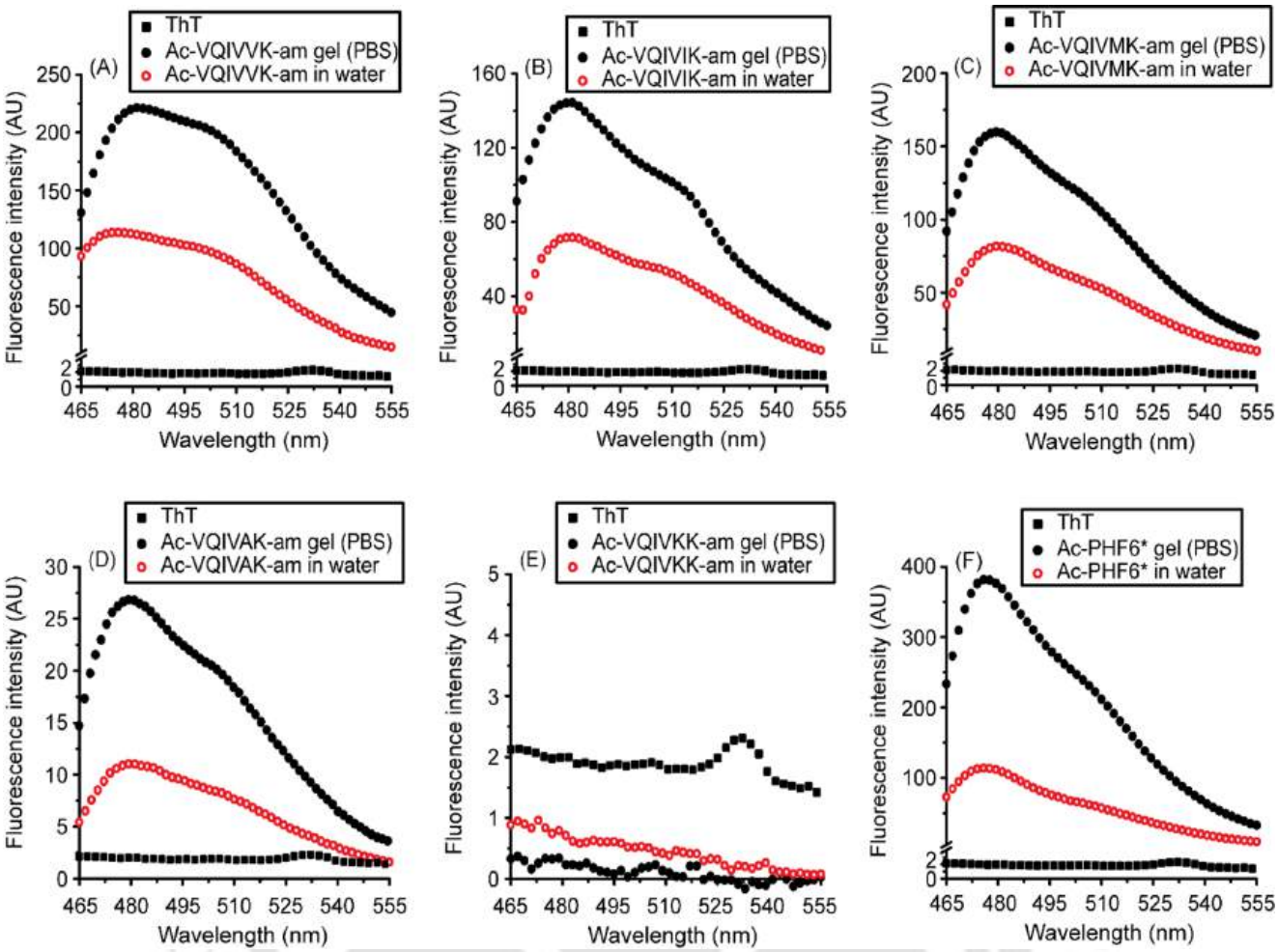

Fig. 3 Thioflavin T fluorescence spectroscopy. ThT fluorescence emission spectra of **A** Ac-VQIVVK-am, **B** Ac-VQIVIK-am, **C** Ac-VQIVMK-am, **D** Ac-VQIVAK-am, **E** Ac-VQIVKK-am, and **F** Ac-PHF6*

ThT concentrations. The samples were excited at 450 nm with a 2.5 nm bandwidth, and fluorescence emission spectra were recorded using an emission bandwidth of 5 nm.

Congo Red (CR) Spectral Shift Assay

Congo red is a dye that binds to amyloid fibrils with high specificity. Binding to amyloid-like fibrils is accompanied by a red shift in the visible region absorption band. A 300 µM CR solution was prepared in 90% PBS and 10% ethanol, as described elsewhere (Klunk et al. 1999). The concentration was estimated using a molar absorption coefficient of 5.93×10^4 $M^{-1}cm^{-1}$ at 505 nm. The 24 h-old peptide gel samples were sheared and CR absorption spectra were recorded at 9 µM concentration with 30 µg/ml peptide concentration.

Circular Dichroism (CD) Spectroscopy

Far-UV electronic CD spectra were recorded on a Jasco J-1500 spectropolarimeter. The 24-hour-old samples were diluted in the respective dispersant (water or PBS) to 200 µM concentration, and spectra were recorded in a 1 mm path-length quartz cell. The spectra were recorded from 260–195 nm at 1 nm bandwidth with a 100 nm/min scanning speed and 8 accumulations. The spectra were corrected by subtracting the respective dispersant spectrum, and the mean residue ellipticity was calculated as described elsewhere (Verma and Chaudhary 2025). The CD spectra were recorded for three replicates, and the data is presented as mean with standard deviations.

Fourier Transform Infrared (FTIR) Spectroscopy

Infrared spectra were recorded on a Shimadzu IRAffinity-1 S spectrometer equipped with a diamond ATR crystal.

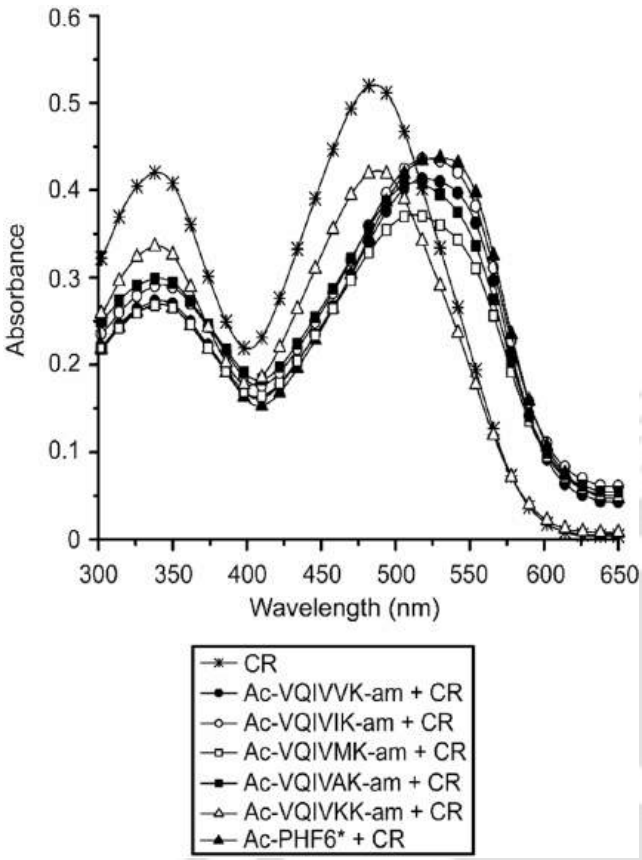

Fig. 4 Congo red absorption spectroscopy. Congo red absorption spectra with peptides obtained after shearing the PBS hydrogels

The 24-hour-old samples were diluted 2-fold, deposited onto the crystal surface, and left to air-dry completely. Each spectrum is the average of 40 scans recorded at a resolution of 4 cm^{-1}.

Transmission Electron Microscopy (TEM)

The 24-hour-old gel samples and the corresponding peptide solutions in water were diluted 2-fold in the respective dispersant and deposited on the carbon-coated copper grids. After about 5 min, the excess solvent was removed using lint-free tissue paper, and the grids were stained with uranyl acetate for a minute before being left to air-dry. The images were captured at 200 kV on a JEM-2100 F TEM (JEOL, Japan).

Cytocompatibility of the Peptides

Cytocompatibility of the peptides was assessed through MTT assay. Ten thousand HEK-293 cells were seeded in a 96-well plate in complete DMEM and incubated at 37 °C with 5% CO_2 for 24 h. The wells were then treated with 50, 100, 150, and 200 µM peptide, and further incubated for 24 h. Following incubation, the growth medium was discarded and 100 µl of MTT in plain DMEM (1 mg/ml) was added to each well and incubated for 3 h. Subsequently, MTT solution was removed, and 100 µl DMSO was added. The absorbance of the purple-colored product was recorded

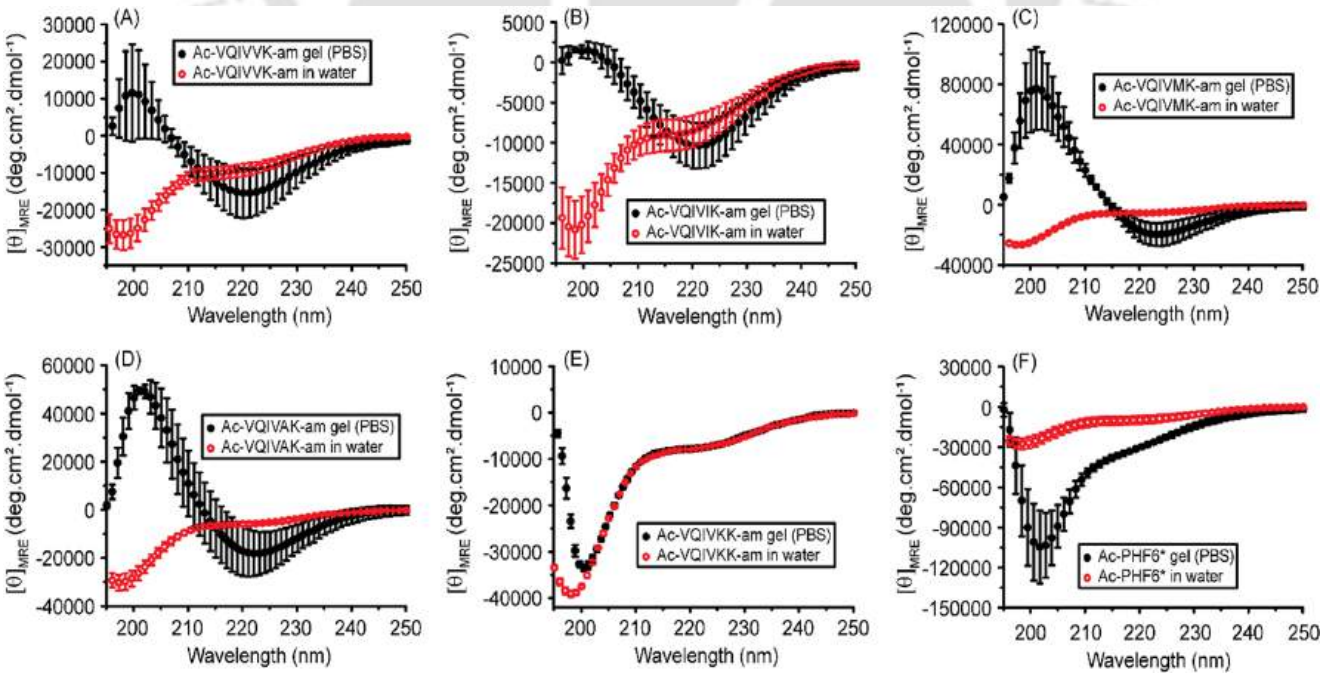

Fig. 5 Circular dichroism spectroscopy. CD spectra of **A** Ac-VQIVVK-am, **B** Ac-VQIVIK-am, **C** Ac-VQIVMK-am, **D** Ac-VQIVAK-am, **E** Ac-VQIVKK-am, and **F** Ac-PHF6*. The data is presented as the mean of three replicates and the error bars represent the standard deviation

at 570 nm using a multi-well plate reader (Multiskan GO, Thermo Scientific).

HEK-293 cells were cultured in a T25 flask using DMEM supplemented with 10% FBS and 1% antibiotic-antimycotic cocktail. The cells were incubated at 37 °C with 5% CO_2 for growth and maintenance. The 10 mM Ac-PHF6* PBS gel was set up in a 96-well plate. The 24-hour-old gel was equilibrated with DMEM for 24 h. The gel was then seeded with 10,000 HEK-293 cells and incubated for 24 h. For studying GAPDH expression, the total RNA was isolated using RNAiso Plus reagent, followed by cDNA synthesis with MultiScribe™ Reverse Transcriptase, and PCR (40 cycles) using primers designed for GAPDH amplification. The cell growth on the hydrogel (5 mM Ac-PHF6*) was assessed through fluorescence imaging. The wells were washed with PBS and treated with a 5 µM calcein AM solution prepared in PBS. The plate was incubated at 37 °C with 5% CO_2 for 30 min. The cells were washed thrice with PBS, and images were captured using a Nikon Eclipse Ts2R fluorescence microscope.

Results and Discussion

Self-assembly, Hydrogelation and Rheology

The primary structure of the peptides employed in this study are shown in Fig. 1A and B. The critical aggregation concentration (CAC) of the peptides in PBS was investigated using 90° light scattering (Fig. S2). All peptides, except Ac-VQIVAK-am and Ac-VQIVKK-am display CAC below 100 µM. Ac-VQIVAK-am displays a CAC around 200 µM whereas Ac-VQIVKK-am CAC was found to be >1 mM. As the Ac-PHF6 hydrogel reported in the literature was prepared at 20 mM concentration, we chose to investigate the aliphatic analogs at the same concentration. All Ac-PHF6 analogs readily dissolved in water to concentrations higher than 20 mM. Ac-PHF6*, however, displayed lower solubility. The concentration higher than ~17 mM could not be achieved. Stock solutions prepared in water were diluted in PBS to achieve the desired concentrations (20 mM for Ac-PHF6 analogs, 10 mM for Ac-PHF6*). All the samples formed hydrogels, as confirmed by inverting the vials. Instant gelation was observed for Ac-PHF6* and all Ac-PHF6 analogs, except Ac-VQIVKK-am. Ac-VQIVKK-am formed a soft gel after about 2 h. The samples were left undisturbed at room temperature for 24 h. The images of the vials containing the 24-hour-old gel samples are shown in Fig. 1C–H. All subsequent experiments, unless mentioned otherwise, were carried out with the peptide samples prepared at the aforementioned concentrations in water and PBS. As hydrogels formed by Ac-PHF6 and its aromatic analogs reported in the literature were characterized for 24-hour-old samples, all assays reported in this study were also carried out after incubating the peptide samples at room temperature for 24 h (Verma et al. 2025; Verma and Chaudhary 2025). Ac-VQIVVK-am and Ac-VQIVIK-am formed transparent hydrogels (Fig. 1C and D), while the gels formed by all other peptides were translucent (Fig. 1E–H).

Rheology was carried out to investigate the viscoelasticity of the hydrogels. Ac-VQIVVK-am and Ac-VQIVIK-am formed hydrogels with storage moduli of around 60 kPa from 100 rad/s down to 0.02 rad/s (Fig. 2A and B). The loss moduli were ~6–10 kPa. The rheology data for 20 mM Ac-PHF6 hydrogel is shown in Fig. 2G. The hydrogel displays storage and loss moduli of ~20 kPa and ~1–5 kPa, respectively. These rheological characteristics are similar to the 20 mM Ac-PHF6 hydrogel reported in the literature (Verma et al. 2025). Substitution of Tyr^{310} in Ac-PHF6 with Val or Ile, therefore, results in stiffer hydrogels. The Ac-VQIVMK-am and Ac-VQIVAK-am formed hydrogels with storage moduli around 30 kPa (Fig. 2C and D). Met and Ala have lower hydrophobicities than those of Val and Ile, and form hydrogels with lower stiffness. Ac-VQIVKK-am formed softer gel with a storage modulus of about 1 kPa (Fig. 2E). We previously investigated Ac-PHF6 analogs wherein the Tyr side chain was replaced with several electron-deficient aromatic groups (Verma and Chaudhary 2025). Interestingly, all analogs formed hydrogels, prompting us to hypothesize that the sole aromatic residue Tyr^{310} in Ac-PHF6 might contribute to self-assembly and hydrogelation more through its hydrophobicity than the aromaticity. Hydrogelation by Ac-PHF6 aliphatic analogs proves that hypothesis. The Ac-PHF6 analogs wherein Tyr is substituted with Val, Ile, Met, and Ala form hydrogels with higher stiffness than that of the Ac-PHF6 hydrogel. The Y310K analog, on the other hand, forms hydrogel with stiffness lower than Ac-PHF6 hydrogel. Besides, unlike all other peptides, the kinetics of gelation is much slower. Whereas all other peptides cause instant PBS gelation, the Y310K analog takes about 2 h to form hydrogel. These data made us wonder if Ac-PHF6*, a tau interaction motif very similar to Ac-PHF6 but lacking an aromatic residue, could also form hydrogel. As Ac-PHF6* displayed lower solubility, the hydrogel could not be set up at 20 mM concentration. Ac-PHF6* hydrogel, therefore, was prepared at 10 mM concentration for all the assays. The 10 mM hydrogel exhibited a storage modulus of about 10 kPa in the 0.02–100 rad/s frequency range. The loss modulus was around one order of magnitude less (Fig. 2F). The viscoelasticity of 10 mM Ac-PHF6 hydrogel is not reported in the literature. Therefore, we prepared 10 mM Ac-PHF6 hydrogel and measured its viscoelasticity to directly compare with that of Ac-PHF6* hydrogel (Fig. 2G). Clearly, the Ac-PHF6* displays higher storage and loss moduli at all

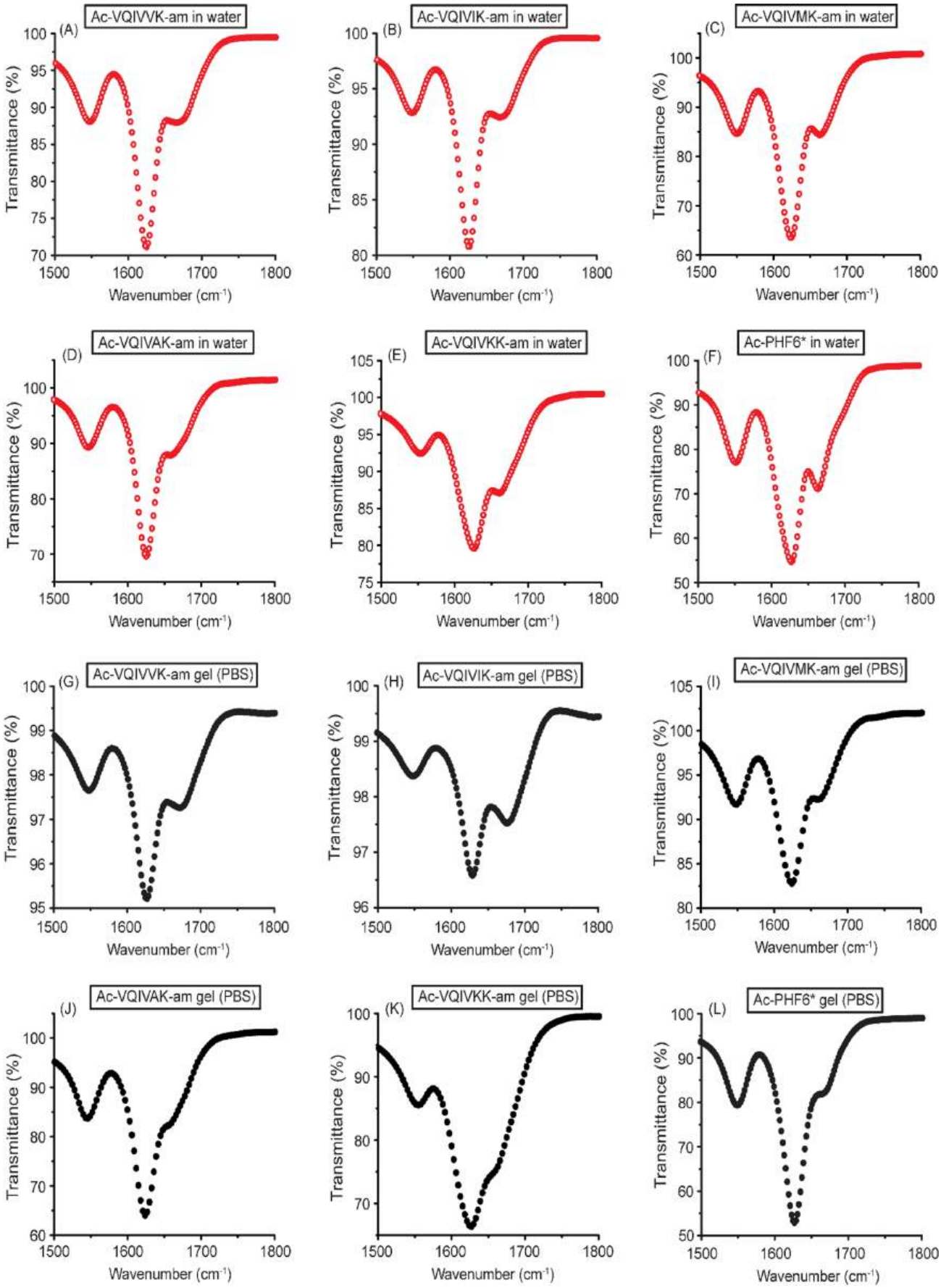

Fig. 6 Infrared spectroscopy. The ATR-FTIR spectra of peptide water samples (panels A-F) and PBS samples (panels G-L)

frequencies. Tyr^{310}, therefore, is superfluous for Ac-PHF6 self-assembly and hydrogelation.

ThT Fluorescence

The structures underlying the hydrogels were investigated using ThT fluorescence, an assay routinely employed to identify the amyloid-like aggregates. The binding of ThT to amyloid-like fibrils causes a large enhancement in its fluorescence intensity. All peptides, except for Ac-VQIVKK-am, caused enhancement in ThT fluorescence intensity (Fig. 3). The enhancement caused by PBS samples is at least 2 times more than that caused by the water samples. This is consistent with the understanding that charge screening of the terminal lysine residue facilitates self-assembly. Notably, the PBS sample of Ac-PHF6* exhibited more than 3-fold higher ThT fluorescence compared to the water sample (Fig. 3F). Eisenberg and coworkers have investigated the steric-zippers formed by VQIVYK and VQIINK peptides (Seidler et al. 2018). VQIINK is reported to form steric zippers with higher shape complementarity and a larger steric zipper interface. Using tau K18 constructs wherein R2 and R3 contain identical hexapeptide motifs, i.e. constructs with two PHF6 or two PHF6*, they further show that PHF6* is a better interaction motif in driving self-assembly. The higher ThT fluorescence intensity observed for Ac-PHF6*, therefore, could be due to its higher aggregation propensity.

Congo Red Spectral Shift Assay

Congo red, a sulfonated diazo dye, displays absorption bands centred around 340 and 496 nm in water. Binding of congo red to amyloid fibrils causes a red-shift in the lower energy band. Figure 4 shows the congo red absorption spectra recorded with the PBS peptide samples. All peptides, except for Ac-VQIVKK-am, exhibit a red shift in the lower energy absorption band. These data are consistent with the ThT fluorescence data. The hydrogel formed by Ac-VQIVKK-am, therefore, is not made up of amyloid-like fibrillar structures.

CD Spectroscopy

The secondary structures of the peptides were analyzed using far-UV CD spectroscopy. The samples were diluted to 200 µM in their respective dispersant for the measurements. In water, CD spectra of all the peptides display a negative band around 198 nm and a lower intensity shoulder around 220 nm (Fig. 5). These spectra are suggestive of a mixture of β-sheet and random coil conformations. In PBS, all Ac-PHF6 analogs, except Ac-VQIVKK-am, show a negative band around 220 nm and a positive band around 200 nm (Fig. 5A–D). These spectra suggest a predominantly β-sheet structure. Ac-VQIVKK-am in PBS displays a spectrum very similar to that observed in water, albeit with a slightly red-shifted higher energy band (Fig. 5E). Ac-PHF6* displays an intense negative band around 202 nm alongside the 220 nm shoulder (Fig. 5F). This CD spectrum comes as a surprise as Ac-PHF6* caused the highest enhancement in ThT fluorescence intensity among all the peptides. Manavalan and Johnson found two distinct types of CD spectra for β-sheet proteins. The one that was eventually designated β_I shows a classical β-sheet signature with a ~ 215–220 nm negative band and a 195–200 nm positive band. The second type of spectrum, known as β_{II}, exhibits a negative band around 200 nm (Manavalan and Johnson 1983; Wu et al. 1992). The Ac-PHF6* CD spectrum in PBS looks similar to that observed in water, but with much higher ellipticity and a slightly red-shifted higher energy band. An ellipticity this large is very atypical of protein CD spectra. Sreerama and Woody assigned such a large ellipticity to poly(Pro) II-like conformation (Sreerama and Woody 2003). A large ellipticity observed for poly(Pro)II implies that a protein with a high poly(Pro)II to β-sheet ratio would give a β_{II} CD signature.

FTIR Spectroscopy

As the CD spectrum observed for Ac-PHF6* in PBS was atypical, the secondary structures were further validated using infrared spectroscopy. The frequency of the amide I band is sensitive to the polypeptide backbone conformation, and is particularly suitable for β-sheet structure. The amide I band for β-sheet in proteins is observed between 1625 and 1640 cm^{-1} (Jackson and Mantsch 1995). Aggregated strands display further lower frequencies with the amide I band lying between 1610 and 1635 cm^{-1} (Jackson and Mantsch 1995; Sarroukh et al. 2013). Infrared spectroscopy, therefore, has emerged as a method of choice for investigating the self-assembled proteins and peptides (Sarroukh et al. 2013; Sassi et al. 2011). Dried samples of all peptides exhibited an amide I band near 1626 cm^{-1} in both PBS and water, clearly establishing the β-sheet conformation of the superstructures underlying the hydrogels (Fig. 6).

Transmission Electron Microscopy

The morphology of the self-assembled structures forming the hydrogels was analyzed using TEM (Fig. 7). Ribbon-like structures were observed for Ac-VQIVVK-am (Fig. 7A) and Ac-VQIVIK-am (Fig. 7B) water samples. Such ribbon-like structures have been reported in the

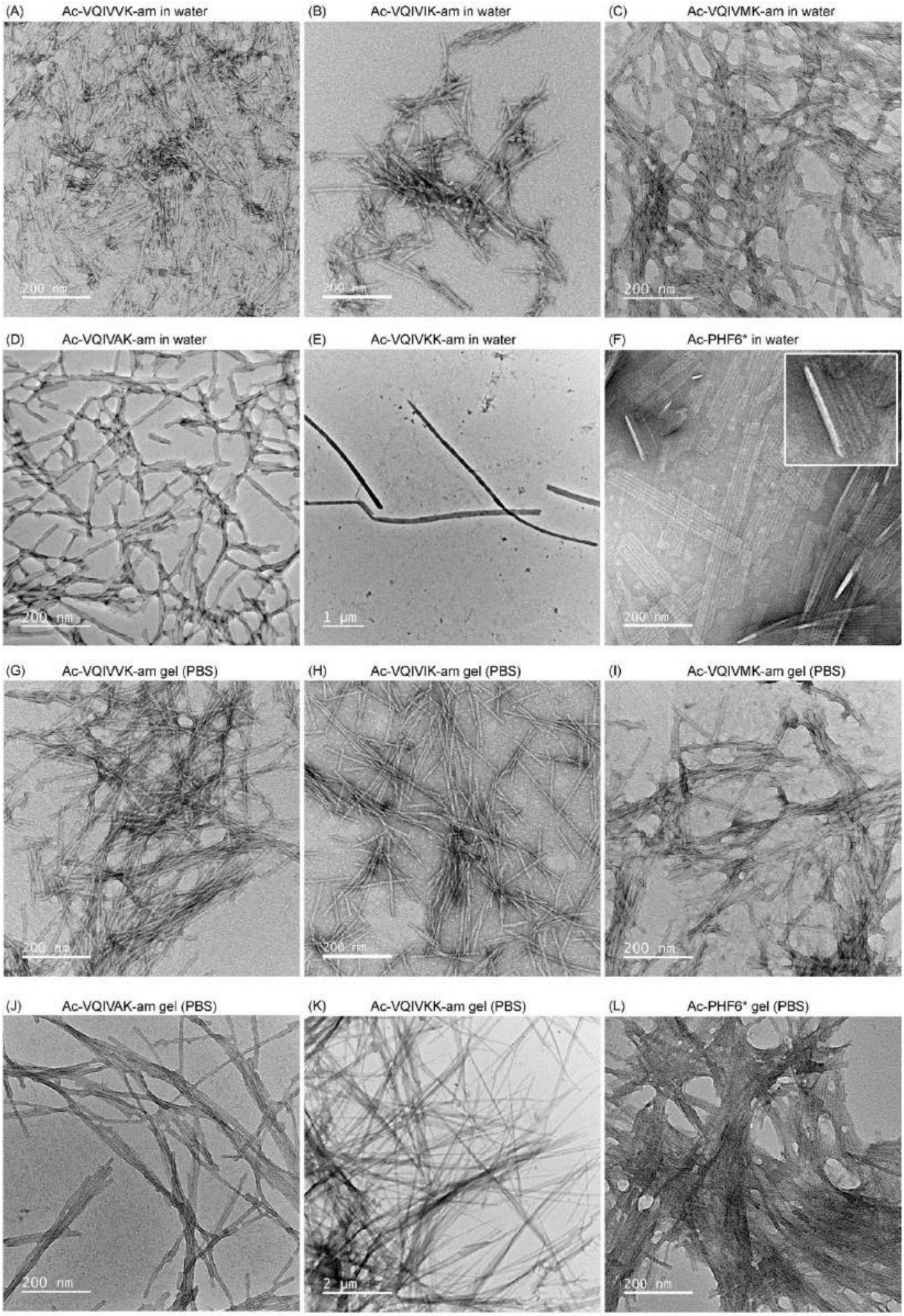

Fig. 7 Transmission electron micrographs. TEM images of water (panels A-F) and PBS hydrogel (panels G-L) samples

literature for Ac-PHF6 (Verma et al. 2025). Ac-VQIVMK-am and Ac-VQIVAK-am form typical amyloid-like filamentous assemblies in water (Fig. 7C and D). Unlike the other Ac-PHF6 analogs that showed abundant fibrillar structures spread throughout the copper grid used for imaging, very few long filamentous structures were found for Ac-VQIVKK-am (Fig. 7E). In PBS, all Ac-PHF6 analogs, except Ac-VQIVKK-am, formed typical amyloid-like fibrils (Fig. 7G–J). The fibrils are rod-like, resembling those previously reported for Ac-PHF6 (Chaudhary et al. 2009; Verma et al. 2025). Ac-VQIVKK-am formed long, straight, and flat ribbon-like structures, suggesting a different mode of assembly (Fig. 7K). Ac-PHF6*, unlike Ac-PHF6 analogs, formed very different superstructures. In water, the peptide self-assembled into long ribbon-like structures that laterally assemble to form flat sheets (Fig. 7F). Some of these sheets appear to curl near the edges (Inset, Fig. 7F). In PBS, Ac-PHF6* formed long, straight but densely entangled fibrous structures (Fig. 7L).

Cytocompatibility of Peptides

The cytocompatibility of peptides was assessed using an MTT cell viability assay. In this assay, viable cells metabolically reduce MTT to formazan crystals, which absorb light at 570 nm. In contrast, non-viable cells lack this activity and do not contribute to the absorbance signal. The cell viability was normalized to untreated control cells (Fig. 8A–F). The cells displayed ~ 80% viability up to 200 µM peptide concentration for all six peptides.

Ac-PHF6 hydrogel has been reported in the literature to support culture of mammalian cells (Verma et al. 2025). We wondered if Ac-PHF6* hydrogel could also support cell culture. The HEK-293 cells were cultured on a 24-hour-old hydrogel (5 mM Ac-PHF6*) for 24 h and then stained with calcein AM, a membrane-permeable, non-fluorescent

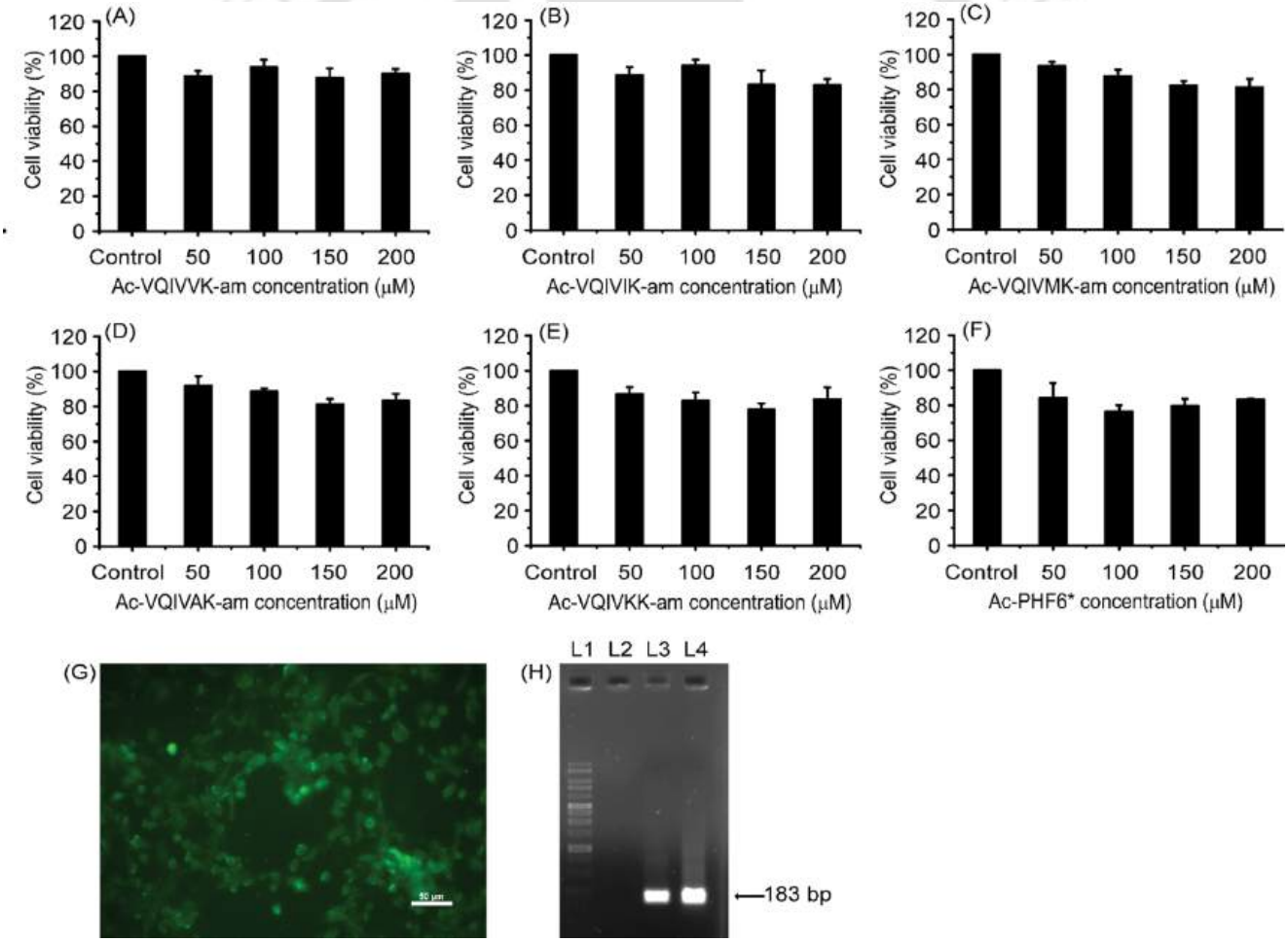

Fig. 8 Cytocompatibility of peptides. HEK-293 cell-viability using MTT assay (**A**–**F**). Cells grown on Ac-PHF6* hydrogel (**G**), and GAPDH expression shown by HEK-293 cells grown on the hydrogel (**H**). The scale bar represents 50 µm. L1 is the 1 kb (250–10,000 bp) DNA molecular weight marker lane, L2 is the negative control, L3 represents the GAPDH amplification from cells cultured in DMEM without peptide (positive control), and L4 represents the GAPDH amplification from cells cultured in Ac-PHF6* hydrogel

probe. Intracellular esterases hydrolyze calcein AM into fluorescent calcein, with fluorescence intensity correlating directly with esterase activity, and therefore, cell viability. Microscopic analysis confirmed HEK-293 cell proliferation in the hydrogel matrix (Fig. 8G). The expression of the housekeeping gene GAPDH was also investigated. Cells grown without Ac-PHF6* (positive control), and in 10 mM hydrogel were harvested, followed by RNA extraction and reverse transcription PCR (RT-PCR). The cells grown in the hydrogel were found to express GAPDH (Fig. 8H).

Conclusion

We previously demonstrated that Ac-PHF6 (CH_3CO-VQIVYK-NH_2) formed an injectable and biocompatible hydrogel in PBS (Verma et al. 2025). The peptide contains a Tyr residue that was believed to facilitate self-assembly through aromatic stacking interactions. In a follow-up study, we examined aromatic analogs of Ac-PHF6 bearing electron-withdrawing substituents on the phenyl ring (Verma and Chaudhary 2025). All the analogs formed hydrogels, prompting us to hypothesize that the Tyr residue may not contribute to self-assembly and gelation due to its aromaticity. Ac-PHF6 analogs wherein Tyr is substituted with amino acids with hydrophobic side chains (Val, Ile, Met, Ala) formed amyloid-like fibrils very similar to those formed by Ac-PHF6. All four peptides caused instant gelation of PBS. The peptide wherein Tyr was substituted with Lys, an amino acid with polar side chain, formed a soft gel with much lower gelation rate. Besides, the assembly of the Y310K analog appears to be different from all other Ac-PHF6 analogs. Ac-PHF6*, a native peptide stretch from the R2 region of tau that lacks an aromatic residue, was also found to form hydrogel. Like Ac-PHF6 hydrogel, Ac-PHF6* hydrogel also supported HEK-293 cell growth. These findings suggest that the role of aromatic residues in peptide self-assembly and hydrogelation may be overemphasized. It is likely that the aromatic residues in many peptides simply contribute through their size and hydrophobicity.

Supplementary Information The online version contains supplementary material available at https://doi.org/10.1007/s10989-026-10803-9.

Acknowledgements SSV and SB acknowledge the Ministry of Education, Govt. of India for fellowship. The authors thank Central Instruments Facility, IIT Guwahati, for transmission electron microscopy and MALDI-TOF mass spectrometry.

Author Contributions S.S.V.: Synthesis, purification, and characterization of the peptides; rheology; all spectroscopy experiments; transmission electron microscopy; writing original draft of the manuscript.S.S.V. and S.B carried out cell culture and cell viability experiments.S.K. provided resources for cell culture experiments, supervised these experiments, and analyzed the data.N.C.: Conceptualization, resources, writing - review & editing, supervision, formal analysis, project administration, funding acquisition.

Funding Funding from the DBT Twinning project No. BT/PR15921/NER/95/140/2015 and SERB project No. SB/YS/LS-316/2013 is acknowledged.

Data Availability The data is provided within the manuscript.

Declarations

Competing Interests The authors declare no competing interests.

References

Belwal VK, Chaudhary N (2020) Amyloids and their untapped potential as hydrogelators. Soft Matter 16:10013–10028

Brøndsted H, Kopeček Ji (1991) Hydrogels for site-specific oral drug delivery: synthesis and characterization. Biomaterials 12:584–592

Chakraborty P, Tang Y, Yamamoto T, Yao Y, Guterman T, Zilberzwige-Tal S, Adadi N, Ji W, Dvir T, Ramamoorthy A, Wei G, Gazit E (2020) Unusual two-step assembly of a minimalistic dipeptide-based functional hypergelator. Adv Mater 32:1906043

Chatterjee S, Upadhyay P, Mishra M, M S, Akshara MR, N K, Zaidi ZS, Iqbal SF, Misra SK (2020) Advances in chemistry and composition of soft materials for drug releasing contact lenses. RSC Adv 10:36751–36777

Chaudhary N, Singh S, Nagaraj R (2009) Morphology of self-assembled structures formed by short peptides from the amyloidogenic protein Tau depends on the solvent in which the peptides are dissolved. J Pept Sci 15:675–684

Das S, Zhou K, Ghosh D, Jha NN, Singh PK, Jacob RS, Bernard CC, Finkelstein DI, Forsythe JS, Maji SK (2016) Implantable amyloid hydrogels for promoting stem cell differentiation to neurons. NPG Asia Mater 8:e304

Datta D, Harikrishna A, Nagaraj R, Chaudhary N (2018) Self-assembly of β-turn motif-connected tandem repeats of Aβ16–22 and its aromatic analogs. Pept Sci. https://doi.org/10.1002/pep2.24099

Datta D, Kumar V, Kumar S, Nagaraj R, Chaudhary N (2019) Limpid hydrogels from β-turn motif-connected tandem repeats of Aβ16–22. Soft Matter 15:4827–4835

Datta D, Kumar V, Kumar S, Nagaraj R, Chaudhary N (2019) Hydrogel formation by an aromatic analogue of a β-amyloid fragment, Aβ16–22: a scaffold for 3D cell culture. ACS Omega 4:620–627

Datta D, Nagaraj R, Chaudhary N (2020) Water-alcohol bigels from fatty acylated dipeptides. J Phys Chem B 124:577–588

Datta D, Chaudhary N (2021) Chap. 8 - Peptide-based hydrogels for biomedical applications. In: Hasija Y (ed) Translational Biotechnology. Academic Press, pp 203–232

Diaferia C, Netti F, Ghosh M, Sibillano T, Giannini C, Morelli G, Adler-Abramovich L, Accardo A (2020) Bi-functional peptide-based 3D hydrogel-scaffolds. Soft Matter 16:7006–7017

Erdogan H, Babur E, Yilmaz M, Candas E, Gordesel M, Dede Y, Oren EE, Demirel GB, Ozturk MK, Yavuz MS, Demirel G (2015) Morphological versatility in the self-assembly of Val-Ala and Ala-Val dipeptides. Langmuir 31:7337–7345

Fichman G, Guterman T, Damron J, Adler-Abramovich L, Schmidt J, Kesselman E, Shimon LJW, Ramamoorthy A, Talmon Y, Gazit E (2016) Spontaneous structural transition and crystal formation in minimal supramolecular polymer model. Sci Adv 2:e1500827

Fleming S, Debnath S, Frederix PWJM, Tuttle T, Ulijn RV (2013) Aromatic peptide amphiphiles: significance of the Fmoc moiety. Chem Commun 49:10587–10589
Fowler DM, Koulov AV, Alory-Jost C, Marks MS, Balch WE, Kelly JW (2006) Functional amyloid formation within mammalian tissue. PLoS Biol 4:e6
Fukuma T, Mostaert AS, Jarvis SP (2006) Explanation for the mechanical strength of amyloid fibrils. Tribol Lett 22:233–237
Gazit E (2002) A possible role for pi-stacking in the self-assembly of amyloid fibrils. FASEB J 16:77–83
Guy M-M, Voyer N (2012) Structure and hydrogel formation studies on homologs of a lactoglobulin-derived peptide. Biophys Chem 163–164:1–10
Haines LA, Rajagopal K, Ozbas B, Salick DA, Pochan DJ, Schneider JP (2005) Light-activated hydrogel formation via the triggered folding and self-assembly of a designed peptide. J Am Chem Soc 127:17025–17029
Hartgerink JD, Beniash E, Stupp SI (2001) Self-assembly and mineralization of peptide-amphiphile nanofibers. Science 294:1684–1688
Hartgerink JD, Beniash E, Stupp SI (2002) Peptide-amphiphile nanofibers: a versatile scaffold for the preparation of self-assembling materials. Proc Natl Acad Sci U S A 99:5133–5138
Hauser CA, Deng R, Mishra A, Loo Y, Khoe U, Zhuang F, Cheong DW, Accardo A, Sullivan MB, Riekel C, Ying JY, Hauser UA (2011) Natural tri- to hexapeptides self-assemble in water to amyloid beta-type fiber aggregates by unexpected alpha-helical intermediate structures. Proc Natl Acad Sci U S A 108:1361–1366
Hendricks MP, Sato K, Palmer LC, Stupp SI (2017) Supramolecular assembly of peptide amphiphiles. Acc Chem Res 50:2440–2448
Hoffman AS (2012) Hydrogels for biomedical applications. Adv Drug Deliv Rev 64:18–23
Jackson M, Mantsch HH (1995) The use and misuse of FTIR spectroscopy in the determination of protein structure. Crit Rev Biochem Mol Biol 30:95–120
Juković M, Ratkaj I, Kalafatovic D, Bradshaw NJ (2024) Amyloids, amorphous aggregates and assemblies of peptides – assessing aggregation. Biophys Chem 308:107202
Kayed R, Head E, Thompson JL, McIntire TM, Milton SC, Cotman CW, Glabe CG (2003) Common structure of soluble amyloid oligomers implies common mechanism of pathogenesis. Science 300:486–489
Klunk WE, Jacob RF, Mason RP (1999) Quantifying amyloid by congo red spectral shift assay. Methods in Enzymology. Academic Press, pp 285–305
Lakshmanan A, Cheong DW, Accardo A, Di Fabrizio E, Riekel C, Hauser CA (2013) Aliphatic peptides show similar self-assembly to amyloid core sequences, challenging the importance of aromatic interactions in amyloidosis. Proc Natl Acad Sci U S A 110:519–524
Li J, Zhang F (2021) Amyloids as building blocks for macroscopic functional materials: designs, applications and challenges. Int J Mol Sci. https://doi.org/10.3390/ijms221910698
Li J, Xing R, Bai S, Yan X (2019) Recent advances of self-assembling peptide-based hydrogels for biomedical applications. Soft Matter 15:1704–1715
Li W, Wu Y, Zhang X, Wu T, Huang K, Wang B, Liao J (2023) Self-healing hydrogels for bone defect repair. RSC Adv 13:16773–16788
Liu H, Wang C, Li C, Qin Y, Wang Z, Yang F, Li Z, Wang J (2018) A functional chitosan-based hydrogel as a wound dressing and drug delivery system in the treatment of wound healing. RSC Adv 8:7533–7549
Liu C, Zhang Q, Zhu S, Liu H, Chen J (2019) Preparation and applications of peptide-based injectable hydrogels. RSC Adv 9:28299–28311
Loic S (2017) In: Asao T (ed) Amino acids modification to improve and Fine-Tune Peptide- based hydrogels. Amino Acid, InTech, Rijeka
Mahler A, Reches M, Rechter M, Cohen S, Gazit E (2006) Rigid, self-assembled hydrogel composed of a modified aromatic dipeptide. Adv Mater 18:1365–1370
Maji SK, Perrin MH, Sawaya MR, Jessberger S, Vadodaria K, Rissman RA, Singru PS, Nilsson KP, Simon R, Schubert D, Eisenberg D, Rivier J, Sawchenko P, Vale W, Riek R (2009) Functional amyloids as natural storage of peptide hormones in pituitary secretory granules. Science 325:328–332
Manavalan P, Johnson WC (1983) Sensitivity of circular dichroism to protein tertiary structure class. Nature 305:831–832
Naiki H, Higuchi K, Hosokawa M, Takeda T (1989) Fluorometric determination of amyloid fibrils in vitro using the fluorescent dye, thioflavin T. Anal Biochem 177:244–249
Nguyen PH, Ramamoorthy A, Sahoo BR, Zheng J, Faller P, Straub JE, Dominguez L, Shea J-E, Dokholyan NV, De Simone A, Ma B, Nussinov R, Najafi S, Ngo ST, Loquet A, Chiricotto M, Ganguly P, McCarty J, Li MS, Hall C, Wang Y, Miller Y, Melchionna S, Habenstein B, Timr S, Chen J, Hnath B, Strodel B, Kayed R, Lesné S, Wei G, Sterpone F, Doig AJ, Derreumaux P (2021) Amyloid oligomers: a joint experimental/computational perspective on Alzheimer's disease, Parkinson's disease, type II diabetes, and amyotrophic lateral sclerosis. Chem Rev 121:2545–2647
Otzen D, Riek R (2019) Functional Amyloids. Cold Spring Harb Perspect Biol. https://doi.org/10.1101/cshperspect.a033860
Pochan DJ, Schneider JP, Kretsinger J, Ozbas B, Rajagopal K, Haines L (2003) Thermally reversible hydrogels via intramolecular folding and consequent self-assembly of a de novo designed peptide. J Am Chem Soc 125:11802–11803
Reches M, Gazit E (2006) Designed aromatic homo-dipeptides: formation of ordered nanostructures and potential nanotechnological applications. Phys Biol 3:S10-19
Rosa E, Diaferia C, Gianolio E, Sibillano T, Gallo E, Smaldone G, Stornaiuolo M, Giannini C, Morelli G, Accardo A (2022) Multicomponent hydrogel matrices of Fmoc-FF and cationic peptides for application in tissue engineering. Macromol Biosci 22:2200128
Ryan DM, Anderson SB, Nilsson BL (2010) The influence of side-chain halogenation on the self-assembly and hydrogelation of Fmoc-phenylalanine derivatives. Soft Matter 6:3220–3231
Sakono M, Zako T (2010) Amyloid oligomers: formation and toxicity of Abeta oligomers. FEBS J 277:1348–1358
Sarroukh R, Goormaghtigh E, Ruysschaert JM, Raussens V (2013) ATR-FTIR: a rejuvenated tool to investigate amyloid proteins. Biochim Biophys Acta 1828:2328–2338
Sassi P, Giugliarelli A, Paolantoni M, Morresi A, Onori G (2011) Unfolding and aggregation of lysozyme: a thermodynamic and kinetic study by FTIR spectroscopy. Biophys Chem 158:46–53
Schneider JP, Pochan DJ, Ozbas B, Rajagopal K, Pakstis L, Kretsinger J (2002) Responsive hydrogels from the intramolecular folding and self-assembly of a designed peptide. J Am Chem Soc 124:15030–15037
Seidler PM, Boyer DR, Rodriguez JA, Sawaya MR, Cascio D, Murray K, Gonen T, Eisenberg DS (2018) Structure-based inhibitors of Tau aggregation. Nat Chem 10:170–176
Shaikh H, Rho JY, Macdougall LJ, Gurnani P, Lunn AM, Yang J, Huband S, Mansfield EDH, Peltier R, Perrier S (2018) Hydrogel and organogel formation by hierarchical self-assembly of cyclic peptides nanotubes. Chem – Eur J 24:19066–19074
Smith AM, Williams RJ, Tang C, Coppo P, Collins RF, Turner ML, Saiani A, Ulijn RV (2008) Fmoc-Diphenylalanine self assembles to a hydrogel via a novel architecture based on π–π interlocked β-Sheets. Adv Mater 20:37–41

Sreerama N, Woody RW (2003) Structural composition of betaI- and betaII-proteins. Protein Sci 12:384–388

Subbalakshmi C, Basak P, Nagaraj R (2017) Self-assembly of t-butyloxycarbonyl protected dipeptide methyl esters composed of leucine, isoleucine, and valine into highly organized structures from alcohol and aqueous alcohol mixtures. Peptide Sci 108:e23033

Sunde M, Serpell LC, Bartlam M, Fraser PE, Pepys MB, Blake CC (1997) Common core structure of amyloid fibrils by synchrotron X-ray diffraction. J Mol Biol 273:729–739

Taief KA, Nemec S, Middleton IA, Kilian KA, Thordarson P (2025) Scrambled RGD hexameric peptide hydrogel supports efficient self-assembly and cell activity. Chem Eur J 31:e202404410

Tao K, Levin A, Adler-Abramovich L, Gazit E (2016) Fmoc-modified amino acids and short peptides: simple bio-inspired building blocks for the fabrication of functional materials. Chem Soc Rev 45:3935–3953

Tyagi G, Sengupta S (2024) Unveiling the multifaceted potential of amyloid fibrils: from pathogenic myths to biotechnological marvels. Biophys Rev 16:737–751

Verma SS, Chaudhary N (2025) Substitution of tyrosine with electron-deficient aromatic amino acids improves Ac-PHF6 self-assembly and hydrogelation. RSC Adv 15:22216–22227

Verma SS, Bhattacharya S, Kumar S, Chaudhary N (2025) The amyloidogenic peptide stretch in human tau, tau306–311 is a promising injectable hydrogelator. Biophys Chem 322:107438

Vijayakanth T, Dasgupta S, Ganatra P, Rencus-Lazar S, Desai AV, Nandi S, Jain R, Bera S, Nguyen AI, Gazit E, Misra R (2024) Peptide hydrogen-bonded organic frameworks. Chem Soc Rev 53:3640–3655

Woerly S (1993) Hydrogels for neural tissue reconstruction and transplantation. Biomaterials 14:1056–1058

Wolf P (1983) A critical reappraisal of waddell's technique for ultraviolet spectrophotometric protein estimation. Anal Biochem 129:145–155

Wu J, Yang JT, Wu CS (1992) Beta-II conformation of all-beta proteins can be distinguished from unordered form by circular dichroism. Anal Biochem 200:359–364

Yang L, Li H, Yao L, Yu Y, Ma G (2019) Amyloid-based injectable hydrogel derived from hydrolyzed hen egg white lysozyme. ACS Omega 4:8071–8080